EVOLUTION OF THE FACE IN MID PLEISTOCENE *HOMO* – 3D SURFACE ANALYSIS OF ONTOGENY, ALLOMETRY AND EVOLUTION

BY

SARAH E. FREIDLINE

A dissertation submitted to the Graduate Faculty in Anthropology in partial fulfillment of the requirements for the degree in Doctor of Philosophy, The City University of New York

2012

© 2012

SARAH E. FREIDLINE

All Rights Reserved

This manuscript has been read and accepted for the
Graduate Faculty in Anthropology in satisfaction of the
dissertation requirements for the degree of Doctor of Philosophy.

__Eric Delson_____

_____ _____

Date Chair of Examining Committee

__Gerald Creed_____

_____ _____

Date Executive Officer

___Katerina Harvati_____

___William Harcourt-Smith_____

___Jean-Jacques Hublin_____

___Philipp Gunz_____

Supervisory Committee

THE CITY UNIVERSITY OF NEW YORK

Abstract

Evolution of the Face in mid Pleistocene *Homo* – 3D Surface Analysis of Ontogeny, Allometry and Evolution

by

Sarah E. Freidline

Advisor: Professor Eric Delson

This dissertation seeks to provide greater insight into the phylogenetic relationships among African and Eurasian Middle Pleistocene humans by placing their facial morphology in a broad evolutionary and developmental context. More specifically, the research goals are to gain a clearer understanding of the developmental variation of facial features and their covariation with size and to identify temporal trends in facial morphology that could potentially clarify the polarity (i.e., primitive or derived) of facial features during Pleistocene human evolution. To do so, I apply a recently developed method, semilandmark geometric morphometrics, to quantify the developmental and adult variability of facial features from childhood to adulthood in archaic and modern humans.

Additionally, this dissertation evaluates the morphology and phylogenetic relationships of specific Middle to Late Pleistocene fossils that are often not included in morphometric analyses because of their fragmentary condition. These fossils include the early Middle Pleistocene fossil ATD6-69 from Atapuerca, Spain, the mid-Middle Pleistocene fossil Zuttiyeh from Israel, and the Late Pleistocene fossil Saint-Césaire from Southwestern France.

Surface and computed tomography scans of modern and Pleistocene fossil humans were acquired and landmarks and semilandmarks were digitized on three-dimensional models created from the scans. Procrustes shape coordinates in shape-space and form-space (i.e., shape and size) were analyzed.

The general results of this dissertation are that some population and species-specific features are already established at the time of birth and that postnatal facial growth further contributes to shape differences among adults. Additionally, this research shows that allometric scaling played an important role in the facial differences between Middle Pleistocene humans and Neanderthals, while modern human facial morphology is the derived condition. The distinctly modern human pattern of facial morphology is already present in Jebel Irhoud 1, dated to around 170 ka. ATD6-69 expresses a mosaic pattern of facial morphology, and several features are certainly modern human-like (e.g., infraorbital depression). Zuttiyeh exhibits a generalized morphology possibly indicative of the population that gave rise to modern humans and Neanderthals. Lastly, the results of the Saint-Césaire study do not provide morphological evidence of admixture between Neandethals and modern humans in this particular specimen.

Dedication

This work is dedicated to my mother, father and brother.

Acknowledgements

Deep gratitude goes to Eric Delson, the supervisor of my doctoral studies in the Department of Anthropology at the City University of New York Graduate Center. I would like to thank him for taking me as his student and for believing in me throughout this process. I would like to acknowledge Jean-Jacques Hublin for mentoring me during my years at the Max Planck Institute for Evolutionary Anthropology. I am grateful for his passionate discussions, enthusiasm for my research, and support, without this I would not have been able to do the projects in my dissertation. Katerina Harvati, formerly at the Max Planck Institute and now at the University of Tübingen, also supervised my dissertation. Katerina has always been an inspiring role model for me, both personally and professionally. I would like to thank her for her support throughout the years. Additionally, I would like to thank Philipp Gunz, a researcher at the Max Planck Institute. Not only was Philipp the mastermind behind the methods used in this dissertation, his intellectual contribution was invaluable. I would like to thank him for his patience with my data and me. He has been an outstanding mentor, both personally and professionally.

I thank all of the curators for access to skeletal material from the following institutions: American Museum of Natural History (New York), Aristotle University of Thessaloniki, Hrvatski Prirodoslovni Muzej (Zagreb), Institut de Paléontologie Humaine (Paris), Musée Archéologique (Rabat), Musée de L'Homme (Paris), Museo Nazionale Preistorico Etnografico "L. Pigorini" (Rome), National Museum of Ethiopia (Addis Ababa), Natural History Museum (London), Naturhistorisches Museum (Vienna), Peabody Museum at Harvard University (Cambridge), Rheinisches Landesmuseum (Bonn), South African Museum (Cape Town), and the University of Cape Town.

In particular, I would like to thank: Dr. Ian Tattersall and Gisselle Garcia for giving me unlimited access to the cast and cranial collection at the AMNH; Drs. Sarah Wurz, Ildiko Pap, Maria

Teschler, Dejana Brajkovic, Ralf Schmitz for their hospitality during my data collection in their institutions; Dr. Fred Grine for allowing me to use a collection of CT scans in my dissertation; Dr. Yoel Rak and Alon Barash for their help while in Tel Aviv and especially for introducing me to the tastiness of Israeli cuisine.

Various aspects of my dissertation research received funding from the Max Planck Society, City University of New York Graduate Center, New York Consortium in Evolutionary Primatology, the National Science Foundation (0333415, 0513660 and 0851756), the L.S.B. Leakey Foundation, Sigma Xi, and the Marie Curie Actions grant MRTN-CT-2005-019564 "EVAN."

I would like to acknowledge Terry Harrison, my undergraduate supervisor at NYU, who influenced me to do graduate studies in physical anthropology, and Shara Bailey, also at NYU, for encouraging me to go to Leipzig to collaborate with members of the Department of Human Evolution at the MPI.

From the MPI I would like to thank the following current and former faculty from the Department of Human Evolution: Tracy Kivell, Matt Skinner, Kornelius Kupczic, Shannon McPherron, Olaf Nehlich, Simon Neubauer, Luke Premo, Amanda Henry, Domingo Carlos Salazar Garcia, Michael Richards, Enza Spinapolice, Fred Spoor, Adam Sylvester, Christine Verna and Bence Viola. From NYCEP: William Harcourt-Smith, Thomas Plummer and Alfie Rosenberger.

Thank you to all of the current and former students and friends in the Department of Human Evolution at the Max Planck Institute, CUNY, NYCEP, University of Tübingen and European Virtual Anthropology Network for their kindness, encouragement and for help making this experience so memorable.

Additionally, I would like to thank the following friends who have made my experience in Leipzig and New York some of my most happiest moments: Matt and Kornelius for your helpful advice and fruitful discussions; Tracy and Louise for our amusing dinners together and their

optimism; Simon for answering all of my silly morphometric questions; my girls Katja, Grit, Mimi, Erin, Esther, Lydia, Emily, Sahra, Nandini, Ellen and Embla. Ellen, you have been such an inspiration for me. Thank you Em, Lydia and Mimi for always making me laugh, even in the hardest times, and without our nights together I don't know how I would have gotten through the last few months. Sahra, thank you for all of the wonderful Italian meals and fortune telling, hopefully some of it will come true. Tomi, for commiserating with me in PhD struggles; our daily lunches and breaks have helped me keep my sanity throughout this process. Thank you Nandini, Hannes and Herni for your friendship. Vicky, your DJ skills greatly assisted me in finishing; Nelson, Karen and Josh thank you for all of your advice, both personal and professional; Jessica for always listening; and Lauren and Andy for being there for me through all of it. Together, your support has meant the world to me.

For their administrative and technical support during my doctoral studies, I would like to thank Ellen DeRiso, Diana Carstens, Cornelia Schicke, Silke Streiber, Rocco Bucholz, Dennis Reinhardt, and Heiko Temming.

Most of all, I would like to thank my mother, father and brother for their unconditional love, support and understanding.

Table of Contents

List of Tables

List of Figures

1. Introduction

1.1.Overview

Facial features are used frequently in species recognition and phylogenetic reconstruction in the human fossil record, and are particularly important in understanding evolutionary relationships among early modern humans, Neanderthals and their precursors in the later stages of human evolution. Neanderthals and modern humans exhibit distinct facial architectures. The patterning of facial morphology of their predecessors, the Middle Pleistocene humans (hereafter MPh), is more mosaic, variously aligning them to *Homo erectus sensu lato*, *H. neanderthalensis* and *H. sapiens*. Facial features that foreshadow the "classic" Neanderthal morphology have been equivocally identified in the European Middle Pleistocene humans (e.g., Arago 21, Sima de los Huesos 5 and Petralona) but are absent in their African and Asian counterparts. If verifiable, the presence of these "incipient" Neanderthal facial features in European MPhs provides compelling evidence for their inclusion in the Neanderthal lineage and an accretionary (gradual and mosaic) model of Neanderthal origins. However, many of these features are discrete and not easily quantifiable using linear morphometrics or even traditional landmark-based geometric morphometrics.

Significant changes in facial size and robusticity occurred throughout Pleistocene human evolution resulting in temporal trends in both facial reduction and enlargement. Moreover, differences in the degree of facial robusticity have been used as evidence to support interbreeding between Neanderthals and modern humans. It is unclear, however, how size affects facial features. This is particularly relevant for MPhs and Neanderthals because together they express the largest faces in the Pleistocene human fossil record.

The fossil ATD6-69 from Atapuerca, Spain dated to ca. 780 ka has been suggested to mark the earliest appearance of modern human facial features. However, as this specimen is a subadult, the interpretation of its facial morphology remains controversial. It is unclear how developmental shape changes would affect the features that link ATD6-69 to modern humans. A better understanding of the ontogeny of facial features and how they are affected by size is critical for evaluating the facial morphology and taxonomic implications of ATD6-69.

This body of work utilizes a recently developed quantitative method, semilandmark geometric morphometrics (SGM; Bookstein, 1997; Gunz et al., 2005, 2009a, b). By enabling one to quantify small-scale features, SGM methods overcome the limitations of linear morphometrics, traditional landmark-based geometric morphometrics, and descriptive methods. We apply SGM to quantify the ontogenetic variability of facial features in modern and Pleistocene humans. In doing so, the development of facial features, their co-variation and allometric scaling are assessed. Ultimately, this body of work seeks to provide greater insight into the phylogenetic relationships between the African and European MPhs, and identify temporal trends in facial morphology that could potentially inform us about the polarity (i.e., primitive or derived) of facial features during Pleistocene human evolution.

1.2.Semilandmark geometric morphometrics

In geometric morphometrics, data take the form of 3-D coordinates of individual landmarks, or of groups of semilandmarks defining curves and surfaces. This is superior to traditional, linear morphometric approaches because it allows for the improved retention and visualization of shape information within a group of specimens, as well as between groups. Semilandmarks make it possible to quantify shape information on curves using coordinate-based statistics. They can be used in geometric-morphometric analyses of shape variation as if they were homologous

landmarks and are therefore particularly helpful in regions where standard osteometric points are sparse (e.g., the neurocranium). Recently it has become possible to capture semilandmarks also from surfaces by creating "patches" over specific morphological features using the software package Landmark Editor (LE). This technique allows researchers for the first time to objectively quantify traits otherwise difficult to measure using traditional linear or even landmark-based geometric morphometrics (e.g., infraorbital plate morphology and orientation). The outcome of this novel approach is that complex features can be quantified as continuous variables, rather than discrete scores, and included in rigorous statistical analyses. Furthermore, SGM methods have been particularly valuable in reconstructing fragmentary fossil specimens (e.g., Gunz, 2005; Gunz et al., 2009).

1.3 Historical background and current perspectives on modern human origins

Since the discovery of the first Neanderthal remains in 1856 at Feldhofer Cave, Neander Valley, Germany, the relationship between modern humans and Neanderthals has been a point of contention among paleontologists and geologists. Despite King's (1864) proposition that the Feldhofer remains should be placed in a separate taxon, *H. neanderthalensis*, the consensus at the time was that it represented an ancient, inferior race of *H. sapiens*. Following the discovery of more Neanderthal remains at Spy Cave (Belgium) and a new and apparently more ape-like fossil in Java (which its discoverer, Eugene Dubois, dubbed *Pithecanthropus erectus*), Schwalbe (1906) presented a phyletic scheme which depicted Neanderthals as an intermediary link between *Pithecanthropus* and modern humans.

At the time, theories of racial succession were popularly incorporated into unilinear interpretations of human evolution. For example, in 1924 Verneau proposed that Neanderthals were the ancestor of *H. sapiens*, and that the "Negroid" race, retaining many primitive Neanderthal

features, represented the earliest modern humans. Similarly, three years later, Hrdlička (1927) proposed that modern humans arose from Neanderthals; however, he believed that Neanderthals exhibited too much variation to be considered a single species, and instead represented a "phase" in an evolutionary series culminating in modern man. Weidenreich (1949), another enthusiast of this theory, modified it to incorporate parallel evolution of modern humans on different continents. This polycentric theory of modern human origins was later emphasized by Coon (1962) and ultimately developed into the Multiregional Theory of human evolution (*see* Wolpoff *et al*., 1984). Although Weidenreich (1949) and Coon (1962) largely focused on the Northern Asian and Australian Pleistocene fossil record as evidence for regional continuity among modern humans, they interpreted the fossil sequence in Africa and Europe in the same manner.

Alternatively, the "Presapiens" hypothesis, proposed by Boule (1911-13) and developed by Vallois during the 1940s and 1950s (e. g., 1954), emphasized separate evolutionary lineages of modern humans and Neanderthals, with Swanscombe and later Fontéchevade representing ancient members of the Presapiens lineage. Concomitantly, Vallois interpreted fossils such as Steinheim as pre-Neanderthals. Therefore, the Presapiens hypothesis implied that modern human ancestors and Neanderthals coexisted in Europe.

Over fifty years later - following improvements in dating techniques, new genetic evidence, and a larger body of fossils - paleoanthropologists are still debating the taxonomy of Middle Pleistocene hominins in Africa and Eurasia, their relationships to Later Pleistocene populations, and the nature of modern human origins. In recent years, two contrasting models have dominated discussions on the origin of modern humans: "Recent African Origin" (Stringer and Andrews, 1988; Stringer, 1994) and "Multiregional Evolution" (Wolpoff *et al*., 1984, 1994, Thorne and Wolpoff, 1992; Wolpoff and Caspari, 1997). The Recent African Origin model proposes that modern humans arose in Africa between 200-100 Ka and migrated throughout the world replacing indigenous archaic populations. Multiregional Evolution, a modification of Weidenreich's and Coon's regional

continuity theories, argues against a strict recent African origin for modern humans and emphasizes a balance between genetic continuity and gene flow between contemporaneous populations. Supporters of this theory argue that modern humans arose not only in Africa but also in Europe and Asia. The "African Hybridization Model" (Bräuer, 1984, 1992; Bräuer and Broeg, 1998) and "The Assimilation Model" (Smith et al., 1989; Smith, 1992) are less extreme versions of these theories. They both support an African origin of modern humans; however, "The African Hybridization Model" allows for a greater or lesser extent of admixture between archaic and modern populations, and "The Assimilation Model" accepts an even greater degree of gene flow, admixture, and changing selection pressures, such that regional continuity in some areas could play an important role in modern human origins.

Most recently, the sequencing of the complete Neanderthal genome revealed that between 1 and 4% of the genomes of people in Eurasia are likely derived from Neanderthals (Green et al., 2010). These authors conclude that low levels of interbreeding between archaic and modern humans most likely occurred in the Near East, when modern humans first left sub-Saharan Africa and before they expanded into Eurasia. Hodgson et al. (2010) propose an alternative scenario in which admixture occurred between Neanderthals and modern humans around 100 ka and then for climatic reasons modern humans retreated back to Africa, severing contact with Neanderthals. They argue that the presence of Neanderthal DNA in Europeans and Asians could be explained by founder effects during range expansion, and that traces of Neanderthal DNA may be present in unsampled modern African populations.

While low levels of interbreeding between Neanderthals and modern humans most likely occurred, its frequency has yet to be determined. Such low levels do not invalidate a sister-species relationship between these two groups. Moreover, within the last ten years a significant amount of genetic (e.g., Krings *et al*., 1997, 2000; Ovchinnikov *et al*., 2000), morphological (e.g., Harvati, 2001, Harvati *et al*., 2004), ontogenetic (e.g., Ponce de Leon and Zollikofer, 2001), and archaeological (e.g.,

Mellars, 2002, 2004, 2006) evidence has accumulated to support a sister-species relationship between modern humans and Neanderthals. Yet, despite the growth of such data, difficulties in defining modern humans morphologically, behaviorally, and archaeologically continue to confound our understandings of modern human origins.

Following Hublin (2009) and Endicott et al. (2010), the current paleoanthropological models for the splitting of modern humans and Neanderthals from an ancestral population can be divided into four chronological categories: the late (~250 ka), middle (~400 ka), and early (~600 ka) periods of the Middle Pleistocene, and the late Early Pleistocene (~800 ka). In the late Middle Pleistocene model, the last common ancestor of *H. neanderthalensis* and *H. sapiens* occurs in Africa and is attributed to the species *H. helmei* (ca. 150-300 ka). This model, also known as the Mode 3 hypothesis, is based on the Florisbad partial cranium dated to ca. 260 ka and presumably associated with a novel lithic technology, Levallois prepared cores (Foley and Lahr, 1997; Lahr and Foley, 2001). In this scenario, *H. helmei* would have migrated out of Africa and introduced the Levallois technology to Europe. Neanderthal and modern human population divergence would have occurred subsequent to the existence of Florisbad at around 260 ka.

The mid-Middle Pleistocene model sees the last common ancestor to *H. neanderthalensis* and *H. sapiens* as a single Euro-African species, which might include fossils such as Arago 21 and Petralona from Europe and Bodo and Kabwe from Africa. Quantitative support for this model has been shown through a combination of qualitative descriptive methods and traditional craniometric techniques, which emphasize the strong similarities in the human fossil record between the two continents. Supporters of this model see the MPh in Europe, Africa and possibly Asia as representing one species, viewed as the last common ancestor of Neanderthals and modern humans (Stringer, 1974, 1983, 1996, 2002; Arsuaga et al., 1997; Rightmire, 1996, 1998a,b, 2001, 2007, 2008; Mounier et al., 2009; Harvati 2009a). A recent landmark-based 3-D geometric morphometrics study (Harvati *et al*., 2010) that was able to quantify some of the relevant facial

morphology supported the link between the African and European MPhs and questioned the assumed polarity of some of these traits. If the Mauer mandible (from Germany) is included in this group then the species name for it is *H. heidelbergensis*. However, Hublin (2009) has argued that this fossil should be excluded because it is primitive and not associated with any cranial material (but see Mounier et al., 2009). Instead, he argues, the Broken Hill (Kabwe) cranium should be given precedence, thus designating the species as *H. rhodesiensis* (Hublin, 2009). The possible age range for this group is between ca. 300 – 650 ka (Stringer, 2002).

The early Middle Pleistocene model identifies the European fossils as a chronospecies of *H. heidelbergensis-H. neanderthalensis*, which is part of a continuum from the early Middle Pleistocene through to the Late Pleistocene. On the other hand, the African fossils, represented as *H. rhodesiensis*, are directly ancestral to *H sapiens*. Using a cladistic approach of qualitatively describing and scoring characters, several researchers (Hublin, 1996, 1998; Arsuaga *et al*., 1997; Dean *et al*., 1998) have noted 'incipient' derived Neanderthal traits in European mid-Pleistocene *Homo* specimens and a gradual accretion of such features through time culminating with the appearance of the 'classic' Neanderthals in the Late Pleistocene. Neanderthal traits that are thought to appear among the earliest European MPh include a degree of midfacial projection, inflation of the maxilla and posteriorly sloping zygomatics. This evidence supports a split between the European and African lineages in the Middle Pleistocene, and a call for separation of the European and African MPh into two species (*H. heidelbergensis* and possibly *H. rhodensiensis*, respectively). Central to this model are the extensive collection of fossils from Sima de los Huesos (SH), Atapuerca, Spain, which display clear Neanderthal affinities (Arsuaga et al., 1997; Rosas, 2001), particularly in the dentition (Martinon-Torres et al., 2007). These fossils have been recently re-dated to a minimum age of ca. 530 ka (Bischoff et al., 2007), and the population divergence between this European lineage and that leading to *H. sapiens* likely preceded 600 ka.

Lastly, the late Early Pleistocene model has a European hominin (*H. antecessor*) as the ancestor to an *H. rhodesiensis-H. sapiens* lineage in Africa and an *H. heidelbergensis-H. neanderthalensis* lineage in Europe. The chronological date for *H. antecessor* is ca. 780 ka (Bischoff et al., 1997), suggesting a population divergence date between these two lineages soon after 800 ka (Bermudez de Castro et al., 1997; Arsuaga et al., 1999).

Our understanding of the timing of divergence between the lineages leading to *H. sapiens* and *H. neanderthalensis* has benefited from recent work combining paleontology and paleogenetics (Noonan et al., 2006; Green et al., 2008, 2010; Endicott et al., 2010). However, it is important to bear in mind that genetic coalescence, population separation and phenotypic differentiation represent chronologically distinct events (Hublin, 2009). In a recent study, Endicott et al. (2010) evaluated the aforementioned four competing paleoanthropological models by using genetic estimates for the time to the most recent common ancestor (MRCA) of modern humans and Neanderthals, obtained using Bayesian phylogenetic analysis of mitochondrial DNA (mtDNA) sequences. To do so, they used a *Pan-Homo* divergence date of between 6.5 to 7.5 Ma. According to their results, the time interval for the most recent common ancestor of Neanderthals and modern humans ranged from 315 to 538 ka. This age interval is compatible with the most recent Neanderthal-modern human molecular divergence dates published by Green et al. (2010). They assumed a *Homo-Pan* divergence date of 5.6 to 8.3 Ma and estimated a Neanderthal and modern human divergence date of between 270 and 440 ka. Similarly, an earlier study by Noonan et al. (2008) on the autosomal genome provided a coalescence time ca. 700 ka and a separation time for Neanderthals and modern human populations ca. 370 ka.

Together, these results postdate the late Early Pleistocene model, ruling out a Eurasian hominin population ancestral to both modern humans and Neanderthals in Europe at 1 Ma to 800 ka. Endicott et al.'s (2010) age range for the MRCA of Neanderthals and modern humans predates the late Middle Pleistocene model, which proposes a timescale for *H. helmei* from ca. 150 to 300 ka.

Moreover, the late Middle Pleistocene model is unlikely because Levallois flake technology occurs in Europe and Africa prior (ca. 300-327 ka; White and Ashton, 2003; Tryon et al., 2005) to the existence of the Florisbad skull (ca. 260 ka), and it does not take into account the proposed Neanderthal features in the European Middle Pleistocene fossils from Swanscombe, Steinheim and Sima de los Huesos (Stringer, 2002; Hublin, 2009).

As the SH material clearly exhibits derived Neanderthal features (Arsuaga et al., 1997; Rosas, 2001; Martinón -Torres et al., 2007), the early Middle Pleistocene model requires a MRCA prior to the existence of this population at around 600 ka (Bischoff et al., 2007). This model falls outside the 95% credible interval for the genetic MRCA. Therefore, according to Endicott et al. (2010) the most plausible model based on genetic estimates is the mid-Middle Pleistocene model, which falls squarely within their proposed time interval of 315-538 ka for the MRCA.

Several researchers have argued for a reappraisal of the SH fossils (e.g., Hublin, 2009; Endicott et al., 2010). These fossils are central to the definition of the *H. heidelberensis-H. neanderthalensis* European continuum; however they display many more derived Neanderthal features than the other European fossils, such as the possibly later Arago 21 specimen (Cook et al., 1982; Lumley et al., 1984; Falguères et al., 2004) and the contemporaneous Mauer mandible (dated to ca. 600 ka, Wagner et al., 2010, 2011). Moreover, the date of the SH (> 530 ka) material is not compatible with Endicott et al.'s (2010) Neanderthal and modern human population divergence dates at no earlier than 538 ka. Taphonomic doubts concerning the deposition of these fossils (see Endicott et al., 2010) suggest that the previous dating of these fossils at between ca. 200-400 ka (Arsuaga et al., 1997; Bischoff et al., 2003) is more appropriate.

The marked heterogeneity of the African fossil hominins during the late Middle Pleistocene contrasts with the early appearance of derived Neanderthal morphology present in the European fossils (Hublin, 2009; Endicott et al., 2010; Harvati et al., 2010). The first well-dated and relatively

complete *H. sapiens* do not appear in Africa until ca. 160 ka at Guomde (Bräuer *et al*., 1997), Herto (White *et al*., 2003) and Omo Kibish (ca. 98- 192 ka). Smith (2002) termed the African fossils from the time span of ca. 250 to 160 ka as the African Transitional Group (ATG). The fossil human remains assigned to this group include Jebel Irhoud 1-4, Florisbad, Ngaloba, Eliye Springs, Guomde and Omo Kibish 2. In addition to the ATG label, the pre-modern phase of *H. sapiens* has also been referred to as *H. helmei* (Stringer, 1996; McBrearty and Brooks, 2000), *H. rhodesiensis* (Hublin, 2009) and archaic *H. sapiens* (Stringer, 2002). The crucial problem when allocating these fossils, however, is diagnosing ancient examples of "modern" humans without a formal definition of modernity (*see* Aiello 1993 and Stringer, 2002 for discussion). Defining modern humans based on recent morphology is problematic because anatomically modern human fossils from the Late Pleistocene are often more robust than more recent *H. sapiens*, and they tend to show mosaic evolutionary patterns (Lahr, 1996; Trinkaus, 1997; Pearson, 2000). Another source of confusion is the relative lack of autapomorphies in *H. sapiens*; the majority of characters used to describe modern human morphology concentrate on cranial globularity (*see* Day and Stringer, 1982 and Stringer *et al*., 1984), and consequently they are not structurally or developmentally independent (Lieberman *et al*., 2002).

In fact, the earliest appearance of modern human facial morphology has been described in the subadult *H. antecessor* specimen ATD6-69 from Gran Dolina, Atapuerca, Spain. This fossil, dated to ca. 780 Ka, shows a modern human-like facial morphology in combination with more primitive craniodental features (Bermúdez de Castro *et al*., 1997). Specifically, the specimen shows a modern human-like canine fossa, coronal orientation of the infraorbital plate, and a horizontal zygomaticoalveolar crest (Bermúdez de Castro *et al*., 1997). Bermúdez de Castro and his co-authors (1997) conclude that the midfacial and subnasal morphology of modern humans may be a retention of a juvenile pattern that was not present in *H. ergaster*, and consequently *H. antecessor* may represent the last common ancestor of the two distinct lineages, Neanderthals and modern humans.

However, that claim cannot be evaluated until the polarity of these traits in the Pleistocene human fossil record is well-understood, and, most importantly, until the pattern of development of these features among recent humans and Neanderthals is known.

Despite its crucial importance in resolving these issues, the ontogeny of facial features and how they are affected by facial size (i.e., allometry) is not well understood. The evidence that exists suggests that population-specific and species-specific craniofacial features occur early in ontogeny in modern humans and Neanderthals (Rak et al., 1994; Zilberman, 1994; Akazawa et al., 1995; Ponce de León and Zollikofer, 2001; Lieberman et al., 2002; Ackermann and Krovitz, 2002; Strand Viðarsdóttir et al., 2002; Williams et al., 2002; Krovitz, 2003; Mitteroecker et al., 2004; Bastir and Rosas, 2004; McNulty et al., 2006; Gunz et al., 2010). However, currently we lack understanding of how specific facial features develop, vary and co-vary. Such an understanding is necessary in order to assess the evolutionary significance of both adult and juvenile facial features and their usefulness in phylogenetic reconstructions of the Pleistocene human fossil record. Establishing these patterns of ontogeny, variation and co-variation and using them to help interpret the later stages of human evolution is one of the major goals of this body of work.

1.4 Objectives

This study demonstrates the applicability of semilandmark geometric morphometrics and contributes to our understanding of facial growth and allometry in Middle to Late Pleistocene human evolution. From a methodological perspective, I set out to quantify the variability of small-scale facial features that were difficult to measure using other approaches, such as linear measurements and traditional geometric morphometrics. In doing so, I wanted to know if more landmarks could provide us with greater discriminatory power between Pleistocene fossil groups and how the shape of particular facial features change with size and through time.

The main objectives of this study are to: 1) use semilandmark geometric morphometric methods to quantify small-scale facial traits (e.g., canine fossa, infraorbital plate orientation, nasal projection, angle of zygomatic, browridge shape) frequently used to define Pleistocene taxa (e.g., *H. erectus*/*ergaster*, *H. antecessor*, *H. heidelbergensis*, *H. neanderthalensis*, *H. sapiens*); 2) quantify the ontogenetic variability of these traits within recent human groups to better assess the development of facial features; 3) quantify the same traits in a large sample of Pleistocene fossil human material for the first time incorporating rarely-used and fragmentary fossils (e.g., ATD6-69; Zuttiyeh and Saint-Césaire); 4) assess the effects of allometry on these facial features; and 5) identify temporal trends in facial morphology. The methods to be used in these analyses are introduced in Chapter 2.

1.5 Research chapter summaries

Chapter 3 evaluates the Middle Pleistocene human face in a broad evolutionary and developmental context. More specifically, we test to see how well facial morphology separates Pleistocene human groups, and we assess the effects of ontogenetic and static allometry on the Pleistocene human face. Ontogenetic and static allometric trajectories were calculated for fossil and modern human groups, and growth simulations were applied to visualize the effects of allometry on the face. We show that facial features can be used to separate Pleistocene humans into temporal clusters. The distinctly modern human pattern of facial morphology is already present in Jebel Irhoud 1, dated to around 170 ka. Species- and population-specific facial features develop before two years of age, and the large-scale facial differences between Neanderthals and Middle Pleistocene humans are mostly due to allometric scaling along a shared allometric trajectory. Among recent modern humans, the facial features most affected by allometric scaling are anterior projection of glabella, nasal aperture height and width, lateral projection of the zygomatic bones, infraorbital surface topography, and lengthening of the subnasal region.

Chapter 4 analyzes the ATD6-69 face in an evolutionary and developmental context. Growth simulations, based on the allometric trajectories of modern humans and Neanderthals, are employed to visualize potential adult shapes of ATD6-69. We show that facial differences between modern and archaic humans are not exclusively allometric. However, as noted above, such differences between Neanderthals and Middle Pleistocene humans are largely due to allometric scaling along a shared trajectory. Between Neanderthals and modern humans, taxon-specific facial morphology develops early in ontogeny and postnatal growth further accentuates their facial differences. These results imply that those features that link ATD6-69's morphology to modern humans would not have been significantly altered in the course of subsequent development. In particular, the infraorbital depression on this specimen would have persisted into adulthood. As a result, its phylogenetic affinities can no longer be overlooked due to its subadult status.

Chapter 5 utilizes SGM to better understand the taxonomic affinities of the Zuttiyeh craniofacial fossil, discovered in Israel in 1925. Radiometric dates and the archaeological context (Acheulo-Yabrudian) bracket the associated cave layers to between 200 and 500 ka making it one of the earliest cranial fossils discovered in the Near East thus far. Its geographic position, at the corridor between Africa and Eurasia, in combination with its probable Middle Pleistocene date, make it a crucial specimen for interpreting later human evolution. Since its discovery, qualitative descriptive and traditional morphometric methods have variously suggested affinities to *Homo erectus* (Zhoukoudian E1; Hrdlička, 1930)*, H. neanderthalensis* (Tabun 1; Keith, 1939), and early *H. sapiens* (Skhul 5; Weidenreich, 1943). To better determine the taxonomic affinities of the Zuttiyeh fossil, this chapter uses 3D semilandmark geometric morphometric techniques and multivariate statistical analyses to quantify its frontal and zygomatic region and compare it to other Middle to Late Pleistocene African and Eurasian hominins.

Our results show that the frontal and zygomatic morphology of Zuttiyeh is most similar to Shanidar 5 (a Near Eastern Neanderthal), Arago 21 (a European Middle Pleistocene hominin), and

Skhul 5 (an early *Homo sapiens*). The shape differences between archaic hominins (i.e., *H. heidelbergensis* and *H. neanderthalensis*) in this anatomical region are very subtle. We conclude that Zuttiyeh exhibits a generalized frontal and zygomatic morphology possibly indicative of the population that gave rise to modern humans and Neanderthals. However, given that it most likely postdates the split between these two lineages, Zuttiyeh might also be an early representative of the Neanderthal lineage. Neanderthals largely retained this generalized overall morphology, whereas recent modern humans depart from this presumably ancestral morphology.

Chapter 6 applies a similar series of analyses to evaluate the morphology of a fragmentary late Neanderthal fossil, Saint-Césaire. Given its fragmentary condition, few metric studies have been performed on the cranial morphology of the Saint-Césaire partial skull. Additionally, its more gracile facial morphology, especially in the supraorbital region, has been used as morphological evidence of admixture between Neanderthals and modern humans. We used a virtually reconstructed Saint-Césaire cranium and applied geometric morphometrics and multivariate statistical analyses to quantify its facial and frontal bone morphology and compared it to other Eurasian Neanderthals and Upper Paleolithic and recent modern humans. Our results strongly support its Neanderthal association and show that the Saint-Césaire facial and frontal bone anatomy is most similar to that of Shanidar 1, a West Asian Neanderthal, and La Ferrassie 1, a European Neanderthal.

Lastly, Chapter 7 summarizes the goals of the dissertation and the key findings. Additionally, the major contributions are outlined and future projects stemming from this body of work are provided.

2. Materials and Methods

2.1 Sample

2.1.1 Fossil human sample

The fossil sample comprises all available Middle to Late Pleistocene subadult and adult fossils that preserve relatively complete faces (see section on Missing Data Reconstruction below). Additionally, some Early Pleistocene fossils were included to provide a comparative framework. Table 2.1 lists the entire fossil sample, their broad geographical location and their chronology. Table 2.2 lists the ontogenetic age estimates for the subadult fossil specimens compiled from the literature. The entire fossil sample was not used in every chapter, but was tailored to each chapter's research question. Therefore, each chapter provides a table of the sample used in the corresponding study. This also applies to the recent modern human specimen sample. Briefly, Chapters 3 and 4 include subadult and adult fossil and recent modern humans, and Chapters 5 and 6 only include adult fossil and recent modern human specimens.

Table 2.1 Fossil specimens used in the studies, their abbreviation (Ab.) and chronology. Subadult individuals are italicized. *cast from AMNH **cast from MPI

Specimen	Ab.	Chronology	Repository
Early Pleistocene: Africa			
ER 1813	1813	1.88-1.90 (Wood, 1991); 1.65 Ma (Gathogo and Brown, 2006)	KNM
ER 3733	ER3733	1.75 Ma (Feibel et al., 1989)	KNM
ER 3883	ER3883	1.50 Ma (Feibel et al., 1989)	KNM

Table 2.1 Continued

*WT 15000**	Tur	1.6 Ma (Feibel et al., 1989)	KNM
Early Pleistocene: Europe			
*ATD6-69**	ATD6-69	> 780 ka (Carbonell 1995;Parés et al., Parés et al., 1999)	CENIEH
Early Pleistocene: Asia			
*Dmanisi 2700**	Dm27	1.7-1.8 Ma (Gabunia et al., 2000)	GNM
Sangiran 17*	S17	1.50 – 1.02 Ma (Larick et al., 2001; Antón, 2003; Antón and Swisher, 2004); > 790 ka (Hyodo et al., 2011)	GM
Middle Pleistocene: Africa			
Bodo	Bd	ca. 600 ka (Clark et al., 1994)	NME
Kabwe	Kb	700 – 400 ka (Klein, 1994); late Middle Pleistocene (Stringer, 2011)	NHM
Middle Pleistocene: Europe			
Arago 21**	Ar	600 – 350 ka (Cook et al., 1982; Falguères et al., 2004)	UM
Petralona	Pt	670 – ca. 250 ka (Harvati et al., 2009)	AUT
Sima de los Huesos 5*	Sm5	ca. 530 ka (Bischoff et al., 2007)	UCM
Middle Pleistocene: Asia			
Dali*	Dl	230 – 180 ka (Chen and Zhang, 1991)	IVPP

Table 2.1 Continued

Zhoukoudian 12 (E1)*	Z12	550 – 520 ka; ca. 580 ka; ca. 770 ka (Grün et al., 1997; Antón, 2003; Shen et al., 2009)	original material missing
Zuttiyeh*	Zt	ca. 350, 500-200 ka (Huxtable, 1990; Bar-Yosef, 1992; Mercier et al., 1995; Mercier and Valladas, 2003)	RM
Late Middle-Late Pleistocene: Africa			
Florisbad*	Fl	290-230 ka (Grün et al., 1996)	NM
Jebel Irhoud 1	I1	ca. 160 ka (Smith et al., 2007)	MA
Late Middle-Late Pleistocene: Europe			
Gibraltar 1	Gb1	71 – 50 to 35 ka (Klein, 1999)	NHM
Guattari	Gt	ca. 50 ka (Schwarcz et al., 1991)	MNPE
Krapina 3	Kr3	140 – 120 ka (Rink and Schwarcz, 1995)	HP
Krapina 6	Kr6	140 – 120 ka (Rink and Schwarcz, 1995)	HP
La Chapelle-aux-Saints	LCh	56 – 47 ka (Grün and Stringer, 1991)	MH
La Ferrassie 1	LF1	71 – 50 to 35 ka (Klein, 1999)	MH
Pech-de-l'Azé I	Pech	51-41 ka (Soressi, 2007)	MH
Saint-Césaire	SC	36 ka (Mercier et al., 1991)	MH

Table 2.1 Continued

Late Middle-Late Pleistocene: Asia

Amud 1*	Am1	ca. 50 ka (Rink et al., 2001)	UT
Liujiang*	Ljg	139 – 111 ka (Shen et al., 2002)	IVPP
Qafzeh 6	Q6	135 – 100 ka (Grün et al., 2005)	UT
Qafzeh 9	Q9	135 – 100 ka (Grün et al., 2005)	UT
Shanidar 1*	Sh1	ca. 50 ka (Trinkaus, 1983)	IM
Shanidar 5*	Sh5	ca. 50 ka (Trinkaus, 1983)	IM
Skhul 5	Sk5	135 – 100 ka (Grün et al., 2005)	PM
*Teshik Tash**	Tesh	57-24 ka (Vishnyatsky 1999)	MSU

Upper Paleolithic: Europe

Brno 2*	Brn2	ca. 23 ka (Holt and Formicola, 2008)	MM
Cro-Magnon 1	Cr1	28 – 27 ka (Holt and Formicola, 2008)	MH
*Grotte des Enfants 6**	GrE6	Gravettian (Henry-Gambier, 2001)	MAP
Mladeč 1	Ml1	ca. 31 ka (Holt and Formicola, 2008)	NM
Předmostí 3*	Pr3	ca. 17 ka (Svoboda, 2008)	original material missing
Předmostí 4*	Pr3	ca. 17 ka (Svoboda, 2008)	original material missing
Oberkassel 1	Ob1	ca. 12 ka (Street, 2002)	RL
Oberkassel 2	Ob2	ca. 12 ka (Street, 2002)	RL

Table 2.1 Continued

Upper Paleolithic: Asia

Zhoukoudian 101**	Zh101	ca. 33 – 13 (Chen et al., 1989; Hedges et al., 1992; Brown, 1993)	original material missing
Zhoukoudian 102**	Zh102	ca. 33 – 13 (Chen et al., 1989; Hedges et al., 1992; Brown, 1992)	original material missing

AMNH, American Museum of Natural History (New York); AUT, Aristotle University of Thessaloniki (Thessaloniki); CNIEH, Centro Nacional Investigación Evolución Humana (Burgos); GM, Geological Museum (Bandung, Indonesia); GNM, Georgia National Museum (Tibilisi); HP, Hrvatski Prirodoslovni Muzej (Zagreb); IM, Iraq Museum (Baghdad); IPH, Institut de Paléontologie Humaine (Paris); IVPP, Institute of Vertebrate Paleontology and Paleoanthropology (Beijing); KNM, National Museum of Kenya (Nairobi); MA, Musée Archéologique (Rabat); MAP, Musee d'Anthropologie Prehistorique (Monte Carlo, Monaco); MH, Musée de l'Homme (Paris); MM, Moravian Museum (Brno); MSU; Moscow State University; NHM, Natural History Museum (London); NM, Naturhistorisches Museum (Vienna); NME, National Museum of Ethiopia (Addis Ababa); MNPE, Museo Nazionale Preistorico Etnografico "L. Pigorini" (Rome); MPI, Max Planck Institute (Leipzig); NM, National Museum (Bloemfontein); PM, Peabody Museum (Cambridge); RL, Rheinisches Landesmuseum (Bonn); RM, The Rockefeller Museum (Jerusalem); UCM, Universidad Complutense de Madrid (Madrid); UM, Université de la Méditerranenée (Marseille); UT, University of Tel-Aviv (Tel-Aviv)

Table 2.2 Ontogenetic age of the subadult fossil specimens used in the analysis.

Specimen	Ontogenetic Age (ca. yr.)
WT 15000	8 (Dean et al., 2001); 12 (Smith, 1994; Smith and Tompkins, 1995)
Dmanisi 2700	> 8 (Vekua et al., 2002); 8 – 16 (Rightmire et al., 2006)
ATD6-69	10 – 11. 5 (Bermúdez de Castro, 1997)
Pech-de-l'Azé I	2 (Tillier, 1996)
Teshik Tash	9 – 11 (Tillier, 1989; Williams et al., 2003)
Grotte des Enfants 6	13 – 15 (Henry-Gambier, 2001)

2.1.2 Recent modern human sample

The adult modern human sample (Table 2.3) is composed of fourteen geographic populations spanning six continents: Australia (South Australian Aborigines), Asia (Mongolia and Thailand), Europe (Austria and Czech Republic), Africa (Khoisan, Egypt and Tanzania), North America (Arizona, Utah, Alaska and Mexico) and South America (Argentina). All adult modern human specimens are from the American Museum of Natural History (AMNH, New York) and from the South African Museum (Cape Town). Adult individuals were sexed according to Howells' (1973) criteria. When possible, an equal number of males and females was included.

Table 2.3 Complete adult recent modern human sample. [1]American Museum of Natural History, New York; [2]South African Museum (Cape Town)

Adult Recent Modern Humans	**N = 234**
Asia	**Total = 10**
Mongolia[1]	5
Thailand[1]	5
Africa	**Total = 44**
Egypt[1]	5
Khoisan, South Africa[1,2]	34
Tanzania[1]	5
Australia	**Total =9**
South Australia[1]	9
Europe	**Total = 58**
Greifenberg, Austria[1]	50
Belgium[1]	2
Czech Republic[1]	6

Table 2.3 Continued

North America	**Total = 108**
Point Hope, Alaska, United States[1]	48
Canyon del Muerto, Arizona, United States[1]	34
Grand Gulch, Utah, United States[1]	18
Mexico[1]	8
South America	**Total = 5**
Tierra del Fuego, Argentina[1]	5

For the growth studies in Chapter 3 and 4, a cross-sectional growth series of recent modern humans was used. This sample is composed of individuals ranging in age from two years to adulthood, from four geographically diverse modern human populations spanning three continents: Africa, North America and Europe (Table 2.4). The African sample consists of an archaeological Khoisan population from South Africa. The North American sample is divided into two groups: a combined Native American archaeological sample from Canyon del Muerto, Arizona and Grand Gulch, Utah, and an archaeological population from Point Hope, Alaska. Lastly, the European sample consists of a temporally more recent combined sample from Strasbourg (France) and Greifenberg (Austria). The recent modern human subadult cranial data were obtained from specimens housed in the American Museum of Natural History (AMNH, New York), South African Museum (Cape Town), University of Cape Town, and Medical Faculty of Strasbourg.

Individual specimens in the human subadult skull collection from the Medical Faculty of Strasbourg have known ages with a precision ranging from one month to one day (Rampont, 1994). Age estimates for all other subadult individuals were assessed according to dental eruption patterns following Ubelaker (1989). Each specimen in the modern human sample was classified by

developmental stage according to dental eruption sequence, as defined in Table 2.4. Table 2.2 lists the number of subadults distributed between each age group within each modern human population. Because of the difficulty and uncertainty in identifying the sex of subadult individuals (Scheuer and Black, 2000), no attempt was made to do so, although studies have shown that size and shape differences occur between males and females throughout ontogeny and are most pronounced during and after adolescence (e.g., Strand Viðarsdóttir et al., 2002; Bulygina et al., 2006).

Table 2.4 Recent modern human adult and subadult specimens used in the analysis. The abbreviation *AG* represents Age Group. Age group one is composed of subadults that only have deciduous dentition, lacking the eruption (as defined by the exposure of cusps) of any permanent teeth; age group two is defined by the eruption of the first molar; age group three is defined by the eruption of the second molar; and age group four is defined by the eruption of the third molar (i.e., complete set of permanent dentition). The specimen sex is denoted as *M* for males and *F* for females.

Population/Geographic Region	**AG 1**	**AG 2**	**AG 3**	**AG 4 (adult)**	**Total**
Khoisan, South Africa[1,2,3]	8	8	4	38 (M: 14; F: 24)	58
Arizona (Canyon del Muerto), Utah (Grand Gulch), USA[3]	7	6	4	52 (M: 25; F: 27)	69
Alaska (Point Hope), USA[3]	6	10	4	48 (M: 26; F: 22)	68
Strasbourg, France[4] and Greifenberg, Austria[3]	7	4	4	49 (M: 27; F: 22)	64

[1]South African Museum
[2]University of Cape Town
[3]American Museum of Natural History
[4]Medical Faculty of Strasbourg

2.2 Measurement protocol

2.2.1 Computed Tomography (CT) and surface scans

Landmarks were digitized on the three-dimensional surface models extracted from surface scans or CT scans. CT scans were made with either an industrial CT scanner (BIR ACTIS 225/300) or a medical CT scanner (Toshiba Aquilion). The pixel size ranged from 0.24 to 0.49 mm, and the slice thickness was between 0.25 and 1.00 mm. Surface scans of the remaining specimens were made with either a Minolta Vivid 910, capable of scanning a resolution of ~ 30 microns in the z plane, or a Breuckmann optoTOP-HE, with a resolution of ~ 6 microns in the z plane. If CT or surface scan data of the original fossil material was not available, surface scans of high quality casts from the Division of Anthropology of the AMNH (New York) or the Max Planck Institute for Evolutionary Anthropology (Leipzig) were made (see Table 2.1). After specimens were surface scanned, scans were processed using either Geomagic Studio or OptoCat (Breuckmann) software, depending on the surface scanner used; for the CT data, three-dimensional surface models were extracted using Avizo (Visualization Sciences Group Inc.). Landmarks on these surfaces were then digitized using Landmark Editor (Wiley et al., 2005).

2.2.2 Landmark data

The complete landmark and semilandmark dataset is illustrated in Figure 2.1a-f, and the landmarks and curve semilandmarks are defined in Appendix A and B. For each study, a landmark and semilandmark subset were extracted from the complete dataset according to the research question. In addition to traditional landmark coordinates, semilandmarks were used to quantify information on curves and surfaces (Bookstein, 1997; Gunz et al., 2005, 2009a,b). The notion of homology employed here is one of geometric correspondence across a sample. Techniques for

surfaces differ substantially from those for curves in that, except for planes and cylinders, there is no straightforward way to distribute the semilandmarks. A mesh of surface-semilandmarks was digitized on one "template" individual (see Fig. 2.1a). This template mesh of surface-semilandmarks was warped into the vicinity of every specimen according to the landmark and curve data using a thin-plate spline (TPS) interpolation between the template individual and each specimen in turn (Gunz et al., 2005). The warped points were then projected onto the surfaces by picking the closest vertices from the specimen's triangulated surface file. This protocol guarantees that every specimen has the same number of curve-semilandmarks and surface-semilandmarks in approximately corresponding locations; a detailed description can be found in Gunz et al. (2005, 2009a,b). This method is different from the option available in Landmark Editor, which automatically transfers landmarks from the "atlas" to a specific scan, and consequently slightly moves the original placement of the landmarks and semilandmarks. The protocol used in this dissertation (i.e., TPS interpolation and multiple projection steps) does not affect the original placement of the traditional and curve semilandmarks, and as a result, the landmarks and semilandmarks do not need to be readjusted after the projection steps. To remove the confounding effects of the arbitrary spacing, these semilandmarks are then allowed to slide along the curves and surfaces prior to the statistical analysis. To linearize the minimization problem (Gunz et al., 2005, 2009a, b), the semilandmarks do not slide on the actual curve or surface but along the tangent vectors to the curve or the tangent planes to the surface. The initially equidistant semilandmarks were slid along tangents to the curves and tangent planes to the surfaces so as to minimize the bending energy of the TPS interpolation between each specimen and the Procrustes consensus configuration. After the sliding step, landmarks and semilandmarks can be treated the same in the subsequent multivariate analysis.

Figure 2.1 a) Complete landmarks and semilandmark dataset digitized on all specimens, [red: biological landmarks; blue: curve-semilandmarks; yellow: surface-semilandmarks] in front-lateral view; b) anterior; c) posterior; d) lateral; e) superior; f) inferior. Biological landmarks are abbreviated. The full names and definitions are listed in Appendix A and B.

a)

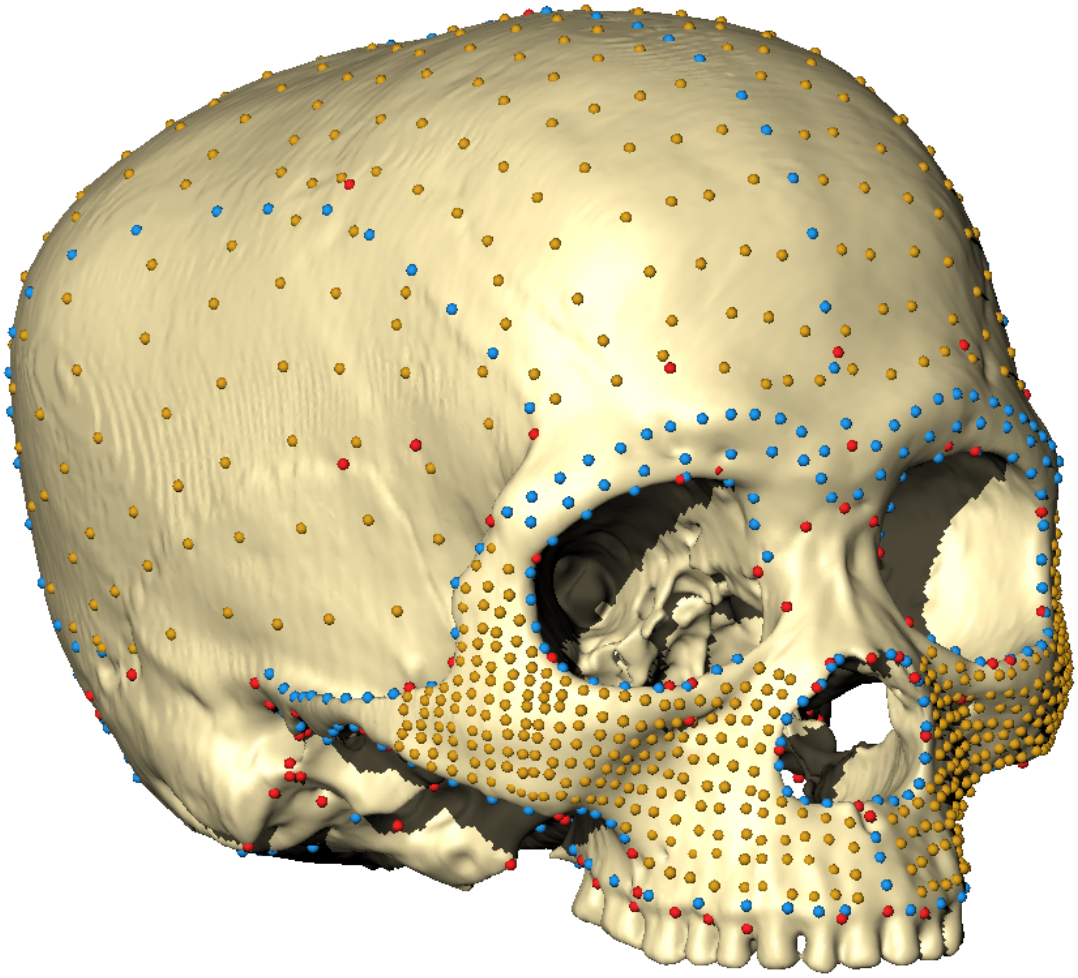

Figure 2.1 Continued: b)

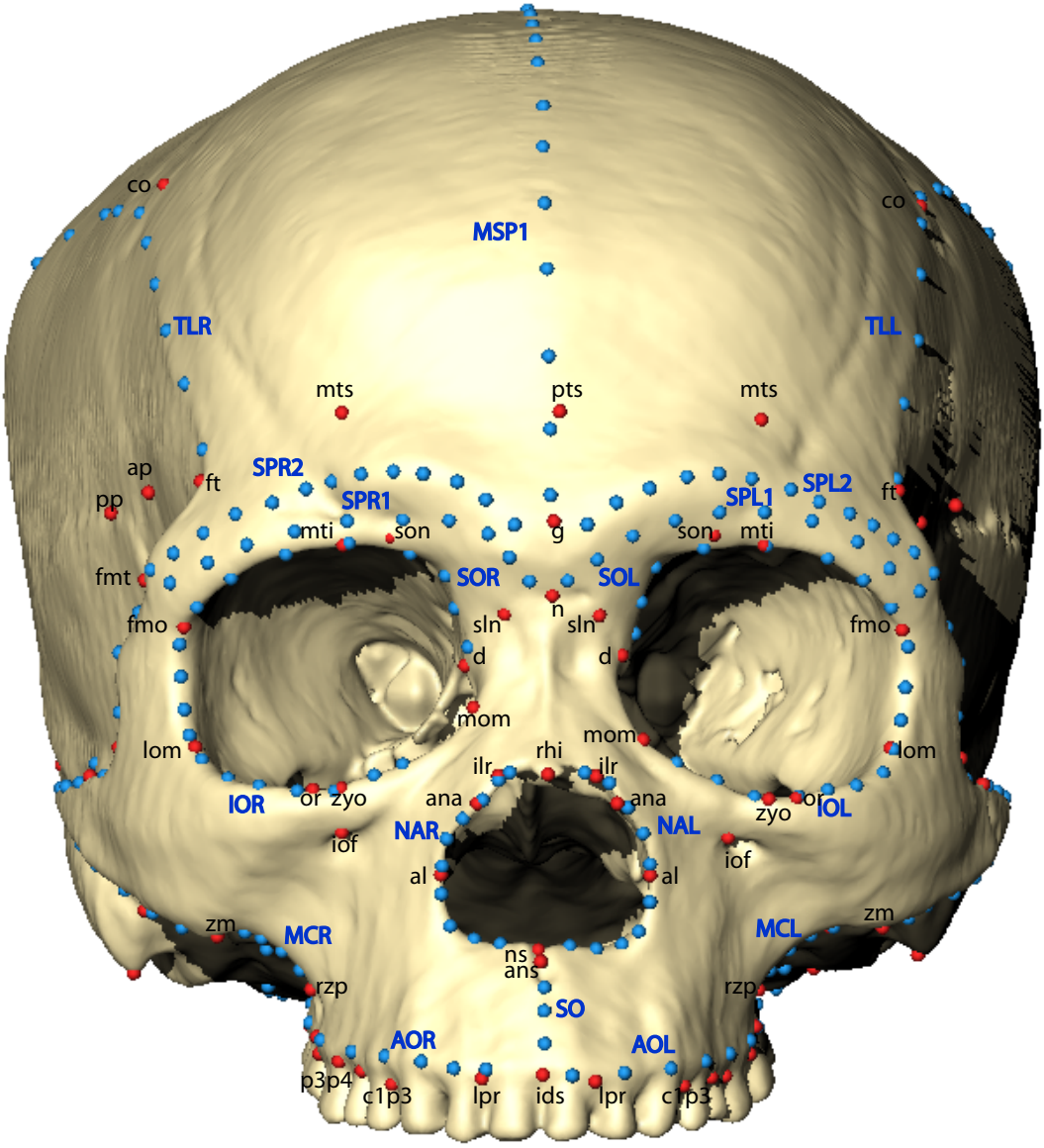

Figure 2.1 Continued: c)

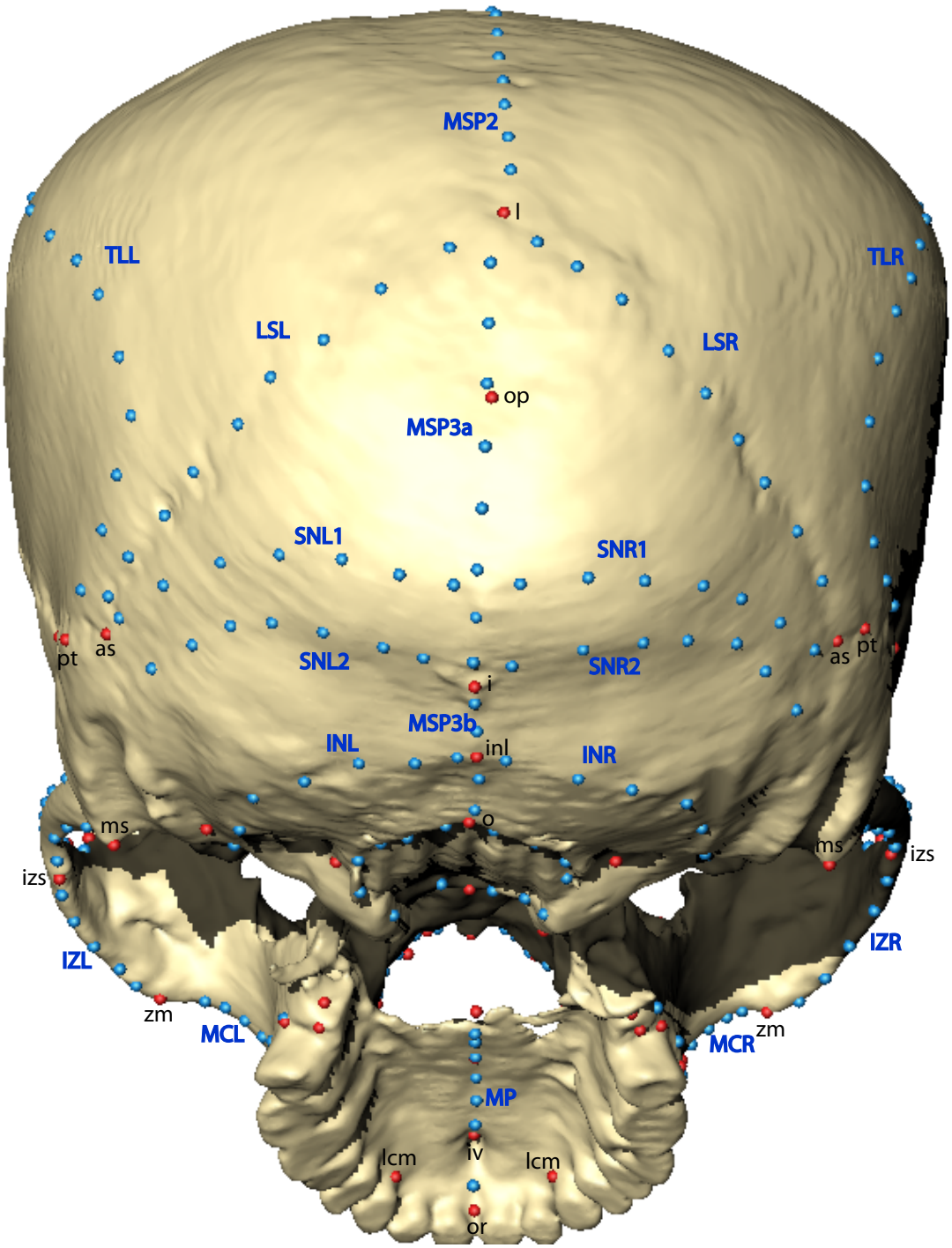

Figure 2.1 Continued: d)

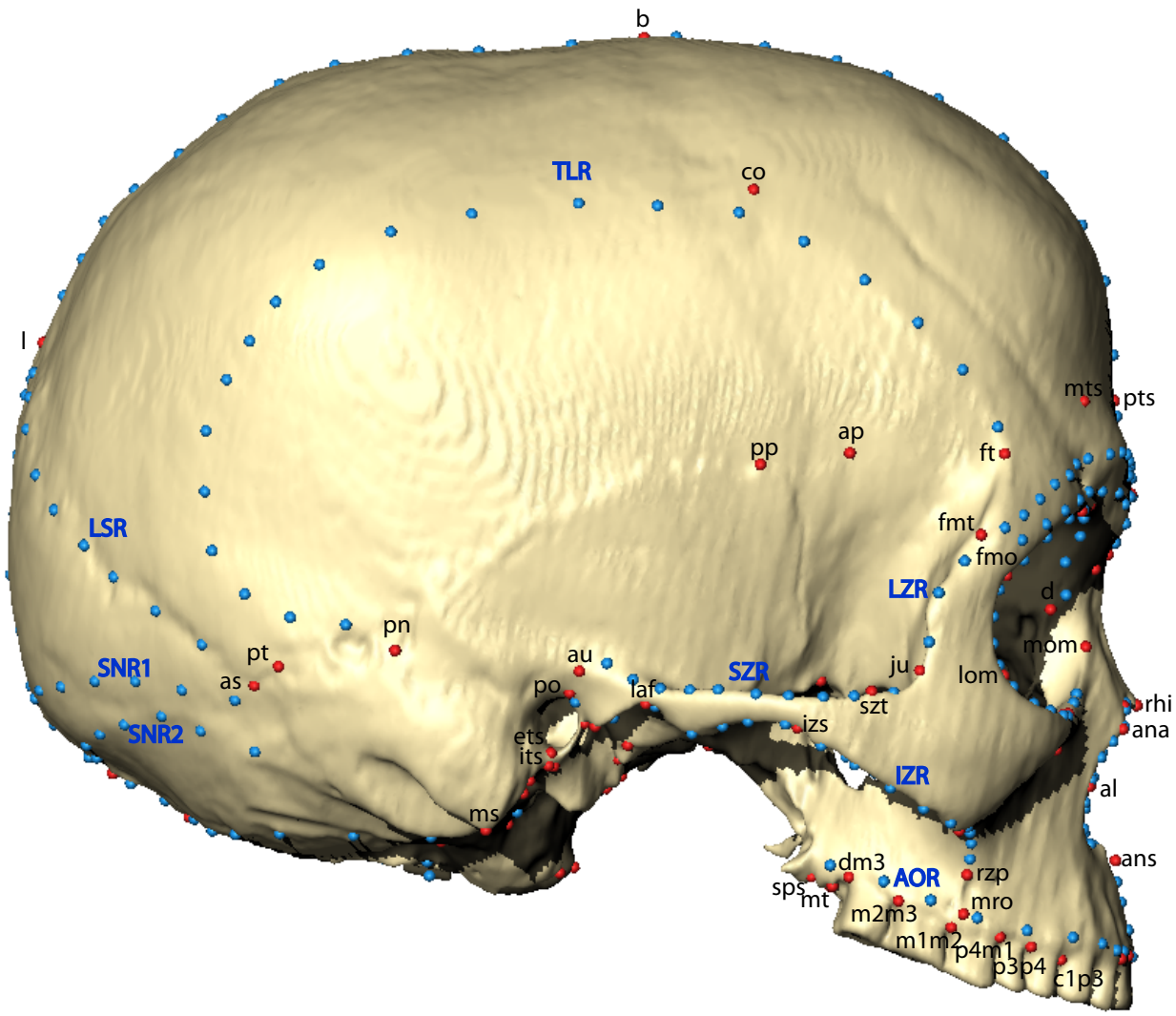

Figure 2.1 Continued: e)

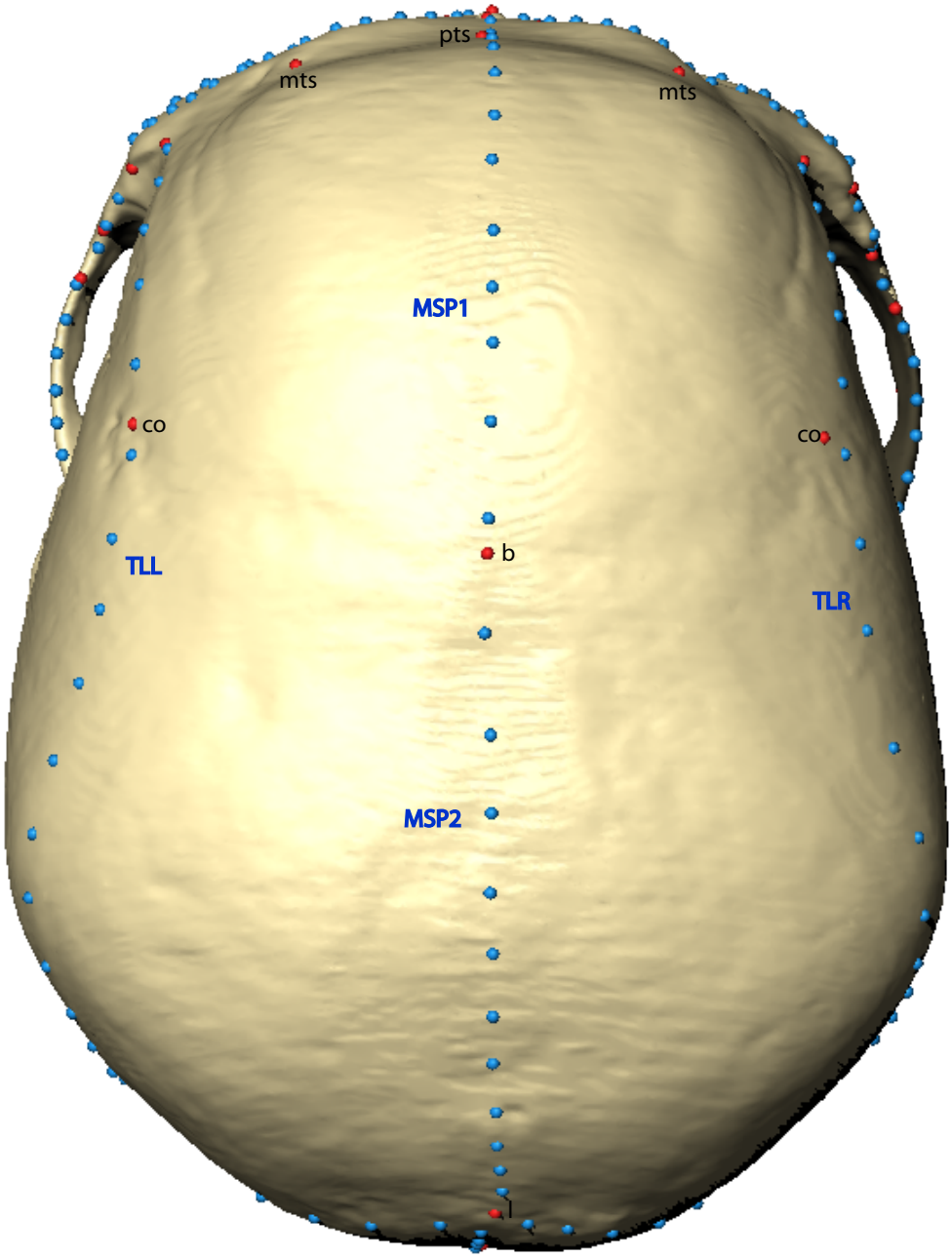

Figure 2.1 Continued: f)

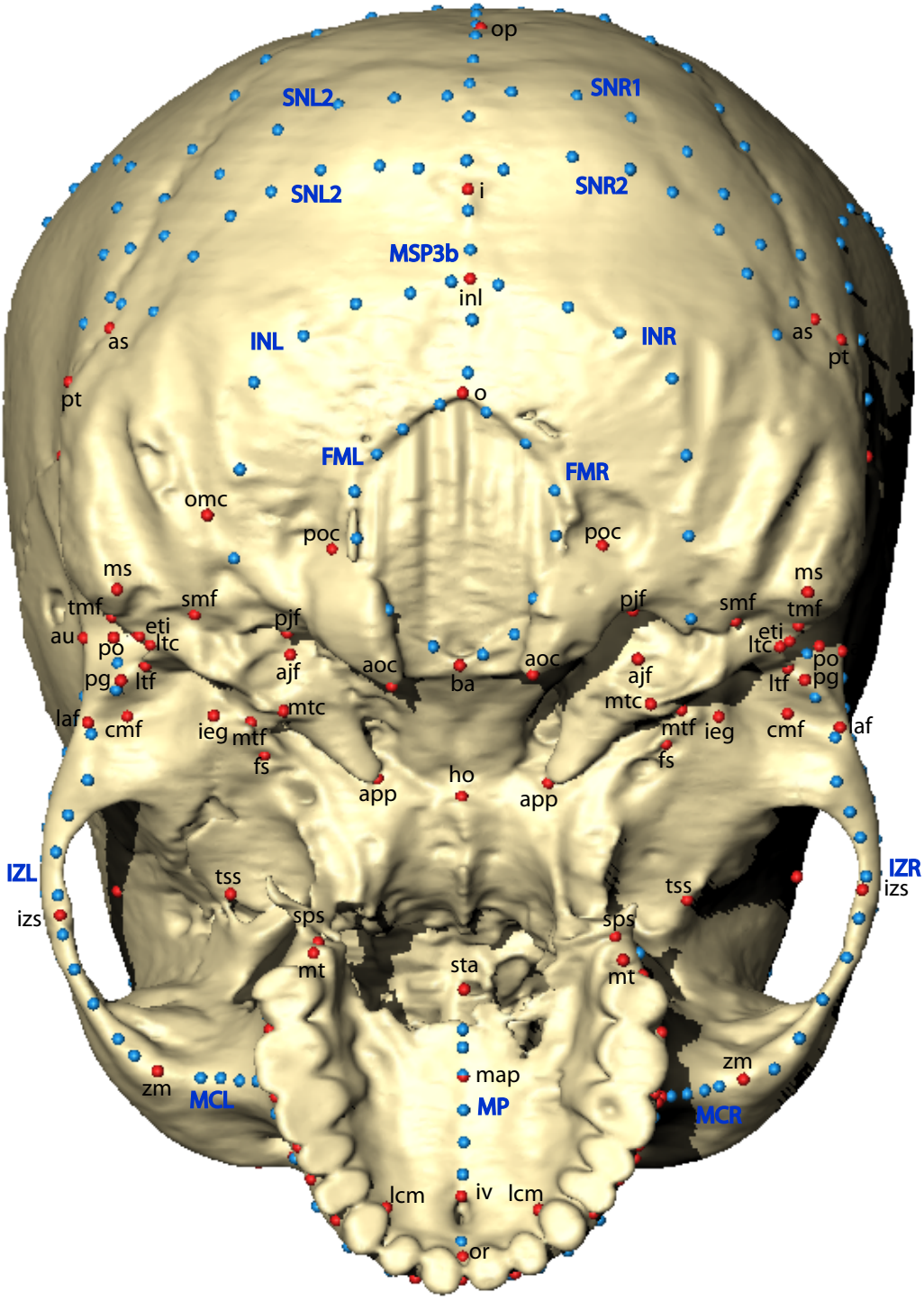

A generalized Procrustes analysis (GPA) was used to superimpose a set of specimen landmark / semilandmark configurations onto the mean (consensus) configuration according to a least-squares criterion. GPA removes the effects of translation and rotation in the raw coordinate data and standardizes each specimen to unit centroid size – the square root of the sum of squared distances from each landmark to the specimen's centroid (Dryden and Mardia, 1998). All data processing and statistical analyses were performed in Mathematica (Wolfram Research) and R (R Development Core Team, 2010).

2.2.3 Missing data reconstruction

As geometric morphometric methods require all specimens to have the same number of homologous points, some minor data reconstruction was necessary for some fossil specimens. First, bilateral symmetry was exploited by mirroring the surface of the better-preserved side along the midsagittal plane using the software Geomagic Studio and Avizo, and then both sides were digitized. The following specimens were completed by mirror-imaging: ATD6-69, Bodo, Cro-Magnon 1, Dali, Florisbad, Gibraltar 1, Guattari, Kabwe, ER 3883, Krapina 3, Krapina 6, La Ferrassie 1, Oberkassel 1, Předmostí 4, Shanidar 1, Zhoukoudian 12, and Zuttiyeh.

Second, if missing data occurred on both sides of the specimen or along the midline, landmarks were estimated using "geometric reconstruction" via TPS following Gunz et al. (2009b). A TPS interpolation function was used to map the missing landmarks / semilandmarks from the sample average onto the target during the semilandmark sliding step (Gunz, 2005; Gunz and Harvati, 2007; Gunz et al., 2009a,b; Grine et al., 2010; Harvati et al., 2010; Stansfield and Gunz, 2011). When a landmark or semilandmark is declared missing it is "fully relaxed" so as to minimize the overall bending energy between the incomplete specimen and the sample Procrustes average (Gunz et al., 2009b). This method of reconstruction has been used in many other geometric

morphometric studies (e.g., Gunz, 2005; Gunz et al., 2007, 2009a,b; Grine et al., 2010; Harvati et al., 2010; Stansfield and Gunz, 2011).

Arago 21 was the most heavily reconstructed fossil. The whole face of Arago 21 (de Lumley and de Lumley, 1971), including the midline, is deformed by what appears to be an almost uniform shear. The virtual reconstruction of the specimen described in Gunz et al. (2009b) was used. A cast of the face of Arago 21 was scanned with a high-resolution optical surface scanner (the cast was of a manual reconstruction and had already corrected for a local plastic deformation on the frontal bone of the original specimen). Points along the midsagittal curve and bilateral landmarks were measured, and reflected relabeling (Mardia et al., 2000; Bookstein, 2005) was used to remove the effects of the taphonomic distortion: the landmarks measured on the cast were reflected across the x-axis and then the corresponding left and right labels of the bilateral point were interchanged. After a least-squares superimposition of the original landmarks and these reflected relabeled landmarks their Procrustes mean shape was computed, thereby creating a perfectly symmetric form (Mardia et al., 2000). Then a TPS interpolation between the original landmark coordinates and the symmetrized configuration was computed and used to warp the vertices of the triangulated surface.

2.3 Analytical methods

2.3.1 Principal component analysis (PCA) in Procrustes shape and form space

In morphometrics a distinction is made between *shape* and *form*. *Shape* refers to the geometric properties of an object that are independent of its overall size, position and orientation, whereas the *form* of an object includes both its shape and size (Mitteroecker and Gunz, 2009). In order to explore the temporal variability in facial morphology among Pleistocene humans, a principal component analysis (PCA) was performed in shape space. A PCA reduces the

dimensionality of high dimensional shape space and provides summaries of large-scale trends within the data (Bookstein, 1991; Rohlf, 1993).

Because several of the studies focus on allometry (Chapters 3 and 4), the inclusion of size in the statistical analyses is essential. Following Mitteroecker et al. (2004, 2005), a PCA in *form* space (also called size-shape space) on the Procrustes landmark and semilandmark coordinates was performed. Form space includes the geometric size (as. ln centroid size) of each specimen (Mitteroecker et al., 2004) and is valuable because the relationship between shape and size can be readily explored. PCAs in shape and form space were used in all studies.

2.3.2 TPS warping along principal components

To visualize the shape changes along the first two principal components (PCs) the Procrustes mean shape was calculated and warped using a thin-plate spline interpolation (see Gunz and Harvati, 2007; Mitteroecker and Gunz, 2009). This was performed in Amira.

2.3.3 Nearest neighbor calculations and visualizations

Additionally, to identify which individuals are most phenetically similar to one another, nearest neighbors were calculated using inter-individual Procrustes distances, the square root of the sum of squared differences of corresponding landmark configuration of two Procrustes-superimposed figures (Slice, 2005). To better illustrate shape differences between Zuttiyeh (in Chapter 5) and Saint-Césaire (in Chapter 6) and their two closest neighbors, their semilandmark and landmark data set was used to warp their surfaces onto their nearest neighbors'. This was performed in Amira.

2.3.4 Linear regression analysis

An ontogenetic trajectory is a sequence of specimens of different dental ages within one population or species in Procrustes shape or form space (Mitteroecker et al., 2004, 2009). As outlined by Mitteroecker et al. (2004, 2005), properties of these trajectories (e.g., length, shape, divergence) can be compared among populations and species. Overlapping trajectories indicate a common pattern of shared development between the groups under investigation; these are the only cases where classic heterochronic terminology should be applied (Mitteroecker et al., 2005). Parallel trajectories reveal that the morphological divergence between groups has already occurred prior to the age of the youngest specimen, and that there is a common pattern of subsequent growth shared between groups; this has been referred to as "generalized heterochrony" (Zollikofer and Ponce de León, 2004). By contrast, divergent trajectories indicate that development further accentuates group differences. Ontogenetic and static allometric trajectories were calculated by linearly regressing Procrustes shape coordinates on the natural logarithm of centroid size (Mitteroecker et al., 2004; Neubauer et al., 2009, 2010). Static allometric trajectories were calculated for all studies whereas ontogenetic trajectories were calculated for only the growth studies in Chapters 3 and 4.

2.3.5 Growth simulations

Growth simulations were performed using the ontogenetic data in Chapters 3 and 4. Although the research questions differ in each study, the same general method was used. Either a mean shape (Chapter 3) or ATD6-69's Procrustes coordinates (Chapter 4) were used to scale to a larger size using the Neanderthal and modern human postnatal ontogenetic allometric trajectories. Shape changes were then visualized by TPS warping. A more detailed description is provided in the Material and Methods sections in Chapters 3 and 4.

2.3.6 Discriminant function analysis (DFA)

In Chapter 5 and 6, a discriminant function analysis (DFA) was computed to assess how well facial morphology separates fossil and modern human groups. This analysis has been applied in previous studies to classify fossil specimens (e.g., Harvati, 2003a; Gunz and Harvati, 2007; Skinner et al., 2008; Glantz et al., 2009; Mounier et al., 2011; Stansfield and Gunz, 2011). DFA utilizes the space of canonical variates, which emphasizes among-group differences relative to within-group differences; the groups were defined *a priori* according to the population grouping shown in Table 1 in Chapters 5 and 6. Zuttiyeh (in Chapter 5) and Saint-Césaire (in Chapter 6) as well as all transitional (Jebel Irhoud 1 and Florisbad), early (Skhul 5, Qafzeh 6 and Luijiang) and Upper Paleolithic *H. sapiens* were treated as individuals with unknown group affinities to be classified by posterior probabilities.

The computation of a DFA requires that the number of variables be smaller than the number of specimens. In order to reduce the dimensionality of the data, the subspace of the first few PCs of the Procrustes shape coordinates was used (see also below). A compromise has to be made between including enough variables (i.e. PCs) to provide a sufficient amount of shape information for discrimination; and using too many variables, thereby creating spurious clusters (for additional discussion of this issue see Skinner et al., 2008; Mitteroecker and Gunz, 2009; Mitteroecker and Bookstein, 2011). As the choice about how many PCs to use for the subspace is arbitrary the DFA was computed multiple times using the first five to sixteen PCs. In order to confirm that too many PCs were not chosen, all specimens were randomly relabeled so as to create false group compositions, and the DFA was repeated. In this test the DFA was not able to discriminate among these random groups; i.e. the clustering observed with the actual group labels in the subspace of the first few PCs was not an artifact of including too many variables.

2.3.7 Posterior probability

Zuttiyeh (in Chapter 5) and Saint-Césaire (in Chapter 6) were classified by posterior probability using four *a priori* groups (see Table 1 in Chapter 5 and 6 for grouping). Several other groups (e.g., transitional, early modern and Upper Paleolithic humans) were also classified via posterior probability. All groups were assigned the same prior probability. Additionally, in Chapter 5, permutation tests (10,000 random permutations) using the Procrustes distances between the mean group shapes were performed to test for significant shape differences between groups.

2.3.8 Visualization of Procrustes superimpositions

To better illustrate the shape differences between Zuttiyeh and the taxonomic groups (e.g., *H. erectus s.l.*, *H. heidelbergensis s.l.*, *H. neanderthalensis* and *H. sapiens*), mean shapes were generated for each group. Then the semilandmark and landmark data set was used to warp the surface of Zuttiyeh to the mean of each group in Avizo. The same was done for Saint-Césaire, but using temporal groupings (e.g., Early, Middle, Late Pleistocene) rather than taxonomic.

3. Middle Pleistocene Human Facial Morphology in an Evolutionary and Developmental Context[1]

3.1 Introduction

Facial morphology is frequently used to distinguish recent modern humans from their Pleistocene ancestors and relatives. Most of the Middle Pleistocene human (MPh) specimens are characterized by their broad and massive faces, projecting browridges, especially in the lateral region (Athreya, 2009), a large interorbital breadth (Trinkaus, 2006), and details of the nasal margin and palate (Rightmire, 2008). They also share several facial features with the Neanderthals, such as facial prognathism, broad nasal apertures, and a lack of concavity in the infraorbital region (Rak, 1986; Trinkaus, 1987; Arsuaga et al., 1997; 2006).

One striking difference between MPh specimens and recent modern humans is facial size. The most complete MPh faces include Bodo and Kabwe (i.e., Broken Hill) from Africa, and Arago 21, Petralona, and Sima de los Huesos 5 from Europe. Given their "mosaic" craniofacial morphology, the taxonomic affinities of these fossils are controversial. Bodo, Kabwe, and Petralona present the largest faces in the human fossil record. However, our understanding of the effects of size on the shape of the face (allometry) is limited. Among hominins, size-correlated shape changes have been observed in the relative breadth of the nasal aperture (Holton and Franciscus, 2008), nasoglabellar profile (Rosas and Bastir, 2002), and infraorbital surface topography (Maddux and Franciscus, 2009). Together, these studies imply that certain facial features may indirectly develop as a result of having a larger face.

[1] The manuscript entitled *Middle Pleistocene human facial morphology in an evolutionary and developmental context*, written by Sarah E. Freidline, Philipp Gunz, Katerina Harvati and Jean-Jacques Hublin, was submitted to the *Journal of Human Evolution* on 12/24/2011 and is currently in review.

The general pattern of craniofacial morphology among the Eurasian and African MPh is characterized by a combination of morphological features, variously aligning them with *H. erectus sensu lato*, *H. neanderthalensis* and *H. sapiens*. The two main competing interpretations are: 1) the MPhs comprise a single, cross-continental taxon, spanning Africa, Europe and possibly Asia; or 2) the European and African MPhs belong to separate clades.

In the first model, the MPhs are assigned to the taxon *H. heidelbergensis* and are considered to be the last common ancestor to both Neanderthals and modern humans. This view is supported by the strong morphological and metric similarities between the European and African specimens (e.g., Stringer, 1974, 1983; Arsuaga et al., 1997; Rightmire, 1998a,b, 2007, 2008; Mounier et al., 2009; Harvati 2009a).

In the second model, the European MPhs are seen as ancestral to Neanderthals and are classified as either *H. neanderthalensis* (Hublin, 1998, 2009) or as the exclusive members of *H. heidelbergensis*, a chronospecies of the Neanderthal lineage (e.g., Arsuaga et al., 1997; Manzi, 2004; but see Wolpoff et al., 1994; Rosas et al., 2006; Tattersall and Schwartz, 2006; Bräuer, 2008 for alternative interpretations of the fossil record). When compared to the African MPhs, the European faces have been described as having more anterolaterally flattened zygomatic bones like Neanderthals (Dean et al., 1998; although see Trinkaus, 1987, 2006) and a more anteriorly placed zygomatic root at the level of the first and second molar (Trinkaus, 1987).

As evidence for the "neanderthalization" process, proponents of this model refer to a series of features on the skeleton that foreshadow the Neanderthal condition and that occur uniquely in the European MPhs (Dean et al., 1998; Hublin, 1998, 2009). The African MPhs, on the other hand, are interpreted as being ancestral to *H. sapiens* and often classified as *H. rhodesiensis* (Hublin, 2009).

The goal of this study is to place the MPhs in an evolutionary and developmental context in order to gain a clearer understanding of how archaic (e.g., MPhs and Neanderthals) and modern human facial features are affected by facial size and how they change through time. Surface semilandmark geometric morphometric techniques are used to quantify facial features that are otherwise difficult to capture, such as the infraorbital surface topography, and growth simulations are applied to visualize the effects of allometry on the face.

3.1.2 Interpretation of ontogenetic allometric trajectories

Conventionally, allometry is defined as the relationship between the total body size of the organism and its shape, anatomy, and physiology among other characteristics. In this study we substitute body size for facial size because we are specifically interested in how differences in facial size influence the expression of facial features and overall facial shape. We recognize three different categories of allometry: ontogenetic, static and evolutionary (Cock, 1966; Klingenberg, 1998). Ontogenetic allometry is the covariation of traits across different age groups (i.e. ontogenetic stages) of a given species. Static allometry occurs within the same ontogenetic stage of a single species. Evolutionary allometry can occur between different phylogenetic lineages, analyzed within one ontogenetic stage.

Recently, Maddux and Franciscus (2009) identified an allometric relationship between facial size and infraorbital surface topography among the genus *Homo*. They found that individuals with large infraorbital regions tend to exhibit flat surface topographies (characteristic of Neanderthals), while individuals with small infraorbital areas possess depressed surface topographies (like modern humans). They argued that depressed versus inflated infraorbital shapes are not two truly dichotomous configurations, but fall along a continuous size gradient. However, they did not include subadult individuals in their regression analyses and therefore they

only explored the effects of static and evolutionary allometry. Additionally, the temporal range of the fossil material was limited to the time span from the Middle Pleistocene to the present.

The present study evaluates the Middle Pleistocene human face in a broad evolutionary and developmental context. More specifically we test to see how well facial morphology separates Pleistocene human groups, ranging from *H. habilis* to recent modern humans, and assess the effects of ontogenetic and static allometry on the Pleistocene human face.

3.2 Materials and methods

3.2.1 Sample

This study includes a comprehensive sample of subadult and adult Early to Late Pleistocene fossil hominins (Table 3.1) and recent modern humans (Table 2.4). The fossil sample was designed to include all available Pleistocene fossils that preserve relatively complete faces (see section on Missing Data Reconstruction Below). Table 3.1 lists the thirty fossils, their broad geographical location and chronology. The modern human sample used in this study consists of the cross-sectional growth series described in Chapter 2 (Table 2.4).

Table 3.1 Fossil specimens used in the analysis, their abbreviation (Ab.) and their chronology. Subadult individuals are italicized.

Specimen	Ab.	Chronology
Early Pleistocene: Africa		
ER 1813	1813	1.88-1.90 (Wood, 1991); 1.65 Ma (Gathogo and Brown, 2006)
*WT 15000**	Tur	1.6 Ma (Feibel et al., 1989)

Table 3.1 Continued

Early Pleistocene: Asia		
*Dmanisi 2700**	Dm27	1.7-1.8 Ma (Gabunia et al., 2000)
Sangiran 17*	S17	1.50 – 1.02 Ma (Larick et al., 2001; Antón, 2003; Antón and Swisher, 2004); > 790 ka (Hyodo et al., 2011)
Middle Pleistocene: Africa		
Bodo	Bd	ca. 600 ka (Clark et al., 1994)
Kabwe	Kb	700 – 400 ka (Klein, 1994); late Middle Pleistocene (Stringer, 2011)
Middle Pleistocene: Europe		
Arago 21*	Ar	600 – 350 ka (Cook et al., 1982; Falguères et al., 2004)
Petralona	Pt	670 – ca. 250 ka (Harvati et al., 2009)
Sima de los Huesos 5*	Sm5	ca. 530 ka (Bischoff et al., 2007)
Late Middle-Late Pleistocene: Africa		
Jebel Irhoud 1	I1	ca. 160 ka (Smith et al., 2007)
Late Middle-Late Pleistocene: Europe		
Gibraltar 1	Gb1	71 – 50 to 35 ka (Klein, 1999)
Guattari	Gt	ca. 50 ka (Schwarcz et al., 1991)
La Chapelle-aux-Saints	LCh	56 – 47 ka (Grün and Stringer, 1991)
La Ferrassie 1	LF1	71 – 50 to 35 ka (Klein, 1999)

Table 3.1 Continued

Pech-de-l'Azé I	Pech	51-41 ka (Soressi 2007)
Late Middle-Late Pleistocene: Asia		
Liujiang*	Ljg	139 – 111 ka (Shen et al., 2002)
Qafzeh 6	Q6	135 – 100 ka (Grün et al., 2005)
Qafzeh 9	Q9	135 – 100 ka (Grün et al., 2005)
Shanidar 1*	Sh1	ca. 50 ka (Trinkaus, 1983)
Shanidar 5*	Sh5	ca. 50 ka (Trinkaus, 1983)
Skhul 5	Sk5	135 – 100 ka (Grün et al., 2005)
Teshik Tash	Tesh	ca. 70 ka (Movius, 1953); 57-24 ka (Vishnyatsky, 1999)
Upper Paleolithic: Europe		
Cro-Magnon 1	Cr1	28 – 27 ka (Holt and Formicola, 2008)
Grotte des Enfants 6	GrE6	Gravettian (Henry-Gambier, 2001)
Mladeč 1	Ml1	ca. 31 ka (Holt and Formicola, 2008)
Předmostí 3*	Pr3	ca. 17 ka (Svoboda, 2008)
Oberkassel 1	Ob1	ca. 12 ka (Street, 2002)
Oberkassel 2	Ob2	ca. 12 ka (Street, 2002)
Upper Paleolithic: Asia		
Zhoukoudian 101*	Zh101	ca. 33 – 13 (Chen et al., 1989; Hedges et al., 1992; Brown, 1993)

Table 3.1 Continued

Zhoukoudian 102*	Zh102	ca. 33 – 13 (Chen et al., 1989; Hedges et al., 1992; Brown, 1992)

*casts

3.2.2 Landmark data

The landmark and semilandmark subset used in this study is shown in Figure 3.1 and the biological landmarks are listed in Table 3.2.

Figure 3.1 671 landmarks and semilandmarks digitized on all specimens, red: biological landmarks; blue: curve-semilandmarks; yellow: surface-semilandmarks. Biological landmarks are abbreviated. The full names are listed in Table 3.2.

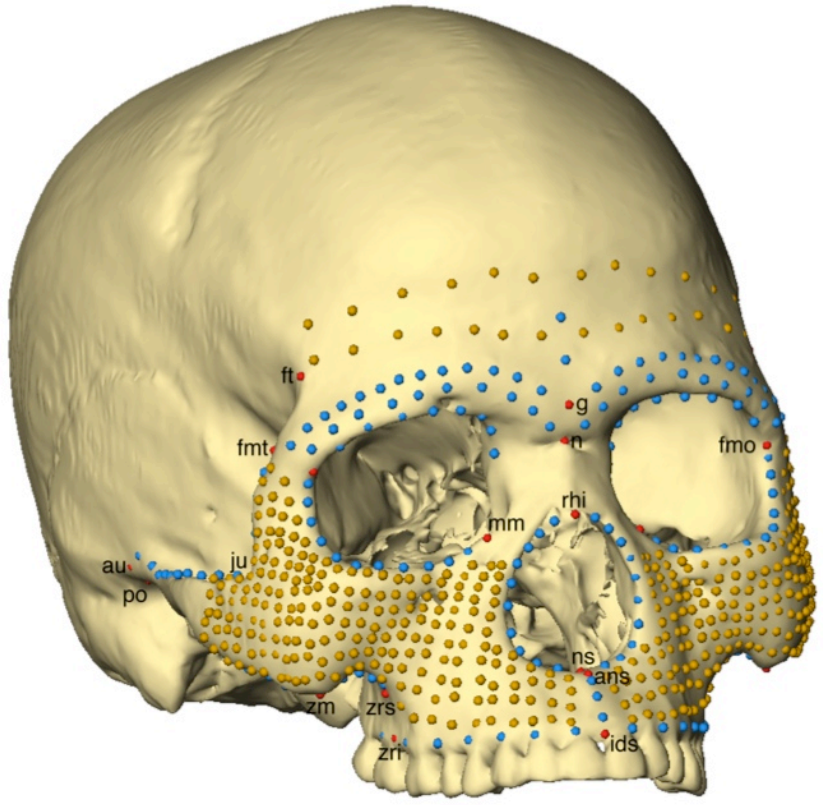

Table 3.2 Biological landmarks used in the analysis.

Landmark	Abbreviation
Alveolare	ids
Anterior nasal spine[1]	ans
Auriculare*	au
Frontomalare orbitale*	fmo
Frontomalare temporale*	fmt
Frontotemporale*	ft
Glabella	g
Jugale*	ju
Medial orbital margin[2]*	mm
Nasion	n
Nasospinale	ns
Porion*	po
Rhinion	rhi
Sphenopalatine suture[3]*	ss
Staphylion	sta
Zygomatic process root inferior[4]*	zri
Zygomatic process root superior[5]*	zrs
Zygomaxillare*	zm

*paired right and left landmarks

3.2.3 Analytical methods

In order to explore the temporal variability in facial morphology among Pleistocene humans, a principal component analysis (PCA) was performed in shape space, and nearest neighbor Procrustes distances were calculated to identify which individuals are most phenetically similar to one another (Slice, 2005). A PCA in form space was performed in order to examine any allometric component in our data, and ontogenetic trajectories were plotted in Procrustes shape and form space for Neanderthals, each of the four modern human populations, and the modern human mean. Additionally, in order to explore the effects of allometry on only the adult facial shape, static

allometric trajectories were calculated and plotted for the adults of each population. Lastly, to see if modern humans and Neanderthals share a common ontogenetic allometric trajectory during postnatal ontogeny, the angle between the two allometric vectors was computed. Following Mitteroecker et al. (2005), the angles were tested for significance using a permutation test based on the null hypothesis that there is no angular difference between the two trajectories.

3.2.4 Growth simulations and visualization techniques

The aim of the series of growth simulations was to identify the shape changes that occur when overgrowing an adult modern human to the size of a MPh. This was performed in order to specifically test the findings of Maddux and Franciscus (2009). To do so, the mean adult modern shape was calculated and scaled following the modern human mean ontogenetic allometric trajectory to the size of a) Kabwe, an African MPh that has a particularly inflated infraorbital surface topography for a MPh and b) Bodo, an African MPh that has the largest face in our sample. Shape changes were visualized by TPS warping of the adult modern human mean shape to the modern human mean scaled to the size of Bodo and Kabwe. The same approach was applied to Neanderthals. The mean adult Neanderthal shape was calculated and scaled following the Neanderthal ontogenetic allometric trajectory to the size of Kabwe and Bodo and the shape changes were visualized.

3.3 Results

3.3.1 Principal component analyses and permutation tests

In order to explore temporal trends in facial morphology a PCA was performed in Procrustes shape space of only the adult individuals; however, in order to increase the *H. erectus* sample size Dmanisi 2700 and WT 15000 were included (Fig. 3.2). The first two principal components (PCs) represent 43.0% of the total shape variation, and neither of the PCs are correlated with size. There is a clear separation between the modern humans, including the early modern and Upper Paleolithic humans, and the archaic humans. Additionally, each temporal group clusters together. However, there is some overlap between Middle Pleistocene humans and Neanderthals. In order to identify which fossils are phenetically most similar to one another, nearest neighbor connections were calculated and plotted in PC space. The black lines indicate that an individual is most similar to an individual outside of its temporal group. Among the Middle Pleistocene humans, Petralona and Kabwe are the most similar to one another; Bodo is most similar to Sima de lost Huesos 5 and the latter specimen is most similar to Arago 21; and Arago 21 is most similar to La Chapelle, a Neanderthal.

Figure 3.2 PCA in shape space of only adult individuals in the sample, except for Dmanisi 2700 and WT 15000. PC 1 represents 23.7 % of total shape variation; PC 2 represents 19.3 % of total shape variation. Convex hulls are drawn for recent modern humans and Upper Paleolithic modern humans. The lines indicate each fossil specimen's nearest neighbor according to inter-individual Procrustes distances. The black lines specify if an individual is most similar to another individual outside of its temporal group. The full names for the fossil specimens are listed in Table 3.1.

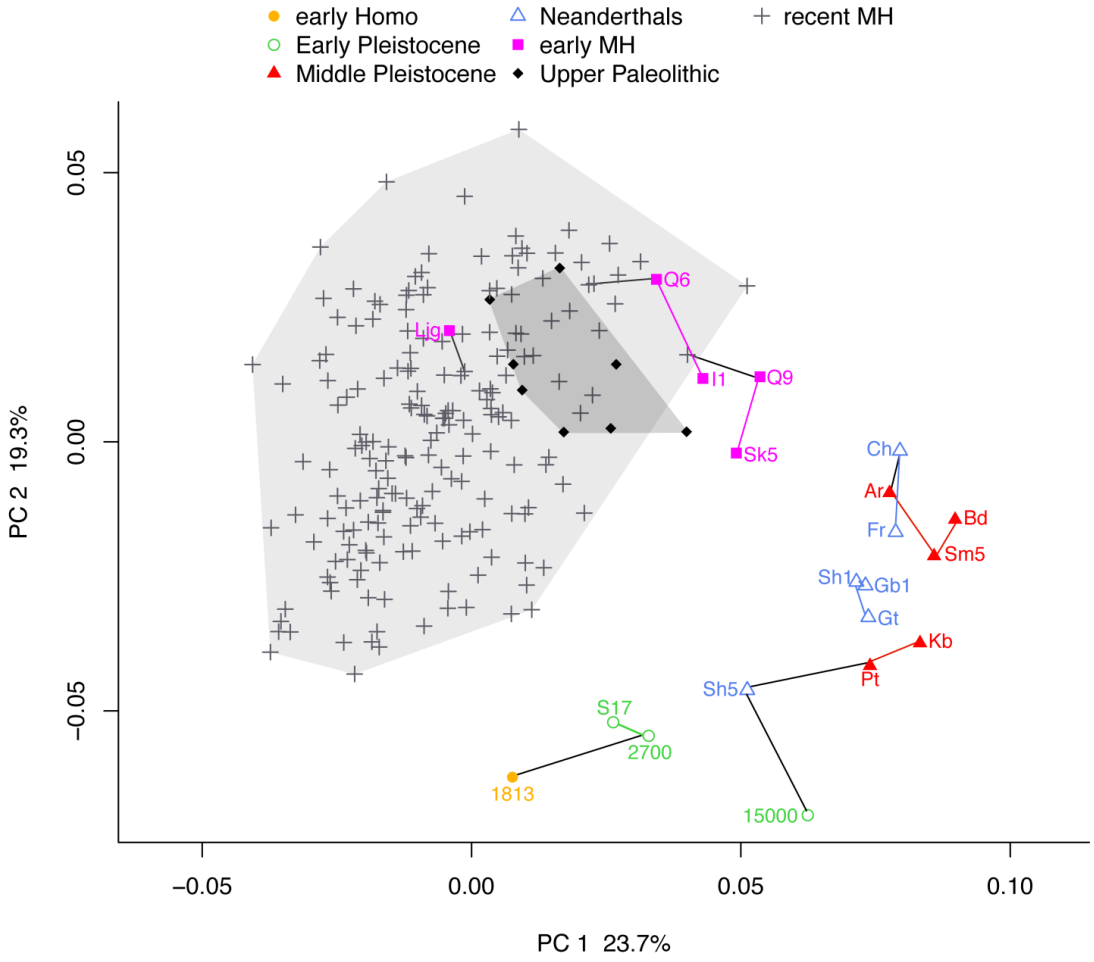

In Figure 3.3, a PCA in Procrustes shape space was performed on the complete sample (i.e. including subadult modern humans and Neanderthals). The first three PCs were plotted and represent 59.1 % of total shape variation. PC 1 is the most correlated with size ($r \cong -0.79$). The solid lines represent the ontogenetic allometric trajectories for each of the four modern human populations and the Neanderthal and mean modern human ontogenetic allometric trajectories. None of the trajectories are overlapping. Because each trajectory has a unique starting point, this

plot shows that population and species-specific facial morphology is present before deciduous teeth erupt. As in Figure 3.2, clusters of temporal groups are also apparent when including the entire sample (i.e. all subadults included). Upper Paleolithic modern humans and early modern humans (eMH) fall within the range of recent human variation; the MPhs cluster near the end of the Neanderthal ontogenetic trajectory; and the Early Pleistocene specimens and ER 1813 are scattered along the right side of the plot (i.e. the positive end of PC 2).

Figure 3.3 PCA in shape space including both subadult and adult fossil and modern humans. The first three PCs are plotted. PC 1 represents 32. 5 % of total shape variation; PC 2 represents 17.8 %; and PC 3 represents 8.8 %. The lines indicate the ontogenetic allometric trajectories for Neanderthals (in blue), the mean modern human trajectory (in dark gray), and the trajectory for each modern human population (in light gray). The trajectories were calculated by regressing shape on ln centroid size. The specimen color-coding is the same as in Figure 3.2.

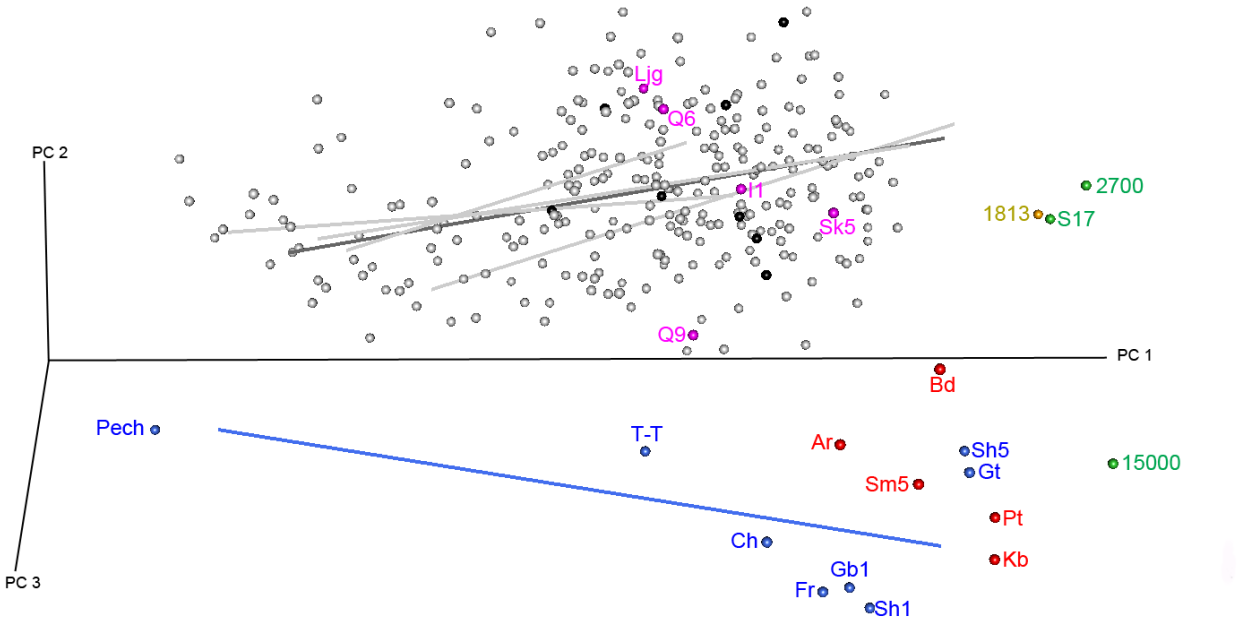

The variance explained by ontogenetic allometry within modern humans is 26.0 % and within Neanderthals it is 59.7 %; a permutation test on the explained variance indicates that either

regression is highly significant. The angle between the modern human and the Neanderthal ontogenetic allometric regression in full shape space is 36.12°. However, a permutation test reveals that the slopes of the Neanderthal and mean MH ontogenetic trajectories are not significantly different ($p \cong 0.33$). Therefore the null hypothesis that the ontogenetic trajectories are parallel cannot be rejected.

In order to further explore the effects of size on facial morphology, a PCA in form space was performed (Fig. 3.4). The longer lines are the Neanderthal and mean modern human ontogenetic allometric trajectories and the shorter lines are the Neanderthal and MPh static allometric trajectories. The ontogenetic trajectories are not overlapping and although they appear to be divergent the angle between the two trajectories is 12.0°. A permutation test cannot reject the null hypothesis that these trajectories are parallel. As expected in a form-space analysis, PC 1 is highly correlated with centroid size ($r = 0.99$). The variance explained by ontogenetic allometry with MH is 80.1 % and within Neanderthals it is 92.4 %. The Neanderthal infant Pech de L'Azé and the youngest MH subadult individuals cluster at the left end of the plot (indicating smaller size) and the individuals with larger faces, e.g., Bodo, Petralona, and Kabwe fall on the opposite end. The MPhs fall at the end of the Neanderthal ontogenetic allometric trajectory and the position of the Neanderthal and MPh static trajectories are very similar. This suggests that allometric scaling explains the large-scale differences in facial shape between the two groups. Apart from Sangiran 17, the Early Pleistocene specimens fall above the Neanderthal ontogenetic trajectory and closer to the subadult individuals along PC 1. This is due to their small facial sizes. The early MH and Upper Paleolithic humans cluster with the adult MH.

Figure 3.4 PCA in form space (including the log centroid size for each individual) of both subadults and adult fossil and modern humans. The first three PCs are plotted. PC 1 represents 79.0 % of total form variation; PC 2 represents 5.0 %; and PC 3 represents 3.3 %. The ontogenetic allometric trajectories for Neanderthals modern humans are in blue and black, respectively. The static allometric trajectory for Neanderthals is in black and for the MPhs is in red. The trajectories were calculated by regressing shape on log centroid size. The two stars demonstrate where the predicted shapes of a modern human overgrown along the mean modern human ontogenetic allometric trajectory to the size of Kabwe and Bodo plot in the PCA (see text for more information). The specimen color-coding is the same as in Figure 3.2.

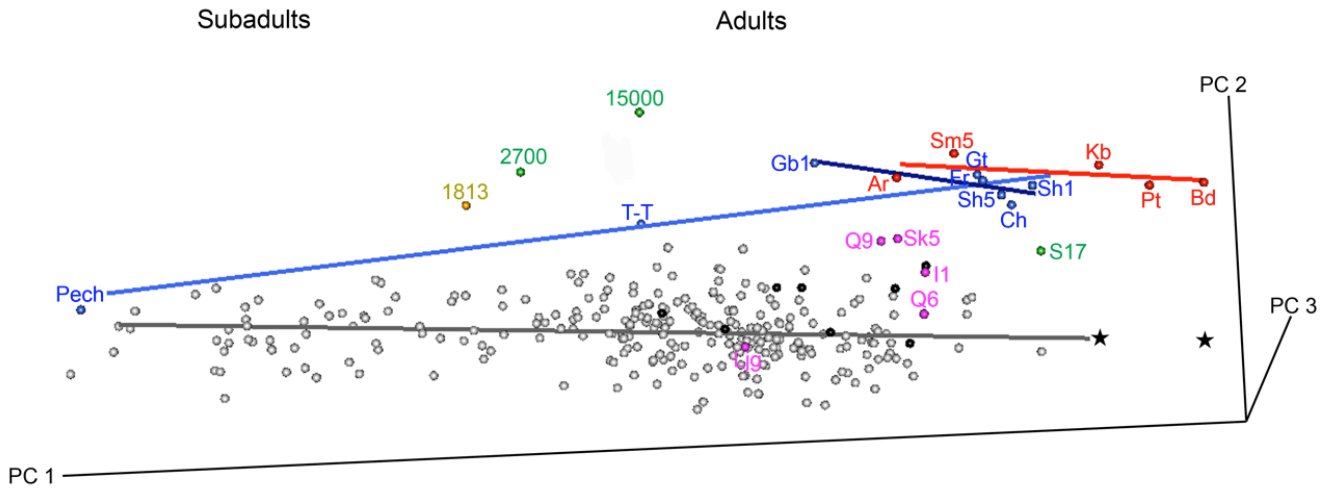

3.3.2 Growth simulations

Figure 3.5 depicts each step of the growth simulations when overgrowing an adult modern human to the size of a MPh. First an adult modern human mean shape was calculated (Fig. 3.5a, e), and then it was overgrown to the size of Kabwe (Fig. 3.5b) and to the size of Bodo (Fig. 3.5f). Among recent modern humans the following allometric shape changes occur as facial size increases: 1) a more anteriorly projecting glabellar region; 2) a slight medio-lateral narrowing and supero-inferior lengthening of the nasal aperture; 3) the zygomatic bones become more laterally projecting; 4) a slight inflation in the infraorbital surface topography; and 5) an elongation of the lower face especially in the subnasal region. Both fossil specimens have an entirely more projecting and

laterally expanded browridge, more prognathic face and inflated infraorbital region compared to a modern human scaled to their size (Fig. 3.5c, d, g, and h). Additionally, in the inferior perspective (Fig. 3.5d) Kabwe's infraorbital plate and zygomatic bone appears to be more sagitally rotated and its nasal aperture is more anteriorly projecting. By contrast, an overgrown modern human has an entirely different facial architecture maintaining two planes: a coronal infraorbital plate combined with lateral (i.e. sagittal) nasal walls, as well as a less projecting nasal aperture. In these features, Bodo also appears to express two midfacial planes, like the modern human condition (Fig. 3.5h); however it exhibits a much more projecting nasal aperture and a more inflated infraorbital surface topography than a modern human scaled to its size.

Figure 3.5 Allometric shape changes of an overgrown modern human to the size of Kabwe (a-d) and to the size of Bodo (e-h); a and e: modern human mean shape; b and f: overgrown to the size of Kabwe (b) and to the size of Bodo (f); c-d, g-h: Procrustes superimposition of overgrown modern human on Kabwe (in transparent purple; c: anterior perspective; d: inferior perspective) and Bodo (in transparent purple; g: anterior perspective; h: inferior perspective).

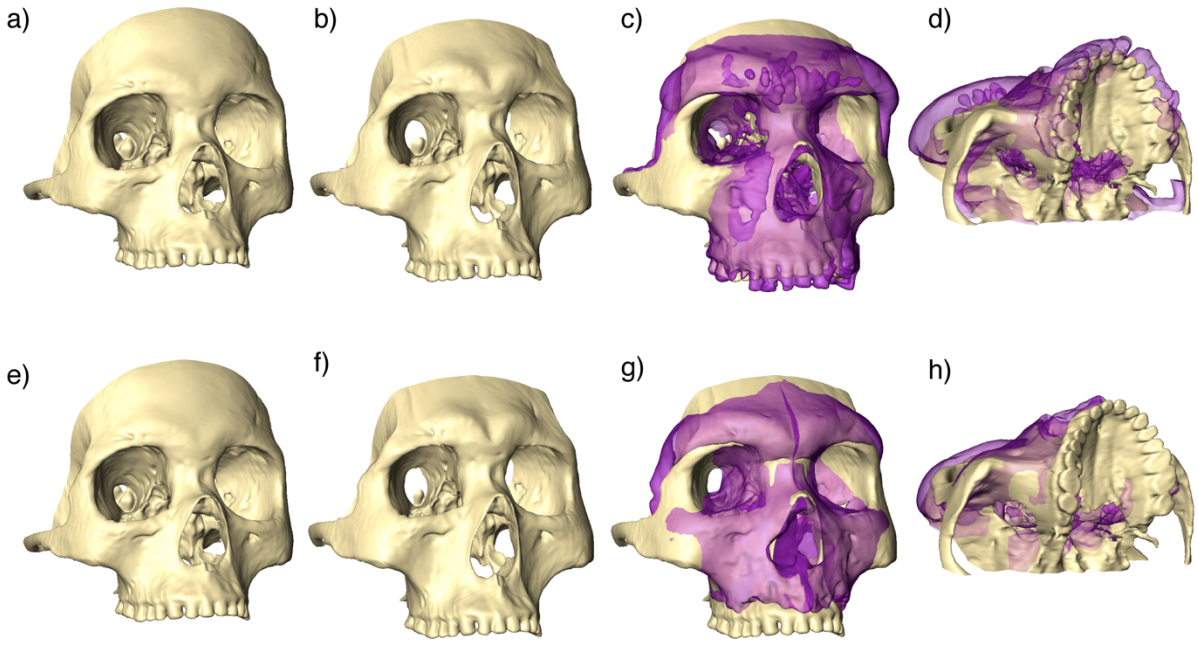

Figure 3.6 visualizes the mean adult Neanderthal facial shape (a, e), overgrown to the size of Kabwe (b) and Bodo (f), and superimposed on them (Kabwe – c, d – and Bodo – g, h – in transparent blue). Kabwe has an entirely more robust and projecting browridge and zygomatic bone when compared to the scaled Neanderthal. Additionally, its zygomatic bone is more antero- laterally projecting and the Neanderthal infraorbital surface topography is more inflated. Despite these differences, however, they share a similar orientation of the infraorbital plate and zygomatic body. The comparisons between Bodo and the scaled Neanderthal are similar to those of Kabwe. The main differences are in the projection of the browridge and the frontal process of the zygomatic. These features are less anteriorly projecting when compared to the scaled Neanderthal. Additionally, Bodo's zygomatic body is more antero-laterally projecting.

Figure 3.6 Allometric shape changes of an overgrown Neanderthal to the size of Kabwe (a-d) and to the size of Bodo (e-h); a and e: Neanderthal mean shape; b and f: overgrown to the size of Kabwe (b) and to the size of Bodo (f); c-d, g-h: Procrustes superimposition of overgrown modern human on Kabwe (in transparent blue; c: anterior perspective; d: inferior perspective) and Bodo (in transparent blue; g: anterior perspective; h: inferior perspective).

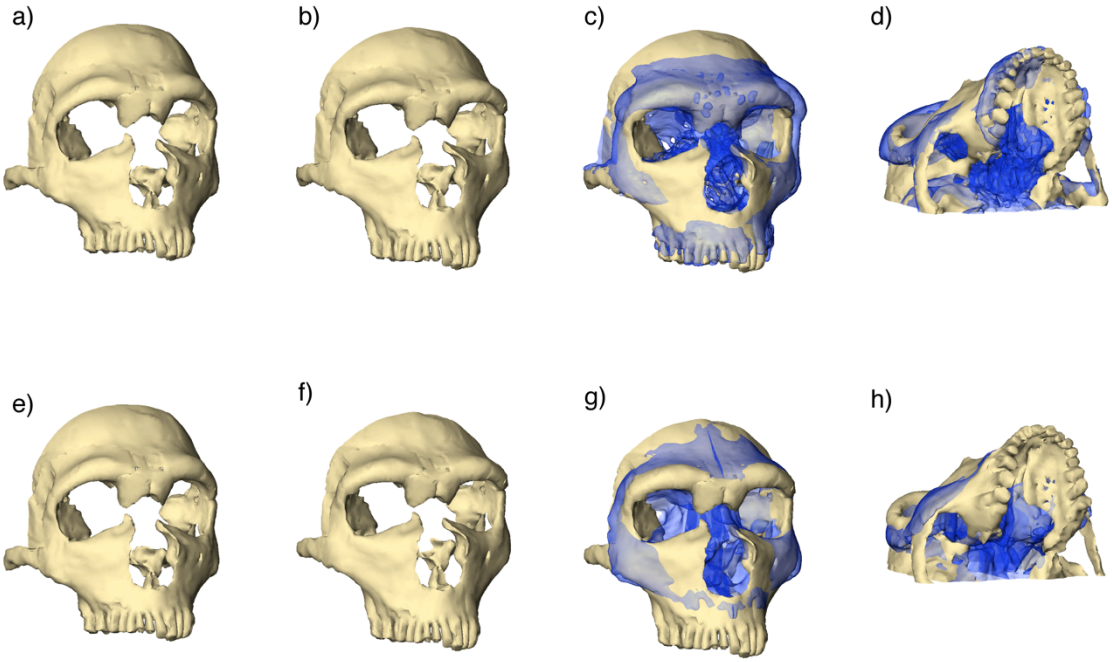

3.4 Discussion

The aim of this study was twofold: first, to explore temporal trends in facial morphology; and second, to identify how changes in facial size affect the morphology of facial features among archaic and recent humans. Our PCA results and nearest neighbor calculations illustrate a temporal trend in facial morphology during Pleistocene human evolution. Inter-individual Procrustes distances indicate that ER 1813, a member of *H. habilis*, is most phenetically similar to Dmanisi hominin 2700 among the specimens included in our sample. *H. habilis*-like cranial and dental features have been described in previous studies on the Dmanisi *H. erectus* populations (e.g., Rightmire et al., 2006; Rightmire et al., 2008; Martinón-Torres et al., 2008). Although MPhs and Neanderthals overlap with one another in Procrustes shape space (Fig. 3.2), each individual is most similar to a member within its respective group. The main exceptions to this are Arago 21, which is most similar to La Chapelle-aux-Saints, and Petralona, being closest to Shanidar 5. Additionally, our PCA results show that there is no clear distinction between African and European MPhs, supporting previous morphometric studies (e.g., Stringer, 1974, 1983; Arsuaga et al., 1997; Rightmire, 1998a, 2007, 2008; Mounier et al., 2009; Harvati, 2009a; Harvati et al., 2010). For example, our nearest neighbor calculations support morphological and metrical similarities between Petralona and Kabwe, as emphasized by Stringer (1983) and Harvati (2009a), as well as between Bodo and Sima de los Huesos 5, as identified by Arsuaga et al. (1997).

The overall position of the MPhs in shape and form space in conjunction with the position of their static allometric trajectory suggests that allometric scaling explains large-scale differences in facial morphology between MPhs and Neanderthals. However, scaling cannot explain the morphological differences between the latter two groups and recent modern humans. Our results confirm previous morphometric studies (e.g., Howells, 1973; Stringer, 1974; Weber et al., 2006; Gunz et al., 2009; Athreya, 2009; Harvati 2009b; Harvati et al., 2010; Stansfield and Gunz, 2011)

showing that modern humans, including the early modern humans, have a facial morphology that is distinct from the archaic humans. All of our modern human groups are most similar to one another based on nearest neighbor calculations, reflecting a high degree of homogeneity among these groups, as well as a clear modern human lineage separation at this later time period. The similarities in facial morphology between our three temporal groups of modern humans (early, Upper Paleolithic and recent modern humans) indicate that the characteristically modern human facial anatomy had already evolved in Jebel Irhoud 1, around 170 Ka. This is not the first study to recognize the "moderness" of its facial morphology (see Hublin, 1992; Harvati, 2009b; Harvati and Hublin, in press). In fact, researchers (Bräuer, 2008; Rightmire, 2009) have proposed that Jebel Irhoud, along with Laetoli 18, Florisbad, Ileret, and several other Late Pleistocene African specimens represent the beginning of the *H. sapiens* lineage.

Lieberman (2008) noted that in many ways MPhs are scaled-up versions of *H. erectus* with larger brains and faces, and that the evolutionary transformation from a MPh to a modern human involves more complex changes in the underlying cranial architecture. In a previous morphometric study on cranial development and integration, Lieberman et al. (2002) demonstrated that the main architectural craniofacial differences between archaic and modern humans can be attributed to differences in the length of the middle cranial fossa and cranial base angles, and that these features explain facial retraction in modern humans. One key aspect of their finding is that the main cranial differences between archaic and modern humans develop early in ontogeny.

Our results are consistent with a growing body of evidence demonstrating that taxon-specific craniofacial morphology among hominin species developed prenatally or very early postnatally (e.g., Ponce de León and Zollikofer, 2001; Lieberman et al., 2002; Ackermann and Krovitz, 2002; Strand Viðarsdóttir et al., 2002; Williams et al., 2002; Krovitz, 2003; Mitteroecker et al., 2004; Bastir and Rosas, 2004; McNulty et al., 2006; Gunz et al., 2010). These morphometric studies largely support earlier descriptive research identifying unique Neanderthal morphology at

an early age (e.g., Rak et al., 1994; Zilberman, 1994; Akazawa et al., 1995). While a wide-range of studies corroborate an early development of many morphological characters across primates, the contribution of postnatal growth to further differentiate populations or species is debated.

Our results suggest that recent modern humans and Neanderthals may share a common pattern of allometric scaling during postnatal growth. In our study, the Neanderthal and modern human allometric trajectories are not overlapping and their slopes share a similar value. Therefore the hypothesis that the Neanderthal and modern human postnatal allometric trajectories are parallel cannot be rejected. While these results are consistent with other comparative morphometric studies on the growth and development of modern humans and Neanderthals (Ponce de León and Zollikofer, 2001; Williams et al., 2002; Krovitz, 2003), this may be an artifact of the small Neanderthal sample size. Therefore, these results should be interpreted with caution.

In their geometric morphometric analysis, Ponce de León and Zollikofer (2001) showed that Neanderthals and modern humans share a common pattern of cranial and mandibular shape change from an early age and onward. The general pattern of shape change comprised a projection and downward elongation of the face and mandible combined with a "contraction" of the cranial vault. They concluded that the craniofacial and mandibular differences between the two groups probably results from differential activity of growth fields early in ontogeny (Ponce de León and Zollikofer, 2001). Similarly, in their geometric morphometric study on facial development in great apes and *Australopithecus africanus*, Ackermann and Krovitz (2002) found that facial features arose very early in development followed by parallel postnatal developmental patterns (with the possible exception of the gorillas). Additionally, they found that aspects of facial growth were more similar between *A. africanus* and modern humans, relative to the great apes. Therefore, their study suggests that our early human ancestors were already demonstrating some human-like aspects of facial growth. The implications of these findings are that one can interchange hominid postnatal growth trajectories without producing significant differences in the end results.

This has been further demonstrated by McNulty et al. (2006). In their study on the taxonomic affinities of the subadult Taung fossil, McNulty et al. (2006) compared developmental simulations of Taung's adult morphology to adults of both *Australopithecus* and *Paranthropus*. In order to evaluate the adult morphology of the Taung child, they grew it up along various hominine developmental trajectories. While they found that the developmental patterns of extant hominine species to be statistically different, the results from their growth simulations indicate that the postnatal developmental differences between hominines has little impact on the estimation of the adult morphology. McNulty et al. (2006) demonstrated that the adult morphology of Taung can be reliably estimated even through the application of an incorrect developmental trajectory.

However, these results are not uniformly accepted. Several geometric morphometric analyses on humans and primates have found that both early postnatal cranial morphology and later postnatal growth contribute to further differentiate populations and species (Richtsmeier et al., 1993; O'Higgins and Jones, 1998; O'Higgins et al., 2001; Strand Viðarsdóttir et al., 2002; Cobb and O'Higgins, 2004; Bastir and Rosas, 2004; Strand Viðarsdóttir and Cobb, 2004; Bastir et al., 2007). In their geometric morphometric analysis on mandibular morphology, Bastir et al. (2007) argued that both pre- and post-natal ontogenetic growth is important in establishing morphological differences in mandibular shape between Neanderthals and modern humans. Their results showed divergent ontogenetic shape changes between Neanderthals and modern humans and significantly different allometric scaling patterns.

Our results do not exclude the possibility that localized differences in facial morphology between Neanderthals and modern humans occur throughout development. The discrepancy between our findings and those of previous studies may be explained by differences in the anatomical region analyzed (e.g., neurocranium versus face), by differing landmark data sets, or by small sample sizes (see Bastir and Rosas, 2004 for further discussion). Different anatomical regions have different rates and patterns of growth. For example, longitudinal data reveal that among

modern humans adult brain size and by extension neurocranial growth is nearly achieved (90-95%) by six years of age; whereas, facial growth continues into puberty, especially among males (Bulygina et al., 2006).

In a recent study testing the effects of evolutionary and static allometry on the midface, Maddux and Franciscus (2009) concluded that differences in infraorbital surface topography across the genus *Homo* can be explained by allometric scaling. At the time of birth, the face of a Neanderthal is already larger than that of a modern human (Ponce de León and Zollikofer, 2001; Ponce de León et al., 2008; Zollikofer and Ponce de León, 2010; Gunz et al., 2010). Additionally, by at least two years of age modern humans express different infraorbital surface topographies than Neanderthals. Therefore, while Neanderthals and modern humans may share a similar pattern of postnatal allometric growth their underlying differences in facial architecture developed early in ontogeny. In agreement with Maddux and Franciscus (2009), our growth simulations demonstrate that shape differences in infraorbital surface topography (inflation/depression) within modern humans change with size. However, a modern human scaled to the size of Bodo clearly displays a less inflated infraorbital surface topography because of the fundamental differences in their craniofacial architecture. Therefore contrary to Maddux and Franciscus (2009), features like infraorbital surface depression or inflation can be used to distinguish between modern and archaic populations. Additionally, we demonstrate that this feature can be used to differentiate between Neanderthals and the African MPhs, Bodo and Kabwe; however, features less susceptible to allometric scaling are more appropriate for determining phylogenetic relationships among closely related hominins.

These findings are consistent with Harvati et al. (2010). In a recent geometric morphometric study evaluating the accretion hypothesis, Harvati et al. (2010) propose that a convex and receding infraorbital profile may be the primitive condition for MPhs and Neanderthals. They found that the infraorbital profile of African and European Middle Pleistocene hominins are

nearly indistinguishable and similar, but not as extreme, to the Neanderthal mean configuration. Harvati et al. (2010) reached a similar conclusion regarding the projection and position of glabella. MPhs, Neanderthals and Jebel Irhoud 1 show an anterioinferior placement of glabella, a condition different from *H. erectus* and recent modern humans (Harvati et al., 2010). Their results indicate that this morphology is most pronounced in the African MPhs (Harvati et al., 2010). Our study and others (e.g., Rosas and Bastir, 2002) demonstrate that there is an allometric relationship between glabellar projection and size. While we cannot comment on the inferior placement of glabella, the large facial sizes of Bodo and Kabwe may explain why the African MPhs show the most anteriorly projecting glabella.

In our study, the facial features most affected by allometric scaling are glabellar projection, nasal aperture width, projection of the zygomatic bones, infraorbital surface topography, and lengthening of the subnasal region. Strand Viðarsdóttir et al. (2002) also identified many of these features as aspects of allometry shared by all modern human populations in her sample. Our findings complement a growing body of research that highlight the important role of allometry in hominin craniofacial development and evolution. Therefore, when making phylogenetic interpretations based on morphology it is preferable to evaluate features that that are less susceptible to allometric scaling and therefore of greater phylogenetic importance.

3.5 Conclusion

In this study we set out to identify temporal trends in facial morphology among Pleistocene humans, and to examine how changes in facial size change the morphology of facial features. Our PCA demonstrates that Pleistocene humans can be divided into temporal groups according to their facial morphology; however, the boundary between the MPhs and Neanderthals is less obvious. Additionally, our nearest neighbor calculations show that the African and European MPhs share an

overall similar facial morphology, although Arago 21 is most similar to a Neanderthal (La Chapelle-aux-Saints). This latter point could suggest that Arago 21 displays incipient Neanderthal facial features.

While the position of the Neanderthal and recent modern human postnatal ontogenetic trajectories suggests that they share a similar pattern of ontogenetic allometric scaling, further studies with a larger subadult Neanderthal sample size are needed to verify these results. Our results show that the distinctive modern human and Neanderthal facial morphology developed early in ontogeny, by at least two years of age. This implies that researchers can use subadult facial morphology to determine taxonomic affinities. However, one must be cautious when using features that are particularly susceptible to allometric scaling, such as glabellar projection, nasal aperture width, and infraorbital surface topography as phylogenetic markers. As for the latter feature, our growth simulations demonstrate that within modern humans there is a subtle change in topography associated with size; modern humans with larger faces generally have a slightly more inflated topography. However, a modern human scaled to the size of Bodo clearly displays a less inflated infraorbital surface topography because of the fundamental differences in their craniofacial architecture.

The overall position of the MPhs in shape and form space in conjunction with the direction of their static allometric trajectory suggests that allometric scaling explains large-scale differences in facial morphology between MPhs and Neanderthals. However, scaling does not explain differences between archaic and modern humans. Jebel Irhoud 1 undoubtedly expresses a modern human pattern of facial morphology, reflecting a clear modern human lineage separation at this later time period.

4. Growth and Allometry of *Homo antecessor* Subadult Facial Morphology[2]

4.1 Introduction

The earliest evidence of a completely modern human facial morphology has been attributed to the juvenile specimen ATD6-69 from Gran Dolina (Aurora Stratum of the TD6 level), Sierra de Atapuerca, Spain (Bermúdez de Castro et al., 1997). The paleomagnetic dates in combination with electron spin resonance (ESR) and uranium series give an age range of between 780-857 ka for the TD6 layer (Falguères et al., 1999). According to its dental formation stage and eruption sequence, it is estimated to have died between the ages of 10 and 11.5 years of age (Bermúdez de Castro et al., 1997). The ATD6-69 specimen has been described as having the following modern human-like facial features: a coronal orientation of the infraorbital plate combined with a sagittal orientation of the lateral nasal walls, a depression in the infraorbital surface, and an arched zygomaticoalveolar crest (Bermúdez de Castro et al., 1997; Arsuaga et al., 1999). However, because of its subadult age the phylogenetic interpretation of its facial morphology has been met with skepticism (see Stringer, 2002). In addition to ATD6-69, the adult right (ATD6-19) and left (ATD6-58) zygomaxillary fragment recovered from the TD6 layer are also described as expressing aspects of modern human morphology (Arsuaga et al., 1999; Bermúdez de Castro et al., 2011).

The Middle Pleistocene fossil locality Sima de los Huesos (SH) is another important site from the same region (Sierra de Atapuerca) with an abundant collection of human remains. The most recent radiometric study places an age for these fossil humans at around 600 ka (Bischoff, et al., 2007). However, the association between this date and the SH remains has been challenged (Endicott et al., 2010). Although these fossils display some aspects of primitive morphology on the

[2] The manuscript entitled *Growth and allometry of* Homo antecessor *subadult facial morphology*, written by Sarah E. Freidline, Philipp Gunz, Katerina Harvati and Jean-Jacques Hublin, will be submitted to the *Journal of Human Evolution* in 2/2012.

face and braincase, the SH hypodigm presents Neanderthal affinities in the dentition (Martinón-Torres et al., 2012), postcrania (Carretero et al., 1997; Gómez-Olivencia et al., 2007), mandible (Rosas, 2001), and several features of the face (Arsuaga et al., 1997). The incipient Neanderthal features and apomorphies present on the SH material, as well as in other European Middle Pleistocene humans, suggests an accretional (mosaic and gradual) appearance of Neanderthal characters in the European human fossil record (Arsuaga et al., 1997; Dean et al., 1998; Hublin, 1998, 2009; although see Martinón-Torres et al. 2012 for alternative interpretations).

Since the initial discovery of the Gran Dolina locality in 1994, over 100 fragmentary cranial and postcranial elements have been recovered from the TD6 level and assigned to a minimum of nine individuals (Bermúdez de Castro et al., 2011). Because of their unique combination of generally primitive (*H. erectus* s.l.-like) dentition and derived (*H. sapiens*-like) facial and postcranial features the specimens recovered from this site have been attributed to a new species *Homo antecessor* (Bermúdez de Castro et al., 1997). The original interpretation of these findings was that modern humans retained this juvenile pattern of midfacial and subnasal morphology and that *H. antecessor* may be the last common ancestor of modern humans and Neanderthals (Bermúdez de Castro et al., 1997; Arsuaga et al., 1999; Bermúdez de Castro et al., 2011). This scenario implies continuity in the European hominin fossil record beginning from ca. 780 ka (or possibly earlier if the material from the site of Sima del Elefante, dated to 1.2 Ma, is assigned to the *H. antecessor*) through the Middle Pleistocene and ending with the Neanderthals. According to this scenario, the European Middle Pleistocene hominins (MPhs) are interpreted as a chronospecies directly ancestral to Neanderthals, whereas a parallel descendant lineage of *H. antecessor* gave rise to *H. sapiens* in Africa (Bermúdez de Castro et al., 2004).

A more recent variant of this scenario is that Europe was colonized from Asia, rather than Africa, and that the African MPhs are a sister-group to this European lineage (Carbonell et al., 2005; Martinón-Torres et al., 2007). This interpretation of human evolutionary history during the early

Middle Pleistocene has been met with criticism (see e.g., Hublin, 2009), and, as a result, there are two prevailing alternative scenarios: (1) the TD6 material is an evolutionary dead-end either belonging to the taxon *H. erectus* (an Asian taxon distinct from *H. ergaster*), or to a separate species and side branch of *H. erectus* (Bermúdez de Castro et al., 2003; Finlayson, 2004); (2) the TD6 material belongs within the taxon *H. antecessor*, or *H. mauritanicus* (Arambourg, 1954) along with the contemporaneous North African hominins, and it is ancestral to both the African and European MPhs. In this latter scenario, the MPhs would either be recognized as a single cross-continental taxon (Rightmire, 1996, 1998; Stringer, 2002), or as separate European and African clades (Hublin, 1998, 2009).

Unfortunately, we have limited knowledge regarding the adult facial morphology of the TD6 population because the few adult fossils that have been recovered from this site are very fragmentary. Therefore, a better understanding of the ontogeny of facial features and how they are affected by size is critical for evaluating the facial morphology and the taxonomic implications of ATD6-69. Quantitative and descriptive studies on facial development in hominins have shown that taxon-specific morphology develops prenatally (Rak et al., 1994; Zilberman, 1994; Akazawa et al., 1995; Ponce de León and Zollikofer, 2001; Lieberman et al., 2002; Ackermann and Krovitz, 2002; Strand Viðarsdóttir et al., 2002; Williams et al., 2002; Krovitz, 2003; Mitteroecker et al., 2004; Bastir and Rosas, 2004; McNulty et al., 2006; Ponce de León et al., 2008; Gunz et al., 2010; Zollikofer and Ponce de León, 2010).

Among hominins, size correlated shape changes (i.e., allometry) have been observed in the relative breadth of the nasal aperture (Holton and Franciscus, 2008), nasoglabellar profile (Rosas and Bastir, 2002) and infraorbital surface topography (Maddux and Franciscus, 2009). This latter feature is particularly relevant to this study because it has been used as one of several key features to suggest a direct phylogenetic relationship between the TD6 hominins and modern humans.

However, our understanding of the variability in infraorbital morphology in fossil and modern humans and how it is affected by size is limited.

This study places the ATD6-69 fossil in an evolutionary and developmental context to assess how facial size affects its morphology. We use three-dimensional landmarks, as well as curve and surface semilandmarks, to quantify its preserved morphology. The application of semilandmarks is particularly useful for capturing the surface topography of the infraorbital region, an anatomical area that is critical to the debate regarding the "modernness" of its morphology. A landmark subset of just the infraorbital region was also created in order to more clearly assess how the shape of this region changes with size (i.e. growth). Additionally, Neanderthal and modern human allometric growth trajectories were used to simulate the development of ATD6-69 from an adolescent to an adult.

4.2 Material and methods

4.2.1 Sample

The fossil sample (Table 4.1) is comprised of Early to Late Pleistocene subadult and adult specimens that preserve the facial morphology present in ATD6-69. The modern human sample used in this study consists of the cross-sectional growth series described in Chapter 2 (Table 2.4).

Table 4.1 Fossil specimens used in the analysis, their abbreviation (Ab.) and chronology. Sub-adult individuals are italicized.

Specimen	Ab.	Chronology
Early Pleistocene: Africa		
ER 1813	1813	1.88-1.90 (Wood, 1991); 1.65 Ma (Gathogo and Brown, 2006)
*WT 15000**	Tur	1.6 Ma (Feibel et al., 1989)
Early Pleistocene: Europe		
*ATD6-69**	ATD6-69	> 780 ka (Carbonell 1995;Parés et al., Parés et al., 1999)
Early Pleistocene: Asia		
*Dmanisi 2700**	Dm27	1.7-1.8 Ma (Gabunia et al., 2000)
Middle Pleistocene: Africa		
Bodo	Bd	ca. 600 ka (Clark et al., 1994)
Kabwe	Kb	700 – 400 ka (Klein, 1994); late Middle Pleistocene (Stringer, 2011)
Middle Pleistocene: Europe		
Arago 21*	Ar	600 – 350 ka (Cook et al., 1982; Falguères et al., 2004)
Petralona	Pt	670 – ca. 250 ka (Harvati et al., 2009a)
Sima de los Huesos 5*	Sm5	ca. 530 ka (Bischoff et al., 2007)

Table 4.1 Continued

Late Middle-Late Pleistocene: Africa		
Jebel Irhoud 1	I1	ca. 160 ka (Smith et al., 2007)
Late Middle-Late Pleistocene: Europe		
Gibraltar 1	Gb1	71 – 50 to 35 ka (Klein, 1999)
Guattari	Gt	ca. 50 ka (Schwarcz et al., 1991)
La Chapelle-aux-Saints	LCh	56 – 47 ka (Grün and Stringer, 1991)
La Ferrassie 1	LF1	71 – 50 to 35 ka (Klein, 1999)
Pech-de-l'Azé I	Pech	51-41 ka (Soressi, 2007)
Late Middle-Late Pleistocene: Asia		
Liujiang*	Ljg	139 – 111 ka (Shen et al., 2002)
Qafzeh 6	Q6	135 – 100 ka (Grün et al., 2005)
Qafzeh 9	Q9	135 – 100 ka (Grün et al., 2005)
Shanidar 1*	Sh1	ca. 50 ka (Trinkaus, 1983)
Shanidar 5*	Sh5	ca. 50 ka (Trinkaus, 1983)
Skhul 5	Sk5	135 – 100 ka (Grün et al., 2005)
*Teshik Tash**	Tesh	ca. 70 ka (Movius 1953); 57-24 ka (Vishnyatsky 1999)
Upper Paleolithic: Europe		
Cro-Magnon 1	Cr1	28 – 27 ka (Holt and Formicola, 2008)
Grotte des Enfants 6	GrE6	Gravettian{Henry-Gambier, 2001}

Table 4.1 Continued

Mladeč 1	Ml1	ca. 31 ka (Holt and Formicola, 2008)
Předmostí 3*	Pr3	ca. 17 ka (Svoboda, 2008)
Oberkassel 1	Ob1	ca. 12 ka (Street, 2002)
Oberkassel 2	Ob2	ca. 12 ka (Street, 2002)
Upper Paleolithic: Asia		
Zhoukoudian 101*	Zh101	ca. 33 – 13 (Chen et al., 1989; Hedges et al., 1992; Brown, 1993)
Zhoukoudian 102*	Zh102	ca. 33 – 13 (Chen et al., 1989; Hedges et al., 1992; Brown, 1992)

*casts

4.2.2 Landmark data

The landmark and semilandmark subset used in this study is shown in Figure 4.1 and the biological landmarks are listed in Table 4.2.

Figure 4.1 Full landmark dataset, red: biological landmarks; blue: curve-semilandmarks; yellow: surface-semilandmarks. Biological landmarks are abbreviated. The full names are listed in Table 4.2.

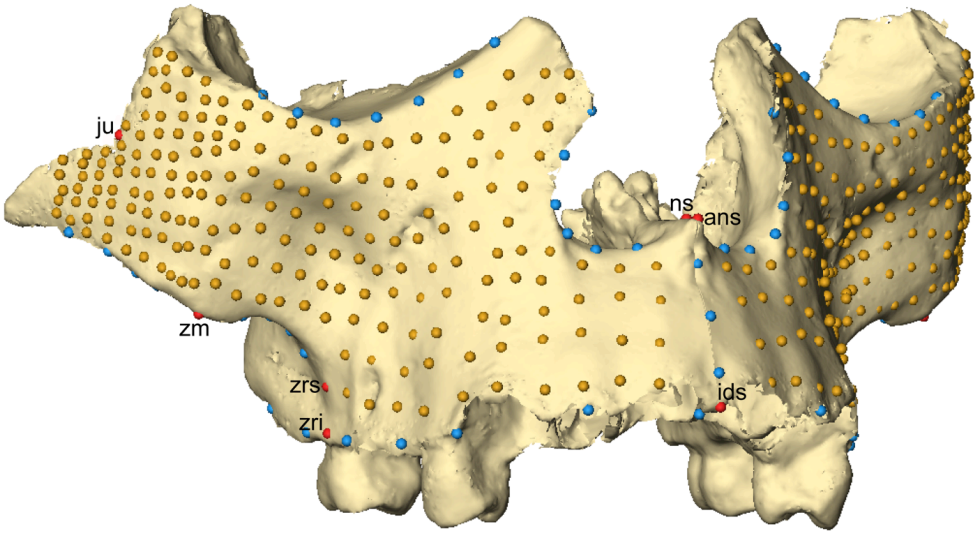

Table 4.2 Biological landmarks used in the analysis.

Landmark	Abbreviation
Alveolare	ids
Anterior nasal spine[1]	ans
Jugale*	ju
Nasospinale	ns
Zygomatic process root inferior[2]*	zri
Zygomatic process root superior[3]*	zrs

Table 4.2 Continued

Zygomaxillare*	zm

*paired right and left landmarks

4.2.3 Missing data reconstruction

Data reconstruction was performed on incomplete fossils following the reconstruction protocol described in Gunz (2005), Gunz et al. (2009a, 2010) and Freidline et al. (in press). Whenever possible, missing parts were reconstructed by mirror-imaging. Because the original ATD6-69 fossil is missing the entire right zygomatic and most of the right maxilla, we mirror-imaged it along its mid-sagittal plane. Two complete zygomatic and maxillary bones enable us to include more landmarks on this anatomical region, and as a result the landmark data set and subsequent analyses are not biased towards the subnasal and alveolar morphology. If missing data occurred bilaterally or along the mid-sagittal plane, then landmarks and semilandmarks were estimated using geometric reconstruction via TPS interpolation (Gunz et al., 2009a). This method of reconstruction was applied in a recent study (Freidline et al., 2012) to several of the same fossils in our sample, and has been used in several other geometric morphometric studies (e.g., Gunz, 2005; Gunz et al., 2007; Gunz et al., 2009a; Gunz et al., 2009b; Grine et al., 2010; Harvati et al., 2010; Stansfield and Gunz, 2011).

4.2.4 Analytical methods

We performed a principal component analysis (PCA) of the Procrustes shape variables on the full landmark and specimen data set and plotted the Neanderthal and modern human ontogenetic allometric trajectories within this space. Both ontogenetic and static allometric

trajectories were plotted in this space. In order to further explore the allometric component in our data, a PCA was also performed in Procrustes form space.

Additionally, in order to explore the developmental changes of the infraorbital surface topography, we extracted a landmark subset of the infraorbital region from the complete facial landmark data set (see Fig. 4.2). Separate PCAs in shape space using this landmark subset were performed on each of the four recent modern human groups (e.g., Khoisan, Arizona / Utah, Alaska, Strasbourg / Greifenberg) and the general pattern and distribution along the first three principal components were similar for each group. Therefore, we chose to report the PCA results of only one group, the Khoisan. Shape changes in this anatomical region were visualized by warping the Procrustes mean shape along the first two principal components (PCs; see Gunz and Harvati, 2007; Mitteroecker and Gunz, 2009).

Figure 4.2 Infraorbital landmark dataset.

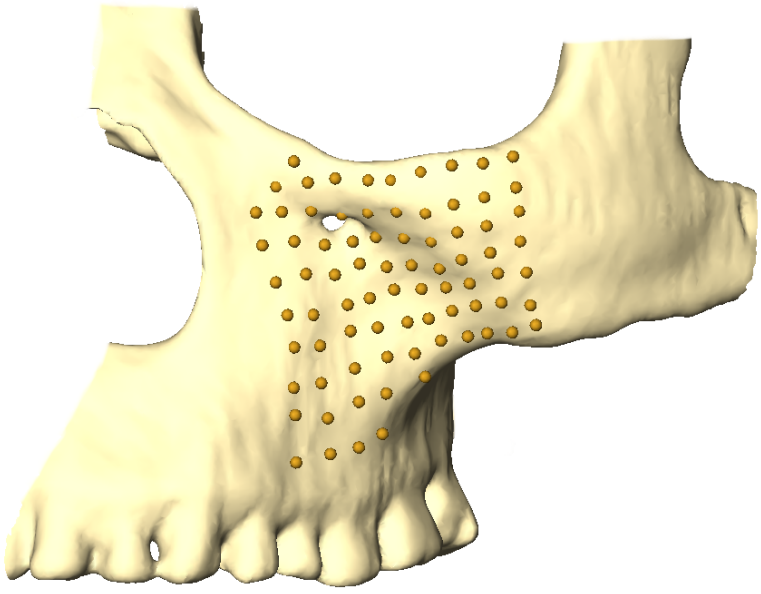

4.2.5 Growth simulations and visualization techniques

Because we lack an adult reference population to model the ontogenetic allometric trajectory of ATD6-69, we cannot directly test how size affects the facial morphology of this specimen. Instead, we used both the Neanderthal and modern human ontogenetic allometric trajectories to scale ATD6-69 to adult size. We computed linear regressions of the Procrustes shape coordinates on ln centroid size, for Neanderthals and modern humans. We then used these two regressions to predict the adult shapes of ATD6-69 using the respective average adult sizes (Fig. 4.3). These simulations therefore visualize what the adult ATD6-69 would have looked like if it had grown up like a Neanderthal, or a modern human. The average size of Neanderthal faces is larger than the modern human average. To visualize the shape differences between the two simulations in Figure 4.4, we therefore predicted the adult shape of ATD6-69 using the same size value, so as not to conflate differences in slope between the modern human and Neanderthal trajectories with differences in "length" along the trajectories.

4.3 Results

4.3.1 PCA: complete landmark and specimen data set

Shape space

We computed a PCA in shape space of the full specimen and landmark dataset. Figure 4.3 shows a plot of the first three PCs representing 62.2 % of total shape variation (PC 1: 29.9 %; PC 2: 24.2 %; PC 3: 8.1%). Among the first three PCs, PC 1 is the most correlated with size ($r \cong -0.53$). The pattern in the first three PCs primarily reflects a contrast between the Neanderthals and MPhs and the recent modern human (MH) morphology. Pech de L'Azé, ATD6-69, Qafzeh 9, Bodo, Skhul 5, Dmanisi 2700 and ER 1813 fall between these two clusters and on the fringe of the recent MH

distribution; whereas, WT-15000 plots closer to the Neanderthal and MPh groups. ATD6-69 plots closer to the Neanderthal ontogenetic trajectory than to the recent MH trajectory. We calculated nearest neighbors based on inter-individual Procrustes distances (PD) in shape space and ATD6-69 is most similar to a European subadult around 12 years of age (PD = 0.066) and an African subadult around 11 years of age (PD = 0.068).

The solid lines represent the recent MH (in gray) and Neanderthal (in blue) ontogenetic allometric trajectories. The position of these trajectories in shape space indicates that species-specific facial morphology has already developed by two years of age. The dashed lines depict the modern human and Neanderthal ontogenetic allometric trajectories used to scale ATD6-69 to a simulated adult, and the solid black circles at the end of each trajectory represent the PC scores for the predicted adult shapes.

Figure 4.3 PCA in shape space of the full landmark and specimen dataset. The first three PCs are plotted. PC 1 represents 29.9 % of total shape variation; PC 2 represents 24.2%; and PC 3 is 8.1 %. The solid lines represent the recent MH (in gray) and Neanderthal (in blue) ontogenetic allometric trajectories. The dashed lines depict the simulated modern human and Neanderthal ontogenetic allometric trajectories used to scale ATD6-69 to an adult, and the solid black circles at the end of each trajectory represent the PC scores for the predicted shapes. The full names for the fossil specimens are listed in Table 4.1.

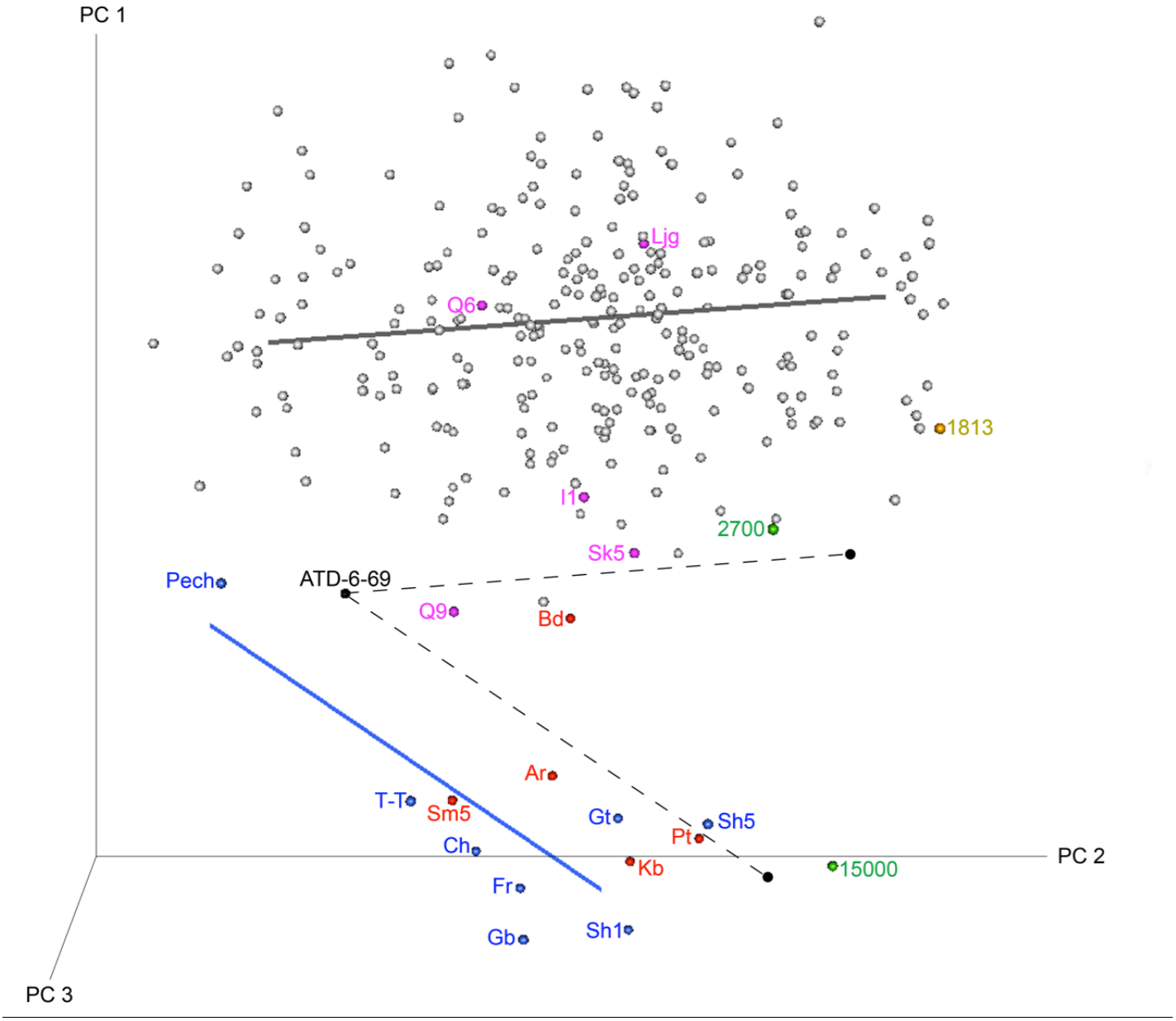

Growth simulations

Figure 4.4 illustrates the predicted shapes of ATD6-69 scaled along the Neanderthal ontogenetic allometric trajectory and the recent MH trajectory. The lines (blue: Neanderthal; gray: recent MH) represent the curve semilandmarks and the black arrows indicate the direction of shape change between the respective shapes for the "modern human ontogeny" and "Neanderthal ontogeny." The differences between the two simulated adult shapes reflect the general facial shape differences between an adult modern human and a Neanderthal. ATD6-69's predicted adult facial morphology grown along the Neanderthal trajectory (blue in Fig. 4.4) has a more oblique zygomaticoalveolar crest, parasagittaly rotated zygomatic bones and infraorbital plate, inflated infraorbital surface topography, inferior position of the infraorbital margin, a larger nasal breadth, a longer subnasal region, and greater projection of the midface. The largest shape differences are associated with the overall orientation of the infraorbital plate and the zygomatic bones. This figure indicates that there are also aspects of postnatal facial growth that further differentiate Neanderthals and MHs. Diverging postnatal trajectories therefore make the facial differences between Neanderthal and recent MH more pronounced during development. Moreover, Neanderthal adults are larger than modern human adults; this further accentuates the adult shape differences between these two human groups.

Figure 4.4 Growth simulations of the predicted shapes of ATD6-69 scaled along the Neanderthal ontogenetic allometric trajectory (blue) and the recent MH trajectory (gray). The lines represent the curve semilandmarks and the black arrows indicate the direction of shape change of the surface semilandmarks between the reference (modern human) and target (Neanderthal) shapes. The length of each arrow describes the amount of shape change.

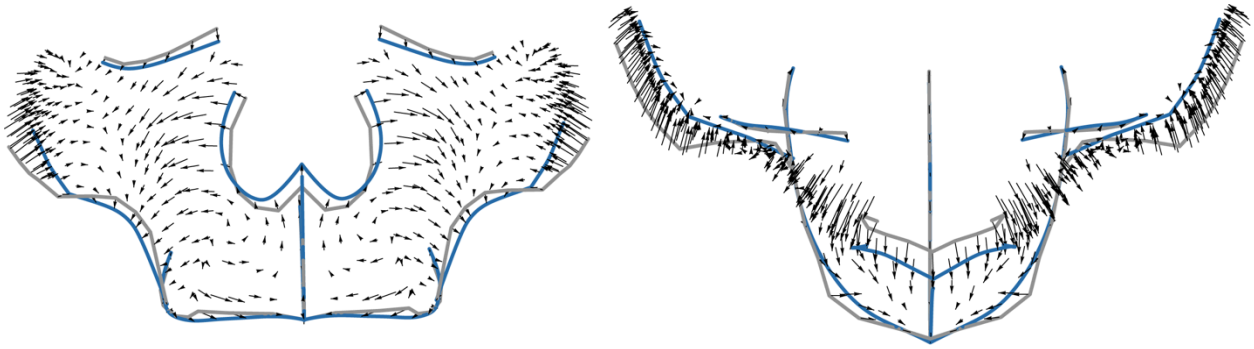

Form space

A PCA of the same landmark and specimen data set was also computed in form space. The first three PCs (Fig. 4.5) represent approximately 91.1 % of the total sample variation (PC 1: 82.3%; PC 2: 5.5 %; PC 3: 3.3 %). As expected, PC 1 represents size ($r \cong 0.999$). The longer lines are the ontogenetic allometric trajectories for modern humans (in gray) and Neanderthals (in blue), and the shorter lines represent the static allometric trajectories (i.e., regression of only the adult data of each group) for Neanderthals (in black) and MPhs (in red). Like in shape space, the ontogenetic allometric trajectories have a unique starting point, indicating that species-specific facial morphology has already developed by two years of age.

Like in Procrustes shape space, ATD6-69 plots closer to the Neanderthal ontogenetic allometric trajectory than to the modern human. ATD6-69 has the same nearest neighbor in form and shape space (European recent modern human subadult). The early MHs fall between the Neanderthal and modern human trajectories, and the MPhs plot along the end of the Neanderthal ontogenetic and static allometric trajectories. The position and slope of the Neanderthal and MPh

static allometric trajectories are very similar to one another indicating that allometric scaling explains the large-scale differences in facial shape between the two groups.

Figure 4.5 PCA in form space (including the log centroid size of each individual) of the complete specimen and landmark dataset. The first PCs are plotted. PC 1 represents 82.3% of total variation; PC 2 represents 5.5 %; and PC 3 is 3.3 %. The longer lines are the ontogenetic allometric trajectories for modern humans (in gray) and Neanderthals (in blue), and the shorter lines represent the static allometric trajectories (i.e., regression of only the adult data of each group) for Neanderthals (in black) and MPhs (in red).

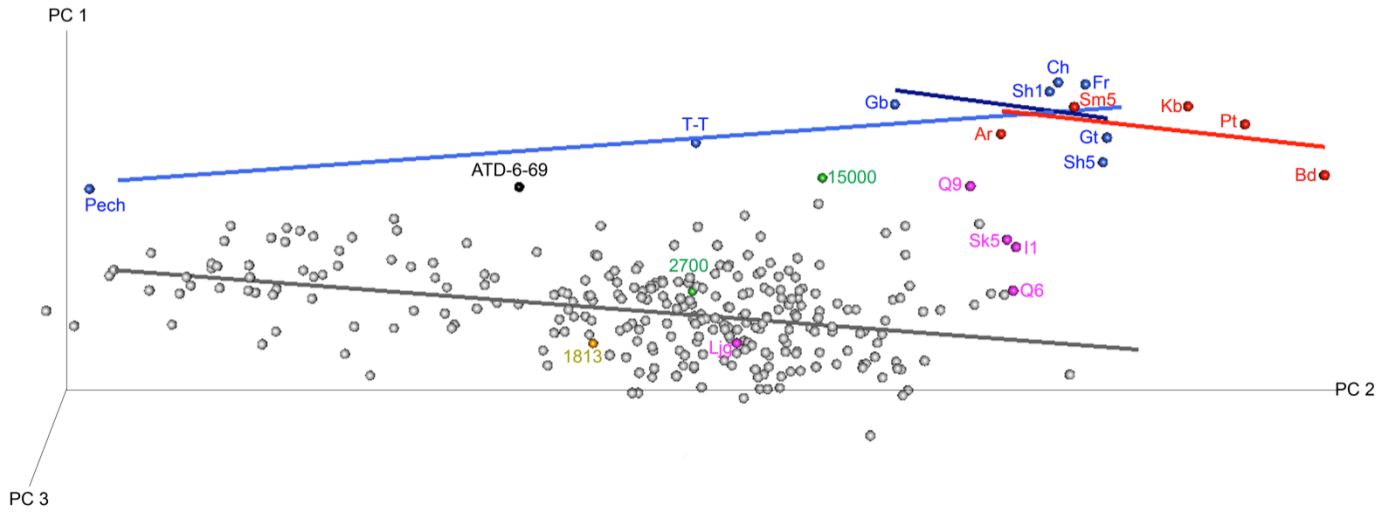

4.3.2 PCA: infraorbital landmark data set

Shape space

In order to explore variation in the infraorbital surface topography in our fossil and modern human sample, we performed a PCA in Procrustes shape space on the infraorbital landmark subset (see Fig. 4.2). Figure 4.6 plots the first three PCs representing 63.1 % of total variation (PC 1: 33.1 %; PC 2: 19.4 %; PC 3: 10.6 %). PC 1 is the most correlated with size (r ≅ -0.53). This plot is similar to the PCA of the complete data set (see Fig. 4.3). The main difference is the position of the Early

Pleistocene specimens Dmanisi 2700 and ER 1813, which plot nearer to one another in this PCA. Like in Figure 4.3, this plot mainly contrasts the recent MH and the Neanderthals and MPhs morphology. ATD6-69 falls along the margin of recent MH variation and the early MH fall within the range of recent MH variation.

Figure 4.6 PCA in shape space using the infraorbital landmark subset (see Fig. 4.2) and the complete specimen sample. The first three PCs are plotted. PC 1 represents 33.1 % of total shape variation; PC 2 represents 19.4 %; and PC 3 is 10.6 %. The solid lines represent the recent MH (in gray) and Neanderthal (in blue) ontogenetic allometric trajectories.

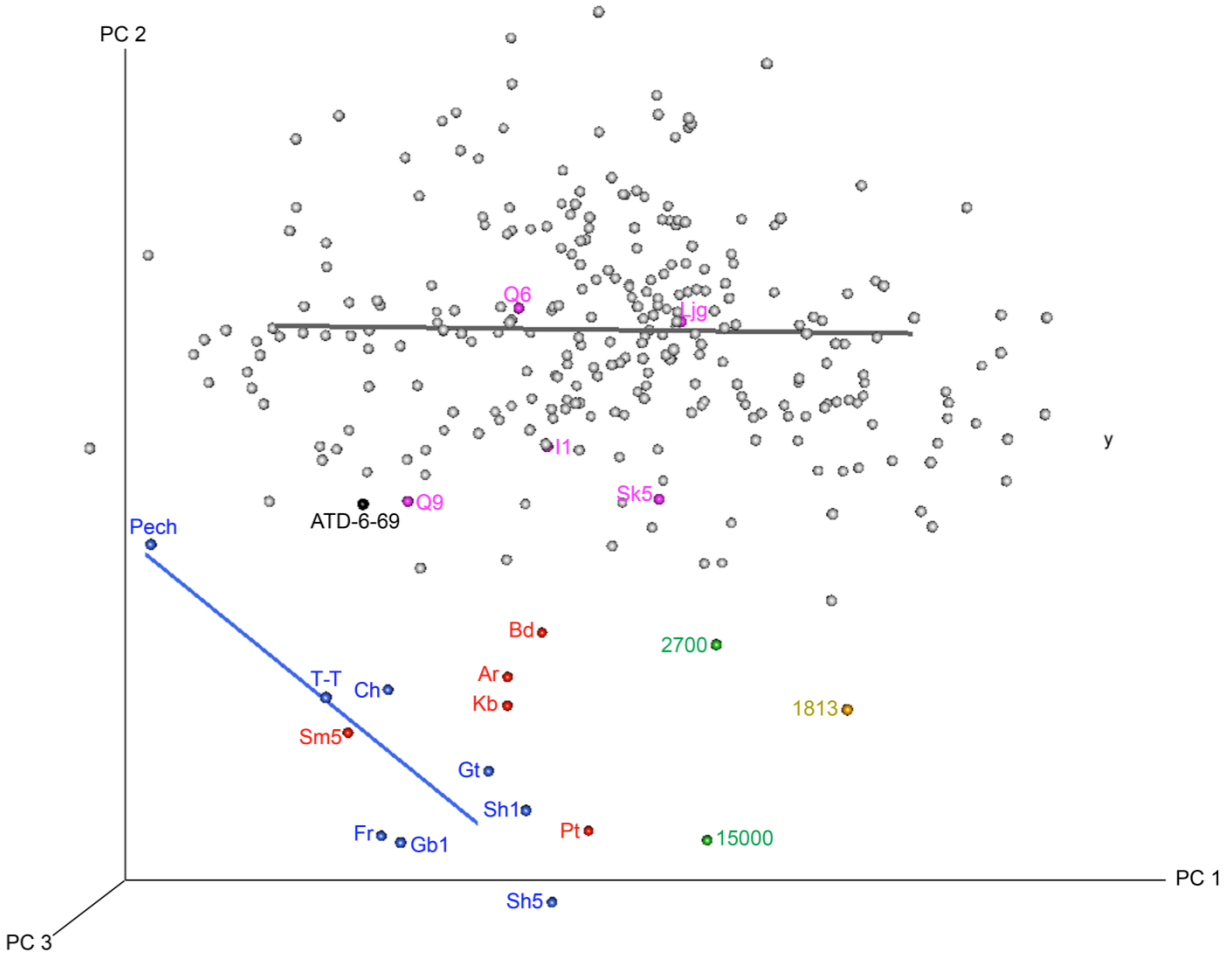

Shape space: Khoisan group

Lastly, in order to elucidate the ontogenetic shape changes of the infraorbital region, we performed a PCA using the infraorbital landmark data set of only the Khoisan individuals. The first three PCs are plotted in Figure 4.7 and they represent 63.8 % of total shape variation (PC 1: 35.0 %; PC 2: 17.1 %; PC 3: 10.8 %): the specimens are labeled according to their age group classification (see Table 4.2 for definitions). The black line represents the ontogenetic allometric trajectory. PC 1 is highly correlated with size ($r \cong 0.82$) and along this component individuals belonging to the same age group cluster together. The youngest and smallest individuals plot at one end of the PC and the adults on the opposite end. Along PC 2 and 3 no clear pattern among age groups emerges, indicating that the infraorbital shape changes along these components is highly variable within the Khoisan group.

Figure 4.7 PCA in shape space using the Khoisan specimen subset and the infraorbital landmark dataset. The first three PCs are plotted. PC 1 represents 35.0 % of total shape variation; PC 2 represents17.1 %; and PC 3 is 10.8 %. The specimens are labeled according to their age group classification (see Table 4.2 for definitions). The black line represents the ontogenetic allometric trajectory.

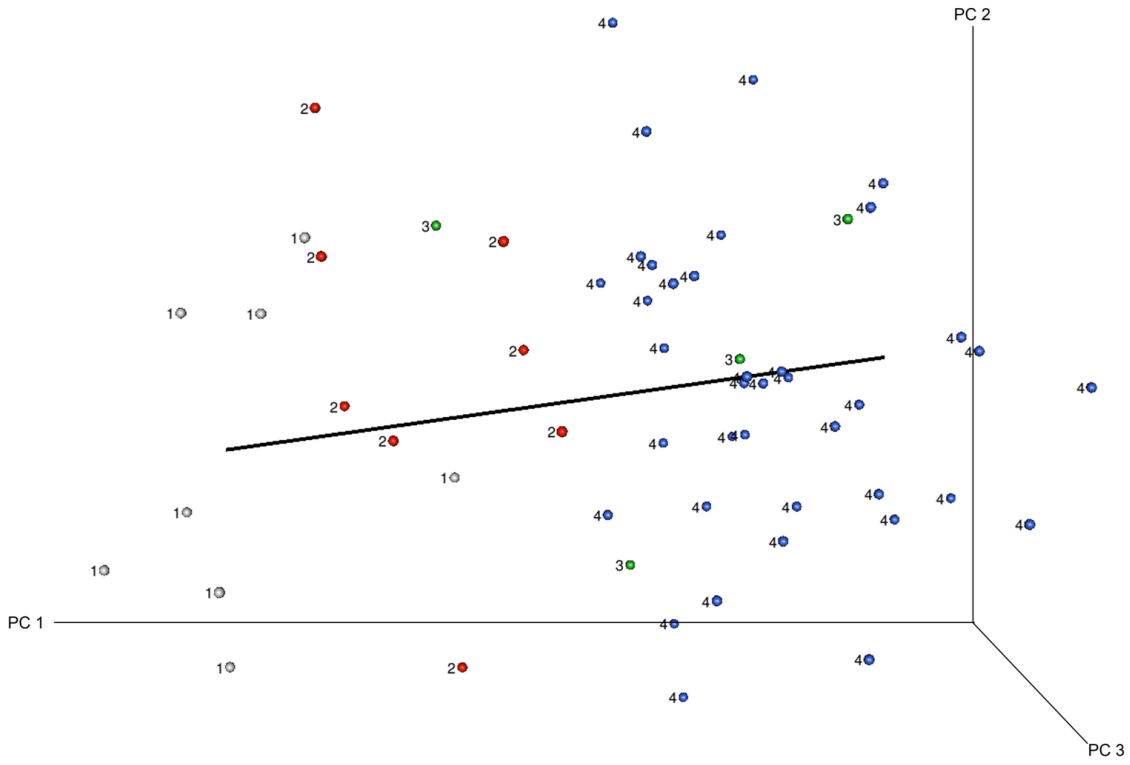

Visualization

Figure 4.8 visualizes the shape changes associated with warping the mean Khoisan infraorbital shape along PC 1 and 2. As PC 1 is highly correlated with size, this component mainly depicts the allometric shape changes in the infraorbital region. These changes include: the curvature and anterior projection of the inferior orbital margin, anterior projection of the lateral nasal walls, and shape of the zygomaticoalveolar curve. PC 1 also comprises some inflation of the infraorbital surface topography associated with size, however it does not affect the "canine fossa." Individuals with superior-inferiorly smaller infraorbital areas (Fig. 4.8a) have a more curved and

anteriorly projecting inferior orbital margin, more anteriorly projecting lateral nasal walls, and a less curved zygomaticoalveolar crest. Whereas, individuals with superior-inferiorly larger infraorbital surface areas (Fig. 4.8b) express a more horizontal inferior orbital margin, less anteriorly projecting lateral nasal walls, greater curvature of the zygomaticoalveolar margin, and the medial aspect of the zygomatic bone (i.e., maxillary process) is more anteriorly projecting.

PC 2 reflects the within-group variability of the infraorbital region (Fig. 4.8c, d). Shape changes along this principal component are mainly associated with the anterior projection of the maxillary process of the zygomatic and the orientation of the anterior surface of the maxilla (i.e., maxillary body facies). Individuals that plot along the negative end of PC 2 have an overall more complex topography than those individuals that plot along the positive end, expressing a more anteriorly projecting maxillary process combined with a posteroinferiorly oriented maxillary body facies. Although PC 2 is not highly correlated with size ($r \cong 0.11$), individuals that plot along the positive end of PC 2 are larger in the superior-inferior dimension.

Figure 4.8 Mean shape changes along the first two PCs in shape space using the Khoisan infraorbital data set; a) mean shape at the negative end of PC 1; b) mean shape at the positive end of PC 1; c) mean shape at the positive end of PC2; d) mean shape at the negative end of PC 2.

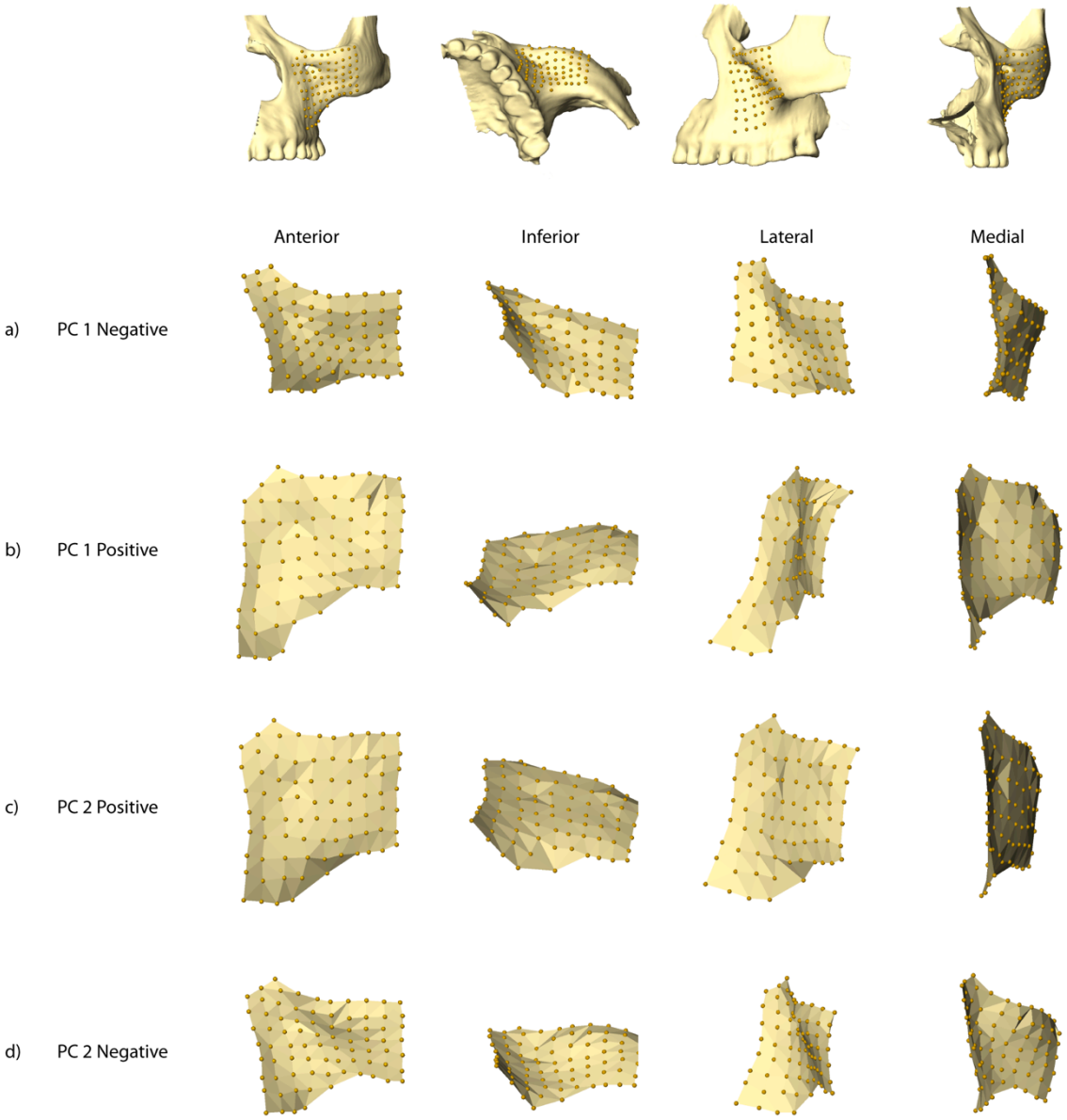

4.4 Discussion

The aim of this study was to evaluate the facial morphology of ATD6-69 in an ontogenetic and evolutionary context. In order to explore allometric trends in our data, we calculated postnatal allometric trajectories for fossil and recent modern humans. The adult facial morphology of ATD6-69 was predicted using these trajectories. Additionally, allometric shape changes in infraorbital surface morphology were visualized along PC axes. The results of our PCA and regression analyses confirm a wide range of studies demonstrating that species-specific facial morphology has already developed prenatally (Ponce de León and Zollikofer, 2001; Ackermann and Krovitz, 2002; Lieberman et al., 2002; Strand Viðarsdóttir et al., 2002; Williams et al., 2002; Krovitz, 2003; Mitteroecker et al., 2004; Bastir and Rosas, 2004). The growth simulations (Fig. 4.4), implementing both the modern human and Neanderthal ontogenetic allometric trajectories to predict the adult facial morphology of ATD6-69, indicate that postnatal development further accentuates the facial differences between modern humans and Neanderthals that are already present early in ontogeny. These results support previous studies on hominin craniofacial growth showing that postnatal growth contributes to further differentiate populations and species (Richtsmeier et al., 1993; O'Higgins and Jones, 1998; O'Higgins et al., 2001; Strand Viðarsdóttir et al., 2002; Cobb and O'Higgins, 2004; Bastir and Rosas, 2004; Strand Viðarsdóttir and Cobb, 2004; Bastir et al., 2007). The results of our growth simulations show that even when we grow ATD6-69 along the Neanderthal ontogenetic allometric trajectory it maintains a curved zygomaticoalveolar crest and some maxillary flexion. Likewise, when we grow it along the modern human ontogenetic allometric trajectory its face remains prognathic. Therefore, while ATD6-69 undoubtedly expresses some aspects of modern human-like facial morphology, such as maxillary flexion, it also displays a total facial prognathism uncharacteristic of recent MH. Additionally, the similarities in the position and direction of the Neanderthal and MPh static allometric trajectories in the PCA in form space (see

Fig. 4.5) strongly suggests that allometric scaling explains the general differences in facial morphology between these two groups.

In his seminal paper on Neanderthal facial architecture, Rak (1986) contrasts a "generalized" or "unmodified" face with that of the western Neanderthal facial skeleton. He describes a generalized face as having a coronally oriented and forward facing infraorbital plate with a surface that slopes down and slightly back; a canine fossa; a distinct angle at the lateral ends of the infraorbital plates that divides the peripheral portion of the face into two parts (lateral and anterior); a curved zygomaticoalveolar crest; and a nasoalveolar clivus that forms an angle with the plane of the nasal aperture. Rak (1986) proposes that, in principle, this morphology is shared by many primates, including modern and fossil humans, such as Skhul IV and V; Zuttiyeh; Jebel Irhoud 1; Steinheim; Qafzeh 6 and 9; and Chinese *H. erectus* (Weidenreich's reconstruction). Several of these generalized facial features have also been noted in the Chinese Middle Pleistocene specimens, such as Dali (Arsuaga et al., 1999), Zhoukoudian (Maxillae III and V, Os Zygomaticum II: Pope, 1992), Yuxian 1 and 2 (Etler, 1996) and Nanjing 1 (Liu et al., 2005). These specimens have been variously described as having a coronal orientation of the cheek bones, a horizontal and high rooted and arched inferior zygomaxillary border, and a canine fossa. While ATD6-69 undoubtedly expresses some aspects of modern human facial morphology, such as maxillary flexion, it also displays a total facial prognathism uncharacteristic of recent MH. According to Rak's theory, the modern human-like facial features in ATD6-69 can be interpreted as being part of a generalized or primitive facial architecture, and aspects of this architecture may have evolved multiple times in human evolution.

With regards to the description of the canine fossa morphology, Rak (1986) does not discriminate between the morphology found in modern humans and *H. erectus*. In some EPhs there is a vertical groove that lies inferior to the infraorbital foramen and lateral to the canine jugum (Weidenreich, 1943; Maureille, 1994). Weidenreich (1943) termed this "sulcus maxillaris" and

Maureille (1994) called it the "fossula canina". Whereas, in modern humans there is an extended depression that covers most of the zygomatic process of the maxilla (Arsuaga et al., 1999) and produces a horizontal incurvation and an incurvation of the zygomaticoalveolar crest (Maureille, 1994). This also appears to be the morphology in ATD6-69.

ATD6-69 expresses a deep infraorbital depression, which cannot entirely be explained by its small size or young age. According to our infraorbital shape analysis (see Fig. 4.8), we can conclude that this depression is most likely due to its anteriorly projecting inferior orbital margin, maxillary process of the zygomatic and lateral nasal walls. These results generally confirm Maddux and Franciscus' (2009) findings on allometric scaling of the infraorbital region in Middle to Late Pleistocene humans. We demonstrate that while size influences the shape and topography of the infraorbital region it is not the only factor. Like Maddux and Franciscus (2009), we also found that the larger the infraorbital area the flatter the topography, the more sloped the inferior orbital rims, and the less everted the lateral nasal margins. Whereas, the smaller the infraorbital surface area, the more depressed the topography, the more projecting the inferior orbital rim and the more everted the lateral nasal walls. These results suggest that infraorbital surface topography is not necessarily a feature in itself, but rather a by-product (i.e. secondarily derived) of the surrounding morphology.

Arsuaga et al. (1999) measured the infraorbital angle in ATD6-69, following Maureille and Houet's (1997) measurement protocol, and found that it was close to the modern human average (ATD6-69: 153 degrees; MH average: 154.7 degrees) and much smaller than Neanderthal (~180 degrees). In our PCA analysis on just the infraorbital landmark data set, ATD6-69 falls on the edge of modern human variation. Our methods, however, cannot prove whether the depression found on ATD6-69 is homologous to the infraorbital depression on modern humans. Studies on bone growth remodeling (e.g., Walters and O'Higgins, 1992; O'Higgins and Jones, 1998; McCollum, 1999; O'Higgins et al., 2001; McCollum, 2008; Rosas and Martinez-Maza, 2010; Martinez-Maza et al.,

2011) of the infraorbital region across hominin taxa could provide us with a better insight regarding the developmental origin of this morphology.

The ATD6-69 face is not the only specimen from this layer to exhibit an arched lower zygomaticoalveolar crest and an infraorbital depression. These features have also been described on several adult human fossil specimens (ATD6-19, ATD6-58) leading Arsuaga et al. (1999) to conclude that these features are invariant through growth. The results of our growth simulations confirm that the shape of these features change little throughout individual growth, although their expression is quite variable within and between modern human populations.

Evolutionary scenarios

Our results indicate that the faces of Neanderthals and modern humans look different throughout postnatal ontogeny, and that diverging postnatal developmental trajectories further accentuate the shape differences between these two groups. In all of our shape analyses ATD6-69 falls on the fringe of recent modern human variation, and its infraorbital depression is reminiscent of modern humans. However, this feature is not a character in the cladistic sense as it covaries with infraorbital size and orientation. Additionally, it displays features associated with facial prognathism that are not found in modern humans. While our results provide us with no justification to include ATD6-69 in the taxon *H. erectus*, we also cannot conclusively support one of the alternative evolutionary scenarios outlined in the introduction.

If *H. antecessor* is an evolutionary side-branch of *H. erectus* and represents a speciation event that occurred in Eurasia – *H. antecessor* – after the first hominin exodus out of Africa (Templeton 2002), then aspects of modern human cranial features may have evolved more than once in Africa and in Europe (Bermúdez de Castro et al., 2004). The possibility that modern human-like facial features evolved multiple times in human evolution does not seem improbable. Our

results demonstrate that facial features such as zygomaticoalveolar curvature and infraorbital topography covary with one another, and that the shape of these features is influenced by infraorbital size. Moreover, our results show that these features are highly variable within modern humans and may have occurred in multiple taxa in the human fossil record.

If *H. antecessor* is the last common ancestor to Neanderthals and modern humans (Bermúdez de Castro et al., 1997; Arsuaga et al., 1999; Bermúdez de Castro et al., 2011), then these two taxa diverged in the early Middle Pleistocene and there was long-term continuity in Africa and Europe. While there is some morphological evidence to support a long-term continuity in Europe (see below), it is inconsistent with both the archaeological record and the Neanderthal and modern human divergence dates based on genetic data. The TD6 hominins are associated with Mode 1 technology although the development of Mode 2 (Acheulean) technology had already occurred in Africa and the Near East by at least 1.6 Ma (Hublin, 2009). Archaeological evidence of Mode 2 technology does not appear in Europe until between 600 and 500 ka. This might be consistent with a replacement scenario in western Eurasia by later populations that were ancestral to Neanderthals. Based on recent modern human genetic data, Templeton (2002, 2005) suggested a second "Out of Africa" migration around 600 ka which was likely associated with larger brained hominins carrying Acheulean technology.

Recent dental and mandibular studies provide an additional level of complexity to this scenario by suggesting that Europe was colonized from Asia, rather than Africa. In a recent study, Martinón-Torres (2007) and her colleagues found that *H. antecessor* shares specific aspects of dental morphology with Eurasian hominins (*H. erectus*, European MPh, and Neanderthals) to the exclusion of African fossil taxa (*A. afarensis*, *A. africanus*, *H. habilis*, *H. ergaster*, and Middle Pleistocene hominins from North Africa). Whereas, contrary to the dental evidence the mandibular morphology of the TD6 hominins does not favor continuity in Europe (Bermúdez de Castro et al., 2008). Carbonell et al. (2005) and Bermúdez de Castro et al. (2008) propose that the TD6

mandibular remains and the Early and Middle Pleistocene Chinese hominins share similarly gracile morphology, unlike the African Early and Middle Pleistocene hominins, and the Sangiran and Dmanisi hominins. However, gracility is a poor phylogenetic marker. We demonstrate that facial size varies considerably during Pleistocene human evolution and affects topographic features of the face that are often used to distinguish hominin taxa.

Therefore, the most convincing evolutionary scenario is that the TD6 hominins, and possibly the contemporaneous North Africa hominins (e.g., Tighenif, Thomas Quarry and Sidi Abderrahman) form a species (e.g., *H. mauritanicus*) that is ancestral to the African and European Middle Pleistocene humans (Hublin, 2001; Stringer, 2002). In this scenario, the origin of the European Middle Pleistocene hominins derives from an African exodus during the Middle Pleistocene probably resembling the Bodo specimen and carrying with it the Mode 2 technology into Europe (Carbonell et al., 1995; Rightmire, 1996; Manzi et al., 2001). This population either replaced the indigenous earlier Pleistocene populations, or there was gene flow between them (Bermúdez de Castro et al., 2003). This scenario can encompass both a wide-ranging MPh taxon (e.g., *H. heidelbergensis s.l.*), or two geographically divided Middle Pleistocene clades: *H. heidelbergensis* or *H. neanderthalensis* in Europe and *H. rhodesiensis* in Africa. This scenario is consistent with the archaeological record and the genetic divergence dates. Recent genetic evidence suggests a divergence date between modern human and Neanderthal mtDNA lineages at around 660 ka (Green et al., 2010). However, it is important to keep in mind that estimates of genetic coalescence time, population separation, and phenotypic differentiation are chronological distinct events that are based on a number of assumptions and are associated with large confidence intervals (Hublin, 2009). The main oppositions to this scenario are the recent dental and mandibular studies that equivocally support continuity in Eurasia from the Early Pleistocene to Neanderthals (Carbonell et al., 2005; Martinón-Torres et al., 2007; Bermúdez de Castro et al., 2008).

Nevertheless, most of the cranial and postcranial morphological evidence can be used to support both of these latter two evolutionary scenarios because in both situations one would expect to find a combination of primitive *H. erectus*/*ergaster* features, as well as derived Middle Pleistocene human, Neanderthal and modern human features. In their initial publication on the dental morphology of the TD6 hominins Bermúdez de Castro et al. (1999) concluded that in some features their dentition suggests an evolutionary continuity between them and the European MPhs, but that overall their dental morphology indicates that they are closest to the African lower and early Middle Pleistocene hominins. In a geometric morphometric study on upper first molar (M^1) morphology, Gómez-Robles et al. (2007) found that the unique M^1 morphology in Neanderthals can be traced back to the *H. antecessor* material and that this morphology is also present in the European MPhs; whereas, modern humans express a primitive M^1 morphology (Gómez-Robles et al., 2007; although see Quam et al., 2009 and Gómez-Robles et al., 2011 for conflicting results). However, the idea of long-term continuity within Europe conflicts with the Neanderthal and modern human genetic divergence dates.

Like the dentition, the TD6 mandibles display a generalized morphology most similar to African and European lower and Middle Pleistocene samples (Bermúdez de Castro et al., 1999). In addition to the interesting, modern human-like facial morphology present on ATD6-69, the TD6 hominins share several derived cranial features with modern humans, Neanderthals and African and European MPhs including a convex superior border of the temporal squama, anterior position of incisive canal, and marked nasal prominence (Bermúdez de Castro et al., 1997; Arsuaga et al., 1999). Lastly, the postcranial remains, which include clavicles, radii, femora, vertebrae and hand and foot remains, are more similar to modern humans than to either Middle Pleistocene humans or Neanderthals (Carretero et al., 1997, 1999; Lorenzo et al., 1999). Critical to the interpretation of these observations, however, is an understanding of the polarity of these postcranial features.

4.5 Conclusions

This is the first study to place the ATD6-69 face in both an evolutionary and developmental context. Our results support previous studies demonstrating that the ATD6-69 hominin exhibits a mosaic pattern of facial morphology, reminiscent of Neanderthals, modern humans and earlier Pleistocene humans. Therefore, our results could support any one of the aforementioned evolutionary scenarios. However, according to the archaeological and genetic evidence it seems unlikely that *H. antecessor* is the last common ancestor to modern humans and Neanderthals. An additional possible scenario that is consistent with our results is that the modern human-like facial morphology present on the ATD6-69 specimen is primitive to what is observed in the Middle Pleistocene humans (Arsuaga et al., 1999), and modern humans independently evolved these features from an African Middle Pleistocene clade. Under this scenario, modern human facial morphology is derived, relative to the Middle Pleistocene human morphology, and evolved sometime in the late Middle Pleistocene by around 170 ka (e.g., Jebel Irhoud 1).

Our PCA results support a wide range of studies showing that many facial features separating Neanderthals and modern humans are already established early in ontogeny. Additionally, our regression analyses and the visualizations of our growth simulations indicate that postnatal growth further accentuates the differences in facial features between Neanderthals and modern humans. Together these results imply that those features that link ATD6-69's morphology to modern humans would not have been significantly altered in the course of subsequent development. Therefore, its subadult status no longer needs to be a limiting factor for interpreting its phylogenetic affinities. In particular the infraorbital depression on this specimen would have persisted into adulthood. However, ATD6-69 also displays features uncharacteristic of modern humans, such as total facial prognathism.

Our data show that there are evident evolutionary changes in the pattern and growth of facial development in modern humans and Neanderthals, and most probably *H. antecessor* also expresses a unique facial growth pattern. In all PCA analyses ATD6-69 plots on the margin of modern human variation and intermediate between them and Middle Pleistocene humans and Neanderthals. As a result, we could expect a postnatal allometric growth trajectory for the TD6 population to also plot in-between the Neanderthals and modern human trajectories. Therefore, finding more complete adult faces from the TD6 layer in Atapuerca will provide us with greater insight on the evolution of facial growth patterns in the human fossil record.

Many of the facial features that ATD6-69 shares with modern humans can be considered to be part of a generalized pattern of facial architecture (sensu Rak, 1986). These features include a coronally oriented infraorbital plate, laterally oriented zyogmatics and a curved zygomaticoalveolar crest. The infraorbital depression on ATD6-69 cannot be explained solely by its small size or young age. The topography of this region is largely influenced by the surrounding anatomical region as well as size. Therefore, infraorbital surface topography is not necessarily a feature in itself, but rather a by-product of the surrounding morphology. Additionally, our results indicate that this feature and the curvature of the zygomaticoalveolar crest are highly variable within and between modern humans. Future work on the developmental mechanisms that underlie hominin facial morphology is needed.

5. A Comprehensive Morphometric Analysis of the Frontal and Zygomatic Bone of the Zuttiyeh Fossil from Israel[3]

5.1 Introduction

The Zuttiyeh fossil human specimen (Turville-Pétre, 1927) was discovered in 1925 in Mugharat el Zuttiyeh (the Cave of the Robbers) near the Sea of Gallilee in Israel. It consists of a nearly complete frontal, right zygomatic and a partial right sphenoid bone and has been dated to the Middle Pleistocene period through correlation with the Tabun archaeological sequence. This sequence is central to understanding the chronology of Western Asia and is frequently used as a reference for interpreting archaeological cultures at other Pleistocene sites, such as Mugharet el Emireh, the Mount Carmel caves, Qafzeh and Kebara (Bar-Yosef, 1992). The Zuttiyeh craniofacial fragment was discovered at the base of the archaeological sequence at Mugharat el Zuttiyeh, under a layer that contained Acheulian-Yabrudian lithics, a pre-Mousterian technology similar to the Tabun E industry (Gisis and Bar-Yosef, 1974; Bar-Yosef, 1988).

Although there are no absolute dates from Mugharat el Zuttiyeh, Acheulo-Yabrudian layers have been radiometrically dated (thermoluminescence, electron spin resonance, and uranium series) from various sites in the Near East and range from > 382 to 200 ka (Yabrud Rockshelter 1: Huxtable, 1990; Bar-Yosef, 1992; Tabun: Mercier et al., 1995; Mercier and Valladas, 2003). Additionally, Tabun E, F, and G have been correlated with Isotope Stages 11-13, extending the age range of Acheulo-Yabrudian to 400-500 ka. Therefore, the Zuttiyeh human fossil is most likely bracketed to between 500 and 200 ka.

[3] The manuscript entitled *A comprehensive morphometric analysis of the frontal and zygomatic bone of the Zuttiyeh fossil from Israel*, written by Sarah E. Freidline, Philipp Gunz, Ivor Janković, Katerina Harvati, and Jean-Jacques Hublin has been published in the *Journal of Human Evolution* Volume 62, Issue 2, February 2012, Pages 225-241.

Since its discovery, the taxonomic and phylogenetic interpretation of the Zuttiyeh fossil has been contentious (for a detailed review see Sohn and Wolpoff, 1993) and influenced by revised and improved dating of the West Asian fossil hominin record and individual and historic perspectives concerning the tempo and mode of later human evolution. At the time of its discovery both the archaeological context of the fossil and the geological antiquity of the site were unclear. Many of the earliest studies incorporating the Zuttiyeh fossil identified morphological similarities to Neanderthals (Keith, 1927; Hrdlička, 1930; McCown and Keith, 1939; Weidenreich, 1943); however, the definition of Neanderthal varied among researchers. For example, Hrdlička (1930) suggested that the fossil showed a strong resemblance to the Asian Early Pleistocene Zhoukoudian E1 cranium, which he believed was a Neanderthal. McCown and Keith (1939) regarded Tabun 1 and Skhul 5 to be Neanderthals of the same population, with Zuttiyeh being more similar to Tabun 1. Weidenreich (1943) stressed its affinities to Skhul 5, which he considered to be an "advanced Neanderthal" intermediate between more "primitive Neanderthals", including Kabwe, Saccopastore, Steinheim, Tabun and Qafzeh, and anatomically modern humans. Additionally, Coon (1963) regarded Zuttiyeh as a possible descendant of a central European Neanderthal such as Krapina or Ehringsdorf. Suzuki and Takai (1970) concluded that Zuttiyeh's morphology was more archaic than the Amud male and most similar to Shanidar 1 and Tabun 1.

Once it became apparent that the Zuttiyeh fossil was actually older than many of the West Asian fossil hominins yet discovered, its interpretation as a Neanderthal relative became less common. Vandermeersch (1989) saw it as transitional between *H. erectus* and the West Asian modern humans (e.g., Skhul and Qafzeh) with no special relationship to Neanderthals, while others (Smith et al., 1989; Trinkaus, 1989; Simmons et al., 1991) interpreted it as a generalized ancestor of all Late Pleistocene West Asian hominins (e.g., Amud, Tabun, Shanidar, Skhul and Qafzeh).

Sohn and Wolpoff (1993) concluded that Zuttiyeh neither expressed uniquely Neanderthal nor modern human features, but instead retained many features similar to those of East Asian

hominins, being particularly similar to the early Middle Pleistocene specimens from Zhoukoudian (e.g., Zhoukoudian 11 and 12). They argued that Zuttiyeh provided a link between East and West Asian hominins, invalidating a unique African origin of modern humans around 200 ka or earlier. More recently, a cladistic analysis placed Zuttiyeh as a sister group to Skhul and these specimens as a sister group to modern humans, and concluded that it is the oldest known *H. sapiens sapiens* (Zeitoun, 2001). Finally, Rightmire's (2009) craniofacial measurements grouped it in a paleocommunity, or *p-deme*, within *H. heidelbergensis* along with Bodo, Elandsfontein, Kabwe, Ndutu, Eyasi, and Omo 2.

Current opinion regarding the phylogenetic relationships between Middle to Late Pleistocene hominins in Western Asia can be divided into three general groups according to the perceived extent of admixture between archaic and modern humans in this region. One view supports complete admixture between the groups and a single species model (e.g., Frayer et al., 1993; Sohn and Wolpoff, 1993; Arensburg and Belfer-Cohen, 1998). Arensburg and Belfer-Cohen (1998) propose that there was regular gene flow between Africa and Asia and that the West Asian hominins represent a continuous chronological sequence from Zuttiyeh to *H. sapiens*. Correspondingly Frayer et al. (1993) and Sohn and Wolpoff (1993) favor West Asian hominins as one species along with all post *H. habilis* specimens, with an Asian rather than African origin. On the opposite end of the spectrum are those who recognize the presence of two species in the Near East: Neanderthals from Shanidar, Amud, Tabun (C1), Kebara (Units X and XII), and Dederiyeh, early *H. sapiens* from Skhul and Qafzeh (levels V-XXIV) and early Upper Paleolithic *H. sapiens* from Ksar Akil and Qafzeh (specimens 1 and 2) (e.g., Bar-Yosef, 1988, 1989; Vandermeersch, 1989). Supporters of this scenario recognize little to no admixture between archaic and modern humans. Lastly, some researchers (Smith, 1992; Trinkaus, 2005) advocate variable levels of admixture between African and Southwest Asian hominins. The assimilation model (Smith et al., 1989; Smith, 1992; Smith et al., 2005; Trinkaus, 2005) posits that anatomically modern humans emerged in Africa and migrated to

Southwest Asia before migrating to southern Asia and higher latitude Eurasia. Rather than replacing the archaic populations they encountered in Eurasia, some level of genetic exchange occurred between the indigenous archaic and the migrating population.

Most recently, the sequencing of the complete Neanderthal genome revealed that between 1 and 4% of the genomes of people in Eurasia are likely derived from Neanderthals (Green et al., 2010). These authors conclude that low levels of interbreeding between archaic and modern humans most likely occurred in the Near East, when modern humans first left sub-Saharan Africa and before they expanded into Eurasia. However, these authors also suggest that ancient population substructuring within Africa could explain their results (see also Gunz et al., 2009a; Wall et al., 2009). Hodgson et al. (2010) propose a third scenario in which admixture occurred between Neanderthals and modern humans around 100 ka and then for climatic reasons modern humans retreated back to Africa, severing contact with Neanderthals. They argue that the presence of Neanderthal DNA in Europeans and Asians could be explained by founder effects during range expansion, and that traces of Neanderthal DNA may be present in unsampled modern Africa populations.

The geographic position of the Zuttiyeh fossil in combination with its probable Middle Pleistocene date makes it an interesting specimen for understanding aspects of later human evolution, including craniofacial morphological variability in Pleistocene human evolution and migration routes between Africa and Eurasia. Here we use three dimensional geometric morphometric methods to quantify the frontal and zygomatic bone morphology of the Zuttiyeh fossil using landmarks and semilandmarks. We apply multivariate statistical analyses to identify which Pleistocene group it is most morphologically similar to: *H. erectus s.l.*, *H. heidelbergensis s.l.*, *H. neanderthalensis*, transitional *H. sapiens*, early *H. sapiens*, Upper Paleolithic *H. sapiens* or recent *H. sapiens*. One of the major advantages of 3-D geometric morphometrics, and specifically curve and surface-semilandmarks, is that it allows researchers to quantify traits otherwise difficult to

measure using traditional linear or even landmark-based geometric morphometrics (e.g., zygomatic orientation and browridge morphology; see Harvati, 2003b; Gunz and Harvati, 2007; Freidline et al., 2008; Harvati et al., 2010; Freidline et al., 2010). Complex features can thus be quantified as continuous variables and included in multivariate statistical analyses.

5.2 Material and methods

5.2.1 Sample

This study includes a comprehensive sample of Early to Late Pleistocene fossil hominins and recent modern humans (Table 5.1). The fossil sample comprises all available Middle Pleistocene (780-128 ka) and West Asian specimens that preserve similar morphology to Zuttiyeh, as well as specimens that had been specifically compared to it in earlier studies. Additionally, some Early and Late Pleistocene fossils were included to provide a comparative framework. Table 5.1 lists the thirty-four fossils, their broad geographical origin, chronology and their attribution to taxonomic groups: *H. erectus s.l.* (N = 4), *H. heidelbergensis s.l.* (N = 6), *H. neanderthalensis* (N = 9) and *H. sapiens* (N = 235). Although we recognize the taxonomy of the Early and Middle Pleistocene groups as controversial, these divisions have been supported in various studies (e.g., *H. erectus s.l.*: Rightmire, 1998a; Asfaw et al., 2002; Antón, 2002, 2003; Potts et al., 2004; Baab, 2008; *H heidelbergensis s.l.*: Stringer, 1983; Rightmire, 1998b, 2008; Harvati, 2009b; Harvati et al., 2010). These prior group designations affect the mean shape calculations and the discriminant function analysis, but not the principal component analysis nor the nearest neighbor computations (see below). The recent modern human sample is composed of only adult individuals from fourteen geographic populations spanning six continents and is listed in Table 2.3.

Table 5.1 Specimens, abbreviation (Ab.) chronology and classification used in the analysis. The classification was only used for the DFA analysis and to calculate group means (see text).

Specimen	Ab.	Chronology	Classification
Early Pleistocene: Africa			
ER 3733	ER3733	1.75 Ma (Feibel et al., 1989)	*H. erectus s.l.*
ER 3883	ER3883	1.50 Ma (Feibel et al., 1989)	*H. erectus s.l.*
Early Pleistocene: Asia			
Sangiran 17*	S17	1.50 – 1.02 Ma (Larick et al., 2001; Antón, 2003; Antón and Swisher, 2004); > 790 ka (Hyodo et al., 2011)	*H. erectus s.l.*
Middle Pleistocene: Africa			
Bodo	Bd	ca. 600 ka (Clark et al., 1994)	*H. heidelbergensis s.l.*
Kabwe	Kb	700 – 400 ka (Klein, 1994)	*H. heidelbergensis s.l.*
Middle Pleistocene: Europe			
Arago 21*	Ar	600 – 350 ka (Cook et al., 1982; Falguères et al., 2004)	*H. heidelbergensis s.l.*
Petralona	Pt	670 – ca. 250 ka (Harvati et al., 2009)	*H. heidelbergensis s.l.*
Sima de los Huesos 5*	Sm5	ca. 530 ka (Bischoff et al., 2007)	*H. heidelbergensis s.l.*

Table 5.1 Continued

Middle Pleistocene: Asia			
Dali*	Dl	230 – 180 ka (Chen and Zhang, 1991)	*H. heidelbergensis s.l.*
Zhoukoudian 12 (E1)*	Z12	550 – 520 ka; ca. 580 ka; ca. 770 ka (Grün et al., 1997; Antón, 2003; Shen et al., 2009)	*H. erectus s.l.*
Zuttiyeh*	Zt	ca. 350, 500-200 ka (Huxtable, 1990; Bar-Yosef, 1992; Mercier et al., 1995; Mercier and Valladas, 2003)	Unclassified
Late Middle-Late Pleistocene: Africa			
Florisbad*	Fl	290-230 ka (Grün et al., 1996)	Unclassified
Jebel Irhoud 1	I1	ca. 160 ka (Smith et al., 2007)	Unclassified
Late Middle-Late Pleistocene: Europe			
Gibraltar 1	Gb1	71 – 50 to 35 ka (Klein, 1999)	*H. neanderthalensis*
Guattari	Gt	ca. 50 ka (Schwarcz et al., 1991)	*H. neanderthalensis*
Krapina 3	Kr3	140 – 120 ka (Rink and Schwarcz, 1995)	*H. neanderthalensis*
Krapina 6	Kr6	140 – 120 ka (Rink and Schwarcz, 1995)	*H. neanderthalensis*

Table 5.1 Continued

La Chapelle-aux-Saints	LCh	56 – 47 ka (Grün and Stringer, 1991)	*H. neanderthalensis*
La Ferrassie 1	LF1	71 – 50 to 35 ka (Klein, 1999)	*H. neanderthalensis*
Late Middle-Late Pleistocene: Asia			
Amud 1*	Am1	ca. 50 ka (Rink et al., 2001)	*H. neanderthalensis*
Liujiang*	Ljg	139 – 111 ka (Shen et al., 2002)	Unclassified
Qafzeh 6	Q6	135 – 100 ka (Grün et al., 2005)	Unclassified
Shanidar 1*	Sh1	ca. 50 ka (Trinkaus, 1983)	*H. neanderthalensis*
Shanidar 5*	Sh5	ca. 50 ka (Trinkaus, 1983)	*H. neanderthalensis*
Skhul 5	Sk5	135 – 100 ka (Grün et al., 2005)	Unclassified
Upper Paleolithic Eurasian modern humans			
Brno 2*	Brn2	ca. 23 ka (Holt and Formicola, 2008)	Unclassified
Cro-Magnon 1	Cr1	28 – 27 ka (Holt and Formicola, 2008)	Unclassified
Mladeč 1	Ml1	ca. 31 ka (Holt and Formicola, 2008)	Unclassified
Předmostí 3*	Pr3	ca. 17 ka (Svoboda, 2008)	Unclassified
Předmostí 4*	Pr4	ca. 17 ka (Svoboda, 2008)	Unclassified

Table 5.1 Continued

Oberkassel 1	Ob1	ca. 12 ka (Street, 2002)	Unclassified
Oberkassel 2	Ob2	ca. 12 ka (Street, 2002)	Unclassified
Zhoukoudian 101*	Zh101	ca. 33 – 13 (Chen et al., 1989; Hedges et al., 1992; Brown, 1992)	Unclassified
Zhoukoudian 102*	Zh102	ca. 33 – 13 (Chen et al., 1989; Hedges et al., 1992; Brown, 1992)	Unclassified
Recent modern humans			
Africa (n = 44): Egypt (5); South Africa (34); Tanzania (5)			*H. sapiens*
Asia (n = 10): Mongolia (5); Thailand (5)			*H. sapiens*
Australia (n = 10)			*H. sapiens*
Europe (n = 58): Austria (50); Belgium (2); Czech Republic (6)			*H. sapiens*
North America (n = 108): United States (100); Mexico (8)			*H. sapiens*
South America (n = 5): Argentina			*H. sapiens*

*casts

5.2.2 Landmark data

The metric data set was designed to include all of the preserved morphology in the Zuttiyeh specimen (Fig. 5.1).

Figure 5.1 291 landmarks and semilandmarks digitized on all specimens, red: biological landmarks; blue: curve-semilandmarks; yellow: surface-semilandmarks. Biological landmarks are abbreviated. The full names are listed in Table 5.2.

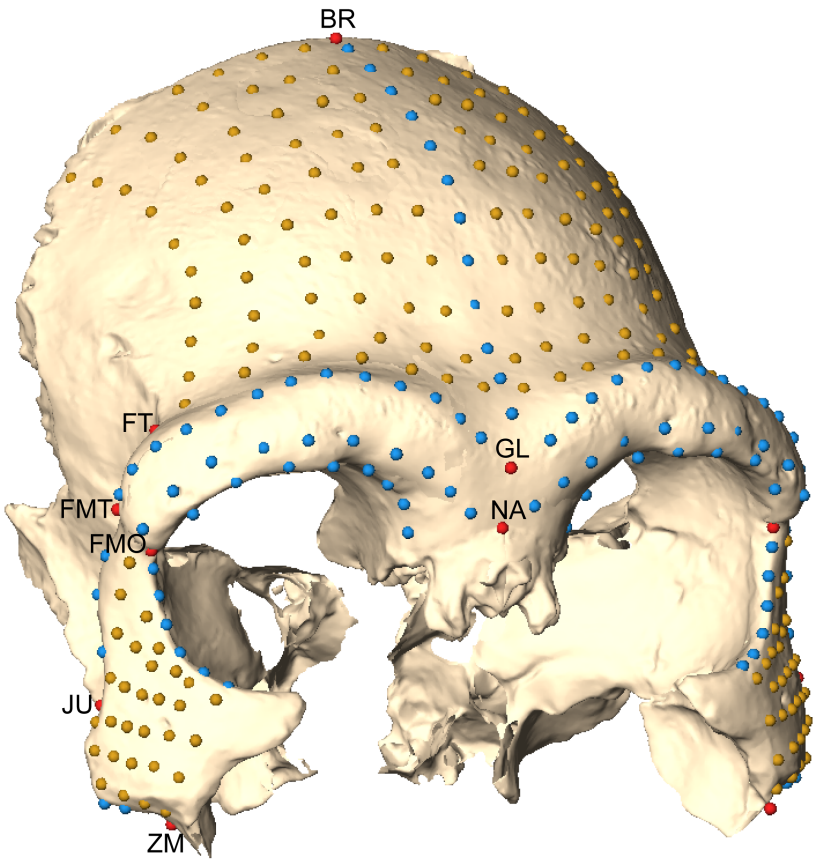

Table 5.2 Biological landmarks used in the analysis.

Landmark	Abbreviation
Bregma	BR
Glabella	GL
Frontomalare orbitale	FMO
Frontomalare temporale	FMT
Frontotemporale	FT
Jugale	JU
Nasion	NA
Zygomaxillare	ZM

5.2.3 Missing data reconstruction

Vandermeersch (1981, 1989) noted that Zuttiyeh's supraorbital torus was divided into medial and lateral components like in modern humans, especially on the right side. However, Simmons and her co-authors (1991) argued that the depression on the right side of the torus is a pathological lesion and does not represent a modern human-like biological separation of the browridge into two components. In order to correct for this possible pathology, we reflected the non-pathological left browridge and merged it to the existing right frontal bone (see Fig. 5.2). Additionally, a large depression is present on the right side of the posterior frontal bone. We repaired this by mirror-imaging aspects of the left posterior frontal bone and merged it to the right frontal bone. Lastly, we reflected the entire right zygomatic bone and merged it to the existing frontal bone creating a complete left zygomatic bone in correct anatomical orientation. Figure 5.2 compares the original cast of Zuttiyeh (Fig. 5.2a) to our reconstruction (Fig. 5.2b).

Figure 5.2 Virtual reconstruction of the Zuttiyeh fossil; a) the original cast of Zuttiyeh which includes two pathologies indicated by the arrows, a possible deformation on the right browridge and a depression on the right posterior frontal bone; b) the virtual reconstruction that was measured and used in the analyses. The left browridge was mirror-imaged and merged onto the right frontal bone indicated in blue, some of the left posterior frontal was mirror-imaged and merged onto the right posterior frontal indicated in blue, and the entire right zygomatic was mirror-imaged and merged onto the left frontal in correct anatomical orientation indicated in transparent gray.

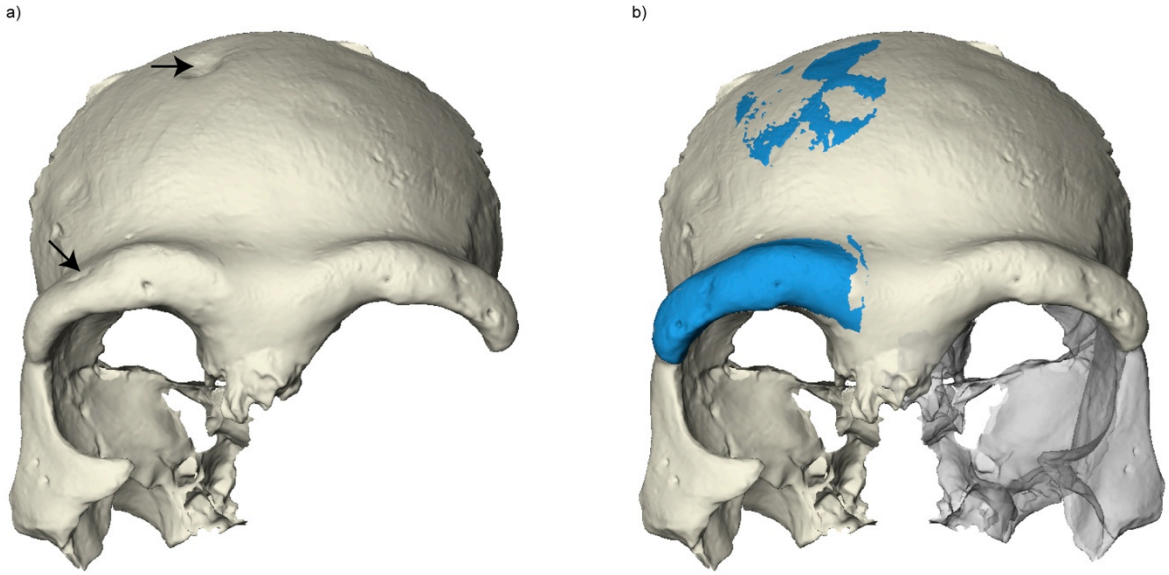

5.2.4 Analytical methods

A principal component analysis (PCA) of all 291 landmarks and semilandmark shape coordinates was performed in order to examine the overall shape variation in the frontal and zygomatic bone and the distribution of each group in shape space. A PCA was also performed in form space (Mitteroecker et al., 2004; Mitteroecker and Gunz, 2009). To determine which individuals are most similar in shape to Zuttiyeh, nearest neighbors in shape space were calculated using Procrustes distances. In order to estimate the range of variation within each taxonomic group (see Table 1 for groupings) and to provide a context for the individual distances between Zuttiyeh

and its nearest neighbors, Procrustes distances were calculated between all possible pairs of individuals within each group.

A discriminant function analysis (DFA) was computed to assess how well the frontal and zygomatic bone morphology separates fossil and modern human groups. The groups were defined *a priori* according to the population grouping shown in Table 1. Zuttiyeh as well as all transitional (Jebel Irhoud 1 and Florisbad), early (Skhul 5, Qafzeh 6 and Luijiang) and Upper Paleolithic *H. sapiens* were treated as individuals with unknown group affinities to be classified by posterior probabilities.

Zuttiyeh was classified by posterior probability using four *a priori* groups: *H. erectus s.l., H. heidelbergensis s.l.*, *H. neanderthalensis* and *H. sapiens* (Table 1). The transitional (Jebel Irhoud 1, Florisbad) and early anatomically modern human specimens (Qafzeh 6, Skhul 5 and Luijiang), and all Upper Paleolithic crania were also classified via posterior probability. Additionally, permutations tests (10,000 random permutations) using the Procrustes distances between the mean group shapes were performed to test for significant shape differences between groups.

To better illustrate the shape differences between Zuttiyeh, *H. erectus s.l.*, *H. heidelbergensis s.l.*, Neanderthals and modern humans, we generated Procrustes mean shapes for each of the aforementioned groups. We then used the semilandmark and landmark data set to warp the surface of Zuttiyeh to the mean of each group in Avizo.

5.3 Results

5.3.1 Principal component analysis

Figure 5.3 displays the first two PCs in shape space, which together account for 61.7% of total shape variation. Convex hulls are drawn for *H. erectus s.l.*, *H. heidelbergensis s.l.*, *H.*

neanderthalensis and *H. sapiens*. The pattern in the first two PCs primarily reflects a contrast between archaic (all fossils excluding the Upper Paleolithic specimens) and modern human morphology. The Upper Paleolithic humans, except for Zhoukoudian Upper Cave 101 and 102, fall within the range of modern human variation. Zuttiyeh, as well as Jebel Irhoud 1 and Florisbad, cluster with the Neanderthals, Skhul 5 and Qafzeh 6 plot between the Neanderthals and modern humans, and Shanidar 5 falls within the range of modern human variation. *Homo heidelbergensis s.l.* and *H. erectus s.l.* cluster separately from all other groups.

Figure 5.3 PCA in shape space. PC 1 represents 31.9 % of total shape variation; PC 2 represents 29.8 % of total shape variation. Convex hulls are drawn for *H. erectus s.l.*, *H. heidelbergensis s.l.*, *H. neanderthalensis* and recent *H. sapiens*; a) mean shape at the negative end of PC 1; b) mean shape at the positive end of PC 1; c) mean shape at the positive end of PC2; d) mean shape at the negative end of PC 2.

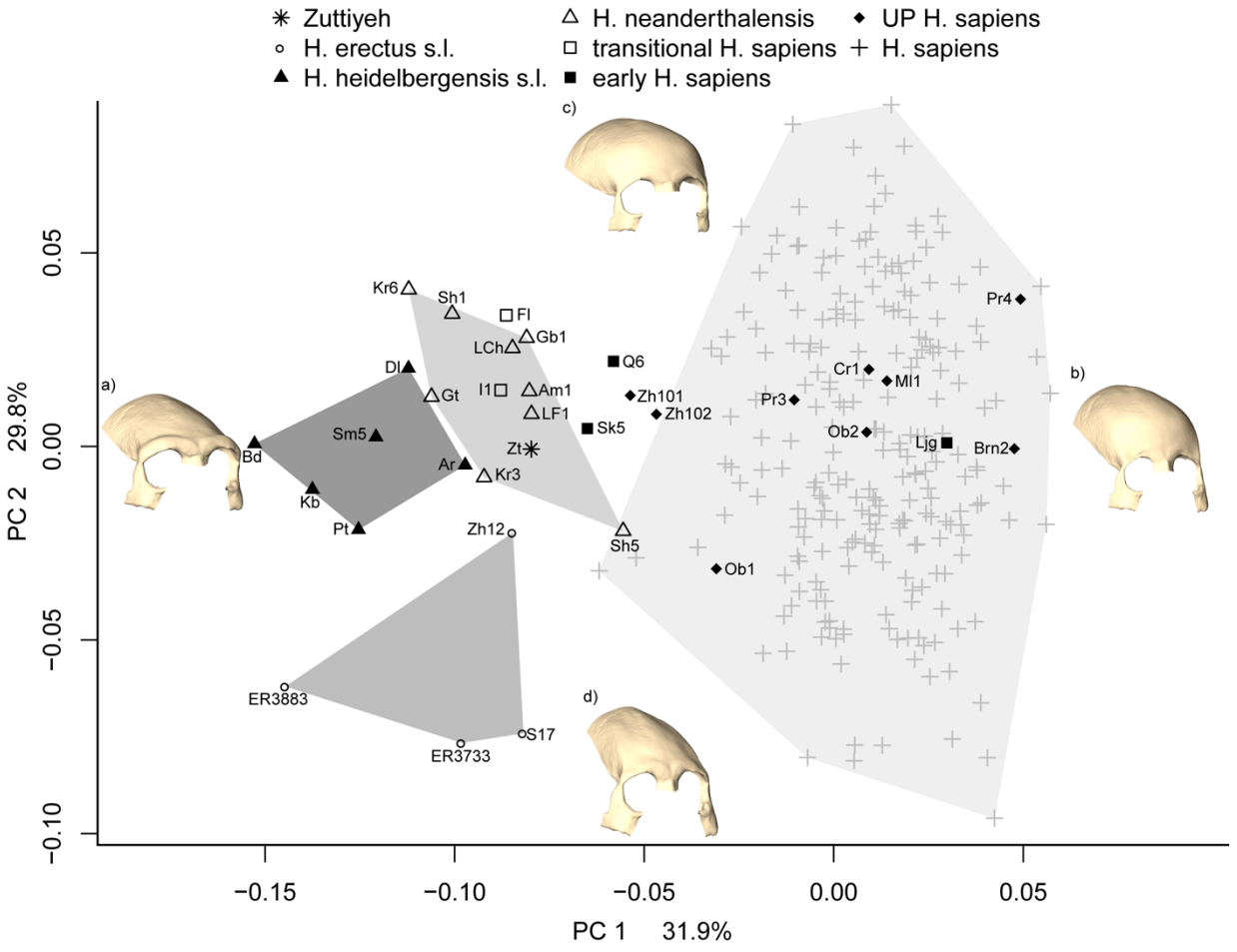

The shape changes along the PC axes are included in the PCA plot (see Fig. 5.3a-d). PC 1 is primarily associated with the overall shape of the frontal bone and the robusticity of the browridge (Figs. 5.3a and b). Individuals at the negative end of PC 1 have a low, receding frontal bone combined with a wide and projecting browridge. Among the fossils, the *H. erectus s.l.* and *H. heidelbergensis s.l*. specimens exhibit the most pronounced browridges and most receding frontal bones. This is especially true for Bodo and ER 3883, which plot at the extreme negative end of PC 1. Skhul 5, Qafzeh 6, Shanidar 5 and Zhoukoudian 101 and 102 are intermediate in this morphology between the more primitive *H. erectus s.l./H. heidelbergensis s.l.* and recent and Upper Paleolithic *H. sapiens*.

Along PC 2, the main shape changes are in frontal bone width and shape and zygomatic size (Fig. 5.3c and 5.3d). Recent modern humans express more variability in these features than the fossil hominins; the European individuals have the widest and most rounded frontal bones plotting at the positive end of PC 2 (Fig. 5.3c) and the North American populations exhibit narrower frontals, falling at the negative end of PC 2 (Fig. 5.3d). Additionally the size and orientation of the zygomatic bone changes along PC 2; individuals that plot at the negative end of PC 2 express much larger zygomatics that are angled more obliquely in the transverse plane. This angle is most apparent along the zygomaxillary arch and the medial section of the zygomatic bodies in Figure 5.3d.

We computed nearest neighbors based on inter-individual Procrustes distances and Zuttiyeh was most similar to Shanidar 5 (Procrustes distance: 0.051), a Near East Neanderthal, Arago 21 (0.061), a European Middle Pleistocene hominin included in the taxon *H. heidelbergensis s.l.*, and Skhul 5 (0.063), an early anatomically modern human. Figure 5.4 plots the Procrustes distances between Zuttiyeh and its ten nearest neighbors in shape space, as well as the Procrustes distances between all possible pairs of individuals within each *a priori* group (*H. erectus s.l.*, *H. heidelbergensis s.l.*, *H. neanderthalensis*, *H. sapiens*). The distance between Zuttiyeh and Shanidar 5 is

well below the median for each group. Except for the *H. erectus s.l.* median, the ranges and medians for each of the *a priori* groups are similar.

Figure 5.4 Procrustes distances between Zuttiyeh and its ten nearest neighbors in shape space and comparisons of intraspecific ranges of Procrustes distances for *H. erectus s.l.*, *H. heidelbergensis s.l.*, *H. neanderthalensis* and *H. sapiens*. The ranges were calculated by computing the Procrustes distances between all possible pairs within the *a priori* groupings shown in Table 5.1. The box plot illustrates the median value, first and third quartiles, and extreme values. Full names of the fossil specimens are listed in Table 5.1.

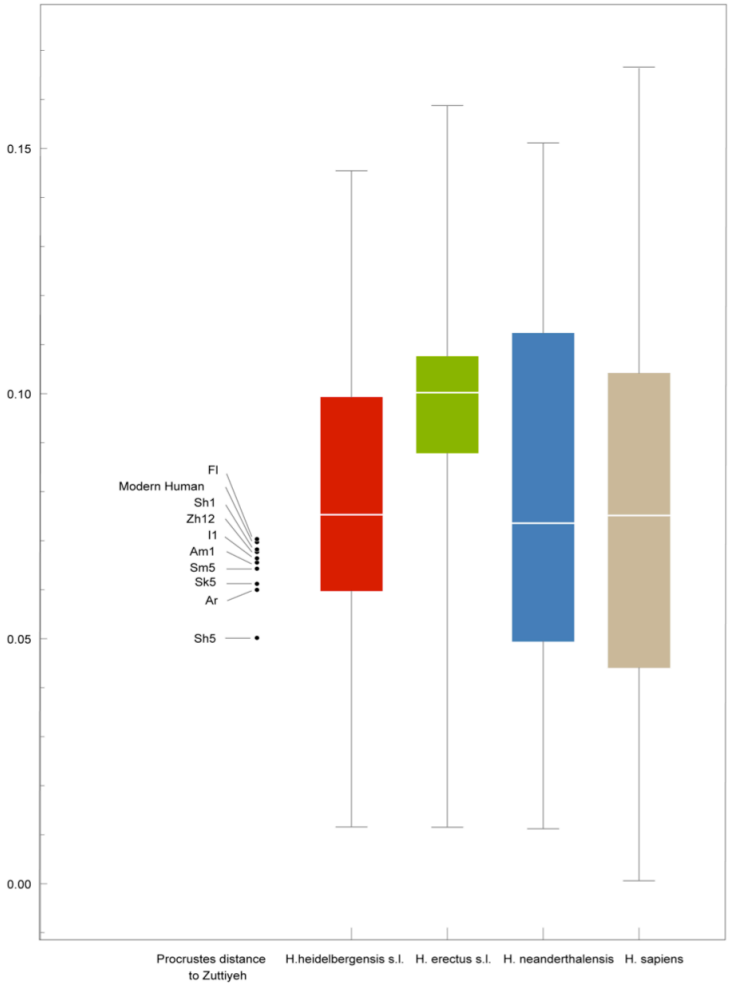

PC 1 (Figs. 5.5 and 5.6) in Procrustes form space (36.4% of total form variation) is highly correlated ($r \cong -0.94$) with log centroid size. Allometric trends (black lines in Figs. 5.5 and 5.6) for *H.*

erectus s.l., H. heidelbergensis s.l., *H. neanderthalensis*, and recent *H. sapiens* were computed by regressing shape on log centroid size. The Middle Pleistocene archaic humans, like Bodo, Petralona and Kabwe, exhibit the largest frontal and zygomatic bones. Like in the first principal component of shape space, PC 2 (21.1 % of total form variation) in form space mainly illustrates a separation between modern and archaic humans. Zuttiyeh plots close to Zhoukoudian 12, its nearest neighbor in form space, along the *H. erectus s.l.* size trend and near the boundary of modern human variation (denoted by the convex hull). In Figure 5.6 we plotted PC 1 against PC 3 (17.0% of total form variation) in form space. In this dimension, Zuttiyeh appears closer to the *H. heidelbergensis s.l.* and Neanderthal allometric trends and within the range of modern human variation.

Figure 5.5 PCA in form space (including the centroid size of each specimen). PC 1 represents 36.4% of total form variation; PC 2 represents 21.1% of total form variation. Convex hulls are drawn for *H. erectus s.l.*, *H. heidelbergensis s.l.*, *H. neanderthalensis* and recent *H. sapiens* and the size trends, calculated by regressing shape on log centroid size, are represented by the black lines.

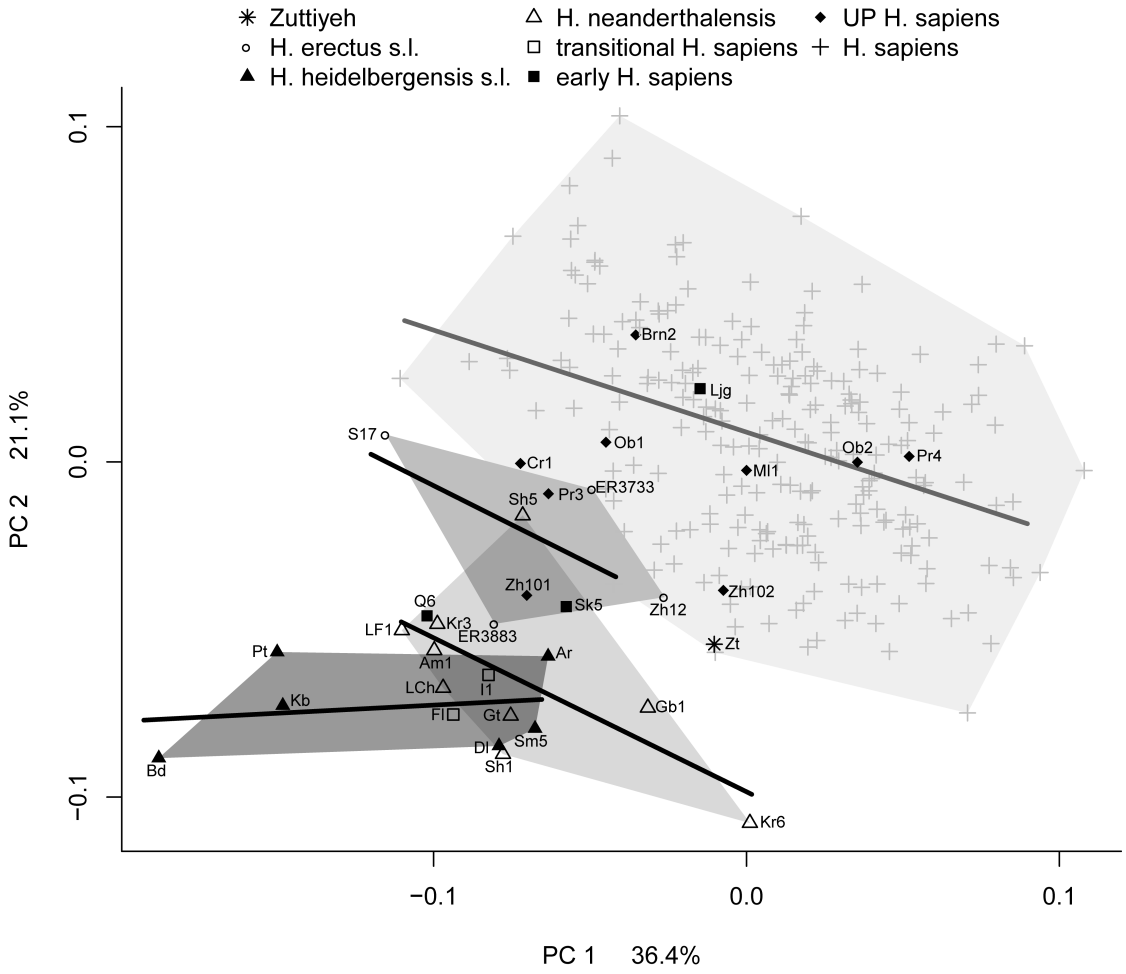

Figure 5.6 PCA in form space (including the centroid size of each specimen). PC 1 represents 36.4% of total form variation; PC 3 represents 17.0% of total form variation. Convex hulls are drawn for *H. erectus s.l.*, *H. heidelbergensis s.l.*, *H. neanderthalensis* and recent *H. sapiens* and the size trends, calculated by regressing shape on log centroid size, are represented by the black lines.

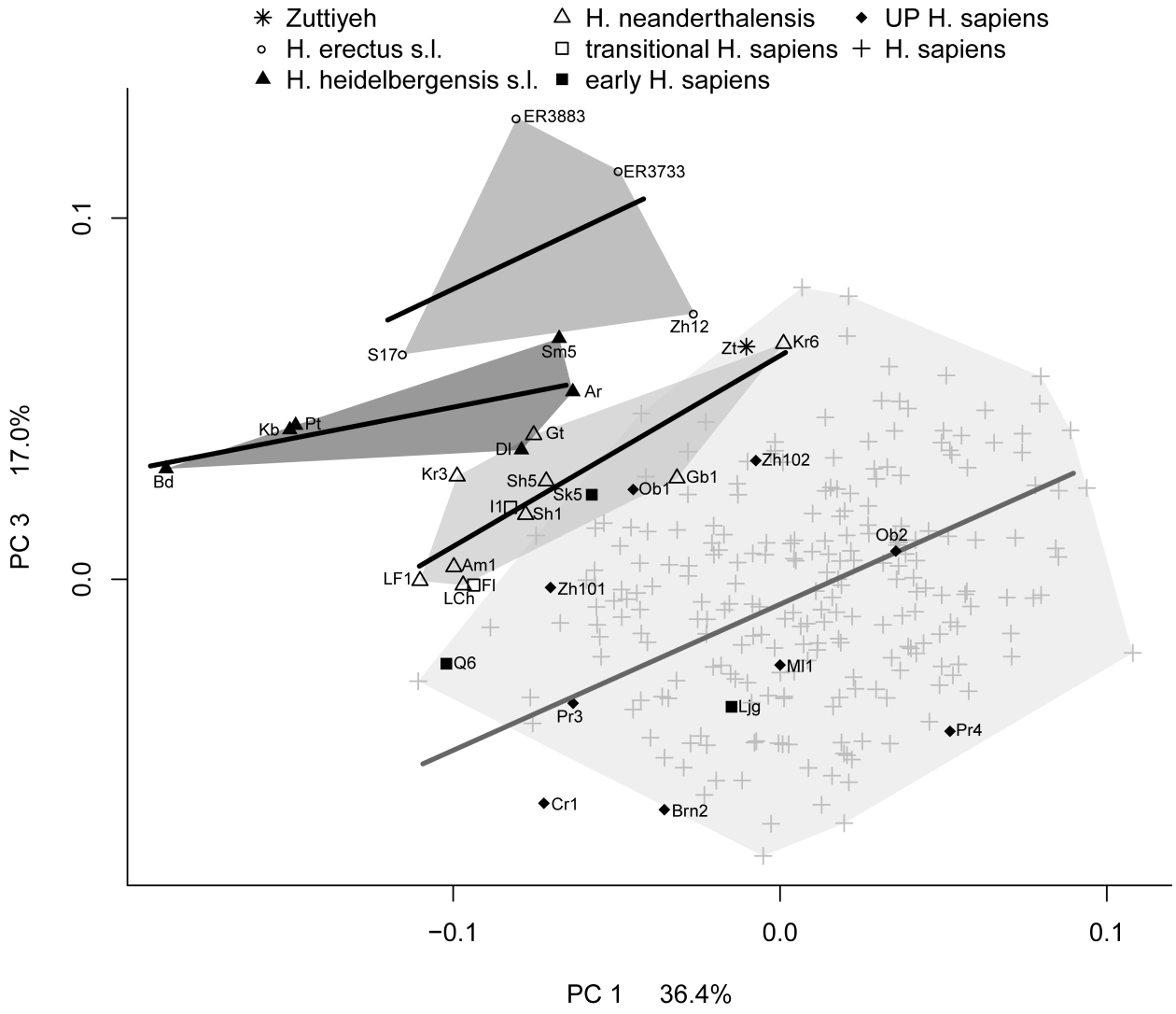

5.3.2 Discriminant function analysis

We performed a DFA (Fig. 5.7) computed in the subspace of the first eight principal components of shape space. As outlined in the methods section, the number of PCs that we report on here is an arbitrary choice that was made because together they represent nearly 90% of total

shape variation. Modern humans clearly separate from the archaic groups and overlap occurs between *H. heidelbergensis s.l.* and *H. neanderthalensis*, and slightly between *H. erectus s.l.* and *H. neanderthalensis*. Zuttiyeh, Jebel Irhoud 1, Dali and Bodo fall within the Neanderthal range, while Florisbad plots outside of all group ranges. Qafzeh 6, Skhul 5, and Zhoukoudian Upper Cave 101 plot adjacent to one another between archaic and modern humans and all Upper Paleolithic *H. sapiens* cluster with the recent modern humans except for Zhoukoudian Upper Cave 101 (see also Harvati, 2009b). We tested the stability of the DFA results by including between five and sixteen principal components of shape space. In all iterations overlap variably occurred between Neanderthals, *H. heidelbergensis s.l.* and *H. erectus s.l.*; modern and Upper Paleolithic humans always clustered separately from the archaic hominins. The position of Zuttiyeh changed very little, always plotting with or near the Neanderthal sample.

Figure 5.7 Discriminant function analysis using the first eight principal components of shape space, representing 87.3 % of total shape variation. Convex hulls are drawn for *H. erectus s.l.*, *H. heidelbergensis s.l.*, *H. neanderthalensis* and recent *H. sapiens*. *A priori* groupings are listed in Table 5.1.

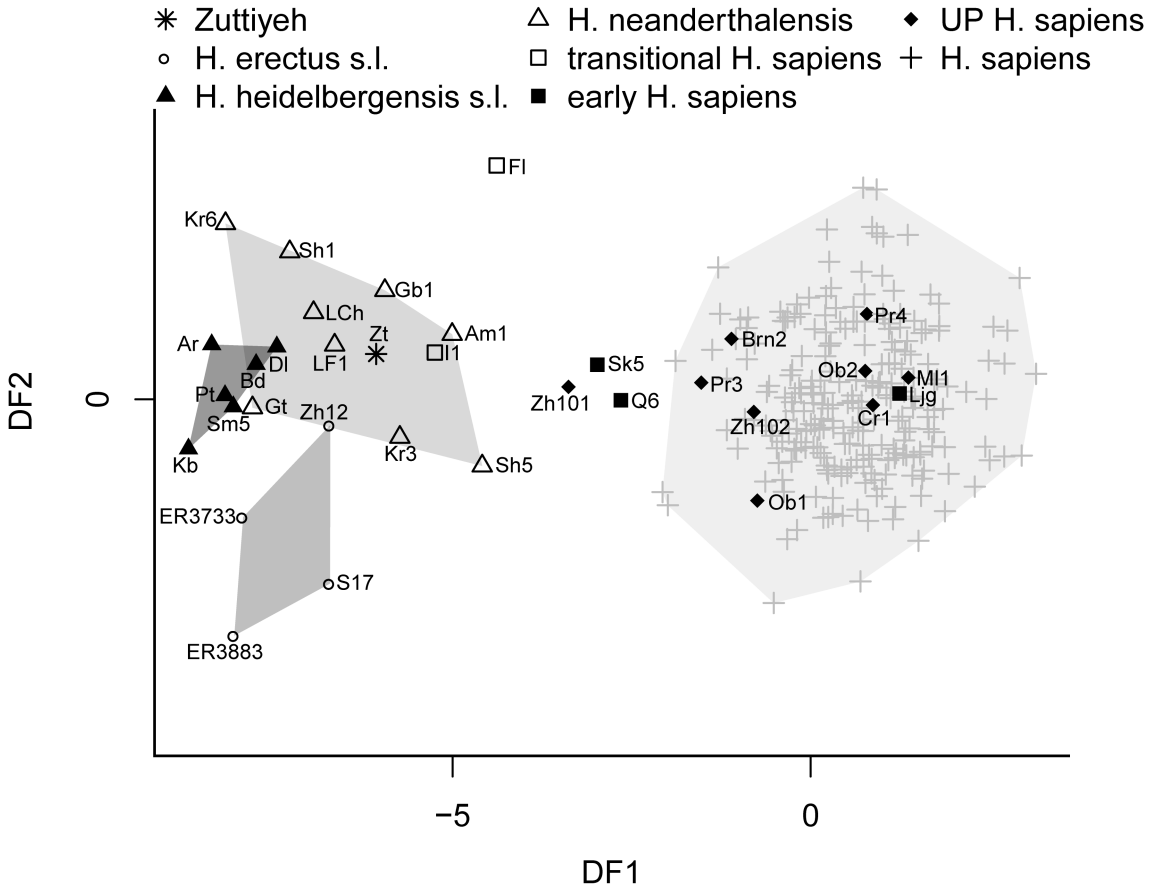

Based on posterior probabilities Zuttiyeh either classified as *H. heidelbergensis s.l.* or as a Neanderthal. Depending on how many principal components were used, the accuracy of correctly classifying fossils ranged from 55% to 73%. Shanidar 5 was most frequently classified as *H. erectus s.l.* and Arago 21 was always misclassified as *H. neanderthalensis* (it was originally assigned to *H. heidelbergensis s.l.*). Additionally, many fossils fluctuated between the three archaic groups (*H. erectus s.l.*, *H. heidelbergensis s.l.* and *H. neanderthalensis*). The result of the permutation test (Table 5.3) indicated that the frontal and zygomatic morphology of *H. sapiens* was significantly different (p

< 0.002) from all groups (*H. erectus s.l.*, *H. heidelbergensis s.l.*, and *H. neanderthalensis*) and that among the fossil groups only *H. neanderthalensis* and *H. erectus s.l.* was significantly different (p < 0.013) from one another.

Table 5.3 Procrustes distances between mean configurations (upper) and significance values (lower). P values were computed using permutation tests on Procrustes distances from the mean. Significant values are denoted in bold.

	H. heidelbergensis s.l.	*H. erectus s.l.*	*H. neanderthalensis*	*H. sapiens*
H. heidelbergensis s.l.	___	0.0694	0.0487	0.1359
H. erectus s.l.	0.2167	___	0.0818	0.1306
H. neanderthalensis	0.3269	**p < 0.0130**	___	0.1025
H. sapiens	**p < 0.0001**	**p < 0.0002**	**p < 0.0001**	___

5.3.3 Visualization – Procrustes superimposition

Zuttiyeh's nearest neighbor in terms of Procrustes distance is Shanidar 5. To illustrate the resemblances between these specimens we superimposed the two individuals (Fig. 5.8a-c). In Figure 5.8, Zuttiyeh is in white and Shanidar 5 is in semitransparent blue; therefore the overlapping areas are represented by the lighter shade of blue. Apart from the long anterior-posterior length of the frontal bone of Shanidar 5, these two specimens have similar frontal widths and frontal bone shapes. They both express a vertical frontal squama that then becomes more convex posteriorly. Shanidar 5 has a deeper medial post-toral sulcus and Zuttiyeh has a flatter glabellar region. Zuttiyeh's mid and upper face is entirely more robust than Shanidar 5 in the following ways: its nasal roots (i.e. area around nasion) project more anteriorly; it has a relatively greater inter-orbital breadth; it has a entirely larger and more projecting browridge; and the frontal process of the zygomatic bone and the posterior margin of the zygomatic body (i.e. *fascia temporalis*) are

relatively wider. The angle at which the zygomatic bone (at the frontal process) meets the frontal bone and the rotation of the zygomatic body are similar between the two specimens.

Zuttiyeh's next nearest neighbor in shape space is Arago 21. In Figure 5.8d-f we superimposed the two individuals; Arago 21 is in red and the overlapping areas are represented by the lighter shade of red. Zuttiyeh's frontal bone is more convex and its frontal squama is more vertical. The width of the frontal bone at frontotemporale is narrower in Zuttiyeh and its frontal bone becomes wider posteriorly. Zuttiyeh expresses a deeper post-toral sulcus region. The entire browridge and glabellar region of Arago 21 is slightly more projecting and is especially more robust at the lateral third. The orbital height is greater in Zuttiyeh, while the breadth and shape are similar between the two. Zuttiyeh has a wider inter-orbital breadth and its nasal root is more anteriorly projecting. The position of the zygomatic bone relative to the frontal bone is very similar. The frontal process of the zygomatic and the zygomatic body is larger and more robust in Arago 21 and the angle of the zygomatic at the medial margin (i.e. near the zygomaxillary suture) is more oblique indicative of its greater midfacial prognathism.

Figure 5.8 Procrustes superimpositions of Zuttiyeh on its nearest neighbors in shape space. Shape information is contained in the landmark and semilandmark data and everything in between these landmarks is interpolated. 5.8a-c (a – anterior perspective, b – superior, c – inferior): Zuttiyeh (white) superimposed on Shanidar 5 (blue), Zuttiyeh's nearest neighbor in shape space based on inter-individual Procrustes distances. 8d-f: Zuttiyeh (white) superimposed on Arago 21 (red), Zuttiyeh's second nearest neighbor in shape space based on inter-individual Procrustes distances.

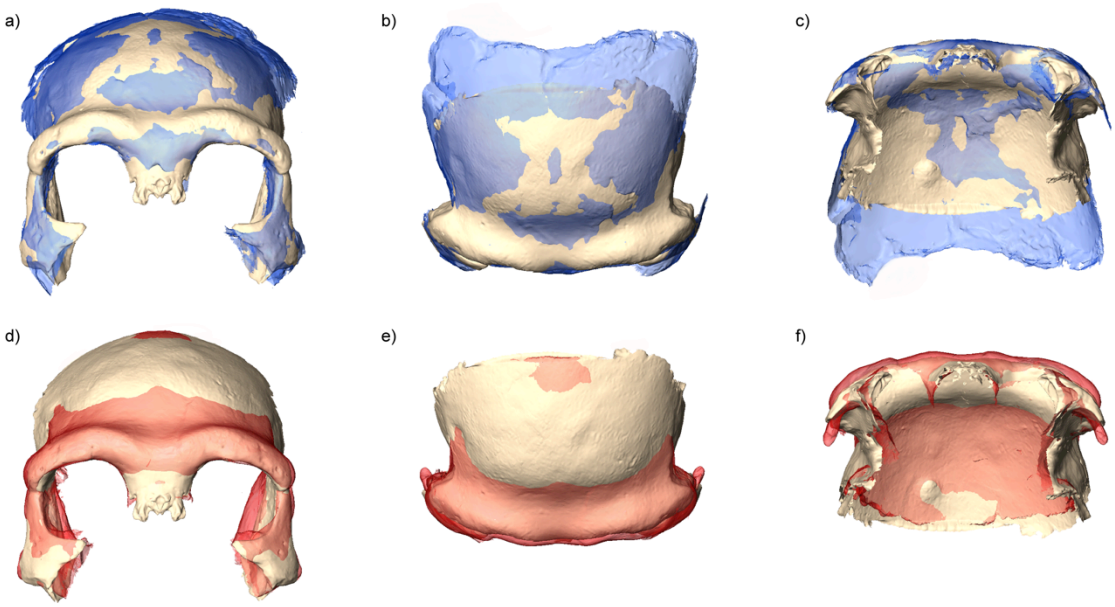

In Figure 5.9a-c we warped Zuttiyeh to the *H. erectus s.l.* mean, in green, and superimposed the two. The frontal bone in Zuttiyeh is more convex and wider. Zuttiyeh has a deeper post-toral sulcus and a wider inter-orbital breadth; the orbital height, breadth and shape are similar between the two. The zygomatic bone in Zuttiyeh is much smaller in all dimensions compared to *H. erectus s.l.* The angle of the zygomatic body is remarkably similar between the two (see Fig. 5.9c), however in Zuttiyeh the angle of the zygomatic at the medial margin (i.e. near the zygomaxillary suture) is more oblique or anteriorly projecting. Overall the mid and upper face is much more robust in *H. erectus s.l.*, which exhibits a more projecting browridge, glabellar region, and nasal root and larger zygomatic bone.

In Figure 5.9d-f we warped Zuttiyeh to the *H. heidelbergensis s.l.* mean, in red, and superimposed them. The frontal bone in Zuttiyeh is more convex and wider along the posterior half. The width at frontotemporale is narrower in Zuttiyeh. The overall browridge is much more robust and projecting in the *H. heidelbergensis s.l.* mean, especially in the medial third of the browridge and glabellar region. In both Zuttiyeh and the *H. heidelbergensis s.l.* mean, the nasal root is posterior to glabella; however it appears more extreme in *H. heidelbergensis* because its glabellar region is much more projecting than Zuttiyeh. Zuttiyeh has a deeper post-toral sulcus. Its orbital height, breadth and shape are similar to the *H. heidelbergensis s.l.* mean, but the inter-orbital breadth is slightly larger in the *H. heidelbergensis s.l*. mean. The zygomatic bones are nearly the same size. The angle of the frontal process of the zygomatic, where the zygomatic bone joins the frontal bone is very similar, but the frontal process of the *H. heidelbergensis s.l.* mean is much more robust and wider. The angle of the zygomatic body is different between the two; in the *H. heidelbergensis s.l*. mean the body is positioned posteriorly and is more sagitally rotated and in Zuttiyeh the zygomatic body is positioned anteriorly and is more coronally rotated.

In Figure 5.9g-i we warped Zuttiyeh to the Neanderthal mean, in blue, and superimposed them. Overall the frontal bone of Zuttiyeh is narrower and the posterior half is more convex. The width of the frontal bone at frontotemporale is nearly the same, but in the Neanderthal mean the frontal bone widens posterior to this region. The browridge shape is very similar between the two however in Zuttiyeh the lateral third of the browridge is much more robust. The Neanderthal glabellar region and nasal root is much more anteriorly projecting. In Zuttiyeh the glabellar region is flattened and nasion and the nasal root are posterior to glabella. Like the comparison to *H. heidelbergensis s.l*., Zuttiyeh has a deeper post-toral sulcus, the orbital height, breadth and shape are similar between the two, but the inter-orbital breadth is slightly larger in the Neanderthal mean. The frontal process of the zygomatic is more robust in Zuttiyeh. In the Neanderthal mean the zygomatic body is positioned posteriorly, rotated sagitally, and is flattened and retreating. In

Zuttiyeh the zygomatic body is positioned anteriorly and is rotated coronally. The Neanderthal zygomatic bones are smaller in all dimensions.

Lastly, in Figure 5.9j-l we warped Zuttiyeh to the modern human mean, in gray, and superimposed them. The modern human frontal bone is entirely more convex. They express a similar frontal bone width. The shape differences between the two are most pronounced in the mid and upper face. In Zuttiyeh all aspects of its browridge size and shape and glabellar region are more robust than modern humans. Zuttiyeh's orbital height and breadth and inter-orbital breadth are larger. Although the zygomatic body in modern humans and in Zuttiyeh are similar in height (superoinferior dimension), the frontal process and posterior margin of the zygomatic body is much more robust in Zuttiyeh. This latter region is wider (e.g., more flaring) and more coronally rotated in Zuttiyeh than in the modern human mean; however the angles of the medial margin of the zygomatic body where it approaches the zygomaxillary suture are similarly coronally rotated in both the modern human mean and Zuttiyeh.

Figure 5.9 Procrustes superimpositions of Zuttiyeh on mean shapes. 5.9a-c (a – anterior perspective, b – superior, c – inferior): Zuttiyeh (white) superimposed on the *H. erectus s.l.* mean (green); 5.9d-f: superimposed on the *H. heidelbergensis s.l.* mean (red); 5.9g-i: superimposed on the *H. neanderthalensis* mean (blue); 5.9j-l: superimposed on the modern human mean (gray).

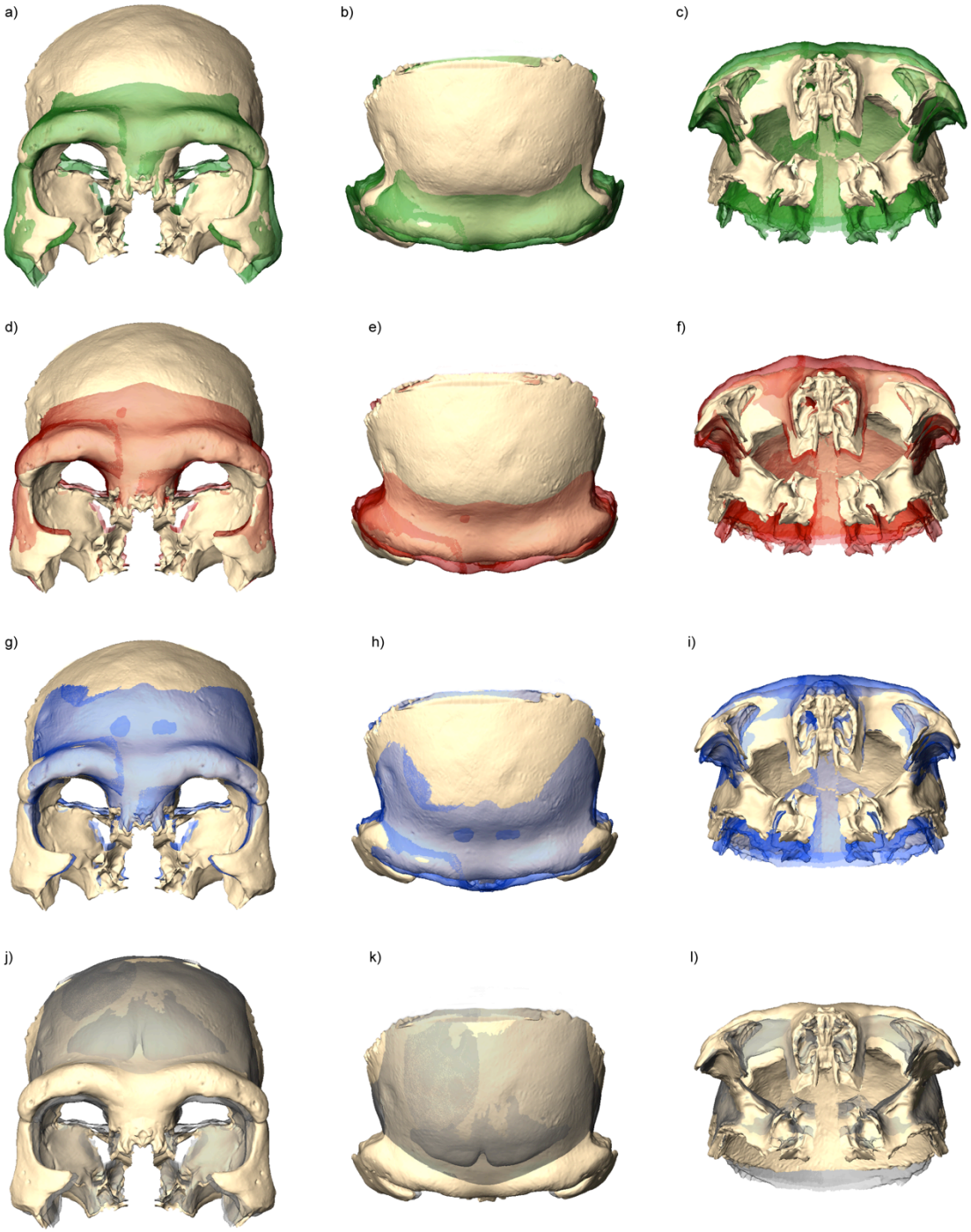

5.4 Discussion

The aim of this study was to assess the morphological affinities of the Zuttiyeh fossil. Semilandmark geometric morphometric methods were employed in order to quantify the overall morphology of its frontal and zygomatic bone, multivariate statistics were performed to analyze the general pattern of morphological variation in Pleistocene fossils and modern humans, and visualization techniques were used to compare both the subtle and gross morphological differences among individual fossils and group means.

5.4.1 Nearest neighbors

Earlier studies have suggested that Zuttiyeh shows a resemblance to fossils such as: Tabun 1 (McCown and Keith, 1939; Suzuki and Takai, 1970), Skhul 5 (Weidenreich, 1943), Ehringsdorf (Coon, 1963), Krapina (Coon, 1963), Zhoukoudian E1 (Hrdlička, 1930; Sohn and Wolpoff, 1993), Shanidar 1 (Suzuki and Takai, 1970), Shanidar 2 and 4 (Trinkaus, 1983) and Amud (Simmons et al., 1991). For various reasons (e.g., undiscovered fossils, different research questions, error in geological dates) most of these studies included a limited fossil sample, primarily consisting of Near Eastern hominins and European Neanderthals. Therefore Zuttiyeh's similarity to other Middle Pleistocene hominins has not been extensively explored.

Our results show that Zuttiyeh is morphologically most similar to Shanidar 5, a Near East Neanderthal, Arago 21, a European Middle Pleistocene hominin, and Skhul 5, an early *Homo sapiens*. The main morphological similarities between Zuttiyeh and Shanidar 5 are the width of the frontal bone, the shape of the frontal squama and the angle of the zygomatic body. Following the original reconstruction of Shanidar 5, Trinkaus (1982, 1983) noted that the unusual combination of a flat frontal bone and curved parietal bone, proportions similar only to Shanidar 1, may be due to artificial cranial deformation in these fossils. Because it was evident to Chech et al. (1999) that what

was purported to be the left lambdoid suture was actually the left squamous suture of the parietal bone, the Shanidar 5 cranium was reconstructed again in 1999. As a result, lambda is not present on the newest reconstruction of the Shanidar 5 cranium thereby eliminating the highly curved parietal arc (measured from bregma to lambda) previously perceived by Trinkaus (1982, 1983). A cast of the new reconstruction was used in this analysis. Apart from its extremely flat frontal bone, which is above the upper limit of the Neanderthal range, Shanidar 5 shows typical Neanderthal facial features (Trinkaus, 1983) and in our analyses (e.g., PCA and DFA) it falls within Neanderthal variation. As a result we support the notion that its flattened frontal bone can be most likely attributed to individual or regional variation rather than artificial deformation (Chech, 1999). Unlike Simmons et al. (1991) and Athreya (2009) our analyses do not show any special affinities between Shanidar 1 and 5 to the exclusion of the other Near East Neanderthals (Tabun 1 and Amud 1). The discrepancy in our results may be due to our differing landmark and specimen data sets.

Among the Middle Pleistocene hominins, the European specimens Arago 21, Petralona and Sima de los Huesos 5, have been described as showing signs of incipient Neanderthal morphology in their midface, including a flattened infraorbital surface topography and obliquely orientated zygomatics (Arsuaga et al., 1997; Dean et al., 1998; Hublin, 1998; but see Harvati, 2009b; Harvati et al., 2010). Our results show that the mid and upper face of Arago 21 is overall more robust compared to Zuttiyeh and that the main features shared between them are in the shape of the browridge and the angle of the zygomatic body. However, on Arago 21 the medial margin of the zygomatic at the zygomaxillary suture is angled more obliquely, indicative of greater midfacial prognathism. Therefore, the midface of Arago 21 is more similar to the Neanderthal condition than to Zuttiyeh.

It has been suggested that the distortion in Arago 21 may make it more gracile than it really is (Guipert, 2005; Guipert et al., 2007). In Guipert's (2005) reconstruction and subsequent analysis of Arago 21 he found it to be most similar to the Ceprano calvarium from Italy (Guipert, 2005;

Guipert et al., 2007) that was recently re-dated to between 430-385 ka (Manzi et al., 2010; Muttoni et al., 2009). The Ceprano calvarium has been the focus of a several morphometric studies (Manzi et al., 2001; Bruner and Manzi, 2005, 2007) and like many of the other Middle Pleistocene neurocranial remains, its morphology is intermediate between *H. erectus* and *H. heidelbergensis/rhodesiensis* making its taxonomic affinities difficult to determine (Bruner and Manzi, 2005, 2007). Most recently, in a study that combined geometric morphometrics and scoring of discrete characters Mounier (2011) suggested that Ceprano was an appropriate representative for the ancestral stock of a wide-ranging *H. heidelbergensis* (Mounier et al., 2011).

5.4.2 Subtle differences in morphology

Hrdlička (1930) and later Sohn and Wolpoff (1993) emphasized the morphological similarities between Zuttiyeh and the Lower Cave Zhoukoudian hominins. In their metrical analysis, Sohn and Wolpoff (1993) found that although Zuttiyeh was most similar to the Near Eastern Neanderthals, it also shared a unique frontal size, curvature, and dimensions of the lateral aspect of the supraorbital torus with the Zhoukoudian hominins. However, it must be noted that their comparative sample was limited to only the Near East Neanderthals, Skhul and Qafzeh, and the Lower Cave Zhoukoudian specimens. Additionally, in their qualitative comparisons Sohn and Wolpoff (1993) found striking similarities between Zuttiyeh and the Zhoukoudian, Gongwangling and Hexian (two Mid/Late Pleistocene hominins from China) *H. erectus* hominins. They claim that these hominins share a similar frontal shape, orbital shape, supraorbital configuration, flattened glabella and superior nasal region, and zygomatic orientation which all contribute to a mid and upper facial flatness common in living Asian populations and their ancestors.

When we superimpose Zuttiyeh on the mean *H. erectus s.l.* shape, our results show clear differences in frontal bone shape. However, in the features related to mid and upper facial flatness

listed by Sohn and Wolpoff (1993) they are quite similar. In both the PCA in shape space and the DFA, Zhoukoudian 12 plots near the Neanderthal range of variation and in the DFA it is consistently misclassified as a Neanderthal. When PC 1 and 2 are plotted in Procrustes form space, Zuttiyeh plots near Zhoukoudian 12. These results suggest that Zhoukoudian 12 clearly shows some derived, possibly "Neanderthal-like", zygomatic and/or frontal bone morphology, but its specific resemblances to Zuttiyeh may be primarily driven by size.

Vandermeersch (1989) argued that except for Zuttiyeh's strong browridge its facial architecture is most similar to that of modern humans. He proposes that fewer morphological changes need to be made to go from Zuttiyeh to a modern human than from Zuttiyeh to a Neanderthal. These changes are: reduction in browridge; increase in frontal squama size; modification of the shape of the orbits from square to rectangular and low; and a reduction in overall robusticity. Features he cites as more modern human-like are an advanced degree of separation of the supraorbital torus into medial and lateral components; vertical frontal squama and high frontal elevation; and an anteriorly facing body of zygomatic.

Our superimposition results (Fig. 5.9a-i) show that the anterior projection of the medial portion of the browridge is similar in all archaic groups and that the main differences between these groups are in the projection of the lateral browridge and glabellar region, which is greatest in *H. heidelbergensis s.l*. In Zuttiyeh, the height of the medial component of the torus is similar to *H. erectus s.l.* and Neanderthals, and the projection and height of the lateral component is smaller than in *H. heidelbergensis s.l.* and greater than *H. erectus s.l.* and Neanderthals. The glabellar region in Zuttiyeh, however, is much more gracile (i.e. less projecting) than in all of these groups. This is consistent with Athreya (2009), possibly supporting a female attribution for Zuttiyeh.

In their multivariate morphometric analysis of Southwest Asian frontal bones, Simmons et al. (1991) show the Zuttiyeh frontal bone to be more similar to Amud 1 than the Skhul/Qafzeh

hominins. They argue that, because their results indicate that Zuttiyeh is more similar to a Neanderthal than an early modern human, their data fail to support the presence of a modern human-like high frontal bone and vertical frontal squama in Zuttiyeh. Our superimpositions (Fig. 5.9j-l) show that the frontal bone elevation and shape in Zuttiyeh is more similar to modern humans than any of the archaic human mean shapes; however, Shanidar 5 (see Fig. 5.8a-c) shares with Zuttiyeh a similar modern human-like vertical height in its frontal squama. The discrepancy between the results of Simmons et al. (1991) and our study is most likely due to methodological differences. Simmons et al. (1991) use traditional linear measurements (following Howells, 1973) to quantify the frontal bone shape. Geometric morphometrics and surface-semilandmarks, however, allow researchers to better capture more subtle morphological features, especially on smooth surfaces where osteometric landmarks are rare, like the frontal bone.

The final feature that Vandermeersch (1989) states as being modern human-like in Zuttiyeh is the anteriorly facing body of the zygomatic. Zuttiyeh's zygomatic body orientation is most like *H. erectus s.l.* mean shape (Fig. 5.9c) and Shanidar 5 (Fig. 5.8c); however the differences among the group mean shapes in this region are very subtle. Although Zuttiyeh is missing both maxillae, the orientation of its zygomatic bones, especially along the zygomaxillary suture, can provide an indication of its overall facial prognathism. When the superimpositions are viewed from an inferior perspective (Figs. 5.9c, f, i, and l) and compared between the archaic and modern human means, one can see that the zygomaxillary border of the zygomatic in Zuttiyeh is more anteriorly projecting than in the *H. erectus s.l.* mean, suggesting a slightly greater midfacial prognathism in the former. Regarding this feature, our results support Simmons et al. (1991) who propose that Zuttiyeh has a total facial prognathism combined with a flat zygomatic, like that of African *H. erectus*, Petralona, Broken Hill and Shanidar 4.

Shanidar 4 along with Shanidar 2, 6, 7, 8 and 9 were found in an archaeological layer lower than Shanidar 1 and 5. The faces of Shanidar 2 and 4 have been described as expressing greater

robusticity and less midfacial prognathism than the later Shanidar Neanderthals 1 and 5 and European Neanderthals (Trinkaus, 1983). According to Trinkaus (1983) these features align them more with the earlier Near East (Zuttiyeh) and European specimens (Petralona, Arago 21, Steinheim). Unfortunately, we were not able to include these specimens in our analysis.

5.4.3 General morphological patterns

The first two dimensions of the PCA in shape space of the frontal and zygomatic bones are dominated by the contrast between fossil and modern humans (including the Upper Paleolithic specimens), with overlap primarily occurring between the Middle to Late Pleistocene groups (*H. heidelbergensis s.l.*, *H. neanderthalensis*, transitional *H. sapiens* and early *H. sapiens*) and Zhoukoudian Upper Cave 101 and 102. The dichotomy in craniofacial morphology between archaic and recent humans has been recognized in past studies (e.g., Howells, 1970; Stringer, 1974) as well as several recent morphometric analyses (Weber et al., 2006; Gunz et al., 2009a; Harvati, 2009b; Athreya, 2009, Stansfield and Gunz, 2011). In Athreya's (2009) quantitative study of frontal bone morphology in Pleistocene fossil hominins, she found that in most aspects archaic human populations (*H. erectus s.l.*, *H. heidelbergensis s.l.*, *H. neanderthalensis*) are not significantly different from each other, and that anatomically modern humans (early, Upper Paleolithic, and recent *H. sapiens*) have the most distinctive frontal bones. Similarly in geometric morphometric analyses of Pleistocene hominin neurocrania and faces, Weber et al. (2006), Gunz et al. (2009a) and Harvati et al. (2007; see also Harvati 2009) show that the greatest shape differences to be between archaic and anatomically modern humans (fossil and recent). In each of these geometric morphometric analyses, the tightest clustering appears to be between the Neanderthals and non-habiline archaic *Homo* (i.e. *H. erectus s.l.* and *H. heidelbergensis s.l.*). Several authors have suggested that Neanderthals and archaic *Homo* share a conserved neurocranial architecture that is different from

modern humans (Lieberman et al., 2002; Bruner et al., 2003; Trinkaus, 2007; Gunz et al., 2009a). Our results also confirm this observation in the frontal bone.

As illustrated in Figures 5.3a-d, the main morphological shape changes along PC 1 are in the width and shape of the frontal bone, projection of the browridge and overall size and robusticity of the mid and upper face. Plotting on the negative end of PC 1, the *H. erectus s.l.* and *H. heidelbergensis s.l.* specimens express one extreme version of this morphology exhibiting a narrower and more receding (i.e. flatter) frontal bone in combination with a wider, more projecting and entirely more robust browridge and larger zygomatic bones in all dimensions. Among the Middle Pleistocene specimens this morphology is most apparent in Bodo, Kabwe and Petralona. Massive supraorbital tori and flattened frontals are two ubiquitous features in *H. erectus* that have been suggested to have been retained in Middle Pleistocene hominins (Rightmire, 2007). Our PCA results in Procrustes shape and form space suggest this might be true for Bodo, Kabwe and Petralona. Athreya (2009),van Vark (1995) and Rightmire (2001) also found these specimens to be the most morphological similar to each other indicating that they are all male and/or part of the same taxonomic group.

Like in the PCA, the results of the DFA show that *H. heidelbergensis s.l.* and *H. neanderthalensis* share a very similar fronto-zygomatic morphology; Dali, Bodo, and Zuttiyeh cluster within the range of Neanderthal variation. The lack of stability in the DFA and classification analysis is caused by the similarities in frontal and zygomatic morphology between these two archaic groups. This is further corroborated by the permutation test, which shows that apart from Neanderthals and *H. erectus s.l.* there are no significant differences in frontal and zygomatic bone shape between the fossil human groups. The similarities between the *H. heidelbergensis s.l.* and Neanderthal morphology are especially apparent in the Procrustes superimposition figures of Zuttiyeh and the Neanderthal mean (Fig. 5.9g-i) and Zuttiyeh and the *H. heidelbergensis* mean (Fig. 5.9d-f). These two groups share an archaic browridge and frontal bone morphology. A great level of

similarity between African and European *H. heidelbergensis* (s.l.) specimens, as well as between them and Neanderthals, in facial morphology was found in previous, landmark-based studies of facial variability (Harvati, 2009b; Harvati et al., 2010), and is confirmed here, although, unlike this previous work, the present study involves only a subset of the face.

Taken together, a comparison of mean shapes shows that subtle differences can be identified in frontal and zygomatic bone morphology among *H. erectus s.l.*, *H. heidelbergensis s.l.,* and *H. neanderthalensis*. However, these shape differences are minor variations on a common theme and not great enough to statistically discriminate distinct morphological groups among the Middle to Late Pleistocene hominins. Our results are congruent with Athreya (2009) and show that the frontal bone morphology is not sufficient for differentiating the Middle to Late Pleistocene human fossil groups.

5.4.4 Evolutionary implications

There are four evolutionary scenarios that might explain the morphology of the Zuttiyeh specimen in the context of the Southwest Asian fossil record. First, Zuttiyeh was a local member of a geographically wide-ranging Middle Pleistocene species also present in Africa and Europe. According to our results, both Zuttiyeh's phenetic similarities to Arago 21 and the clustering of the African and European Middle Pleistocene hominins in our PCA and DFA supports this scenario. This scenario is in accordance with the late divergence model of modern human origins, which emphasizes the strong similarities in the human fossil record between Africa, Europe and possibly Asia (Hublin, 2009). Supporters of this model see the Middle Pleistocene hominins across these continents as representing one species, possibly *H. heidelbergensis* (or *H. rhodesiensis* if the Mauer mandible is not included in this group; see Hublin, 2009), the last common ancestor of

Neanderthals and modern humans (Rightmire, 1998b; Stringer, 2002; Mounier et al., 2009; Mounier et al., 2011).

Second, according to the accretionary model of Neanderthal evolution (see Dean et al., 1998; Hublin, 1998, 2009), there was a long term *in situ* evolution of Neanderthals in Western Eurasia and Zuttiyeh was a Southwestern member of this group designated as *H. neanderthalensis* (Hublin, 2009) or as *H. heidelbergensis s.s.* (Arsuaga et al., 1997), a chronospecies directly ancestral to Neanderthals. Phenetic similarities shared between Zuttiyeh and Shanidar 5 may support this scenario.

Third, there was regular gene flow between Africa and Western Asia during the Middle to Late Pleistocene and Zuttiyeh was a member of the population ancestral to *H. sapiens* in Africa. Following Woodward (1921), *H. rhodesiensis* has been proposed as the name of the taxon for the African group. Our results do not support any direct link between Zuttiyeh and the African Middle Pleistocene humans to the exclusion of the contemporaneous European populations, or to *H. sapiens*. However, the new Middle Pleistocene dental remains from the site of Qesem Cave in Israel, dated to between 400 to 200 ka, equivocally suggest a closer similarity to the Skhul and Qafzeh material than to Neanderthals (Hershkovitz et al., 2011). In addition to being from the same region and possibly the same time period, Zuttiyeh and the Qesem material also shared the Acheulo-Yabrudian lithic technology. Therefore, they may be part of the same local Middle Pleistocene *Homo* population; however, because they lack similarly preserved morphology we cannot directly compare them. Nevertheless, if they were members of the same population, then they were characterized by a mosaic pattern of craniodental morphology.

Fourth, Zuttiyeh and the Southwest Asian hominins (e.g., Skhul, Qafzeh and the Neanderthals) represent either a regional lineage of *H. sapiens* (Wolpoff et al., 1984) or, together with the African Mid-Late Pleistocene humans, they constitute a "deep-rooted" *H. sapiens* lineage

(Arensburg and Belfer-Cohen, 1998). According to this scenario, Zuttiyeh should show its closest affinities to the Southwest Asian hominins.

Our results can support any one of these models. According to our Procrustes distance calculations, the diversity of fossil types (e.g., African and European Middle Pleistocene humans, Near East Neanderthal and modern humans, Asian *H. erectus*, recent modern human) to which it is most morphologically similar to (Fig. 4) strongly suggest that it exhibits a generalized morphology, which one would expect to see in the last common ancestor of Neanderthals and modern humans. Therefore, while our results do not show strong support for one particular taxonomic allocation for the Zuttiyeh fossil, we advocate that its mosaic morphological pattern is indicative of the population that gave rise to Neanderthals and modern humans.

Neanderthals retained aspects of this ancestral frontal bone morphology and through time developed apomorphies on other parts of the cranium (e.g., suprainiac fossa, inflated maxillary region) that are characteristic of the classic European Neanderthals dated to Oxygen Isotope Stages 3 and 4 (Dean et al., 1998; Hublin, 1998, 2009). The evolutionary processes responsible (i.e. natural selection or genetic drift) for producing cranial differences between modern humans and Neanderthals are difficult to prove (see Lieberman, 2008); however recent quantitative genetic and morphological studies suggest that genetic drift (neutral evolution) may have played an important role (Weaver et al., 2007; Roseman and Weaver, 2007; von Cramon-Taubadel and Lycett, 2008; Schillaci, 2008), although selection has also been suggested, especially for some aspects of the face (Weaver et al., 2007; Hubbe et al., 2009). Further evidence for the role of genetic drift in shaping the Neanderthal cranium is the gradual accumulation of Neanderthal features in the fossil record for over a period of >300,00 years (Hublin, 1998, 2009; Weaver, 2009).

This study is limited to the available anatomical information preserved on the Zuttiyeh fossil, namely the frontal and zygomatic morphology. Although the efficacy of using craniodental

morphology to reconstruct phylogenetic hypothesis about human evolution has been questioned (see Collard and Wood, 2000), multiple recent studies on modern humans have found that overall cranial morphology reflects population history (e.g., Relethford, 1994, 2004a,b; Roseman, 2004; Harvati and Weaver, 2006a,b; Smith, 2009; Hubbe et al., 2009; von Cramon-Taubadel, 2009). However, the phylogenetic value of different anatomical regions (such as e.g. the face, vault or basicranium) remains open to debate. With reference to the specific anatomy preserved on Zuttiyeh, the cranial vault has been reported to be relatively highly correlated with population history (e.g., neutral genetic data or geographic distances; Roseman, 2004; Harvati and Weaver, 2006a,b; Hubbe et al., 2009), while the phylogenetic usefulness of facial morphology has been questioned, being potentially affected by climatic variables and / or mastication (e.g., Skelton and McHenry, 1992; Wood and Lieberman, 2001; Lieberman et al., 2004; Lieberman, 2008). Recent work testing this hypothesis has produced somewhat contradictory results (see Harvati and Weaver 2006b, Hubbe et al., 2009; Smith, 2009). A study by von Cramon-Taubadel (2009) examined individual cranial bones as well as cranial regions among geographically diverse modern human populations and found that the maxilla, the zygomatic and the occipital bone are less reliable for reconstructing phylogenetic relationships. However, the majority of these studies were conducted on the microevolutionary scale, and therefore may not be relevant for higher-level systematics.

5.5 Conclusion

This is the most detailed metrical study on the fronto-zygomatic region of Zuttiyeh to date. In the PCA and DFA, Zuttiyeh plots in the middle of the Neanderthal variation, and according to Procrustes distances it is phenetically most similar to Shanidar 5. In addition to sharing some similarities in zygomatic bone morphology, Shanidar 5 and Zuttiyeh also express a vertical frontal

squama, a feature that is most often attributed to modern humans. However, in all other aspects its mid and upper facial morphology expresses a combination of features seen in Early to Late Pleistocene archaic humans. Overall, it is morphologically most similar to, a Near East Neanderthal (Shanidar 5), a Middle Pleistocene hominin (Arago 21), and a Near East early modern human (Skhul 5).

This raises the intriguing possibility that the generalized morphology present in Zuttiyeh characterizes a population ancestral to both Neanderthals and modern humans, or a population immediately postdating their divergence. Hopefully, future fossil discoveries from this time period and geographical region, like in Qesem Cave in Israel, will shed more light on this issue. We conclude that Neanderthals largely retained a generalized morphology, while the modern human frontal and zygomatic bone represents a significant departure from this presumably ancestral morphology. Furthermore, these results show that the frontal and zygomatic bones are not sufficient for distinguishing archaic humans and that additional anatomical features should be used to allocate fossils.

Through the application of semilandmark geometric morphometric methods we are able to provide quantitative support for the subtle differences in frontal and zygomatic bone morphology often described, or qualitatively identified, between the different archaic human groups used in this study (*H. erectus s.l.*, *H. heidelbergensis s.l.*, and *H. neanderthalensis).* However, the morphological differences among these groups are ultimately minor variations on a common theme and do not reflect underlying architectural differences. There is significant overlap between *H. heidelbergensis s.l.*, Neanderthals and even early *H. sapiens* indicating that all of these groups resemble the ancestral morphology. Only recent and most Upper Paleolithic modern humans depart from this pattern.

6. The Craniofacial Morphology of Saint-Césaire: A Semilandmark Geometric Morphometrics Analysis[4]

6.1 Introduction

The Saint-Césaire skeleton comprises most of the right side of the cranium including parts of the parietal bone, most of the squamous portion of the temporal bone, a nearly complete frontal and zygomatic bone, parts of the maxilla and complete maxillary and mandibular dentition (LI2-RM3). The cranial morphology has been described as exhibiting a combination of typical Neanderthal features in the infraorbital and mandibular morphology combined with a more gracile supraobital torus and narrow nose (Lévêque and Vandermeersch, 1980; Cartmill and Smith, 2009). Postcranially its body proportions are "hyper-arctic" like the European Neanderthals; however researchers have noted that it also expresses some modern human-like morphology (Lévêque and Vandermeersch, 1980; Stringer et al., 1984; Trinkaus et al., 1998, 1999). This morphology may indicate differences in locomotor patterns and activities, such as extensive daily ranging and less forceful movements of the arm, that are more similar to Upper Paleolithic human behavior than to Neanderthals (Trinkaus et al., 1998, 1999).

The Saint-Césaire skeleton is one of the latest known Neanderthals, dated by theromoluminescence techniques on burned flints to around 36 Ka (Mercier et al., 1991), and it is one of the few clearly diagnostic specimens associated with the Châtelperronian industry. The extent of contact, culturally and genetically, between Neanderthals and Upper Paleolithic humans in Europe is controversial. Researchers have argued that the Châtelperronian industry was developed either by an acculturation process through direct contact of Neanderthals with modern humans or

[4] The manuscript entitled *The craniofacial morphology of Saint-Césaire: a semilandmark geometric morphometric analysis*, written by Sarah E. Freidline, Philipp Gunz, Marcia S. Ponce de León, Christoph P. E. Zollikofer, and Jean-Jacques Hublin, will be submitted in 02/2012 as a book chapter in the following edited volume: *The Saint-Césaire Human Fossil and its Context,* edited by J-J. Hublin and B. Vandermeersch, New York: Springer.

imitation of modern human stone tool technology by Neanderthals (Harrold, 1989; Hublin et al., 1996; Mellars, 1999), or that it was established independently of modern human influence (d'Errico et al., 1998; Zilhão and d'Errico, 1999). In the recent sequencing of the Neanderthal genome, low levels of gene flow were detected between recent modern humans and Neanderthals, prior to the divergence of the Eurasian groups from each other (i.e., before 50 ka) and most likely in the Middle East. However, the genetic and morphological evidence for interbreeding in Europe during the Upper Paleolithic remains unclear.

Supporters of the Assimilation (e.g., Smith et al., 1989) and Multiregional (e.g., Wolpoff et al., 1984) models of modern human origins argue that evidence of regional continuity in Europe can be seen in specific aspects of modern human cranial morphology such as high frequencies of occipital bunning, presence of a suprainiac fossa, the degree of upper midfacial projection, and the morphological pattern of the supraorbital torus (Frayer et al., 1993; Wolpoff et al., 2001; Smith et al., 2005; Cartmill and Smith, 2009). Researchers have claimed that the Saint-Césaire skull shows a number features approaching the "modern" condition, such as a markedly reduced lateral supraorbital torus, a narrow nasal breadth, squared orbits, an incipient chin, and anterior tooth size reduction (Frayer et al., 1993). Temporal trends in the reduction of facial and supraorbital robusticity in Neanderthals, while maintaining total facial prognathism, have also been used as evidence for regional continuity in Europe (Smith and Ranyard, 1980; Wolpoff et al., 1981; Frayer et al., 1993; Wolpoff, 1999). In addition to Saint-Césaire, other fossils that have been argued to show morphological evidence of Neanderthal and Upper Paleolithic human admixture are from Mladeč (Czech Republic), Vindija (Croatia), Peştera cu Oase, Peştera Muierii and Peştera Cioclovina (Romania; but see Harvati et al., 2007 regarding the latter specimen), and Abrigo do Velho (Portugal).

Because of its fragmentary condition, few metric studies have been performed on the Saint-Césaire craniofacial material. Here we use three dimensional geometric morphometric methods to

quantify its preserved facial and frontal bone morphology. The study will place Saint-Césaire in a comparative morphometric context with other chronologically and geographically relevant groups such as the older Middle Pleistocene hominins (*Homo heidelbergensis s.l.*), Neanderthals, and contemporaneous Upper Paleolithic and more recent modern humans. Being one of the latest surviving Neanderthals, this specimen can provide us with a clearer understanding of temporal trends in facial morphology in Neanderthals and could potentially yield greater insight into morphological evidence of interbreeding between Neanderthals and Upper Paleolithic modern humans.

6.2 Material and methods

6.2.1 Sample

The fossil sample (Table 6.1) consists of Pleistocene hominin specimens from Africa, Europe and Asia that retain nearly complete facial and frontal bone morphology. Crucial to this study are the Middle Paleolithic Eurasian Neanderthals (n = 5) and the Upper Paleolithic European modern humans (n = 6). Unfortunately, Neanderthals that were contemporaneous (ca. 30 – 35 ka) with the Saint-Césaire specimen could not be included in this study because the few that have been discovered either do not preserve enough facial morphology (e.g., Vindija, Arcy-sur-Cure) or are immature (e.g., Mezmaiskaya). In order to more clearly interpret the evolutionary trajectory of facial morphology, adult individuals temporally both older (Early and Middle Pleistocene hominins) and younger (Latest Pleistocene and Holocene) than Saint-Césaire were also included in this study. The recent modern human (MH) sample (Table 2.3) comprises fourteen morphologically diverse geographic populations spanning six continents: Australia (South Australian Aborigines), Asia (Mongolia and Thailand), Europe (Austria and Czech Republic), Africa (Khoe-San, Egypt and Tanzania), North America (Arizona, Utah, Alaska and Mexico) and South America (Argentina). Apart

from two Early Pleistocene subadult specimens (WT 15000 and Dmanisi 2700), only adult crania were included (according to spheno-occipital fusion and eruption of permanent dentition).

Table 6.1 Specimens used in the analysis and their abbreviation (Ab.). *casts

Specimen	Ab.
Early Pleistocene: Africa	
ER 1813	1813
ER 3733	ER3733
ER 3883	ER3883
WT 15000*	Tur
Early Pleistocene: Asia	
Dmanisi 2700*	Dm27
Sangiran 17*	S17
Middle Pleistocene: Africa	
Bodo	Bd
Kabwe	Kb
Middle Pleistocene: Europe	
Arago 21*	Ar
Petralona	Pt
Sima de los Huesos 5*	Sm5

Table 6.1 Continued

Middle Pleistocene: Asia	
Dali*	Dl
Late Middle-Late Pleistocene: Africa	
Jebel Irhoud 1	I1
Late Middle-Late Pleistocene: Europe	
Gibraltar 1	Gb1
Guattari	Gt
La Chapelle-aux-Saints	LCh
La Ferrassie 1	LF1
Saint-Césaire	SC
Late Middle-Late Pleistocene: Asia	
Liujiang*	Ljg
Qafzeh 6	Q6
Qafzeh 9	Q9
Shanidar 1*	Sh1
Shanidar 5*	Sh5
Skhul 5	Sk5
Upper Paleolithic Eurasian modern humans	
Cro-Magnon 1	Cr1

Table 6.1 Continued

Mladeč 1	Ml1
Předmostí 3*	Pr3
Předmostí 4*	Pr4
Oberkassel 1	Ob1
Oberkassel 2	Ob2
Zhoukoudian 101*	Zh101
Zhoukoudian 102*	Zh102

6.2.2 Landmark data

The landmark data set was designed to capture all of the preserved craniofacial morphology of the Saint-Césaire reconstructed cranium (see below; Fig. 6.1) and the traditional osteometric landmarks are listed in Table 6.2.

Figure 6.1 482 landmarks and semilandmarks digitized on all specimens. Biological landmarks are abbreviated. The full names are listed in Table 6.2.

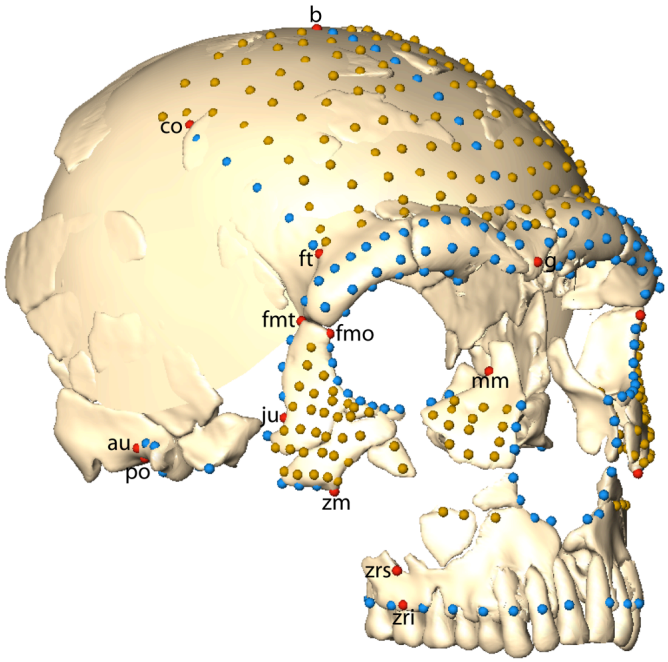

Table 6.2 Biological landmarks used in the analysis.

Landmark	Abbreviation
Auriculare*	au
Bregma	b
Coronale*	co
Glabella	g
Frontomalare orbitale*	fmo
Frontomalare temporale*	fmt
Frontotemporale*	ft

Table 6.2 Continued

Jugale*	ju
Medial orbital margin[1]*	mm
Porion*	po
Zygomatic process root inferior[2]*	zri
Zygomatic process root superior[3]*	zrs
Zygomaxillare*	zm

*paired right and left landmarks

6.2.3 Missing data reconstruction

In addition to the data reconstruction steps described in Chapter 2, we interpolated the morphology that was missing between the existing bone fragments (Fig. 6.2a-d) using Amira.

Figure 6.2 a, c) original Saint-Césaire reconstruction; b, d) reconstruction of morphology between missing frontal bone fragments.

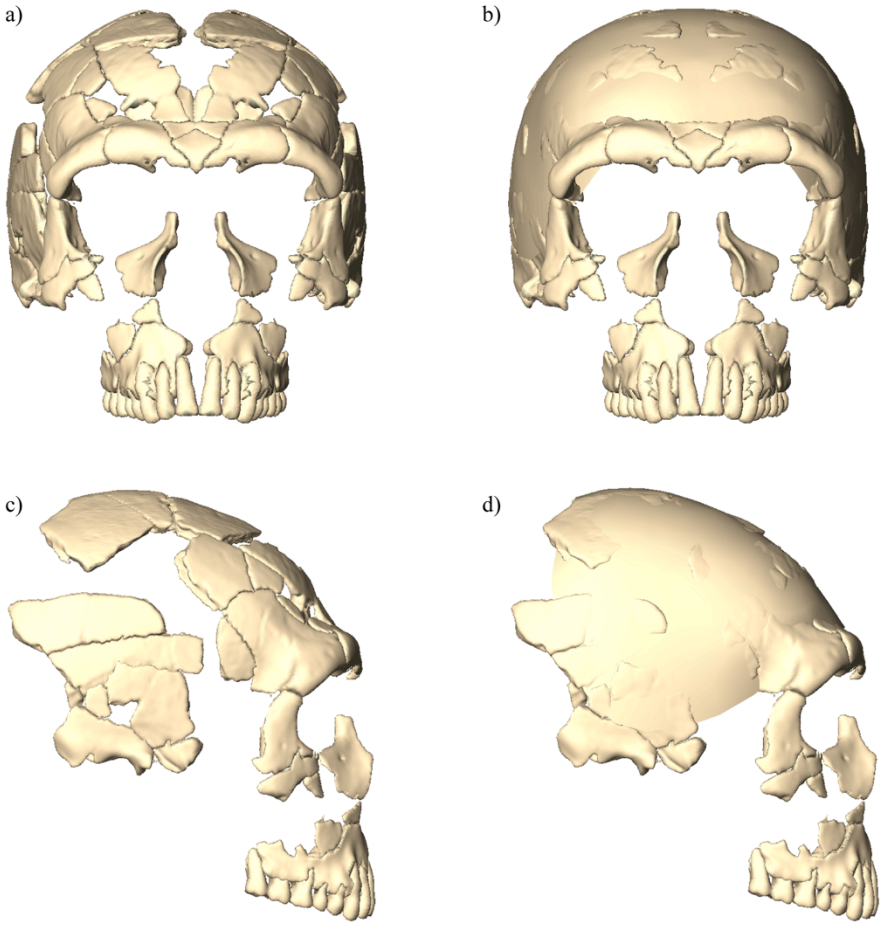

6.2.4 Analytical methods

A Principal Component Analysis (PCA) was performed on the 482 landmark and semilandmark Procrustes shape coordinates in order to explore overall facial and frontal bone shape variation and possible temporal trends in the data. Shape changes were visualized along the first two principal component (PC) axes by TPS warping of the Procrustes mean shape (see Gunz and Harvati, 2007; Mitteroecker and Gunz, 2009). To identify which individuals are most similar in Procrustes shape space nearest neighbors were calculated. A PCA was also performed in Procrustes

form space in order to identify any temporal trends associated with a reduction in craniofacial robusticity and size within the Neanderthal group (Mitteroecker et al., 2004; Mitteroecker and Gunz, 2009).

A discriminant function analysis (DFA) was performed to evaluate how well facial and frontal bone morphology separates the Pleistocene human groups. Individuals were classified according to four *a priori* group assignments: Early Pleistocene, Middle Pleistocene, Neanderthals and recent modern humans. Table 6.3 lists each specimen's *a priori* group assignment. Saint-Césaire, as well as ER 1813, the early MHs and Upper Paleolithic humans were treated as having unknown group affinities to be classified by posterior probability; all groups were assigned the same prior probability.

Table 6.3 *A priori* group assignments used for the fossils in the Canonical Variates Analysis. All recent modern humans were assigned to the recent modern humans group.

Specimen	**Group Assigment**
ER 1813	Early Pleistocene
ER 3733	Early Pleistocene
ER 3883	Early Pleistocene
WT 15000	Early Pleistocene
Dmanisi 2700	Early Pleistocene
Sangiran 17	Early Pleistocene
Bodo	Middle Pleistocene
Kabwe	Middle Pleistocene
Arago 21	Middle Pleistocene
Petralona	Middle Pleistocene
Sima de los Huesos 5	Middle Pleistocene

Table 6.3 Continued

Dali	Middle Pleistocene
Gibraltar 1	Neanderthal
Guattari	Neanderthal
La Chapelle-aux-Saints	Neanderthal
La Ferrassie 1	Neanderthal
Shanidar 1	Neanderthal
Shanidar 5	Neanderthal

In order to visualize the shape difference in the facial and frontal bone morphology we created a series of superimpositions of Saint-Césaire and the group means of Middle Pleistocene hominins, Neanderthals and recent MH. We used TPS interpolations computed from the landmarks and semilandmarks to warp the surface of Saint-Césaire to the respective group means.

6.3 Results

6.3.1 Principal component analysis

Figure 6.3 displays the first two PCs in shape space, which together represent 51.5% of total shape variation. Convex hulls are drawn for the Early and Middle Pleistocene groups, Neanderthals and recent MH; here the *a priori* group assignment only affects the symbol, not the position of the individual in the plot. The Upper Paleolithic modern humans fall within the range of recent MH variation and each temporal group clusters together with some overlap occurring between the Middle Pleistocene hominins and the Neanderthals. The pattern in the first two PCs shows a clear separation between the modern (Upper Paleolithic humans and recent MH) and archaic humans

(Early and Middle Pleistocene hominins and Neanderthals). The early MH and Zhoukoudian 101 fall between the Neanderthals and modern humans and Saint-Césaire falls near the center of the plot and within the ranges of Neanderthal and recent MH variation.

Figure 6.3 Principal Component Analysis in Shape Space. Convex hulls are drawn for Early and Middle Pleistocene hominins, Neanderthals and recent modern humans (MH).

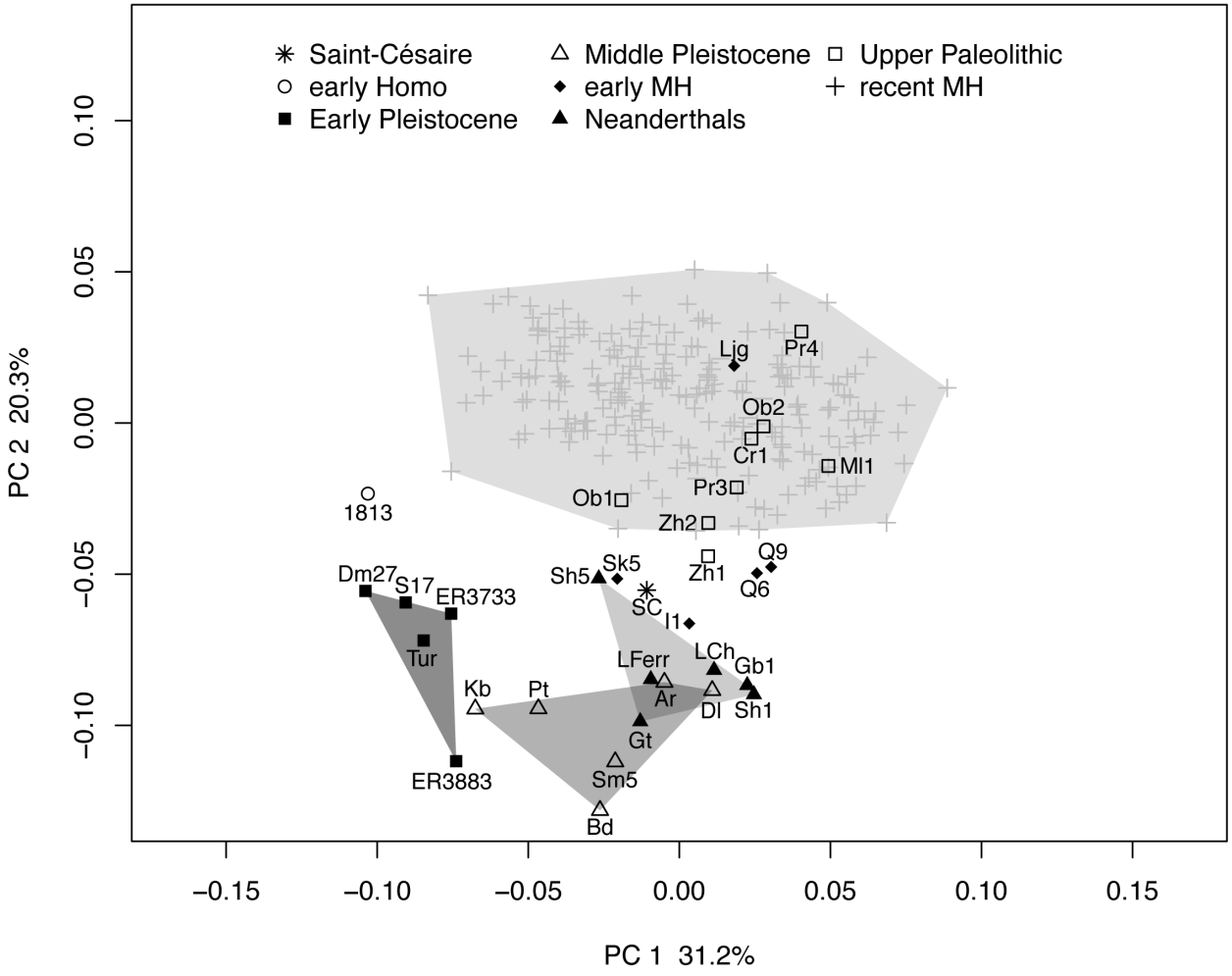

Figure 6.4 illustrates the shape changes that occur along the first two PC axes. Individuals that plot along the negative extreme of PC 1 (e.g., ER 1813 and Dmanisi 2700) have a narrower, receding frontal bone, a more pronounced browridge and glabellar region, a coronally rotated

infraorbital plate, and an overall larger and more robust mid-and lower face (Fig. 6.4a). The shape changes that are associated with the negative end of PC 2 (Fig. 6.4c) include a receding frontal bone, robust and projecting supraorbital torus, widening of the upper face (along the frontal process of the zygomatics), a more sagittal rotation of the zygomatic and maxillary bones, straight zygomaticoalveolar crest, inflated infraorbital surface topography, larger nasal aperture, and larger palatal arch. These features are most extreme in Bodo, an African Middle Pleistocene fossil.

Figure 6.4 Mean shape changes along PC 1 and 2, a): mean shape at the negative end of PC 1, b) mean shape at the positive end of PC 1; c) mean shape at the negative end of PC 2, d) mean shape at the positive end of PC 2.

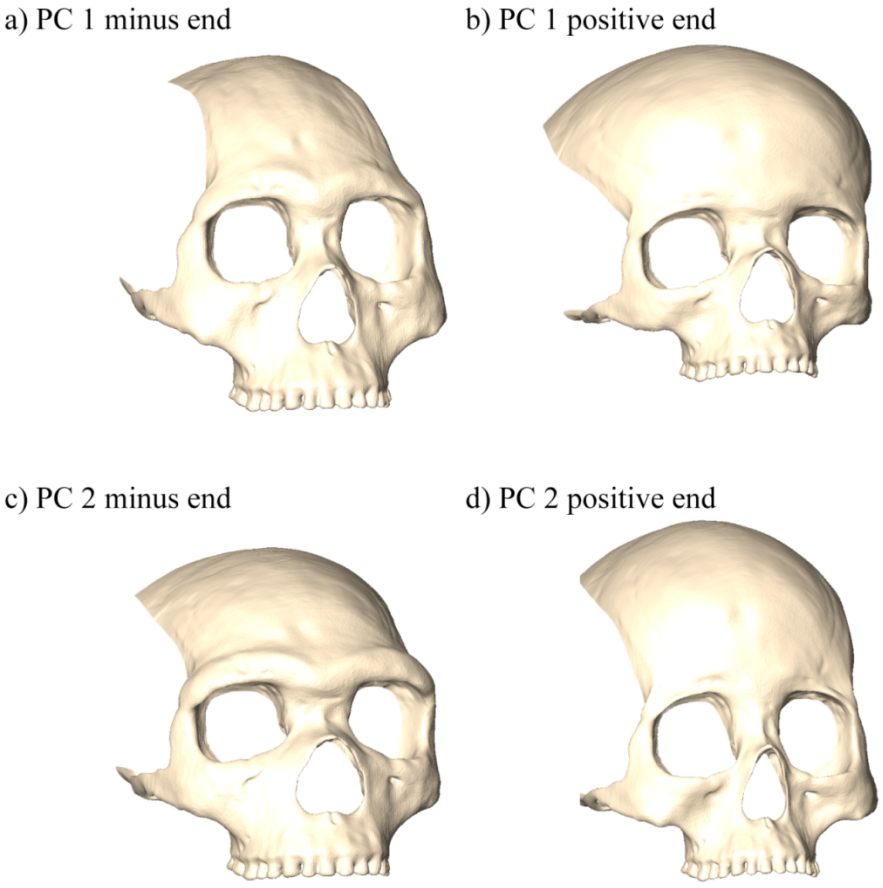

Table 6.4 lists Saint-Césaire's five nearest neighbors in shape space based on inter-individual Procrustes distances and Figure 6.5 illustrates the cluster of its nearest neighbors in Procrustes space. It is most similar to Shanidar 1 (0.068), a West Asian Neanderthal, and La Ferrassie 1 (0.070), a European Neanderthal. Saint-Césaire and Shanidar 1 (Fig. 6.6) share a similar tall and narrow nasal aperture, anteriorly projecting lower face, size and shape of the alveolar and subnasal region, and both express a superiorly-inferiorly long (i.e., tall) and narrow face that tapers downward (Fig. 6.6a, b). The frontal bone, especially along the midline is particularly flat (i.e. low and receding) in Shanidar 1. Trinkaus (1983) has suggested that this may be a due to artificial cranial deformation. Shanidar 1 has a smaller and more sagitally rotated zygomatic bone, projecting nasal region, robust mid- and lateral browridge, smaller and less projecting glabellar region, and a more downward distending inferolateral corner of orbit (Fig. 6.6a, b).

Table 6.4 Procrustes distances of Saint-Césaire's top five nearest neighbors in shape space listed in ascending order.

Specimen	Procrustes Distance to Saint-Césaire
Shanidar 1	0.068
La Ferrassie 1	0.070
La Chapelle-aux-Saints	0.074
Shanidar 5	0.076
Arago 21	0.076

Figure 6.5 Cluster of Saint-Césaire's nearest neighbors in Procrustes space. The line length is arbitrary.

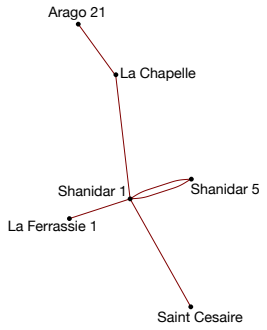

Although similar in shape, the frontal bone of Saint-Césaire is more receding along the midline than La Ferrassie 1 (Figure 6.6c). They share the classic Neanderthal double arched supraorbital tori, however Saint-Césaire's tori and glabellar region are less projecting and its lateral tori are more robust. Additionally they both have an overall superiorly-inferiorly long face that tapers inferiorly and a projecting nasal, subnasal and alveolar region. La Ferrassie 1 has a broader interorbital breadth, larger nasal aperture, more sagitally rotated zygomatic bones, and a more downward distending inferolateral corner of orbit.

Figure 6.6 Procrustes superimpositions of Saint-Césaire on its nearest neighbors in shape space. Shape information is contained in the landmark and semilandmark data and everything in between these landmarks is interpolated. 6.5a, b: Saint-Césaire (white) superimposed on Shanidar 1 (purple), Saint-Césaire's nearest neighbor in shape space based on inter-individual Procrustes distances. 6.5c, d: Saint-Césaire (white) superimposed on La Ferrassie 1 (purple), Saint-Césaire's second nearest neighbor in shape space based on inter-individual Procrustes distances.

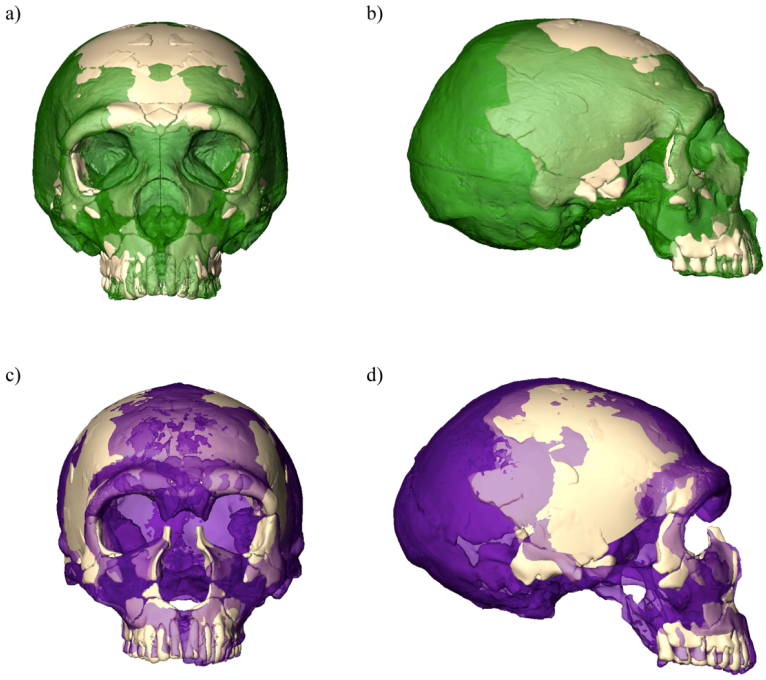

PC 1 (Fig. 6.7) in Procrustes form space (40.8% of total form variation) is highly correlated ($r \cong 0.97$) with log centroid size. Size trajectories for the Early and Middle Pleistocene hominins, Neanderthals and recent MH were plotted by regressing shape on log centroid size and are represented by the black lines in Figure 6.7. The Middle Pleistocene humans, Bodo, Petralona and Kabwe, exhibit the largest faces. Among the Neanderthals, La Ferrassie 1 has the largest face and Gibraltar 1 has an unusually small face. Saint-Césaire plots near the Neanderthal range of variation and like the early MH, it plots in between Neanderthals and recent MH along PC 2.

Figure 6.7 Principal component analysis in form space (including the log centroid size of each specimen). Convex hulls are drawn for Early and Middle Pleistocene hominins, Neanderthals and recent modern humans, and the size trajectories, calculated by regressing shape on log centroid size, are represented by the black lines.

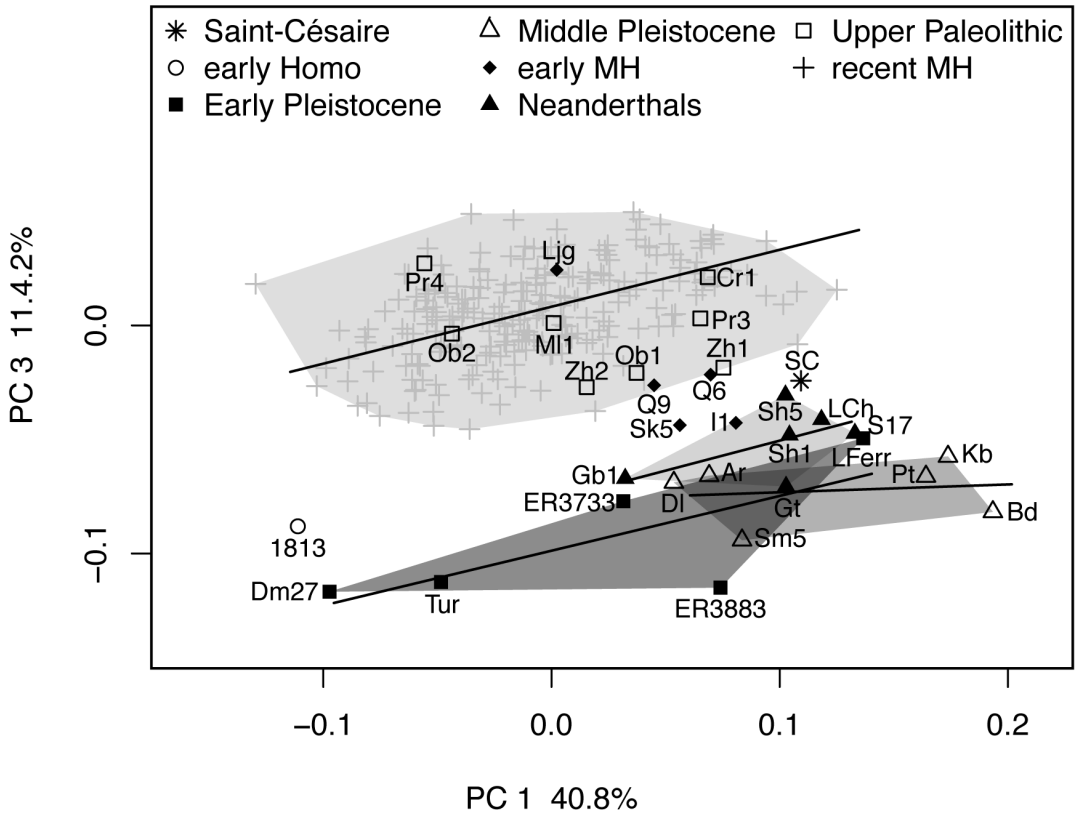

6.3.2 Discriminant function analysis

A DFA (Fig. 6.8) was performed using the first ten PCs of shape space representing 80.9% of total shape variation. Overall there is a clear separation between the four *a priori* groups: Early and Middle Pleistocene hominins, Neanderthals and recent MH; however slight overlap occurs between Neanderthals and Middle Pleistocene humans. Similar to the PCA, the Upper Paleolithic humans fall within the range of recent MH variation, except for Zhoukoudian 101, and the early MH cluster between the modern and the archaic groups. Saint-Césaire plots near the Neanderthal range of variation. To test the stability of the DFA, we included between five and fifteen principal

components of shape space. Although overlap variably occurred between the archaic groups, the early MH, Upper Paleolithic humans and recent MH never plotted within any of the archaic groups range of variation. Saint-Césaire plotted within the Neanderthal range of variation in all iterations. Based on posterior probabilities Saint-Césaire was always classified as a Neanderthal. The accuracy of correctly classifying fossil specimens ranged from 71.4% to 85.7% depending on how many principal components were used. Arago 21 was always misclassified as a Neanderthal, Dali was most frequently classified as an Early Pleistocene hominin and Shanidar 5 as a Middle Pleistocene hominin. Modern humans were never misclassified and Upper Paleolithic humans were always classified as recent MH.

Figure 6.8 Discriminant function analysis using the first ten principal components of shape space, representing 80.9 % of total shape variation. Convex hulls are drawn for Early and Middle Pleistocene hominins, Neanderthals and recent modern humans.

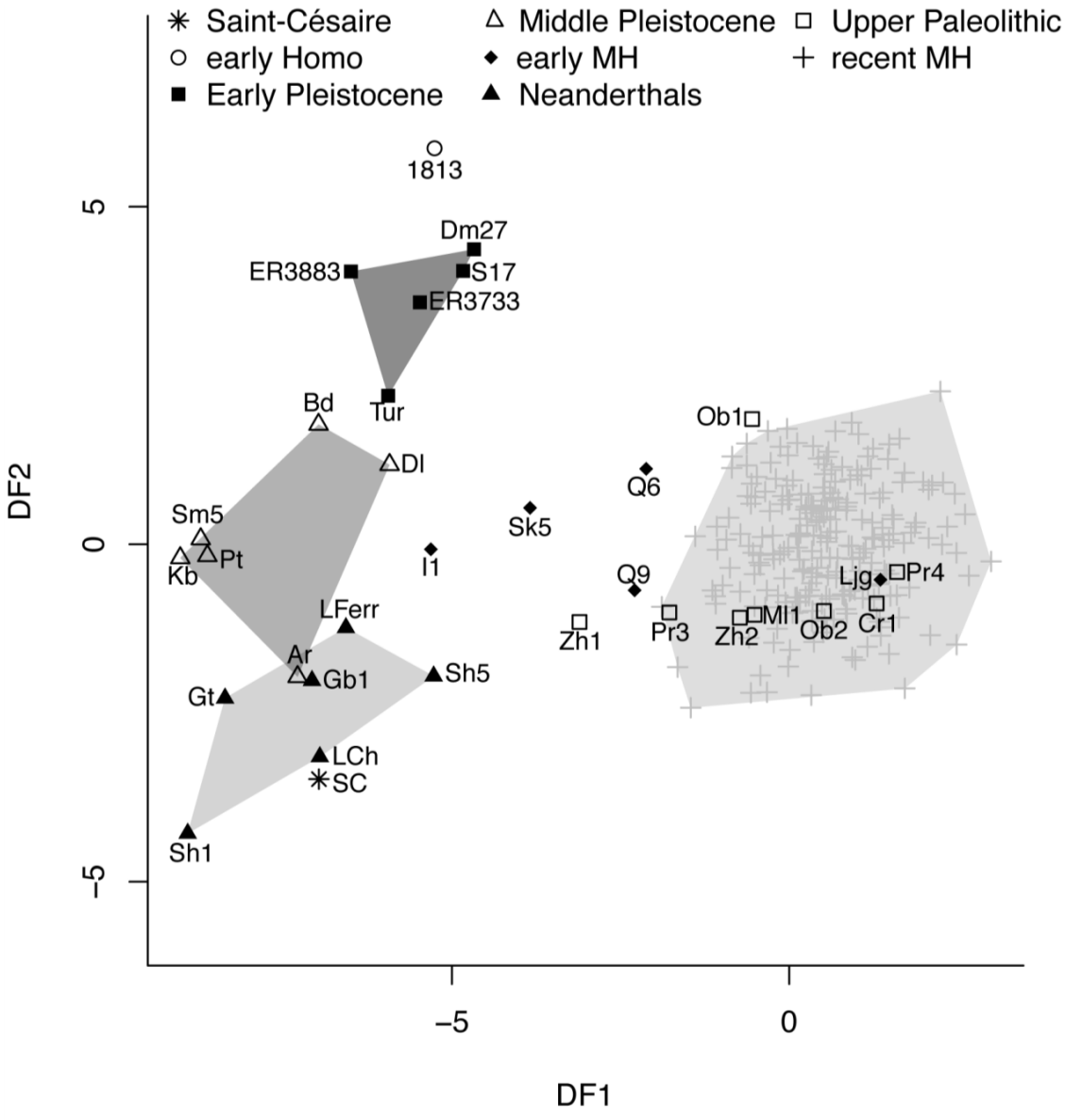

6.3.3 Visualization – Procrustes superimposition

To visualize the shape differences between Saint-Césaire and the Middle Pleistocene human mean (Fig. 6.9), we warped the surface of Saint-Césaire to the average shape of the Middle

Pleistocene humans based on the landmarks and semilandmarks in Figure 6.1. Saint-Césaire has a more vertical frontal bone shape; narrower midface; smaller browridge, zygomatic bones and nasal aperture; more projecting nasal region; and superiorly-inferiorly longer face. In Figure 6.9c and d, we warped Saint-Césaire to the Neanderthal mean shape, in blue, and superimposed them. They share a similar browridge shape, although in Saint-Césaire its middle and lateral third is more robust and the central portion is more gracile; facial width; subnasal and alveolar shape; and equally projecting nasal region. Additionally, the zygomatic bones are similar in size and shape; however it is more sagitally rotated in the Neanderthal mean. Saint-Césaire has a more vertical frontal bone; less projecting glabellar region; a narrower nasal aperture and a superiorly-inferiorly longer face. Lastly, in Figure 6.9e and f, we warped Saint-Césaire to the recent MH mean, in gray, and superimposed the two. Saint-Césaire has a more receding frontal bone; projecting and robust browridge; sagitally rotated zygomatic bones; projecting nasal, subnasal and alveolar region; larger nasal aperture; and a longer face.

Figure 6.9 Procrustes superimpositions of Saint-Césaire on mean shapes. 6.9a, b: Saint-Césaire (white) superimposed on the Middle Pleistocene mean (red); 6.9c, d: Saint-Césaire (white) superimposed on the Neanderthal mean (blue); 6.9e, f: Saint-Césaire (white) superimposed on the recent MH mean (gray).

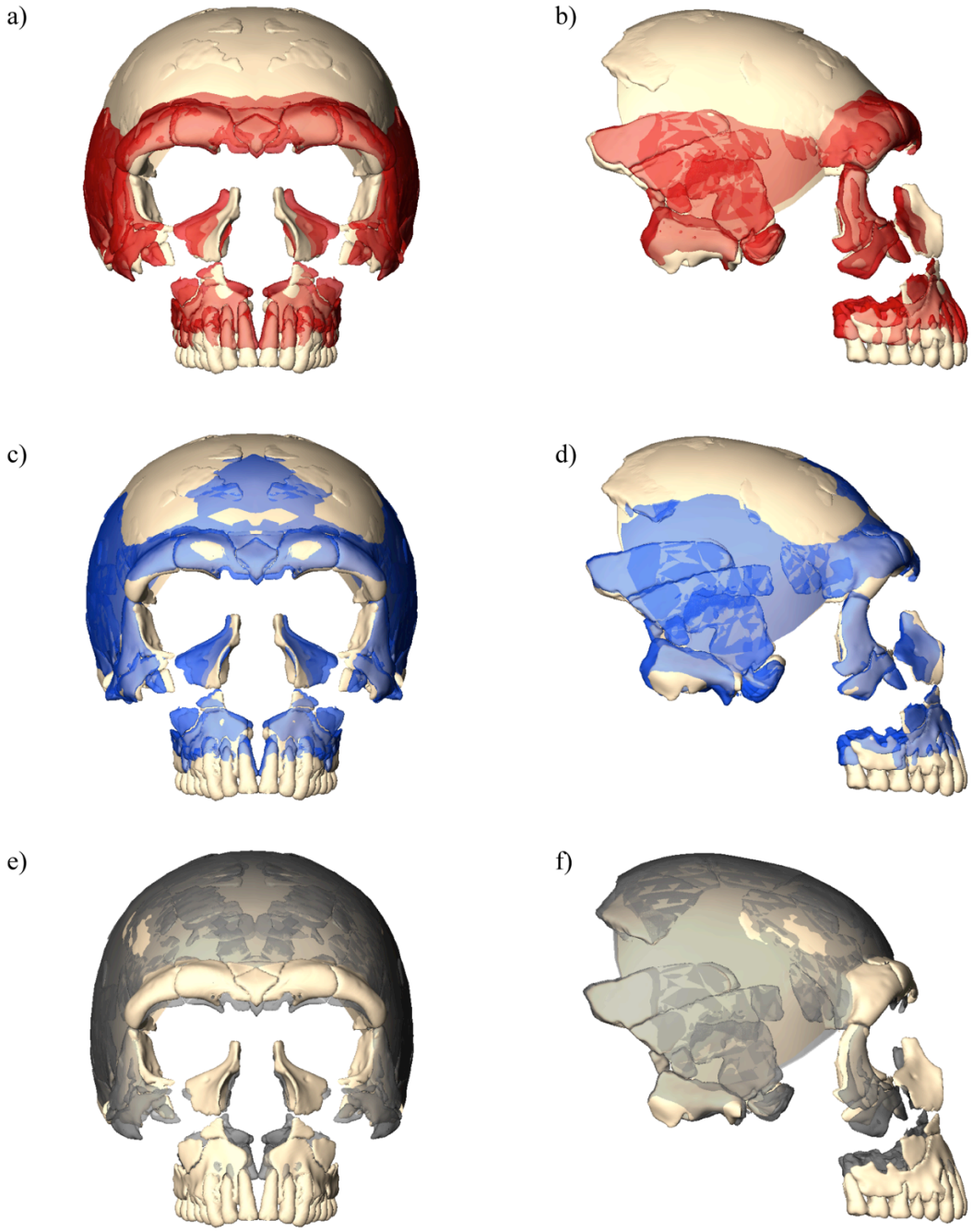

6.4 Discussion

The results of our multivariate statistical analyses show that the facial and frontal bone morphology of the Saint-Césaire specimen unquestionably resembles that of a Neanderthal. In Procrustes shape space Saint-Césaire is closest to the Neanderthal mean (Table 6.5). Specific features that it shares with Neanderthals are a receding frontal bone; projecting nasal region; inflated midfacial topography; broad upper face that tapers inferiorly; and double arched supraorbital tori (Fig. 6.9c, d). When compared to the Neanderthal mean, it has a narrower nasal aperture, superiorly-inferiorly longer face, the zygomatic bone is less sagittaly rotated, and it lacks a downward distending inferolateral corner of orbit.

Frayer et al. (1993) states the reduced lateral supraorbital torus, narrow nasal aperture and subrectangular orbital morphology in Saint-Césaire is transitional between Neanderthals and modern humans. However, an equally narrow nasal aperture can be observed in Shanidar 1, Saint-Césaire's nearest neighbor in shape space. Additionally, the lateral supraorbital morphology of Saint-Césaire appears to be more robust than the Neanderthal mean shape (Fig. 6.9c, d). Therefore our results indicate that these features more likely reflect individual Neanderthal variation rather than evidence for interbreeding between Neanderthals and Upper Paleolithic humans. However, a clearer understanding of the developmental integration of these features within the cranium and their covariation with size are necessary in order to interpret their phylogenetic relevance (Lieberman, 1995; Lieberman et al., 2002; Maddux and Franciscus, 2009; Freidline et al., 2010).

Our results show a clear evolutionary trajectory in facial morphology through time beginning with *H. habilis* (ER 1813) and ending with the Upper Paleolithic and recent MH. According to our PCA and DFA, the Upper Paleolithic humans fall within the variation of recent MH and their combination of facial and frontal bone morphology is fundamentally different from

archaic humans (Early and Middle Pleistocene humans and Neanderthals). These results are consistent with other recent studies that use Upper Paleolithic facial (e.g., Harvati, 2009b; Harvati et al., 2010) and neurocranial morphometric data (e.g., Weber et al., 2006; Gunz et al., 2009a; Harvati, 2009b; Harvati et al., 2010). As illustrated in Fig. 6.4b and d, features that distinguish the Upper Paleolithic and recent MH from archaic humans are a vertical frontal squama, more gracile browridge, coronally rotated infraorbital plate, slightly depressed infraorbital surface topography, smaller nasal aperture, and less projecting mid and lower face. These features have been documented extensively in the literature (e.g., Day and Stringer, 1982; Bräuer, 1984; Stringer et al., 1984; Habgood, 1989; Howells, 1989; Frayer et al., 1993; Lieberman, 1995; Lahr, 1996; Lieberman et al., 2002).

In addition to the clear morphological differences among the temporal groups, the PCA in form space indicates that there is a general trend in a reduction in facial size and robusticity between Middle Pleistocene humans and Neanderthals. A similar temporal trend within Neanderthals is not as evident. Except for Gibraltar 1, Saint-Césaire and the other Neanderthals cluster tightly along the first PC in form space indicating that they have similar facial sizes. However along PC 3 Saint-Césaire plots between Neanderthals and recent MH. Because Saint-Césaire is similar in size to the other Neanderthals, its more gracile features cannot be explained entirely by allometric scaling. This could demonstrate a trend in facial reduction and supraorbital robusticity while maintaining total facial prognathism as described by others (e.g., Frayer et al., 1993). More late Neanderthals specimens are needed in order to more accurately test this hypothesis.

There are several outliers in each temporal group in the PCA and DFA. Arago 21 clusters with the Neanderthals and is always classified as a Neanderthal in posterior probability, suggesting that its facial morphology is more like Neanderthals than the contemporaneous Middle Pleistocene hominins. These results have been recognized in previous studies (Arsuaga et al., 1997; Dean et al., 1998; Hublin, 1998; but see also Harvati et al., 2010). Dali clusters with the Neanderthals in the

PCA; however, it is most frequently classified as an Early Pleistocene hominin in posterior probability. Zhoukoudian 101 plots outside the range of modern human variation but it is always classified as a recent MH in posterior probability. These results are similar to Harvati's (2009) morphometric analysis of the Zhoukoudian Upper Cave cranial vaults data set, but differ from her facial analysis. Lastly, the Luijiang specimen shows stronger affinities to modern humans than the more contemporaneous early MH specimens.

6.5 Conclusion

Our landmark and semilandmark-based analyses of facial shape and form conclusively align Saint-Césaire with Neanderthals. With regards to facial shape it most closely resembles Shanidar 1 and La Ferrassie 1. Beginning with the Early Pleistocene each temporal group has a unique craniofacial morphology except for the Upper Paleolithic human specimens, which fall within the variation of recent modern humans: as illustrated in both the PCA and DFA the Upper Paleolithic humans consistently cluster with the recent MH. Our results suggest that the overall architecture of the modern human facial morphology is derived with respect to the presumably ancestral pattern observed in Early and Middle Pleistocene *Homo*. Early recent MH crania (Irhoud 1, Qafzeh 6 & 9, Skhul 5) are intermediate between recent modern humans and archaic *Homo*. Aspects of the Saint-Césaire craniofacial morphology that have been argued to represent admixture between Neanderthals and Upper Paleolithic humans are more likely either a result of individual variation within Neanderthals or indicative of a temporal trend towards facial gracilization in later Neanderthals. More late Neanderthal fossils are needed in order to accurately test these hypotheses.

7. Summary and Conclusions

7.1 Summary

The main objectives of the dissertation were to 1) use semilandmark geometric morphometric (SGM) methods to quantify small-scale facial traits (e.g., infraorbital plate orientation and topography, nasal projection, angle of zygomatic, browridge shape) frequently used to define Pleistocene taxa (e.g., *H. erectus*/*ergaster*, *H. antecessor*, *H. heidelbergensis*, *H. neanderthalensis*, *H. sapiens*); 2) quantify the ontogenetic variability of these traits within recent human groups to better assess the development of facial features; 3) quantify the same traits in a large sample of Pleistocene fossil human material for the first time incorporating rarely-used material (e.g., ATD6-69, Zuttiyeh and Saint-Césaire); 4) assess the effects of allometry on these facial features; and 5) identify temporal trends in facial morphology.

In this context, four specific studies were carried out, each of which utilized a unique landmark dataset that was designed according to the specific research question.

- Chapter 3 evaluated the Middle Pleistocene human (MPh) face in a broad evolutionary and developmental context and assessed the effects of ontogenetic and static allometry on the Pleistocene human face.
- Chapter 4 analyzed the *H. antecessor* subadult (ATD6-69) facial morphology in an evolutionary and developmental context and employed growth simulations to visualize potential adult shapes of ATD6-69.
- Chapter 5 utilized SGM to better understand the taxonomic affinities of the Zuttiyeh craniofacial fossil.
- Chapter 6 applied a similar series of analyses as Chapter 5 in order to evaluate the morphology of the fragmentary, Late Pleistocene Neanderthal fossil Saint-Césaire.

7.1.1 Facial growth and allometry

The results of our ontogenetic studies (Ch. 3 and 4) indicate that population and taxon-specific facial morphology develops prenatally or very early postnatally. In each of the recent modern human groups in our sample (South African, French/Austrian, Native American), distinctive population-specific facial morphology was present in the youngest specimens, i.e., before the eruption of permanent dentition. Additionally, the facial features that are used to discriminate between Neanderthals and recent modern humans have also developed by this time point. Our results regarding the contribution of postnatal facial growth to further differentiate modern humans and Neanderthals are more ambiguous however.

The angle between the Neanderthal and recent modern human allometric vectors was calculated and tested for significance using a permutation test. Our results suggest that Neanderthals and recent modern humans share a common pattern of allometric scaling during postnatal facial growth (Chapter 3). However, our growth simulations incorporating the *H. antecessor* dataset (Chapter 4), demonstrate that postnatal development further accentuates the facial differences between recent modern humans and Neanderthals that were already established at birth. Although the landmark datasets analyzed in these two studies are not identical, the overall pattern and distribution of individuals in Procrustes shape and form space, as well as the position and direction of the Neanderthal and modern human postnatal ontogenetic allometric trajectories, are very similar in both studies. Most likely, the angle between the modern human and Neanderthal slopes was not statistically significant because of the small Neanderthal sample size. Because we demonstrate visually that there are allometric shape changes between Neanderthals and modern humans during postnatal ontogeny, both pre- and postnatal ontogenetic growth is important in establishing morphological differences in facial shape between Neanderthals and recent modern humans. The results imply that the adult morphology of ATD6-69 would be similar to its subadult morphology, but more pronounced.

MPhs and Neanderthals overlap in all mid- and lower-facial analyses. The large-scale facial differences between these two groups can be mainly attributed to allometric scaling along a shared ancestral trajectory. In all ontogenetic analyses Arago 21 and SH 5 plot on one end of the MPh static allometric trajectory, and Petralona, Kabwe and Bodo fall on the opposite end, indicating that the latter group of hominins express larger faces. This signal may suggest sexual dimorphism within the MPhs sample, Arago 21 and SH 5 being small females and Bodo, Kabwe and Petralona being large males. Sexual dimorphism is potentially a major source of variation. However, assigning sex to fossil hominins can be problematic because sexual dimorphism is determined on the same feature used for sex diagnosis. Among the MPhs in our sample Arago 21, Bodo, Kabwe, Petralona and Dali have been described as males in earlier studies (Keith, 1927; Lumley and Lumley, 1973; Pope, 1992). However, the sex assignment of SH 5 is more ambiguous. Compared to other specimens from the SH assemblage, as well as other MPhs and Neanderthals, Arsuaga et al. (1997) notes that the calvarial and cranial base measurements suggest that SH 5 is a small male or a female, but on the other hand Rosas (1997) assigns the SH 5 mandible to a male. While we cannot rule out the possibility that the size discrepancy between these MPhs is due to sexual dimorphism, the variation seen in these fossils could also be attributed to interpopulation variation, directional trends or diachronic fluctuations.

The results in Chapter 3 indicate that facial features most affected by allometric scaling include: anterior glabellar projection, nasal aperture width, lateral projection of the zygomatic bones, infraorbital surface topography, and lengthening of the subnasal region. Because these features are susceptible to allometric scaling, one should be cautious when using them to make phylogenetic associations. One caveat concerning these results is the size bias in the modern human population from Point Hope, Alaska. Individuals from this population exhibit the largest faces in the modern human sample and therefore allometric scaling among this population may be driving these particular shape changes. Future studies will test this by excluding the Point Hope

individuals, recalculating the modern human ontogenetic allometric trajectories, and comparing the shape changes associated with allometry.

Our results indicate that an infraorbital depression is a variable feature within and between modern human populations, but that its shape changes very little throughout individual development. While size influences the shape and topography of the infraorbital region, it is not the only factor. Using growth simulations, we demonstrate that a modern human scaled to the size of Bodo clearly displays a less inflated surface topography because of the fundamental differences in their craniofacial architectures. The shape and depression of this feature covaries with the eversion of the lateral nasal walls and the projection of both the inferior orbital rim and maxillary process of the zygomatic. Therefore our results suggest that infraorbital topography is not necessarily a feature in itself, but rather a by-product (i.e., secondarily derived) of the surrounding morphology. Thus, the infraorbital depression, or the canine fossa, is not a character in the cladistic sense, and because the face appears to be so highly integrated facial features should be used with caution in cladistic analyses. Moreover, neither our methods, nor cladistics, can demonstrate that the depression in ATD6-69 is homologous to that found in modern humans. Studies on bone growth remodeling of this region could provide us with greater insight.

7.1.2 Temporal trends

The most apparent trend in all analyses is the distinctiveness of modern human (both recent and Upper Paleolithic) facial morphology. Regardless of the dataset used, modern humans always cluster together, and there is a clear division between them and archaic *Homo* (e.g., Early and Middle Pleistocene humans and Neanderthals). Zhoukoudian 101 and 102 are the main exceptions to this pattern. In the Zuttiyeh analysis, they fall on the fringe of modern human variation due to their robust browridge morphology. A possible explanation for the division

between archaic and modern humans in all analyses is a sampling bias in recent modern human individuals. In all studies there are significantly more recent modern human than fossil specimens. Subsampling of the recent modern humans and/or resampling of the fossil specimens is one way to test for this potential problem and will be addressed in future studies.

The mid- and lower-faces of Jebel Irhoud 1 and Near Eastern early *H. sapiens* (Skhul 5, Qafzeh 6 and 9) fall within the range of modern human variation; however, when their upper faces (i.e., browridge and frontal bone) are included in the PCA they plot between modern and archaic humans. Smith (2002) termed the African fossils from the time span of ca. 250 to 160 ka as the African Transitional Group. The fossil human remains assigned to this group include Jebel Irhoud 1-4, Florisbad, Ngaloba, Eliye Springs, Guomde and Omo Kibish 2. In addition to Jebel Irhoud 1, the only other transitional modern human included in our analyses was Florisbad. Like Jebel Irhoud 1, the upper face of Florisbad is more archaic-like; however because its mid- and lower-face morphology is not preserved we cannot comment on the extent of its modernness. According to the fossils included in our analyses, the similarities in facial morphology between these four temporal groups (transitional, early, Upper Paleolithic and recent modern humans) indicate that the characteristically modern human facial morphology had already evolved in Jebel Irhoud 1, at around 170 ka. Yet, the transitional and early modern human specimens, especially Jebel Irhoud 1, express morphologically more primitive frontal bones.

This pattern is also true for Bodo. Our PCA analyses reveal that Bodo expresses a primitive upper-face and frontal bone combined with a more derived, modern human-like, mid- and lower-face. In fact, in the analyses that include the entire frontal bone (Chapters 5 and 6), Bodo plots on the extreme end of the archaic *Homo* variation, opposite to modern humans. Bodo, as well as Petralona and Kabwe, exhibits a narrow and receding frontal bone in combination with a wider, more projecting and entirely more robust browridge and larger zygomatic bones in all dimensions, like the *H. erectus s.l.* sample. These results suggest that primitive features have been retained in

these specimens. This raises interesting questions about the pattern of integration between the mid- and upper-face that could be addressed in future studies.

In addition to Jebel Irhoud 1 and Bodo, Dali and ATD 6-69 also plot on the edge of modern human variation in mid- and lower-facial analyses. These results present a complex picture regarding the polarity of facial features and demonstrate that modern human-like facial morphology is intermittently present in hominins from four distinct chronological periods in Middle Pleistocene human evolution in Europe, Africa and Asia. The modern human-like features that are present on ATD6-69, Dali and Jebel Irhoud 1 include a coronal orientation of the infraorbital plate, curved zygomaticoalveolar crest, and infraorbital depression, and the only modern human-like facial feature in Bodo is the coronal orientation of the infraorbital plate. There are three possible explanations for the presence of these features on each of these hominins. They are either (collectively or independently): 1) primitive retentions; 2) shared derived (i.e., synapomorphies); and/or 3) result from convergent evolution.

The problem with identifying these features as synapomorphic is that they are not present in the mid-Middle Pleistocene fossil hominins from Africa, the immediate ancestors of *H. sapiens*, yet they occur in earlier forms (e.g., ATD6-69) and the African "transitional" group (e.g., Jebel Irhoud 1-4, Ngaloba, Eliye Springs, Guomde and Omo Kibish 2). The most parsimonious explanation is that the modern human-like facial features (identified above) are part of a generalized, or primitive, facial architecture (following Rak, 1986), and aspects of this facial morphology, such as a curved zygomaticoalveolar crest, coronal orientation of the cheek bones, and possibly the infraorbital depression, may have evolved multiple times in human evolution. This explanation is consistent with our morphometric analysis on the infraorbital region in Chapter 4, which demonstrates how the topography of this region covaries with both size and the surrounding morphology. Moreover, these facial features have been variously identified in the Asian *H. erectus* fossil material (see Pope, 1992). Future work will compare the facial morphology of ATD6-69 by

means of Procrustes superimposition to earlier forms such as *H. erectus* and later forms such as Bodo in order to gain greater clarity regarding the polarity of these facial features.

One potential problem that is in need of further discussion is the taphonomic damage and subsequent facial reconstruction of the Dali specimen. While this fossil undoubtedly expresses a curved zygomaticoalveolar crest and infraorbital depression its proximity to modern humans in our PCAs may be due to our reconstruction methods. After reflecting the more complete side of the face (the right side), we reconstructed its damaged and/or missing morphology around the alveolar region using geometric reconstruction methods via TPS according to the modern human mean shape. In other words, its damaged and/or missing morphology was estimated following a modern human reference. In future studies, aspects of the Dali cranium will also be reconstructed following the Neanderthal and possibly the Middle Pleistocene human mean shape and the three results will be compared. For the present, we do not consider Dali to be a member of *Homo sapiens*, even though its position in our graphs is similar to that of Jebel Irhoud 1, which is included in *H. sapiens* as defined here.

To summarize, modern human-like, or "generalized", facial features were present in varying degrees in more primitive forms, such as Asian *H. erectus* and *H. antecessor*, were generally "lost" in the Middle Pleistocene hominins in Africa and Europe, evolved again in the African "transitional" fossils, and have since been retained in recent modern humans. Therefore the morphological evidence in combination with the geographical location and chronology of relevant fossils all suggest that the beginning of the *H. sapiens* lineage coincides with the African "transitional" hominins. While I acknowledge that our fossil sample from this time period is limited, our results consistently emphasize the distinctiveness of the modern human morphology, including both the African transitional and Near East Skhul and Qafzeh material, suggesting a distinct cladogenetic event. Therefore, I would argue that the nomenclature for these specimens should be *H. sapiens*, rather than "African Transitional Group," transitional *H. sapiens* or early *H. sapiens*.

As discussed in the previous section, MPhs and Neanderthals overlap in all mid- and lower-facial analyses, and the large-scale facial differences between these two groups can be mainly attributed to allometric scaling. The following Neanderthal features are shared with MPhs, but are less pronounced: parasagittally oriented zygomatic bones and infraorbital plate; flat or inflated infraorbital surface topography; and mid-facial prognathism. The growth analyses in Chapter 3 suggest that scaling a Neanderthal face to the size of a large MPh face will result in more laterally projecting zygomatic bones and a less parasagittally oriented face. However, both the inflation of the infraorbital surface topography and midfacial prognathism are maintained and are more pronounced in Neanderthals when compared to similarly sized MPh faces. Therefore, the high degree of infraorbital inflation and midfacial prognathism can be seen as features uniquely present in Neanderthals. According to our PCA and DFA analyses, MPhs and Neanderthals differ more in their upper-face and frontal bone morphology. The MPhs do not share the characteristically Neanderthal double-arched supraorbital torus. Their browridge is entirely more anteriorly projecting and robust, especial at the lateral edges, and their frontal bone is more receding. However, permutation tests indicate that except for Neanderthals and *H. erectus s.l.*, there are no significant differences in frontal and zygomatic bone shape between fossil groups.

Our results show that there is no *clear* distinction between African and European MPh facial morphology; however, among the MPhs, Arago 21 and SH 5 appear to be most similar to one another, and Bodo, Petralona and Kabwe consistently cluster together. As mentioned earlier these two groupings can be partly explained by size. Arago 21 and SH 5 are smaller than Bodo, Petralona and Kabwe and since our findings show that allometric scaling explains some of the morphological differences between the MPhs and Neanderthals, the smaller MPhs – Arago 21 and SH 5 – cluster with the Neanderthals. In all PCA analyses Arago 21 is most similar to a Neanderthal (either La Chapelle-aux-Saints or Guattari) and SH 5 is most often similar to Arago 21. This latter point could suggest that Arago 21 and possibly SH 5 display incipient Neanderthal features, as put forward in

the accretion hypothesis. Whether the African and European Middle Pleistocene specimens are conspecific (i.e., *H. heidelbergensis*) or the European MPhs are pre-Neanderthals that look like African *H. rhodesiensis* due to symplesiomorphies cannot be clearly determined with our data. However, one intriguing alternative possibility is that Arago 21 and SH 5 are early members of the Neanderthal lineage and Petralona, Bodo, Kabwe and possibly Zuttiyeh form a Middle Pleistocene group that is either part of a separate lineage leading to *H. sapiens*, or a persistence of the common ancestral species of *H. sapiens* and *H. neanderthalensis*. A more comprehensive analysis including the entire cranium could provide us with greater insight.

7.1.3 Evolutionary implications

ATD6-69 and Zuttiyeh: early to mid-Middle Pleistocene evolutionary scenarios

Our results regarding the phylogenetic relationships of ATD6-69 and Zuttiyeh to earlier and later humans, and its implications for early to mid-Middle Pleistocene human evolution are equivocal. ATD6-69 expresses a mosaic pattern of facial morphology, and several features are certainly modern human-like (e.g., infraorbital depression). However, as discussed above, its modern human-like facial features are part of a generalized morphology that most likely evolved several times in human evolution, and therefore they do not exclusively link *H. antecessor* to *H. sapiens*. Dental studies, on the other hand, emphasize continuity in Europe between Gran Dolina and the Sima de los Huesos material (Gómez-Robles et al., 2007; Martinón-Torres, 2007; Gómez-Robles et al., 2011). If *H. antecessor* is the last common ancestor to Neanderthals and modern humans (Bermúdez de Castro et al., 1997, 2011; Arsuaga et al., 1999), then these two taxa diverged in the early Middle Pleistocene and there was long-term continuity in Africa and Europe. While there is some morphological evidence to support a long-term continuity in Europe, it is inconsistent with both the Neanderthal and modern human divergence dates based on genetic data and the archaeological record.

The date of the *H. antecessor* material at around 780 ka, or possibly earlier (1.2 Ma) if the Sima de Elefante material is included in this taxon, predates the molecular results estimating that the most recent common ancestor (MRCA) of Neanderthals and modern humans occurred during the time interval of 315 to 538 ka (Endicott et al., 2010). Moreover, there is no record of the Acheulean industry in Europe prior to 600 ka, although it appeared in Africa over 1.6 Ma (Hublin, 2009). The occurrence of the Acheulean industry in Europe can be best explained by a second migration of large brained hominins out of Africa carrying this technology into Europe at around 600 ka (Templeton, 2002, 2005). Therefore all lines of evidence – morphological, genetic, and archaeological - most strongly support the hypothesis that *H. antecessor* is ancestral to both the European and African MPhs and is not the last common ancestor to *H. neanderthalensis* and *H. sapiens*.

Overall, the diversity of fossils to which Zuttiyeh is most similar morphologically (e.g., Shanidar 5, Arago 21, Skhul 5, Sima de los Huesos 5, Amud 1) strongly suggests that it exhibits a generalized morphology, which one would expect to see in the last common ancestor of Neanderthals and modern humans. Our results support either 1) a late divergence time (ca. 300 ka) between Neanderthals and modern humans from a Eurasian and African Middle Pleistocene species; 2) an accretionary model of Neanderthal evolution, in which Zuttiyeh would have been an early member of a Eurasian Neanderthal lineage; or 3) an interpretation of Zuttiyeh as a late-surviving member of an early to mid-Middle Pleistocene species (e.g., 800-500 ka), which gave rise to Neanderthals and modern humans earlier in time than the Zuttiyeh population. All three of these scenarios are consistent with Endicott et al.'s MRCA time interval estimate (315-538 ka) and both Noonan et al.'s (2008) and Green et al.'s (2010) Neanderthal and modern human genetic divergence dates of ca. 370 ka and between 270-440 ka, respectively. Hopefully, future fossil discoveries from sites in southwestern Asia, like Qesem Cave, will shed more light on Middle Pleistocene human evolution in this region.

Therefore, given the results present in this body of work, in combination with the archaeological evidence and recent genetic divergence estimates between Neanderthals and modern humans, the most convincing early to late Middle Pleistocene evolutionary scenario is as follows:

- *H. antecessor* is an early Middle Pleistocene species present in Europe and possibly North Africa. If the *H. antecessor* material and the contemporaneous North African material are conspecific then the nomen *H. mauritanicus* might be considered to have priority[5]. This species originated via a distinct speciation event from an earlier *H. erectus/ergaster* –like form in Africa or Europe around 1.3-1 Ma (depending upon affinities of the Elefante fossils). If *H. antecessor* and the North African material are conspecific then migration and gene flow occurred between these two continents.
- The mid-Middle Pleistocene fossils in Africa and Europe form a wide-ranging species, *H. heidelbergensis* or *H. rhodesiensis* (if the Mauer mandible is not included), that originated in Africa or Europe from an *H. antecessor* –like form. Regardless of whether it originated in Africa or Europe, this species presumably migrated between the two continents and carried with it Acheulean technology. Petralona, Bodo and Kabwe and are definitely included in this group; however, the inclusion of Arago 21, SH 5 and Zuttiyeh (less so) is more equivocal. These latter fossils may represent the beginning of the Neanderthal lineage and possibly a chronospecies of *H. neanderthalensis*. Under this model, *H. rhodesiensis* is ancestral to *H. sapiens* in Africa. According to this model, substantial levels of genetic drift are responsible for the origins of Neanderthals in Europe and modern humans in Africa (see Endicott et al. 2010). The primary problem with this model is the date of the SH material. The morphology of this SH hominins is too derived in the Neanderthal direction for such an early geological

[5] However, following Arambourg (1955), *H. mauritanicus* (or *Atlanthropus mauritanicus*) appears to have been named provisionally, which renders it unavailable.

date of ca. 600 ka. If the taphonomic doubts concerning the SH material is substantiated and the previous dates of between 200 and 400 ka are correct, then this scenario becomes more plausible.

- The origin of *H. sapiens* occurs in Africa during the late Middle Pleistocene. This speciation event is associated with the African "transitional" group and includes fossils from sites such as Jebel Irhoud, Omo Kibish, Herto and Guomde among others.

Saint-Césaire: Late Pleistocene evolutionary scenario

Lastly, our results do not provide morphological evidence for Neanderthal and modern human admixture in the Saint-Césaire specimen. The facial and frontal morphology of Saint-Césaire unquestionably resembles that of a Neanderthal, and it is most similar to Shanidar 1 and La Ferrassie 1. Its more gracile features that have been used to suggest interbreeding with modern humans cannot be explained entirely by allometric scaling. There may be a trend in facial reduction and supraorbital robusticity while still maintaining total facial prognathism as described by others (e.g., Frayer et al., 1993), or this could simply be a result of individual variation within Neanderthals. More well-preserved late Neanderthals are needed to accurately test these hypotheses.

7.2 Contributions

This was the first set of studies to use semilandmark geometric morphometric methods to quantify small-scale facial features on recent and archaic humans. By doing so, we have demonstrated that this method is superior to more traditional approaches, such as scoring features, because it is both objective and repeatable. An additional advantage to this method is its strength in

visualization. Not only have these small-scale features been quantified, but we were also able to visualize how they change with size and through time, and how they covary with other features. For these reasons, these studies improve our understanding of growth and allometry in Middle Pleistocene *Homo*, Neanderthals and modern humans.

This was also the first analysis to include the subadult *H. antecessor* (ATD6-69) specimen in both an evolutionary and developmental context and use growth simulations to predict its adult morphology. We demonstrate that its adult morphology would have been very similar to its current morphology, just more pronounced. These results imply that subadult fossil remains of Middle to Late Pleistocene *Homo* can also be used to reconstruct phylogenetic relationships and should no longer be overlooked for this purpose.

Additionally, this was the most comprehensive morphometric study on both the Zuttiyeh fossil and the reconstructed Saint-Césaire Neanderthal fossil. The results of the Zuttiyeh study underscore its generalized morphology, and the results of the Saint-Césaire study demonstrate that admixture between Neanderthals and Upper Paleolithic modern humans cannot be detected in the morphology of this specimen. Together these studies contribute to our understanding of the evolution of facial morphology from the early Middle Pleistocene to present times, as well as the phylogenetic relationships between the taxa over this time period.

7.3 Future directions

The analysis presented in this dissertation both provides the opportunity to build on current research by incorporating new fossil specimens and opens up several new avenues of study on the ontogeny of hominin facial morphology. While this dissertation demonstrates that postnatal development further accentuates the facial differences between recent modern humans and Neanderthals, we were unable to show statistically that the growth trajectories between modern

humans and Neanderthals were significantly different from one another. Increasing the subadult Neanderthal sample size would increase our understanding of Neanderthal facial ontogeny and the differences between them and modern humans. There are several subadult Neanderthal facial specimens that could not be included in the analyses because they require extensive reconstruction, including: Le Moustier 2, La Quina 18 and Roc de Marsal. Additionally, several subadult early *H. sapiens* specimens (e.g., Qafzeh 10, 11, and Skhul 1) from Israel were recently scanned by the Max Planck Institute. A study on the comparison of facial growth between them, recent modern humans and Neanderthals would complement a growing body of research on dental (e.g., Smith et al., 2007) and brain (e.g., Gunz et al., 2010) development that seeks to understand when the uniquely modern human pattern of growth and development originated.

The results from our studies consistently show that there were differences in timing between the evolution of the mid- and lower-face compared to the upper-face and frontal bone, indicating that craniofacial evolution occurred in a mosaic manner. Additionally, our results clearly demonstrate that facial features covary with one another suggesting that at least the mid- and lower-face are highly integrated. The data collected in this dissertation could be used to address questions of craniofacial integration. Moreover, this would be an exciting opportunity to collaborate with other researchers (e.g., Neubauer et al., 2009, 2010; Gunz et al., 2010), who share a similar semilandmark endocranial dataset, to pursue a large-scale study on integration.

Further investigation into facial development within our modern human sample is another avenue of research worth investigating. An interesting result from the dissertation is that population specific facial morphology has developed early postnatally or possibly prenatally. Comparing the rate and development of facial growth among the recent modern human populations in our sample would provide us with a greater insight to recent modern human facial variation.

Lastly, a methodologically new avenue to explore, and the next logical step, is research on bone growth remodeling of the face. As bone is a dynamic tissue that is constantly changing throughout an individual's lifetime, evolutionary changes in facial morphology have often been interpreted as adaptive. However, the developmental mechanisms that underlie bone growth on a microscopic scale are largely unexplored. The pioneering work of Enlow (1962, 1963, 1966a, b) and Bromage (1987, 1989) revealed that structural differences in the human craniofacial skeleton are reflected in specific patterns at the microscopic level through bone deposition and resorption (i.e., removal). However, Enlow's studies are restricted to only a few populations because of the invasive techniques applied. Therefore, linking large-scale changes in facial growth observed during childhood with changes in specific patterns at the microstructural level would be an exciting and novel research avenue to pursue. To do so, patterns of bone remodeling would be visualized using microscopy, and data would be collected from several geographically diverse populations of modern humans across age groups and compared between the groups. Additionally, incorporating fossil material could provide us with greater insight into the homology of specific facial features across taxa, such as the infraorbital depression.

Appendix A: Craniofacial Landmarks and Definitions

DORSAL (Midsagittal, 12)

1. [i] **Inion** – an ectocranial midline point at the base of the external occipital protuberance[1]

2. [op] **Opisthocranion** – an instrumentally determined point at the rear of the cranium. It is defined as the midline ectocranial point at the farthest chord length from glabella[1]

3. [l] **Lamdba** – the ectocranial midline point where the sagittal and the lambdoidal sutures intersect; when in doubt, choose the point where the lateral halves of the lambdoidal suture and the lower end of the sagittal suture would be projected to meet.[1] The apex of the occipital bone at its junction with the parietals, in the midline; there is often an intercalary or apical bone at the site, in which case lambda is to be found by extending the general curving course of each half of the lambdoid suture to their intersections with the midline (or halfway between these intersections)[2]

4. [ap] **Apex** – an instrumentally determined, ectocranial midline point placed where a coronal plane through the right and left poria intersects the midsagittal skull outline[1]

5. [b] **Bregma** – the ectocranial point where the coronal and sagittal sutures intersect.[1] The posterior border of the frontal bone in the median plane; the general course of the suture as a whole should be lightly drawn with a pencil, and the bregma established on this; the sutures may meet with rounded external edges, resulting in a cleft or depression at their junction. Bregma is then to be established "in the air," i.e., its correct position is at the level of the general surface of the bone[2]

6. [pts] **Midline post-toral sulcus** – the minima of concavity on midline post-toral frontal squama[3]

7. [g] **Glabella** – the most anterior midline point on the frontal bone, usually above the frontonasal suture[1] (in Frankfurt Horizontal)

8. [n] **Nasion** – the intersection of the fronto-nasal suture and the median plane; if there is irregularity near the midline, rectify the general curve of the fronto-nasal suture with a pencil so as to find the correct level for nasion[2]

9. [rhi] **Rhinion** – the midline point at the inferior free end of the internasal suture[1]

10. [ns] **Nasospinale** – the point where a line tangent to the inferiormost points of the two curves of the inferior nasal aperture margin (edge, rim) crosses the midline[1] (this point is inferior to anterior nasal spine)

11. [ans] **Anterior nasal spine** – thin projection of bone on the midline at the inferior margin of the nasal aperture[1]

12. [ids] **Alveolare (infradentale superius)** – the midline point at the inferior tip of the bony septum between the upper central incisors[1]

DORSAL (Bilateral, 33)

13. [iof] **Infraorbital foramen** – located below the inferior orbital rim on the facial surface[1] (taken at the most superior point)

14. [ilr] **Inferolateral rhinion** – the most inferior end point of the nasomaxillary suture; this point defines the inferior lateral corner of the nasal bone[4]

15. [ana] **Anterior nasal aperture** – the most anterior point on the margin of the nasal aperture, usually superior to alare[4] (the point is best viewed laterally)

16. [al] **Alare** – instrumentally determined as the most lateral point on the margin of the nasal aperture[1]

17. [zm] **Zygomaxillare** – the most inferior point on the zygomaticomaxillary suture[1]

18. [zyo] **Zygoorbitale** – the point where the orbital rim intersects the zygomaticomaxillary suture[1]

19. [mom] **Medial orbital margin** – the point of maximal concavity on the medial inferior corner of the orbital margin, where the orbital margin and the frontal process of the maxilla meet at a right angle[4]

20. [sln] **Superolateral nasion** – the superior lateral point where the frontonasal and nasomaxillary sutures cross; this point defines the superior lateral corner of the nasal bone[4]

21. [d] **Dacryon** – the point where the lacrimomaxillary suture meets the frontal bone[1]

22. [son] **Supraorbital notch** – the point of greatest projection of notch into the orbital space[3] (on the orbit, laterally. if there is a foramen, take on orbital rim on the lateral side of the foramen; if there is no notch, take on lateral side of foramen)

23. [lom] **Lateral orbital margin** – the point of maximal concavity on the lateral inferior corner of the orbital margin[4]

24. [or] **Orbitale** – the lowest point on the orbital margin[1] (considerable variation exists and this point is not always located on the inferior lateral margin of the orbit)

25. [fmt] **Frontomalare temporale** – the point where the frontozygomatic suture crosses the temporal line (or outer orbital rim)[1]

26. [fmo] **Frontomalare orbitale** – the point where the frontozygomatic suture crosses the inner orbital rim[1]

27. [mti] **Mid-torus inferior** – the point on inferior margin of supraorbital torus (superior margin of the orbit) roughly at middle of orbit[5]

28. [mts] **Mid-torus superior** – the superior to MTI on superior most point of the supraorbital torus when viewed in Frankfurt Horizontal[5] (in modern humans, the supraorbital torus is divided into (1) a superior supraciliary arch and glabellar region (medial), (2) a supraorbital sulcus (midway in between), and (3) a supraorbital arch (lateral). MTS should be taken on the superior border of (3) the supraorbital arch, between (1) and (3)[4]

29. [fsm] **Frontosphenomalare** – the point on external cranial vault where frontal, sphenoid and malar bones join[3]

30. [ap] **Anterior pterion** – a region, rather than a point, where frontal, temporal, parietal, and sphenoid meet on the side of the vault. The sutural contact pattern is this area is highly variable[1] (where the coronal suture intersects the sphenofrontal or sphenoparietal sutures)

31. [pp] **Posterior pterion** – the point posterior to anterior pterion, where the sphenotemporal, squamosal, and sphenoparietal sutures intersect[4] (sutural pattern in the pterion region is highly variable and this bilateral landmark may or may not be present due to sutural fusion on either or both sides)

32. [szt] **Superior zygomaticotemporal suture** – the anterosuperior point of zygomaticomaxillary suture (taken at orbital rim)[5]

33. [ju] **Jugale** – the point in the depth of the notch between the temporal and frontal processes of the zygomatic[1]

34. [po] **Porion** – the uppermost point on the margin of the external auditory meatus[1]

35. [au] **Auriculare** – a point vertically above the center of the external auditory meatus at the root of the zygomatic process, a few millimeters above porion[1] (found on the suprameatal crest)

36. [ets] **Infero-lateral ectotympanic tube superior** – the point on superior border of inferior margin of ectotympanic tube, directly inferior to porion[6] (taken a bit inward)

37. [eti] **Infero-lateral ectotympanic tube inferior** – the point on inferior border of inferior margin of ectotympanic tube, directly inferior to porion[6] (taken as the most inferior point)

38. [mro] **Malar root origin** – the point where malar root arises from the maxilla (often a point of concavity between molar juga and malar root)[3]

39. [rzp] **Root of the zygomatic process** – the malar root origin projected onto buccal alveolar surface[7]

40. [co] **Coronale** – the point on the coronal suture where the breadth of the frontal bone is greatest[1]

41. [st] **Stephanion** – the point where the coronal suture crosses the temporal line.[1] The intersection of the coronal suture and the limit of the temporal muscle (the superior temporal line)[2]

42. [ft] **Frontotemporale** – the point where the temporal line reaches its most anteromedial position on the frontal[1]

43. [pn] **Parietal notch** – forms on the posterosuperior border of the temporal where the squamosal and parietomastoid sutures meet[1] (sutural pattern in this region can be variable, but the point is usually found posterior to the supramastoid crest; it is best to locate the parietomastoid and squamosal sutures first)

44. [ast] **Asterion** – the point where the lambdoidal, parietomastoid, and occipitomastoid sutures meet.[1] If the meeting point is occupied by a wormian bone (os astericum), extend the lambdoid suture onto its surface, and then extend the other two sutures (temporo-parietal, temporo-occipital) to the first line, finding asterion as the point midway between the intersections if these do not coincide; use only the part of the last two sutures (ca. 1 cm) which is nearest the point, in finding these directions. If the lambdoid (or other) suture is complex or composed of wormian

bones, trace a pencil line along the center of the area covered by the complexity, as well as can be done, to find the main axis of the suture[2]

45. [ptl] **Posterior temporal line** – the point of intersection of the superior temporal line and parietomastoid suture (extrapolated if necessary)[6] (this may be a difficult landmark, but it is usually found between parietal notch and asterion where the parietal bone is raised; this morphology is much like the raised supramastoid crest as it is the "end extension" of the inferior temporal line)

VENTRAL (Midsagittal, 8)

46. [inl] **Inferior nuchal line** – the midline point where the (transverse) inferior nuchal line and the (sagittal) median nuchal line meet; these two lines form a cross, point should be taken at the center[4]

47. [o] **Opisthion** – the midline point at the posterior margin of the foramen magnum[1]

48. [ba] **Basion** – the midline point on the anterior margin of the foramen magnum[1]

49. [ho] **Hormion** – the most posterior midline point on the vomer[1] (taken on the sphenoid, directly below the posterior midline point of the vomer)

50. [sta] **Staphylion** – the point on the interpalatal suture where a line drawn between the deepest parts of the notches (free edges) at the rear of the palate crosses the midline[1]

51. [map] **Midline anterior palatine** – the anterior most point on the midline of transverse palatine bone[6]

52. [iv] **Incisivion** – midline point at posterior margin of the incisive foramen (oral)[3]

53. [ol] **Orale** – the midline point on the hard palate where a line drawn tangent to the posterior margins of the central incisor alveoli crosses the midline[1]

VENTRAL (Bilateral, 33)

54. [izs] **Inferior zygomaticotemporal suture** – anteroinferior point of zygomaticomaxillary suture, in antero-lateral view[5]

55. [poc] **Posterior occipital condyle** – most posterior point on long axis of occipital condyle, taken on condyle[6]

56. [aoc] **Anterior occipital condyle** – most anterior point on long axis of occipital condyle, taken on condyle[6]

57. [ms] **Mastoidale** – the most inferior point on the mastoid process[1]

58. [jme] **Juxtamastoid eminence** – taken on the most inferior point. This eminence is located between the digastric fossa (lateral) and the groove for occipital artery (medial)–in other words, it's the peak between two valleys[4,7]

59. [omc] **Occipitomastoid crest** – most inferior point on the occipitomastoid suture. In modern humans, the crest is medial to the juxtamastoid crest and the groove for occipital artery (this point corresponds to Baab[6], not Harvati[7])

60. [tmf] **Tympanomastoid fissure** – point on lateral border of the tympanomastoid fissure[6]

61. [mtc] **Medial petrotympanic crest** – most medial point of petrotympanic crest at level of carotid canal[8] (where crest meets the canal)

62. [ltc] **Lateral petrotympanic crest** – lateral origin of petrotympanic crest[8] (taken where the mastoid and the margin of EAM meets; if crest splits, take the posterior branch by the mastoid)

63. [smf] **Stylomastoid foramen** – taken on the posterior border[7]

64. [ajf] **Anterior jugular fossa** – most antero-medial point of the jugular fossa[7] (on the edge of the fossa; this measures the diagonal, maximum length of the jugular fossa)

65. [pjf] **Posterior jugular fossa** – most postero-lateral point of the jugular fossa[7] (on the edge of the fossa; this measures the diagonal, maximum length of the jugular fossa)

66. [pg] **Postglenoid** – infero-lateral-most point posterior to glenoid fossa and anterior to ectotympanic tube (corresponds to postglenoid tuberosity[5] or postglenoid crest)

67. [ieg] **Inferior entoglenoid** – most inferior point on the entoglenoid pyramid[7] (medial portion of glenoid fossa, bump forms next to suture)

68. [laf] **Lateral articular fossa** – deepest point on the lateral margin of the articular eminence (root of the articular eminence)[7] (point of maximum concavity, on the edge of mandibular fossa)

69. [cmf] **Center of mandibular fossa** – point of intersection of the long axis and the axis perpendicular to the long axis of the mandibular fossa[6]

70. [mtf] **Medial squamotympanic fissure** – intersection of squamotympanic fissure / petrotympanic fissure with medial edge of mandibular fossa[6]

71. [ltf] **Lateral squamotympanic fissure** – intersection of squamotympanic fissure with lateral edge of mandibular fossa[6] (usually by the lateral edge of the EAM, behind postglenoid, if possible)

72. [fs] **Foramen spinosum** – point on posterolateral border of foramen spinosum[6]

73. [app] **Anterior petrous pyramid of tympanic** – antero-medial-most point on petrous pyramid of tympanic, visible in basal view[6] (taken on the sphenoid bone, just anterior to the most antero-medial point of the pyramid)

74. [sps] **Spheno-palatine suture** – suture between palatine and sphenoid bones[7] (taken posterior and inferior to maxillary tuberosity)

75. [tss] **Temporo-sphenoid suture** – point where sphenotemporal suture passes from squama to cranial base, often on infratemporal crest[6]

76. [lpr] **Lateral prosthion** – antero-inferior-most point on premaxilla, equivalent to prosthion, but between central and lateral incisors[5]

77. [lcm] **Lingual canine margin** – most lingual aspect of canine alveolar process[3]

78. [c1p3] **Canine-P3 contact** – point of contact projected onto buccal alveolar surface[3]

79. [p3p4] **P3-P4 contact** – point of contact projected onto buccal alveolar surface[3]

80. [p4m1] **P4-M1 contact** - point of contact projected onto buccal alveolar surface[3]

81. [m1m2] **M1-M2 contact** – projected (laterally) onto alveolar margin[5]

82. [m2m3] **M2-M3 contact** - point of contact projected onto buccal alveolar surface[3]

83. [dm3] **Distal M3** – distal midpoint projected (laterally) onto alveolar margin[5]

84. [mt] **Maxillary tuberosity** – most posterior point on 'occlusal' surface of alveolus[3]

[1]White and Folkens, 2000; [2]Howells, 1973; [3]McNulty, 2003; [4]new landmarks, defined here; [5]Frost et al., 2003; [6]Baab, 2007 [7]Harvati, 2001; [8]Harvati, 2003

Appendix B: Craniofacial Curve Semilandmarks and Definitions

1. [NAR/NAL] **Nasal aperture right/left –** lateral rhinion to lateral anterior nasospinale along nasal margin; 10 semilandmarks (sl)

2. [AOR/AOL] **Alveolar outline right/left** – anterior sphenopalatine suture to lateral alveolare; 10 sl

3. [SO] **Subnasal outline** – superior alveolare to inferior anterior nasal spine; 3 sl

4. [MCR/MCL] **Maxillary contour left/right** – superior root of zygomatic process to medial zygomaxillare; 4 sl

5. [IZR/IZL] **Inferior zygomatic outline right/left** – lateral zygomaxillare to anterior porion; 12 sl

6. [SZR/SZL] **Superior zygomatic outline right/left** – anterior auriculare to posterior jugale; 10 sl

7. [LZR/LZL] **Lateral zygomatic outline right/left** – superior jugale to inferior frontomalare temporale; 3 sl

8. [SPR1/SPL1] **Supraorbital profile 1 right/left** – most anterior projection of browridge from between frontomalare and orbitale (highest point) to lateral nasion; 10 sl

9. [TLR/TLL] **Temporal line right/left** – posterior frontotemporale to superior posterior temporal line along superior temporal line; 20 sl

10. [IOR/IOL] **Inferior orbital margin right/left** – lateral medial orbital margin to inferior frontomalare orbitale; 11 sl

11. [SOR/SOL] **Superior orbital margin right/left** – superior frontomalare orbitale to superior medial orbital margin; 8 sl

12. [MSP1] **Midsagittal profile 1** – superior nasion to anterior bregma; 12 sl

13. [MSP2] **Midsagittal profile 2** – posterior bregma to anterior lambda; 11 sl

14. [LSR/LSL] **Lambdoidal suture right/left** – medial asterior to lateral lambda; 9 sl

15. [SNR2/SNL2] **Superior nuchal line 2 right/left** – lateral asterior to medial inion; 7 sl

16. [INR/INL] **Inferior nuchal line right/left** – posterior jugale to inferior nuchal landmarks; 7 sl

17. [MSP3a] **Midsagittal profile 3a** – inferior lambda to superior inion; 8 sl

18. [MSP3b**] Midsagittal profile 3b** – superior inion to superior opisthion; 4 sl

19. [FMR/FML] **Foramen magnum right/left** – lateral opisthion to lateral basion; 7 sl

20. [MP] **Midsagittal palate** – anterior staphylion to posterior orale; 7 sl

21. [SNR1/SNL1] **Supreme nuchal line right/left** – lateral asterion to most center point along crest/line; 7 sl

22. [SPR2/SPL2] **Supraorbital profile 2 right/left** – frontomalare temporale to lateral/superior glabella, following browridge shape; 13 sl

References

Ackermann, R.R., Krovitz, G.E., 2002. Common patterns of facial ontogeny in the hominid lineage. Anat. Rec. 269, 142-147.

Aiello, L. 1993. The fossil evidence for modern human origins in Africa: a revised view. American Anthropologist 95, 73-96.

Akazawa, T., Muhesen, S., Dodo, Y., Kondo, O., Mizoguchi, Y., 1995. Neanderthal infant burial. Nature 377, 585-586.

Antón, S.C., 2002. Evolutionary significance of cranial variation in Asian *Homo erectus.* Am. J. Phys. Anthropol. 118, 301-323.

Antón, S.C., 2003. Natural history of *Homo erectus.* Am. J. Phys. Anthropol. S37, 126-170.

Antón, S.C., Swisher III, C.C., 2004. Early dispersals of *Homo* from Africa. Ann. Rev. Anthropol. 33, 271-296.

Arambourg, C. 1954. L'Hominien fossile de Ternifine (Algérie). Comptes Rendus à l'Académie des Sciences de Paris 239, 893-895.

Arambourg, C., 1955. A recent discovery in human paleontology Atlanthropus of Ternifine (Algeria). Am. J. Phys. Anthropol. 13, 191-201.

Arensburg, B., Belfer-Cohen, A., 1998. Sapiens and Neandertals: Rethinking the Levantine Middle Paleolithic Hominids. In: Akazawa, T., Aoki, K., Bar-Yosef, O. (Eds.), Neandertals and Modern Humans in Western Asia. Plenum Press, New York, pp. 311-322.

Arsuaga, J.L., Martínez, I., Gracia, A., Lorenzo, C., 1997. The Sima de los Huesos crania (Sierra de Atapuerca, Spain). A comparative study. J. Hum. Evol. 33, 219-281.

Arsuaga, J.L., Martinez, I., Lorenzo, C., Gracia, A., Munoz, A., Alonso, O., Gallego, J., 1999. The human cranial remains from Gran Dolina Lower Pleistocene site (Sierra de Atapuerca, Spain). J. Hum. Evol. 37, 431-457.

Asfaw, B., Gilbert, W.H., Beyene, Y., Hart, W.K., Renne, P.R., Wolde Gabriel, G., Vrba, E.S., White, T.D., 2002. Remains of *Homo erectus* from Bouri, Middle Awash, Ethiopia. Nature 416, 317-320.

Athreya, S., 2009. A comparative study of frontal bone morphology among Pleistocene hominin fossil groups. J. Hum. Evol. 57, 786-804.

Baab, K.L., 2008. The taxonomic implications of cranial shape variation in *Homo erectus.* J. Hum. Evol. 54, 827-847.

Bar-Yosef, O., 1988. The date of South-West Asian Neandertals. In: Otte, M. (Ed.), L'Homme de Neandertal. Etudes et Recherches Archéologiques de l'Université de Liège, Liège, pp. 31-38.

Bar-Yosef, O., 1989. Geochronology of the Levantine Middle Paleolithic. In: Mellars, P., Stringer, C. (Eds.), The human revolution. Edinburgh University Press, Edinburgh, pp. 589-610.

Bar-Yosef, O., 1992. The role of Western Asia in modern human origins. Phil. Trans. R. Soc. 337, 193-200.

Bastir, M., O'Higgins, P., Rosas, A., 2007. Facial ontogeny in Neanderthals and modern humans. Proc. Biol. Sci. 274, 1125-1132.

Bastir, M., Rosas, A., 2004. Facial heights: evolutionary relevance of postnatal ontogeny for facial orientation and skull morphology in humans and chimpanzees. J. Hum. Evol. 47, 359-381.

Bermúdez de Castro, J.M., Arsuaga, J.L., Carbonell, E., Rosas, A., Martinez, I., Mosquera, M., 1997. A hominid from the lower Pleistocene of Atapuerca, Spain: possible ancestor to Neandertals and modern humans. Science. 276, 1392-1395.

Bermúdez de Castro, J.M., Martinón-Torres, M., Carbonell, E., Sarmiento, S., Rosas, A., van der Made, J., Lozano, M., 2004. The Atapuerca sites and their contribution to the knowledge of human evolution in Europe. Evol. Anthropol. 13, 25-41.

Bermúdez de Castro, J.M., Perez-Gonzalez, A., Martinón-Torres, M., Gómez-Robles, A., Rosell, J., Prado, L., Sarmiento, S., Carbonell, E., 2008. A new early Pleistocene hominin mandible from Atapuerca-TD6, Spain. J. Hum. Evol. 55, 729-735.

Bermúdez de Castro, J.M., Rosas, A., Nicolas, M.E., 1999. Dental remains from Atapuerca-TD6 (Gran Dolina site, Burgos, Spain). J. Hum. Evol. 37, 523-566.

Bermúdez de Castro, J.M., Martinón-Torres, M., Gómez-Robles, A., Margvelashvili, A., Arsuaga, J.L., Carretero, J.M., Martinez, I., Sarmiento, S., 2011. The Gran Dolina-TD6 human fossil remains and the origins of Neanderthals. In: Condemi, S., Weniger, G.-C. (Eds.), Continuity and Discontinuity in the People of Europe: One Hundred Fifty Years of Neanderthal Study. Springer, New York, pp. 67-75.

Bermúdez de Castro, J.M., Martinón-Torres, M., Prado, L., Gómez-Robles, A., Rosell, J., López-Polín, L., Arsuaga, J.L., Carbonell, E., 2010. New immature hominin fossil from European Lower Pleistocene shows the earliest evidence of a modern human dental development pattern. Proc. Natl. Acad. Sci. U. S. A. 107, 11739-11744.

Bermúdez de Castro, J.M., Martinón-Torress, M., Sarmiento, S., Lozano, M., 2003. Gran Dolina-TD 6 versus Sima de los Huesos dental samples from Atapuerca: evidence of discontinuity in the European Pleistocene population. Journal of Archaeological Science 30, 1421-1428.

Bermúdez de Castro, J.M., Rosas, A., Carbonell, E., Nicolás, M.E., Rodríguez, J., Arsuaga, J.L., 1999. A modern human pattern of dental development in lower Pleistocene hominids from Atapuerca-TD6 (Spain). Proc. Natl. Acad. Sci. U. S. A. 96, 4210-4213.

Bischoff, J.L., Williams, R.W., Rosenbauer, R.J., Aramburu, A., Arsuaga, J.L., Garcia, N.,

Cuenca-Bescos, G., 2007. High-resolution U-series dates from the Sima de los Huesos hominids yields 600+/- kyrs: implications for the evolution of the early Neanderthal lineage. J. Archaeol. Sci. 34, 763-770.

Bischoff, J.L., Shamp, D.D., Aramburu, A., Arsuaga, J.L., Carbonell, E., Bermúdez de Castro, J.M., 2003. The Sima de los Huesos hominids date to beyond U/Th equilibrium (> 350 kyr) and perhaps to 400-500 kyr: new radiometric dates. J. Archaeol. Sci. 30, 275-280.

Bookstein, F.L., 1991. Morphometric Tools for Landmark Data: Geometry and Biology. Cambridge University Press, Cambridge.

Bookstein, F.L., 1997. Landmark methods for forms without landmarks: Morphometrics of group differences in outline shape. Med. Image. Anal. 1, 225-243.

Bookstein, F.L., 2005. After landmarks. In: Slice, D.E. (Ed.), Modern morphometrics in physical anthropology. KluwerAcademic/Plenum Publishers, New York, pp. 49–71.

Boule, M. 1911-13. L'Homme fossile de La Chapelle-aux-Saints. Annales de Paleontologie 6, 106-72; 7, 21-192; 8, 1-70.

Bräuer, G., 1984. A craniological approach to the origins of anatomically modern *Homo sapiens* in Africa and implications for the appearance of modern humans. In: Smith, F. H. and Spencer, F. (Eds.), The Origins of Modern Humans: A World Survey of the Fossil Evidence. Alan R. Liss, New York, pp. 327-410.

Bräuer, G., 1992. Africa's place in the evolution of *Homo sapiens.* In: Bräuer, G., Smith, F.H. (Eds.), Continuity or Replacement: Controversies in *Homo sapiens* Evolution. A. A. Balkema, Rotterdam/Brookfield, pp. 83-98.

Bräuer, G., 2008. The origin of modern anatomy: By speciation or intraspecific evolution? Evol. Anthropol. 17, 22-37.

Bräuer, G., Broeg, H., 1998. On the degree of Neandertal-modern continuity in the earliest Upper Paleolithic crania from the Czech Republic: evidence from nonmetrical features. In: Omoto, K., Tobias, P. (Eds.), The Origins of Past Modern Humans; Toward Reconciliation. World Scientific, Singapore, pp. 106-125

Bräuer, G., Yokoyama, Y., Falgueres, C. and Mbua, E. 1997. Modern human origins backdated. Nature 386, 337-338.

Bromage, T.G., 1987. The scanning electron microscopy/replica technique and recent applications to the study of fossil bone. Scan. Microsc. 1, 607-613.

Bromage, T.G., 1989. Ontogeny of the early hominid face. J. Hum. Evol. 18, 751-773.

Brown, P., 1992. Recent human evolution in East Asia and Australasia. Philos. Trans. R. Soc. Lond. 337, 235-242.

Bruner, E., Manzi, G., 2005. CT-based description and phyletic evaluation of the archaic human calvarium from Ceprano, Italy. Anat. Rec. A. 285, 643-658.

Bruner, E., Manzi, G., 2007. Landmark-based shape analysis of the archaic *Homo* calvarium from Ceprano (Italy). Am. J. Phys. Anthropol. 132, 355-366.

Bruner, E., Manzi, G., Arsuaga, J.L., 2003. Encephalization and allometric trajectories in the genus *Homo*: evidence from the Neandertal and modern lineages. Proc. Natl. Acad. Sci. 100, 15335-15340.

Bulygina, E., Mitteroecker, P., Aiello, L., 2006. Ontogeny of facial dimorphism and patterns of individual development within one human population. Am. J. Phys. Anthropol. 131, 432-443.

Carbonell, E., Bermúdez de Castro, J.M., Arsuaga, J.L., Diez, J.C., Rosas, A., Cuenca-Bescos, G., Sala, R., Mosquera, M., Rodriguez, X.P., 1995. Lower Pleistocene hominids and artifacts from Atapuerca-TD6 (Spain). Science. 269, 826-830.

Carbonell, E., Bermúdez de Castro, J.M., Arsuaga, J.L., Allue, E., Bastir, M., Benito, A., Cáceres, I., Canals, T., Díez, J.C., et al., 2005. An Early Pleistocene hominin mandible from Atapuerca-TD6, Spain. Proc. Natl. Acad. Sci. U. S. A. 102, 5674-5678.

Carretero, J.M., Arsuaga, J.L., Lorenzo, C., 1997. Clavicles, scapulae and humeri from the Sima de los Huesos site (Sierra de Atapuerca, Spain). J. Hum. Evol. 33, 357-408.

Carretero, J.M., Lorenzo, C., Arsuaga, J.L., 1999. Axial and appendicular skeleton of *Homo antecessor*. J. Hum. Evol. 37, 459-499.

Cartmill, M., Smith, F., 2009. The Human Lineage. Wiley-Blackwell, Hoboken.

Chech, M., Groves, A., Thorne, A., Trinkaus, E., 1999. A new reconstruction of the Shanidar 5 cranium. Paléorient. 25, 143-146.

Chen, T., Hedges, R.E.M., Yuan, Z., 1989. Accelerator radiocarbon dating for the Upper Cave of Zhoukoudian. Acta Anthropol. Sinica 8, 216-221.

Chen, T., Zhang, Y., 1991. Paleolithic chronology and possible coexistence of *Homo erectus* and *Homo sapiens* in China. World. Archaeol. 23, 147-154.

Clark, J.D., De Heinzelin, J., Schick, K.D., Hart, W.K., White, T.D., Wolde Gabriel, G., Walter, R.C., Suwa, G., Asfaw, B., Vrba, E., 1994. African *Homo erectus*: old radiometric ages and young Oldowan assemblages in the Middle Awash Valley, Ethiopia. Science 264, 1907.

Cobb, S.N., O'Higgins, P., 2004. Hominins do not share a common postnatal facial ontogenetic shape trajectory. J. Exp. Zool. B. Mol. Dev. Evol. 302, 302-321.

Cock, A.G., 1966. Genetical aspects of metrical growth and form in animals. Q. Rev. Biol. 41, 131-190.

Collard, M., Wood, B., 2000. How reliable are human phylogenetic hypotheses? Proc. Natl. Acad. Sci. 97, 5003-5006.

Cook, J., Stringer, C.B., Currant, A.P., Schwarcz, H.P., Wintle, A.G., 1982. A review of the

chronology of the European Middle Pleistocene hominid record. Am. J. Phys. Anthropol. 25, 19-65.

Coon, C.S., 1963. Origin of Races. Knopf, New York.

Day, M.H., Stringer, C.B., 1982. A reconsideration of the Omo-Kibish remains and the *erectus-sapiens* transition. In: Lumley, M.A. (Ed.), L'homo Erectus Et La Place De L'homme De Tautavel Parmi Les Hominidés Fossiles. Centre National de la Recherche Scientifique. Nice, pp. 814-46.

Dean, C., Leakey, M.G., Reid, D., Schrenk, F., Schwartz, G.T., Stringer, C., Walker, A., 2001. Growth processes in teeth distinguish modern humans from Homo erectus and earlier hominins. Nature 414, 628-631.

Dean, D., Hublin, J.J., Holloway, R., Ziegler, R., 1998. On the phylogenetic position of the pre-Neandertal specimen from Reilingen, Germany. J. Hum. Evol. 34, 485-508.
d'Errico, F., Zilhao, J., Julien, M., Baffier, D., Pelegrin, J., 1998. Neanderthal acculturation in Western Europe? A critical review of the evidence and its interpretation. Curr. Anthropol. 39, S1-S44.

Dryden, I.L., Mardia, K.V., 1998. Statistical shape analysis. John Wiley & Sons, Chichester.

Endicott, P., Ho, S.Y., Stringer, C., 2010. Using genetic evidence to evaluate four palaeoanthropological hypotheses for the timing of Neanderthal and modern human origins. J. Hum. Evol. 59, 87-95.

Enlow, D.H., 1962. A study of the post-natal growth and remodeling of bone. Am. J. Anat. 110, 79-101.

Enlow, D.H., 1963. Principles of bone remodeling. Charles C. Thomas Publisher, Springfield, Illinois.

Enlow, D.H., 1966a. A morphogenetic analysis of facial growth. Am. J. Orthod. 52, 283-299.

Enlow, D.H., 1966b. A comparative study of facial growth in *Homo* and *Macaca*. Am. J. Phys. Anthropol. 24, 293-308.

Etler, D.A., 1996. The fossil evidence for human evolution in Asia. Annual Review of Anthropology 25, 275-301.

Falguères, C., Yokoyama, Y., Shen, G., Bischoff, J.L., Ku, T.L., de Lumley, H., 2004. New U-series dates at the Caune de l'Arago, France. J. Archaeol. Sci. 31, 941-952.

Falguères, C., Bahain, J.J., Yokoyama, Y., Arsuaga, J.L., Bermúdez de Castro, J.M., Carbonell, E., Bischoff, J.L., Dolo, J.M., 1999. Earliest humans in Europe: the age of TD6 Gran Dolina, Atapuerca, Spain. J. Hum. Evol. 37, 343-352.

Feibel, C.S., Brown, F.H., McDougall, I., 1989. Stratigraphic context of fossil hominids from the Omo group deposits: northern Turkana Basin, Kenya and Ethiopia. Am. J. Phys. Anthropol. 78, 595-622.

Finlayson, C., 2004. Neanderthals and Modern Humans: An Ecological and Evolutionary Perspective. Cambridge University Press, Cambridge.

Foley, R., Lahr, M.A., 1997. Mode 3 technologies and the evolution of modern humans. Cambridge. Archaeol. J. 7, 3-36.

Frayer, D.W., Wolpoff, M.H., Thorne, A.G., Smith, F.H., Pope, G.G., 1993. Theories of modern human origins: the paleontological test. Am. Anthropol. 95, 14-50.

Freidline, S.E., Gunz, P., Harvati, K., Delson, E., Hublin, J.J., 2008. How three-dimensional surface data can be used to reconstruct fragmentary fossils. Am. J. Phys. Anthropol. S46, 99.

Freidline, S.E., Gunz, P., Harvati, K., Hublin, J., 2010. 3D semilandmark geometric morphometric quantification of modern human facial development. Am. J. Phys. Anthropol. S50, 93.

Freidline, S.E., Gunz, P., Janković, I., Harvati, K., Hublin, J.-J. in press. A Comprehensive Morphometric Analysis of the Frontal and Zygomatic Bone of the Zuttiyeh Fossil from Israel. J. Hum. Evol. doi:10.1016/j.jhevol.2011.11.005.

Gabunia, L., Vekua, A., Lordkipanidze, D., Swisher, C.C., Ferring, R., Justus, A., Nioradze, M., Tvalchrelidze, M., Anton, S.C., et al., 2000. Earliest Pleistocene hominid cranial remains from Dmanisi, Republic of Georgia: taxonomy, geological setting, and age. Science 288, 1019-1025.

Gathogo, P.N., Brown, F.H., 2006. Revised stratigraphy of Area 123, Koobi Fora, Kenya, and new age estimates of its fossil mammals, including hominins. J. Hum. Evol. 51, 471-479.

Gómez-Olivencia, A., Carretero, J.M., Arsuaga, J.L., Rodríguez-García, L., García-González, R., Martínez, I., 2007. Metric and morphological study of the upper cervical spine from the Sima de los Huesos site (Sierra de Atapuerca, Burgos, Spain). J. Hum. Evol. 53, 6-25.

Gómez-Robles, A., Martinón-Torres, M., Bermúdez de Castro, J.M., Margvelashvili, A., Bastir, M., Arsuaga, J.L., Perez-Perez, A., Estebaranz, F., Martinez, L.M., 2007. A geometric morphometric analysis of hominin upper first molar shape. J. Hum. Evol. 53, 272-285.

Gómez-Robles, A., de Castro, J.M., Martinón-Torres, M., Prado-Simón, L., 2011. Crown size and cusp proportions in Homo antecessor upper first molars. A comment on Quam et al. 2009. J. Anat. 218, 258-262.

Gisis, I., Bar-Yosef, O., 1974. New excavations in Zuttiyeh Cave. Paléorient. 2, 175-180.

Glantz, M., Athreya, S., Ritzman, T., 2009. Is Central Asia the eastern outpost of the Neandertal range? A reassessment of the Teshik-Tash child Am. J. Phys. Anthropol. 138, 45-61.

Green, R.E., Krause, J., Briggs, A.W., Maricic, T., Stenzel, U., Kircher, M., Patterson, N., Li, H., Zhai, W., et al., 2010. A draft sequence of the Neandertal genome. Science 328, 710-722.

Green, R.E., Malaspinas, A.S., Krause, J., Briggs, A.W., Johnson, P.L., Uhler, C., Meyer, M., Good, J.M.,

Maricic, T., et al., 2008. A complete Neandertal mitochondrial genome sequence determined by high-throughput sequencing. Cell 134, 416-426.

Grine, F.E., Gunz, P., Betti-Nash, L., Neubauer, S., Morris, A.G., 2010. Reconstruction of the late Pleistocene human skull from Hofmeyr, South Africa. J. Hum. Evol. 59, 1-15.

Grün, G.R., 1996. A re-analysis of electron spin resonance dating results associated with the Petralona hominid. J. Hum. Evol. 30, 227-241.

Grün, G.R., Huang, P.-H., Wu, X., Stringer, C.B., Thorne, A.G., McCulloch, M., 1997. ESR analysis of teeth from the palaeoanthropological site of Zhoukoudian, China. J. Hum. Evol. 32, 83-91.

Grün, G.R., Stringer, C.B., 1991. ESR dating and the evolution of modern humans. Archaeometry. 33, 153-199.

Grün, G.R., Stringer, C.B., McDermott, F., Nathan, R., Porat, N., Robertson, S., Taylor, L., Mortimer, G., Eggins, S., McCulloch, M., 2005. U-series and ESR analyses of bones and teeth relating to the human burials from Skhul. J. Hum. Evol. 49, 316-334.

Guipert, G., 2005. Reconstitution et position phylétique des restes crâniens de l'homme de Tautavel (Arago 21-47) et de Biache-Saint-Vaast 2 apports de l'imagerie et de l'analyse tridimensionelles. Ph.D. Dissertation, Université Paul Cézane.

Guipert, G., Mafart, B., de Lumley, M.-A., 2007. Virtual restoration of the fossil Arago 21-47 and phyletic position (Abstract). Paleoanthropology Society, Philadelphia, PA.

Gunz, P., 2005. Statistical and geometric reconstruction of hominid crania: reconstructing australopithecine ontogeny. Ph.D. Dissertation, University of Vienna.

Gunz, P., Bookstein, F.L., Mitteroecker, P., Stadlmayr, A., Seidler, H., Weber, G.W., 2009a. Early modern human diversity suggests subdivided population structure and a complex out-of-Africa scenario. Proc. Natl. Acad. Sci. 106, 6094-6098.

Gunz, P., Harvati, K., 2007. The Neanderthal "chignon": variation, integration, and homology. J. Hum. Evol. 52, 262-274.

Gunz, P., Mitteroecker, P., Bookstein, F., 2005. Semilandmarks in three dimensions. In: Slice, D.E. (Ed.), Modern Morphometrics in Physical Anthropology. Plenum Publishers, New York, pp. 73-98.

Gunz, P., Mitteroecker, P., Neubauer, S., Weber, G.W., Bookstein, F.L., 2009b. Principles for the virtual reconstruction of hominin crania. J. Hum. Evol. 57, 48-62.

Gunz, P., Neubauer, S., Maureille, B., Hublin, J.J., 2010. Brain development after birth differs between Neanderthals and modern humans. Curr. Biol. 20, R921-R922.

Habgood, P.J., 1989. The origin of anatomically modern humans in Australasia. In: Mellars, P. and Stringer, C.B. (Eds.), The Human Revolution: Behavioural and Biological Perspectives on the Origins of Modern Humans. Edinburgh University Press, Edinburgh, pp. 245-73.

Harrold, F.B., 1989. Mousterian, Châtelperronian, and Early Aurignacian in Western Europe: Continuity or discontinuity? In: Mellars, P. and Stringer, C.B. (Eds.), The Human Revolution: Behavioural and Biological Perspectives on the Origins of Modern Humans. Edinburgh University Press, Edinburgh, pp. 677-713.

Harvati, K., 2001. The Neanderthal problem: 3-D geometric morphometric models of cranial shape variation within and among species. Ph.D. Dissertation, City University of New York.

Harvati, K., 2003a. The Neanderthal taxonomic position: models of intra- and inter-specific craniofacial variation. J. Hum. Evol. 44, 107-132.

Harvati, K., 2003b. Quantitative analysis of Neanderthal temporal bone morphology using three-dimensional geometric morphometrics. Am. J. Phys. Anthropol. 120, 323-338.

Harvati K. 2009a. Petralona: Link between Africa and Europe? In: Schepartz, L. Bourbou, C and Fox, S. (Eds.), New Directions in the Skeletal Biology of Greece. Wiener Laboratory Series, ASCSA, Athens, pp. 31-47.

Harvati, K., 2009b. Into Eurasia: a geometric morphometric re-assessment of the Upper Cave (Zhoukoudian) specimens. J. Hum. Evol. 57, 751-762.

Harvati, K., Frost, S.R., and McNulty, K.P. 2004. Neanderthal taxonomy reconsidered: implication of 3D primate models of intra- and interspecific differences. Proc. Natl. Acad. Sci. 101, 1147-1152.

Harvati, K., Gunz, P., Grigorescu, D., 2007. Cioclovina (Romania): affinities of an early modern European. J. Hum. Evol. 53, 732-746.

Harvati K., Hublin J.-J. In press. Morphological continuity of the face in the late Middle and Upper Pleistocene Hominins from North Western Africa – A 3-D geometric morphometric analysis. In: Hublin, J.-J. and McPherron, S. (Eds.), Modern Origins: A North African Perspective. Springer.

Harvati, K., Hublin, J.J., Gunz, P., 2010. Evolution of middle-late Pleistocene human cranio-facial form: A 3-D approach. J. Hum. Evol. 59, 445-464.

Harvati, K., Panagopoulou, E., Runnels, C., 2009. The paleoanthropology of Greece. Evol. Anthropol. 18, 131-143.

Harvati, K., Weaver, T.D., 2006a. Human cranial anatomy and the differential preservation of population history and climate signatures. Anat. Rec. A. 288, 1225-1233.

Harvati, K., Weaver, T.D., 2006b. Reliability of cranial morphology in reconstructing Neanderthal phylogeny. Neanderthals revisited: new approaches and perspectives. Springer, Dordrecht, pp. 239-254.

Hedges, R.E.M., Housley, R.A., Bronk, C.R., Van Klinken, G.J., 1992. Radiocarbon dates from the Oxford AMS system: Archaeometry Datelist 14 Archaeometry 34, 141-159.

Henry-Gambier, D. 2001. la Sépulture des enfants de Grimaldi (Baoussé-Roussé): anthropologie et palethnologie des populations de la fin du paléolitique supérieur. Comite Des Travaux Historiques Et scientifiques, Paris.

Hershkovitz, I., Smith, P., Sarig, R., Quam, R., Rodríguez, L., García, R., Arsuaga, J.L., Barkai, R., Gopher, A., 2011. Middle Pleistocene dental remains from Qesem Cave (Israel). Am. J. Phys. Anthropol. 144, 575-592.

Hodgson, J.A., Bergey, C.M., Disotell, T.R., 2010. Neandertal genome: the ins and outs of African genetic diversity. Curr. Biol. 20, R517-R519.

Holt, B.M., Formicola, V., 2008. Hunters of the Ice Age: The biology of Upper Paleolithic people. Am. J. Phys. Anthropol. S47, 70-99.

Holton, N.E., Franciscus, R.G., 2008. The paradox of a wide nasal aperture in cold-adapted Neandertals: a causal assessment. J. Hum. Evol. 55, 942-951.

Howells, W.W., 1970. Mount Carmel man: morphological relationships. Proceedings, 8th International Congress of Anthropological and Ethnological Sciences 1, 269-272.

Howells, W.W., 1973. Cranial Variation in Man: A Study by Multivariate Analysis of Patterns of Differences among Recent Human Populations. Papers of the Peabody Museum of Archaeology and Ethnology, Harvard, Cambridge.

Howells, W.W., 1989. Skull Shapes and the Map. Papers of the Peabody Museum of Archaeology and Ethnology 79, Harvard, Cambridge.

Hrdlička, A. 1927. The Neanderthal phase of man. Huxley Memorial Lecture, 1927. J. R. Anthrop. Inst. 57, 249-274.

Hrdlička, A., 1930. The skeletal remains of early man. Smithsonian Institution Annual Report for 1928. The Smithsonian Institution, Washington D.C., pp. 593-623.

Hubbe, M., Hanihara, T., Harvati, K., 2009. Climate signatures in the morphological differentiation of worldwide modern human populations. Anat. Rec. 292, 1720-1733.

Hublin, J.-J., 1992. Recent human evolution in northwestern Africa. Philos. Trans. R. Soc. Lond. B. Biol. Sci. 337, 185-191.

Hublin, J-J. 1996. The first Europeans. Archaeology 49, 36-44.

Hublin, J.-J., 1998. Climate changes, paleogeography, and the evolution of the Neandertals. In: Akazawa, T., Bar-Yosef, O. (Eds.), Neandertals and Modern Humans in Western Asia. Plenum Press, New York, pp. 295-310.

Hublin, J.-J., 2001. Northwestern African Middle Pleistocene hominids and their bearing on the emergence of *Homo sapiens.* In: Barham, L., Robson-Brown, K. (Eds.), Human Roots: Africa and Asia in the Middle Pleistocene. Western Academic & Specialist Press, Bristol, pp. 99-122.

Hublin, J.-J., 2009. Out of Africa: modern human origins special feature: the origin of Neandertals. Proc. Natl. Acad. 106, 16022-16027.

Hublin, J.-J., Spoor, F., Braun, M., Zonneveld, F., Condemi, S., 1996. A late Neanderthal associated with Upper Palaeolithic artefacts. Nature, 381, 224-226.

Huxtable, J., 1990. Burnt flint date for Yabrud Shelter I Ancient TL Date Lists No. 4 Entry 43.

Hyodo, M., Matsu'ura, S., Kamishima, Y., Kondo, M., Takeshita, Y., Kitaba, I., Danhara, T., Aziz, F., Kurniawan, I., Kumai, H., 2011. High-resolution record of the Matuyama-Brunhes transition constrains the age of Javanese Homo erectus in the Sangiran dome, Indonesia. Proc. Natl. Acad. Sci. 108, 19563-19568.

Keith, A., 1927. A report on the Galilee skull. In: Turville-Pétre, F. (Ed.), Researches in Prehistoric Galilee, 1925-1926. Council of the British School of Archaeology in Jerusalem, London, pp. 593-623.

King, W. 1864. On the reputed fossil of man of the Neanderthal. Quarterly Journal of Science London 1, 88-97.

Klein, R.G., 1994. Southern Africa before the Iron Age. In: Corruccini, R.S. (Ed.), Integrative Paths to the Past: Paleoanthropological Advances in Honor of F. Clark Howell. Prentice Hall, Engelwood Cliffs, NJ, pp. 471-519.

Klein, R.G., 1999. The Human Career. The University of Chicago Press, Chicago.

Klingenberg, C.P., 1998. Heterochrony and allometry: the analysis of evolutionary change in ontogeny. Biol. Rev. Camb. Philos. Soc. 73, 79-123.

Krings, M., Stone, A., Schmitz, R.W., Krainitzki, H., Stoneking, M., and Paabo, S. 1997. Neanderthal DNA sequences and the origin of modern humans. Cell 90, 19-30.

Krings, M. Capelli, C., Tschentscher, F., Geisert, H., Meyer, S., von Haeseler, A., Grossschmidt, K., Possnert, G., Paunovic, M., Paabo, S. 2000. A view of Neanderthal genetic diversity. Nature Genetics 26, 144-146.

Krovitz, G.E., 2003. Shape and growth differences between Neandertals and modern: Grounds for a species-level distinction. In: Thompson, J.L., Krovtiz, G.E., Nelson, A.J. (Eds.), Patterns of growth and development in the genus *Homo.* Cambridge University Press, Cambridge, pp. 320-342.

Lahr, M.M., 1996. The evolution of modern human cranial diversity: A study in cranial variation. Ph.D. Dissertation, Cambridge University Press.

Lahr, M.M., Foley, R.A., 2001. Mode 3, *Homo helmei*, and the pattern of human evolution in the Middle Pleistocene. In: Barham, L., Robson-Brown, K. (Eds.), Human Roots: Africa and Asia in the Middle Pleistocene. Western Academic & Specialist Press, Bristol, pp. 23-29.

Larick, R., Ciochon, R.L., Zaim, Y., Sudijono, Suminto, Rizal, Y., Aziz, F., Reagan, M., Heizler, M., 2001. Early Pleistocene $^{40}Ar/^{39}Ar$ ages for Bapang Formation hominins, Central Java,

Indonesia. Proc. Natl. Acad. Sci. 98, 4866-4871.

Lévêque, F., Vandermeersch, B., 1980. Découvertes de restes humains dans un niveau castelperronien à Saint-Césaire (Charente-Maritime). Comptes Rendus De L'académie Des Sciences Paris. 291D, 187-189.

Lieberman, D.E., 1995. Testing hypotheses about recent human evolution from skulls. Curr. Anthropol. 36, 159-197.

Lieberman, D.E., 2000. Ontogeny, homology, and phylogeny in the hominid craniofacial skeleton: the problem of the browridge. In: O'Higgins, P., Cohn, M.J. (Eds.), Development, Growth and Evolution: Implications for the Study of the Hominid Skeleton. Academic Press, San Diego, pp. 85-122.

Lieberman, D.E., 2008. Speculations about the selective basis for modern human craniofacial form. Evol. Anthropol. 17, 55-68.

Lieberman, D.E., Krovitz, G.E., Yates, F.W., Devlin, M., St Claire, M., 2004. Effects of food processing on masticatory strain and craniofacial growth in a retrognathic face. J. Hum. Evol. 46, 655-677.

Lieberman, D.E., McBratney, B.M., Krovitz, G., 2002. The evolution and development of cranial form in *Homo sapiens.* Proc. Natl. Acad. Sci. 99, 1134-1139.

Liu, W., Zhang, Y., Wu, X., 2005. Middle Pleistocene human cranium from Tangshan (Nanjing), Southeast China: a new reconstruction and comparisons with Homo erectus from Eurasia and Africa. Am. J. Phys. Anthropol. 127, 253-262.

Lorenzo, C., Arsuaga, J.L., Carretero, J.M., 1999. Hand and foot remains from the Gran Dolina Early Pleistocene site (Sierra de Atapuerca, Spain). J. Hum. Evol. 37, 501-522.

de Lumley, H., 1984. L'industrie du Pleistocène inférieur de la grotte du Vallonet Roquebrune-Cap-Martin, Alpes-Maritime. L'Anthropologie 92, 501-614.

de Lumley, H., de Lumley, M.-A., 1971. Découverte de restes humaines anténéandertaliens datés au début de Riss à la Caune d'Arago (Tautavel, Pyrénées-Orientales). C. R. Acad. Sci., Paris. 272, 1729-1742.

de Lumley, H., de Lumley, M.-A., 1973. Pre-neanderthal remains from Arago cave in southwestern France. Yearb. Phys. Anthropol. 17, 162-168.

Maddux, S.D., Franciscus, R.G., 2009. Allometric scaling of infraorbital surface topography in *Homo*. J. Hum. Evol. 56, 161-174.

Manzi, G., 2004. Human evolution at the Matuyama-Brunhes boundary. Evol. Anthropol. 13, 11-24.

Manzi, G., Magri, D., Milli, S., Palombo, M.R., Margari, V., Celiberti, V., Barbieri, M., Barbieri, M., Melis, R.T., et al., 2010. The new chronology of the Ceprano calvarium (Italy). J. Hum. Evol. 59, 580-585.

Manzi, G., Mallegni, F., Ascenzi, A., 2001. A cranium for the earliest Europeans: phylogenetic position of the hominid from Ceprano, Italy. Proc. Natl. Acad. Sci. 98, 10011-10016.

Mardia, K.V., Bookstein, F., Moreton, I.J., 2000. Statistical assessment of bilateral symmetry of shapes. Biometrika 87, 285-300.

Martinez-Maza, C., Rosas, A., García-Vargas, S., Estalrrich, A., de la Rasilla, M., 2011. Bone remodelling in Neanderthal mandibles from the El Sidrón site (Asturias, Spain). Biol. Lett. 7, 593-596.

Martinón-Torres, M., Bermúdez de Castro, J.M., Gómez-Robles, A., Arsuaga, J.L., Carbonell, E., Lordkipanidze, D., Manzi, G., Margvelashvili, A., 2007. Dental evidence on the hominin dispersals during the Pleistocene. Proc. Natl. Acad. Sci. U. S. A. 104, 13279-13282.

Martinón-Torres, M., Bermúdez de Castro, J.M., Gómez-Robles, A., Margvelashvili, A., Prado, L., Lordkipanidze, D., Vekua, A., 2008. Dental remains from Dmanisi (Republic of Georgia): morphological analysis and comparative study. J. Hum. Evol. 55, 249-273.

Martinón-Torres, M., Bermúdez de Castro, J.M., Gómez-Robles, A., Prado-Simón, L., Arsuaga, J.L., 2012. Morphological description and comparison of the dental remains from Atapuerca-Sima de los Huesos site (Spain). J. Hum. Evol. 62, 7-58.

Maureille, B., 1994. La face chez *Homo erectus* et *Homo sapiens*: recherche sur la variabilité morphologique et métrique. Ph.D. Dissertation, University of Bordeaux I.

Maureille, B., Houët, F., 1997. Nouvelles données sur caractéristiques dérivées du mastif facial supérieur des Néandertaliens. Anthrop. et Préhistoire 108, 89-98.

McBrearty, S., Brooks, A.S., 2000. The revolution that wasn't: a new interpretation of the origin of modern human behavior. J. Hum. Evol. 39, 453-563.

McCollum, M.A., 1999. The robust australopithecine face: a morphogenetic perspective. Science. 284, 301-305.

McCollum, M.A., 2008. Nasomaxillary remodeling and facial form in robust *Australopithecus*: a reassessment. J. Hum. Evol. 54, 2-14.

McCown, T., Keith, A., 1939. The stone age of Mount Carmel, Vol. 2, the fossil human remains from the Levallois-Mousterian. Clarendon, Oxford.

McNulty, K.P., 2003. Geometric morphometric analyses of extant and fossil hominoid craniofacial morphology. Ph.D. Dissertation, City University of New York.

McNulty, K.P., Frost, S.R., Strait, D.S., 2006. Examining affinities of the Taung child by developmental simulation. J. Hum. Evol. 51, 274-296.

Mellars, P., 1999. The Neanderthal problem continued. Curr. Anthropol. 40, 341-64.

Mellars, P. 2002. Archaeology and the origins of modern humans: European and African

perspectives. Proceedings of the British Academy 106, 31-46.

Mellars, P. 2004. Neanderthals and the modern colonization of Europe. Nature 431, 461-465.

Mellars, P. 2006. A new radiocarbon revolution and the dispersal of modern humans in Eurasia. Nature 439, 931-935.

Mercier, N., Valladas, H., 2003. Reassessment of TL age estimates of burnt flints from the Paleolithic site of Tabun Cave, Israel. J. Hum. Evol. 45, 401-409.

Mercier, N., Valladas, H., Joron, J. L., Reyss, J. L., Lévêque, F. & Vandermeersch, B., 1991. Thermoluminescence dating of the late Neanderthal remains from Saint-Césaire. Nature 351, 737-739.

Mercier, N., Valladas, H., Valladas, G., Reyss, J.L., Jelinek, A., Meignen, L., Joron, J.L., 1995. TL dates of burnt flints from Jelinek's excavations at Tabun and their implications. J. Archaeol. Sci. 22, 495-509.

Mitteroecker P, Bookstein F.L., 2011. Linear discrimination, ordination, and the visualization of selection gradients in modern morphometrics. Evol. Biol. 38, 100-114.

Mitteroecker, P., Gunz, P., 2009. Advances in geometric morphometrics. Evol. Biol. 36, 235-247.

Mitteroecker, P., Gunz, P., Bernhard, M., Schaefer, K., Bookstein, F.L., 2004. Comparison of cranial ontogenetic trajectories among great apes and humans. J. Hum. Evol. 46, 679-697.

Mitteroecker, P., Gunz, P., Bookstein, F.L., 2005. Heterochrony and geometric morphometrics: a comparison of cranial growth in *Pan paniscus* versus *Pan troglodytes*. Evol. Dev. 7, 244-258.

Mounier, A., Condemi, S., Manzi, G., 2011. The stem species of our species: a place for the archaic human cranium from Ceprano, Italy. PLoS One 6, e18821.

Mounier, A., Marchal, F., Condemi, S., 2009. Is *Homo heidelbergensis* a distinct species? New insight on the Mauer mandible. J. Hum. Evol. 56, 219-246.

Muttoni, G., Scardia, G., Kent, D.V., Swisher, C.C., Manzi, G., 2009. Pleistocene magnetochronology of early hominin sites at Ceprano and Fontana Ranuccio, Italy. Earth and Planetary Science Letters. 286, 255-268.

Neubauer, S., Gunz, P., Hublin, J.J., 2009. The pattern of endocranial ontogenetic shape changes in humans. J. Anat. 215, 240-255.

Neubauer, S., Gunz, P., Hublin, J.J., 2010. Endocranial shape changes during growth in chimpanzees and humans: A morphometric analysis of unique and shared aspects. J. Hum. Evol. 59, 555-566.

Noonan, J.P., Coop, G., Kudaravalli, S., Smith, D., Krause, J., Alessi, J., Chen, F., Platt, D., Paabo, S., et al., 2006. Sequencing and analysis of Neanderthal genomic DNA. Science. 314, 1113-1118.

O'Higgins, P., 2000a. Quantitative approaches to the study of craniofacial growth and evolution: advances in morphometric techniques: development, growth and evolution. Academic Press, San Diego.

O'Higgins, P., 2000b. The study of morphological variation in the hominid fossil record: biology, landmarks and geometry. J. Anat. 197 (Pt 1), 103-120.

O'Higgins, P., Chadfield, P., Jones, N., 2001. Facial growth and the ontogeny of morphological variation within and between the primates *Cebus apella* and *Cercocebus torquatus.* Journal of Zoology. 254, 337-357.

O'Higgins, P., Jones, N., 1998. Facial growth in *Cercocebus torquatus*: an application of three-dimensional geometric morphometric techniques to the study of morphological variation. J. Anat. 193 (Pt 2), 251-272.

Ovchinnikov, I.V., Gotherstrom, A., Romanova, G.P., Kharitonov, V.M., Liden, K., Goodwin, W. 2000. Molecular analysis of Neanderthal DNA from the northern Causcasus. Nature 404, 490-493.

Parés, J.M., Pérez-González, A., 1995. Paleomagnetic age for hominid fossils at Atapuerca archaeological site, Spain. Science 269, 830-832.

Parés, J.M., Pérez-González, A., 1999. Magnetochronology and stratigraphy at Gran Dolina section, Atapuerca (Burgos, Spain). J. Hum. Evol. 37, 325-342.

Pearson, O.M. 2000 Postcranial remains and the origin of modern humans. Evol. Anthropol. 9, 229-247.

Ponce de León, M.S., Golovanova, L., Doronichev, V., Romanova, G., Akazawa, T., Kondo, O., Ishida, H., Zollikofer, C.P., 2008. Neanderthal brain size at birth provides insights into the evolution of human life history. Proc. Natl. Acad. Sci. U. S. A. 105, 13764-13768.

Ponce de León, M.S., Zollikofer, C.P., 2001. Neanderthal cranial ontogeny and its implications for late hominid diversity. Nature. 412, 534-538.

Pope, G.G., 1992. Craniofacial evidence for the origins of modern humans in China. Yearbook of Physical Anthropology 35, 243-298.

Potts, R., Behrensmeyer, A.K., Deino, A., Ditchfield, P., Clark, J., 2004. Small mid-Pleistocene hominin associated with East African Acheulean technology. Science 305, 75-78.

Quam, R., Bailey, S., Wood, B., 2009. Evolution of M1 crown size and cusp proportions in the genus *Homo*. J. Anat. 214, 655-670.

R Development Core Team. 2010. R: A language and environment for statistical computing. R Foundation for Statistical Computing, Vienna, Austria.

Rak, Y., 1986. The Neanderthal: A new look at an old face. J. Hum. Evol. 15, 151-164.

Rak, Y., Kimbel, W.H., Hovers, E., 1994. A Neandertal infant from Amud cave, Israel. J. Hum.

Evol. 26, 313-324.

Rampont, M., 1994. Les squelettes, os et dents de foetus, nouveaux-né et enfants du musée anatomique de Strasbourg. Aspect historiques et catalogues. Ph.D. Dissertation, Université Louis Pasteur.

Relethford, J.H., 1994. Craniometric variation among modern human populations. Am. J. Phys. Anthropol. 95, 53-62.

Relethford, J.H., 2004a. Boas and beyond: migration and craniometric variation. Am. J. Hum. Biol. 16, 379-386.

Relethford, J.H., 2004b. Global patterns of isolation by distance based on genetic and morphological data. Hum. Biol. 76, 499-513.

Richtsmeier, J.T., Corner, B.D., Grausz, H.M., Cheverud, J.M., Danahey, S.E., 1993. The role of postnatal growth pattern in the production of facial morphology. Syst. Biol. 42, 307.

Rightmire, G.P. 1996. The human cranium from Bodo, Ethiopia: evidence for speciation in the Middle Pleistocene. J. Hum. Evol. 31, 21-39.

Rightmire, G.P., 1998a. Evidence from facial morphology for similarity of Asian and African representatives of *Homo erectus.* Am. J. Phys. Anthropol. 106, 61-85.

Rightmire, G.P., 1998b. Human evolution in the Middle Pleistocene: the role of *Homo heidelbergensis.* Evol. Anthropol. 6, 218-227.

Rightmire, G.P., 2001. Morphological diversity in Middle Pleistocene *Homo.* In: Wood, B., Tobias, P.V. (Eds.), Humanity from African Naissance to Coming Millenia: Colloquia in Human Biology and Paleoanthropology. Firenze University Press, Firenze, pp. 135-140.

Rightmire, G.P., 2007. Later Middle Pleistocene *Homo.* In: Henke, W., Tattersall, I. (Eds.), Handbook of Paleoanthropology. Springer, Heidelberg, pp. 1695-1715.

Rightmire, G.P., 2008. *Homo* in the Middle Pleistocene: Hypodigms, variation, and species recognition. Evol. Anthropol. 17, 8-21.

Rightmire, G.P., 2009. Out of Africa: Modern Human Origins Special Feature: Middle and later Pleistocene hominins in Africa and Southwest Asia. Proc. Natl. Acad. Sci. 16046-16050.

Rightmire, G.P., Lordkipanidze, D., Vekua, A., 2006. Anatomical descriptions, comparative studies and evolutionary significance of the hominin skulls from Dmanisi, Republic of Georgia. J. Hum. Evol. 50, 115-141.

Rightmire, G.P., Van Arsdale, A.P., Lordkipanidze, D., 2008. Variation in the mandibles from Dmanisi, Georgia. J. Hum. Evol. 54, 904-908.

Rink, W.J., Schwarcz, H.P., 1995. ESR ages for Krapina hominids. Nature 378, 24.

Rink, W.J., Schwarz, H.P., Lee, H.K., Rees-Jones, J., Rabinovich, R., Hovers, E., 2001. Electron

spin resonance (ESR) and thermal ionization mass spectrometric (TIMS) $^{230}Th/^{234}U$ dating of teeth in Middle Paleolithic layers at Amud Cave, Israel. Geoarchaeology 16, 701-717.

Rohlf, F.J., 1993. Relative warp analysis and an example of its application to mosquito wings. In: Marcus, L.F., Bello, E., García-Valdecasas, A. (Eds.), Contributions to Morphometrics. Museo Nacional de Ciencies Naturales, Madrid, pp. 131–159.

Rosas, A., 2001. Occurrence of neanderthal features in mandibles from the Atapuerca-SH site. Am. J. Phys. Anthropol. 114, 74-91.

Rosas, A., Bastir, M., 2002. Thin-plate spline analysis of allometry and sexual dimorphism in the human craniofacial complex. Am. J. Phys. Anthropol. 117, 236-245.

Rosas, A., Martinez-Maza, C., 2010. Bone remodeling of the *Homo heidelbergensis* mandible; the Atapuerca-SH sample. J. Hum. Evol. 58, 127-137.

Rosas, A., Martínez-Maza, C., Bastir, M., García-Tabernero, A., Lalueza-Fox, C., Huguet, R., Ortiz, J.E., Julià, R., Soler, V., et al., 2006. Paleobiology and comparative morphology of a late Neandertal sample from El Sidron, Asturias, Spain. Proc. Natl. Acad. Sci. U. S. A. 103, 19266-19271.

Roseman, C.C., 2004. Detecting interregionally diversifying natural selection on modern human cranial form by using matched molecular and morphometric data. Proc. Natl. Acad. Sci. 101, 12824-12829.

Roseman, C.C., Weaver, T.D., 2007. Molecules versus morphology? Not for the human cranium. Bioessays 29, 1185-1188.

Scheuer, L., Black, S.M., 2000. Developmental juvenile osteology. Elsevier Academic Press, San Diego.

Schillaci, M.A., 2008. Human cranial diversity and evidence for an ancient lineage of modern humans. J. Hum. Evol. 54, 814-826.

Schwalbe, G. 1906. Studien zur Vorgeschichte des Menschen. I. Zur Frage der Abstammung des Menschen. E. Scheizerbart, Stuttgart.

Schwarcz, H.P., Bietti, A., Buhay, W.M., Stiner, M.C., Grün, R., Segre, A., 1991. On the reexamination of Grotta Guattari: Uranium-series and electron-spin-resonance dates. Curr. Anthropol. 32, 313-316.

Shen, G., Gao, X., Gao, B., Granger, D.E., 2009. Age of Zhoukoudian *Homo erectus* determined with (26)Al/(10)Be burial dating. Nature. 458, 198-200.

Shen, G., Wang, W., Wang, Q., Zhao, J., Collerson, K., Zhou, C., Tobias, P.V., 2002. U-Series dating of Liujiang hominid site in Guangxi, Southern China. J. Hum. Evol. 43, 817-829.

Simmons, T., Falsetti, A.B., Smith, F.H., 1991. Frontal bone morphometrics of southwest Asian Pleistocene hominids. J. Hum. Evol. 20, 249-269.

Skelton, R.R., McHenry, H.M., 1992. Evolutionary relationships among early hominids. J. Hum. Evol. 23, 309-349.

Skinner, M.M., Wood, B.A., Boesch, C., Olejniczak, A.J., Rosas, A., Smith, T.M., Hublin, J.J., 2008. Dental trait expression at the enamel-dentine junction of lower molars in extant and fossil hominoids. J. Hum. Evol. 54, 173-186.

Slice, D.E., 2005. Modern Morphometrics in Physical Anthropology. Kluwer Academic, New York.

Smith, B.H., 1994. Patterns of dental development in *Homo*, *Australopithecus*, *Pan*, and *Gorilla*. Am. J. Phys. Anthropol. 94, 307-325.

Smith, B.H., Tompkins, R.L., 1995. Toward a life history of the Hominidae. Annual. Review. of. Anthropology. 24, 257-279.

Smith, F.H., 1982. Upper Pleistocene hominid evolution in South-Central Europe: a review of the evidence and analysis of trends. Curr. Anthropol. 23, 667-703.

Smith, F.H., 1992. Models and realities in modern human origins: the African fossil evidence. Philos. Trans. R. Soc. Lond. 337, 243-250.

Smith, F.H., 2002. Migrations, radiations and continuity: Patterns of Middle and Late Pleistocene humans. In: Hartwig, W.C. (Ed.), The Primate Fossil Record. Cambridge University Press, Cambridge, pp. 437-456.

Smith, F.H., Falsetti, A.B., Donnelly, S.M., 1989. Modern human origins. Am. J. Phys. Anthropol. 32, 35-68.

Smith, F.H., Janković, I., Karavanic, I., 2005. The assimilation model, modern human origins in Europe, and the extinction of Neandertals. Quat. Int. 137, 7-19.

Smith, F.H., Ranyard, G.C., 1980. Evolution of the supraorbital region in Upper Pleistocene fossil hominids from South-Central Europe. Am. J. Phys. Anthropol. 53, 589-610.

Smith, H.F., 2009. Which cranial regions reflect molecular distances reliably in humans? Evidence from three-dimensional morphology. Am. J. Hum. Biol. 21, 36-47.

Smith, T.M., Tafforeau, P., Reid, D.J., Grün, R., Eggins, S., Boutakiout, M., Hublin, J.-J., 2007. Earliest evidence of modern human life history in North African early *Homo* sapiens. Proc. Natl. Acad. Sci. 104, 6128-6133.

Sohn, S., Wolpoff, M.H., 1993. Zuttiyeh face: a view from the east. Am. J. Phys. Anthropol. 91, 325-347.

Soressi, M., Jones, H.L., Rink, W.J., Maureille, B., Tillier, A.M., 2007. The Pech-de-l'Azé I Neandertal child: ESR, uranium-series, and AMS 14C dating of its MTA type B context. J. Hum. Evol. 52, 455-466.

Svoboda, J.A., 2008. The upper paleolithic burial area at Předmostí: ritual and taphonomy. J. Hum. Evol. 54, 15-33.

Stansfield Nee Bulygina, E., Gunz, P., 2011. Skhodnya, Khvalynsk, Satanay, and Podkumok calvaria: Possible upper paleolithic hominins from European Russia. Journal of Human Evolution, 60, 129-144.

Strand Viðarsdóttir, U., Cobb, S., 2004. Inter- and intra-specific variation in the ontogeny of the hominoid facial skeleton: testing assumptions of ontogenetic variability. Ann. Anat. 186, 423-428.

Strand Viðarsdóttir, U., O'Higgins, P., Stringer, C., 2002. A geometric morphometric study of regional differences in the ontogeny of the modern human facial skeleton. J. Anat. 201, 211-229.

Street, M., 2002. Ein Wiedersehen mit dem Hund von Bonn-Oberkassel. Bonn Zool. Beitr. 50, 269-290.

Stringer, C.B., 1974. Population relationships of later Pleistocene Hominids: A multivariate study of available crania. J. Archaeol. Sci. 1, 317-342.

Stringer, C.B., 1983. Some further notes on the morphology and dating of the Petralona hominid. J. Hum. Evol. 12, 731-742.

Stringer, C.B. 1994. Out of Africa – a personal history. In: Nitecki, M.H. and Nitecki, D.V. (Eds.), Origins of Anatomically Modern Humans. Plenum Press, New York, pp. 150-174.

Stringer, C.B. 1996. Current issues in modern human origins. In: Meikle,W., Howell, F. C. and Jablonski, N. (Eds.), Contemporary Issues in Human Evolution. California Academy of Science Memoir 21, 115-134.

Stringer, C.B., 2002. Modern human origins: progress and prospects. Philos. Trans. R. Soc. Lond. 357, 563-579.

Stringer, C.B., 2011. The Chronological and evolutionary position of the Broken Hill cranium. Am. J. Phys. Anthropol. S52, 287.

Stringer, C.B., Andrews, P., 1988. Genetic and fossil evidence for the origin of modern humans. Science. 239, 1263-1268.

Stringer, C.B., Hublin, J.-J., Vandermeersch, B., 1984. The origins of anatomically modern humans in Western Europe. In: Smith, F.H. and Spencer , F. (Eds.), The Origins of Modern Humans: A World Survey of the Fossil Evidence. Alan R. Liss, New York, pp. 51-135.

Suzuki, H., Takai, F., 1970. The Amud Man and His Cave Site. University of Tokyo Press, Tokyo.

Tattersall, I., Schwartz, J.H., 2006. The distinctiveness and systematic context of *Homo neanderthalensis.* In: Harvati, K., Harrison, T. (Eds.), Neanderthals revisited: New

approaches and perspectives. Dordrecht, New York, pp. 9-22.

Templeton, A., 2002. Out of Africa again and again. Nature. 416, 45-51.

Templeton, A.R., 2005. Haplotype trees and modern human origins. Am. J. Phys. Anthropol. Suppl 41, 33-59.

Thorne, A., Wolpoff, M., 1992. The multiregional evolution of humans. Scientific American 266, 76-83.

Tillier, A.-M., 1989. The evolution of modern humans: evidence from young Mousterian individuals. In: Mellars, P., Stringer, C. (Eds.), The Human Revolution: Behavioural and Biological Perspectives on the Origins of Modern Humans. Princeton University Press, New Jersey, pp. 286-297.

Tillier, A.M., 1996. The Pech de l'Azé and Roc de Marsal children (Middle Paleolithic, France): skeletal evidence for variation in Neanderthal ontogeny. Human. Evolution 11, 113-119.

Trinkaus, E., 1983. The Shanidar Neandertals. Academic Press, New York.

Trinkaus, E., 1987. The Neandertal face: evolutionary and functional perspectives on a recent hominid face. J. Hum. Evol. 16, 429-443.

Trinkaus, E., 1989. Issues concerning human emergence in the later Pleistocene. In: Trinkaus, E. (Ed.), The Emergence of Modern Humans: Biological Adaptations in the Later Pleistocene. Cambridge University Press, Cambridge, pp. 1-17.

Trinkaus, E. 1997. Apppendicular robusticity and the paleobiology of modern human emergence. Proc. Natl. Acad. Sci. 94, 13367-13373.

Trinkaus, E., 2005. Early modern humans. Ann. Rev. Anthropol. 34, 207.

Trinkaus, E., 2006. Modern human versus Neandertal evolutionary distinctiveness. Current Anthropology 47, 597-620.

Trinkaus, E., 2007. European early modern humans and the fate of the Neandertals. Proc. Natl. Acad. Sci. 104, 7367-7372.

Trinkaus, E., Churchill, S.E., Ruff, C.B., Vandermeersch, B., 1999. Long bone shaft robusticity and body proportions of the Saint-Césaire 1 Châtelperronian Neanderthal. J. Archaeol. Sci. 26, 753-773.

Trinkaus, E., Ruff, C.B., Churchill, S.E., Vandermeersch, B., 1998. Locomotion and body proportions of the Saint-Césaire 1 Châtelperronian Neandertal. Proc. Natl. Acad. Sci. 95, 5836-5840.

Tryon, C.A., McBrearty, S., Texier, P.-J., Levallois lithic technology from the Kapthurin Formation, Kenya: Acheulian origin and Middle Stone Age diversity. Arf. Archaeol. Rev. 22, 199-229.

Turville-Pétre, F., 1927. Researches in Prehistoric Galilee, 1925-26. Council of the British

School of Archaeology in Jerusalem, London.

Ubelaker, D., 1989. Human Skeletal Remains. Taraxacum Press, Washington D.C.

Vallois, H.V. 1954. Neandertals and Presapiens. Journal of the Royal Anthropological Institute of Great Britain and Ireland 84, 111-130.

Vandermeersch, B., 1981. Les hommes fossiles de Qafzeh (Israël). Editions du Centre national de la recherche scientifique, Paris.

Vandermeersch, B., 1989. The evolution of modern humans: recent evidence from southwest Asia. In: Mellars, P.A., Stringer, C. (Eds.), The human revolution. Edinburgh University Press, Edinburgh, pp. 155-164.

van Vark, G.N., 1995. The study of hominid skeletal remains by means of statistical methods. In: Boas, N.T., Wolfe, G.D. (Eds.), Biological Anthropology: The State of the Science. Oregon State University Press, Corvallis, pp. 71-90.

Vekua, A., Lordkipanidze, D., Rightmire, G.P., Agusti, J., Ferring, R., Maisuradze, G., Mouskhelishvili, A., Nioradze, M., De Leon, M.P., et al., 2002. A new skull of early *Homo* from Dmanisi, Georgia. Science. 297, 85-89.

Vishnyatsky, L., 1999. The Paleolithic of Central Asia. Journal of World. Prehistory 13, 69-122.

von Cramon-Taubadel, N., 2009. Congruence of individual cranial bone morphology and neutral molecular affinity patterns in modern humans.. Am. J. Phys. Anthropol. 140, 205-215.

von Cramon-Taubadel, N., Lycett, S.J., 2008. Brief communication: human cranial variation fits iterative founder effect model with African origin. Am. J. Phys. Anthropol. 136, 108-113.

Vishnyatsky, L., 1999. The Paleolithic of Central Asia. Journal. of. World. Prehistory. 13, 69-122.

Wagner, G.A., Krbetschek, M., Degering, D., Bahain, J.J., Shao, Q., Falguères, C., Voinchet, P., Dolo, J.M., Garcia, T., Rightmire, G.P., 2010. Radiometric dating of the type-site for *Homo heidelbergensis* at Mauer, Germany. Proc. Natl. Acad. Sci. U. S. A. 107, 19726-19730.

Wagner, G.A., Maul, L.C., Löscher, M., Schreiber, H.D., 2011. Mauer – the type site of *Homo heidelbergensis*: palaeoenvironment and age. Quaternary. Science. Reviews. 30, 1464-1473.

Wall, J.D., Lohmueller, K.E., Plagnol, V., 2009. Detecting ancient admixture and estimating demographic parameters in multiple human populations. Mol. Biol. Evol. 26, 1823-1827.

Walters, M., O'Higgins, P., 1992. Factors influencing craniofacial growth: a scanning electron microscope study of high resolution facial replicas. Proc. Austral. Soc. Hum. Biol. 5, 391-402.

Weaver, T.D., 2009. The meaning of Neandertal skeletal morphology. Proc. Natl. Acad. Sci. 106, 16028.

Weaver, T.D., Roseman, C.C., Stringer, C.B., 2007. Were Neandertal and modern human cranial

differences produced by natural selection or genetic drift? J. Hum. Evol. 53, 135-145.

Weber, G.W., Gunz, P., Mitteroecker, P., Stadlmayr, A., Bookstein, F.L., Seidler, H., 2006. External geometry of Mladeč neurocrania compared with anatomically modern humans and Neandertals. Early Modern Humans at the Moravian Gate: Mladeč Caves and their Remains. Springer, Heidelberg, pp. 453-471.

Weidenreich, F., 1943. The skull of *Sinanthropus pekinensis*: a comparative study on a primitive hominid skull. Geological Survey of China, Pehpei, Chungking.

Weidenreich, F. 1949. Interpretation of the fossil material. Early Man in the Far East. A Symposium. Stud. Phys. Anthrop. 1, 149-158.

White, M., Ashton, N., Palaeolithic core technology and the origins of the Levallois method in northwestern Europe. Current Anthropology 44, 598-609.

White, T.D., Asfaw, B., DeGusta, D., Gilbert, H., Richards, G.D., Suwa, G., and Howell, F.C. 2003. Pleistocene *Homo sapiens* from Middle Awash, Ehtiopia. Nature 423, 742-747.

Wiley, D.F., Amenta, N., Alcantara, D.A., Deboshmita, G., Kil, Y.J., Delson, E., Harcourt-Smith, W., Rohlf, F.J., St John, K., Hamann, B., 2005. Evolutionary morphing. Proceedings of IEEE Visualizations.

Williams, F.L., Godfrey, L.R., Sutherland, M.R., 2002. Heterochrony and the evolution of Neandertal and modern human craniofacial form. In: Minugh-Purvis, N., McNamara, K.J. (Eds.), Human Evolution through Developmental Change. The John Hopkins University Press, Baltimore, pp. 405-441.

Wolpoff, M.H., 1999. Paleoanthropology. McGraw-Hill, New York.

Wolpoff, M. and Caspari, R. 1997. Race and human evolution: a fatal attraction. Simon & Schuster, New York.

Wolpoff, M.H., Hawks, J., Frayer, D.W., Hunley, K., 2001. Modern human ancestry at the peripheries: a test of the replacement theory. Science 291, 293-297.

Wolpoff, M.H., Smith, F.H., Malez, M., Radovčić, J., Rukavina, D., 1981. Upper Pleistocene human remains from Vindija cave, Croatia, Yugoslavia. Am. J. Phys. Anthropol. 54, 499-545.

Wolpoff, M.H., Thorne, A.G., Jelinek, J., Yinyun, Z., 1994. The case for sinking *Homo erectus*. 100 years of *Pithecanthropus* is enough! Cour. Forsch. Inst. Senckenberg. 171, 341-361.

Wolpoff, M.H., Wu, X. and Thorne, A.G. 1984. Modern *Homo sapiens* origins: a general theory of hominid evolution involving the fossil evidence from east Asia. In Smith, F.H. and Spencer, F. (Eds.), The Origins of Modern Humans: A World Survey of the Fossil Evidence. Alan R. Liss, New York, pp. 411-483.

Wood, B., 1991. Koobi Fora Research Project, vol. 4: Hominid Crania Remains. Clarendon Press, Oxford.

Wolpoff, M.H., Wu Xinzhi, Thorne, A.G., 1984. Modern *Homo sapiens* origins: A general theory of hominid evolution involving the fossil evidence from east Asia. In: Smith, F.H., Spencer, F. (Eds.), The origins of modern humans: a world survey of the fossil evidence. Alan R. Liss, New York, pp. 411-483.

Wood, B., Lieberman, D.E., 2001. Craniodental variation in *Paranthropus boisei*: a developmental and functional perspective. Am. J. Phys. Anthropol. 116, 13-25.

Woodward, A.S., 1921. A new cave man from Rhodesia, South Africa. Nature 108, 371-372.

Zeitoun, V., 2001. The taxinomical position of the skull of Zuttiyeh. C. R. Acad. Sci., Paris. 332, 521-525.

Zelditch, M.L., Lundrigan, B.L., Garland, T., 2004. Developmental regulation of skull morphology I. Ontogenetic dynamics of variance. Evol. Dev. 6, 194-206.

Zilberman, P.S., 1994. A Neanderthal infant from the Barakai Cave, western Caucasus. J. Hum. Evol. 27, 405-415.

Zilhão, J. & d'Errico, F., 1999. The chronology and taphonomy of the earliest Aurignacian and its implications for the understanding of Neandertal extinction. Journal of World Prehistory 13, 1-68.

Zollikofer, C.P., Ponce de León, M.S., 2004. Kinematics of cranial ontogeny: heterotopy, heterochrony, and geometric morphometric analysis of growth models. J. Exp. Zool. B. Mol. Dev. Evol. 302, 322-340.

Zollikofer, C.P., Ponce de León, M.S., 2010. The evolution of hominin ontogenies. Semin. Cell. Dev. Biol. 21, 441-452.